# LHC - CHALLENGES IN HANDLING BEAMS EXCEEDING 100 MJ

R. Schmidt, CERN, Geneva, Switzerland

*Abstract*

The Large Hadron Collider (LHC) at CERN operates at 4 TeV with high intensity beams, with bunch intensities exceeding the nominal value by several 10 %. The energy stored in each beams is beyond 130 MJ, less than a factor of three from the nominal value at 7 TeV. With these parameters, operation entered into a regime where various effects due to high intensity bunches are observed (instabilities, beam-beam effects, e-cloud effects). The highly efficient collimation system limits beam losses that threaten to quench superconducting magnets. The correct functioning of the machine protection systems is vital during the different operational phases. Already a small fraction of the stored energy is sufficient to damage accelerator equipment or experiments in case of uncontrolled beam loss. Safe operation in presence of such high intensity proton beams is guaranteed by the interplay of many different systems: beam dumping system, beam interlocks, beam instrumentation, equipment monitoring, collimators and absorbers. The experience gained with the key systems of machine protection and collimation will be discussed.

## INTRODUCTION

The LHC has a long history. Even before the drawing-board stage, the farsighted John Adams noted in 1977 that the tunnel for the future LEP collider should also be big enough to accommodate another ring of magnets. In 1984 a workshop was organised under the joint sponsorship of ECFA and CERN to discuss the feasibility of large hadron colliders in the LEP tunnel [1]. The design converged later to a collider with an energy of 7 TeV and a nominal luminosity of $10^{34} cm^{-2} s^{-1}$. It took about 25 years from 1984 to first proton collisions in 2009, followed by runs in 2010, 2011 and 2012. Due to nonconformities of the interconnections between magnets the energy was limited to 3.5 TeV in 2010 and 2011, and to 4.0 TeV in 2012. Integrated and peak luminosities during 2012 are shown in Figure 1 and Figure 2. The peak luminosity is more than $7.5 \times 10^{33} cm^{-2} s^{-1}$ and an integrated luminosity of more than $14\, fb^{-1}$ was recorded by the experiments. Despite the operation at lower energy, the LHC experiments published already exciting results, a new particle with a mass of about 125 GeV with parameters that are compatible with the Standard-Model Higgs [2]. The nominal parameters for the LHC are compared with the parameters for 2011 and 2012 in Figure **3**.

## HIGH LUMINOSITY

The LHC nominal luminosity exceeds the luminosity of other hadron colliders by a factor of 20. This is achieved by operating with a large number of bunches in two separated beam pipes, only crossing in the four experiments. For nominal operation at 7 TeV the energy stored in each beam exceeds with more than 360 MJ the values for other accelerators by two orders of magnitude. Figure 4 shows the nominal parameters for operation at 7 TeV and the parameters in 2011 and 2012. When operating at 4 TeV instead of 7 TeV, a peak luminosity of $7.5 \times 10^{33} cm^{-2} s^{-1}$ was achieved despite operating with bunches every 50 ns instead of nominal 25 ns. This was only possible with emittances much smaller than nominal, and bunch currents more than 30% higher than nominal.

The luminosity depends on the emittance and the intensity per bunch (=> high brightness beams), determined to a large extent by the chain of injectors (LINAC, Booster, PS and SPS). The beam structure (25 ns or 50 ns bunch spacing) and the number of bunches is also prepared in the injectors. A large amount of work is going on to understand and improve the beam parameters in the injector complex, with a direct impact on LHC performance (see several papers in this workshop). An ambitious improvement program is on the way during the next decade to further improve the beam parameters that can be delivered to LHC as well as to other physics experiments at CERN [3].

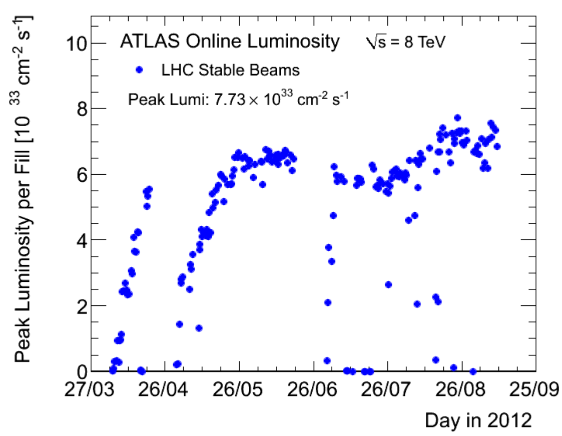


Figure 1: Peak luminosity for fills in 2012.

## EXPERIMENTAL INSERTIONS

In four of the eight LHC insertions the beams are brought together into a common vacuum over ~260 m to collide in the experiments. To avoid a large number of head-on collisions the beams are crossing in the experiment at an angle. The total crossing angle is about 300 µrad. When the beams are travelling through the common chamber, there are a number of parasitic crossings. A separation of about 10 σ between the beams is required for all parasitic crossings, about 64 when operating with 1380 bunches (50 ns bunch spacing).

ISBN 978-3-95450-118-2

# J-PARC RECOVERY STATUS

K. Yamamoto on behalf of J-PARC Accelerator Group, J-PARC, Tokai-mura, Japan


*Abstract*

The beam commissioning of the Japan Proton Accelerator Research Complex (J-PARC) facilities started in November 2006. After that a provided beam power was increased by the beam commissioning. Just before the Great East Japan Earthquake in March 2011, the Rapid-Cycling Synchrotron (RCS) of the J-PARC provided 200kW proton beam to neutron users, and Main Ring (MR) provided 145kW proton beam to Neutrino target. However, the facilities of J-PARC were seriously damaged by the Earthquake. We completed not only the recovery work in only nine months, but also improved some devices. A beam operation after recovery work shows that those improvements enabled further high power operation. In the Linac and RCS, output power was not only reproduced but also increased to 275kW. In MR, extraction beam power in both modes (Slow extraction for Hadron experimental hall and Fast extraction for Neutrino target) were increased as well.


## INTRODUCTION

The Japan Proton Accelerator Research Complex (JPARC) is a multipurpose facility for the physical experiments. The J-PARC facilities were constructed in the Tokai site of the Japan Atomic Energy Agency (JAEA). The accelerator complex consists of a linac (acceleration energy is 181 MeV so far and it will upgrade to 400 MeV by installing annular-ring coupled structure cavity (ACS) in 2013), a 3 GeV Rapid-Cycling Synchrotron (RCS), and a 50 GeV Main Ring synchrotron (MR) [1]. At the beginning, the beam commissioning of the linac started in November 2006 [2,3,4]. Construction of another accelerators and experimental facilities were continued afterwards, the RCS started to deliver proton beam to the MLF and MR in May 2008 [5]. The user operation for MLF started in December 2008 [6]. Concerning the MR, it has two extraction lines. One is the slow extraction line which deliver a proton beam to the hadron experimental hall, and the other is the fast extraction line which deliver the beam to the neutrino target for the T2K (Tokai-to-Kamioka) experiment. In January 2009, we achieved slow extraction for hadron beam line [7]. And neutrino beam line commissioning started in April 2009. The regular T2K experiment started in January 2010 to take the physics data [8]. After that, the beam power for users was increased and user operation was continued just before the Great East Japan earthquake in March 2011 [9,10]. However, the catastrophic earthquake caused many serious damages to all J-PARC facilities.

## INFLUENCE OF THE EARTHQUAKE

### *LINAC*

The linac is composed of an utility building of about 330 m length, a building of the Linac-3GeV RCS Beam Transport Line(L3BT) and the accelerator tunnel in the underground. The earthquake broke the ground around the linac and the water supply/drain pipes. Figure 1 shows the entrance to the linac building. At the inside of the building, some cranes were damaged. An air conditioning system and some water pipes were also broken, but the klystrons were able to work. There were ground water leakage in the tunnel and the floor is covered with water. The maximum depth of water reached 10cm. We immediately pumped up it by temporary power generators. It was found that there was no contamination by the radioactive nuclides in the water, but pH of water was 11. Therefore we neutralized it by a sulphuric acid before drain. After draining the water, we investigated the tunnel wall and floor. Then we found many cracks to be on the floor near the cavities of the separated drift tube linac(S-DTL). Due to the flood, a number of dry scroll pumps and pre-amplifiers that were directly put on the floor were damaged. Furthermore, some beam position monitors and Current transformers are broken and vacuum leakage occurred from those chambers. We checked the resonant frequency of the acceleration cavities such as RFQ (radio frequency quadrupoles), DTLs and S-DTLs, and there were no serious problems.

Figure 1: The entrance to the linac building, where a footpath subsided.

Measurement result of all magnet positions indicated that the maximum displacement of linac magnets is 25mm in horizontal plane and 40mm in vertical plane. The maximum displacement point is near the cracks on the floor. The margin of the adjuster of the base is not



ISBN 978-3-95450-118-2

# HIGH INTENSITY ISSUES AT FAIR

O. Kester#, GSI, Helmholtzzentrum für Schwerionenforschung, Darmstadt,
Institut für Angewandte Physik, Goethe-Universität Frankfurt, Germany

*Abstract*

The facility for antiproton and ion research – FAIR – will produce secondary beams of unprecedented intensities [1]. In order to produce such intense secondary beams and to provide intense beams for the CBM [2] and APPA [3] collaboration, primary heavy ion beams of highest intensities will be required. The main driver accelerator of FAIR will be the SIS100 synchrotron. The GSI heavy ion accelerator facility will be the injector of ion beams for SIS100. In order to reach the final intensities above $10^{11}$ ions per cycle, the injector chain has to be modified accordingly and the SIS100 has to be tailored to the needs. Therefore an intensity upgrade program of the GSI accelerator facility has been started, which comprises improvements of ion sources, of the injector linacs and of the heavy ion synchrotron SIS18. In addition, high energy beam transport and the SIS100 need to have a dedicated design, in order to handle beam losses. The issues of the upgrade program and of the SIS100 design will be addressed.

## INTRODUCTION

FAIR will provide worldwide unique accelerator and experimental facilities allowing for a large variety of unprecedented fore-front research in physics and applied science. The main thrust of FAIR research focuses on the structure and evolution of matter on both a microscopic and on a cosmic scale – deepening our fundamental understanding of questions of the complex structure of matter. To answer these fascinating and crucial questions, FAIR is being constructed in Darmstadt, Germany. This is a highly sophisticated accelerator complex which will provide high-energy, precisely-tailored beams of antiprotons as well as ions from stable and exotic isotopes. A key feature of the FAIR facility is a highly sophisticated accelerator system that will allow the parallel and versatile production of an unprecedented range of particle beams.

The corresponding four pillars of FAIR physics comprise experiments studying exotic particles that will explore fundamental processes which are thought to have happened in the early phases and still happen in the ongoing evolution of the universe. These processes produced the basic constituents of matter and overall structure we see now in the universe. In addition, a range of experiments will be possible in which different forms of matter are compressed. The experiments will simulate conditions in the early Universe, in ultra-dense stars and at the cores of giant planets like Jupiter. FAIR will explore, in a unique way, the properties of fundamental particles and how they combine into more complex forms of matter under a wide range of astrophysical conditions.

#o.kester@gsi.de

The experiments will be truly complementary to those carried out at other future facilities like FRIB [4]. Based on cost estimates and the firm commitments on funding of FAIR Member States, a Modularized Start Version (MSV) has been agreed upon. This version provides for outstanding and world-leading research programmes in all four scientific areas of FAIR. It provides also a unique scientific and technological environment for educating the next generations of students.

## ACCELERATOR OVERVIEW

The FAIR accelerator facility of the MSV is shown in figure 1. The central part of the FAIR accelerator facility is a synchrotron accelerator ring with maximum magnetic rigidity of 100 Tm – the SIS100. The synchrotron will have a circumference of about 1100. The magnets employed will be new, rapidly cycling superconducting magnets in order to minimize construction and operating costs. For the highest intensities, it is planned to operate the SIS100 at a repetition rate of 1 Hz and therefore with ramp rates of the dipoles up to 4 T/s. The goal is to achieve intense pulsed $U^{28+}$ beams with $4 \cdot 10^{11}$ ions per pulse at 1.5 GeV/u and intense ($2 \cdot 10^{13}$) pulsed proton beams at 29 GeV. For the high-intensity proton beams, as required for antiproton production, a dedicated proton linac delivering 35 mA and 70 MeV protons is needed.

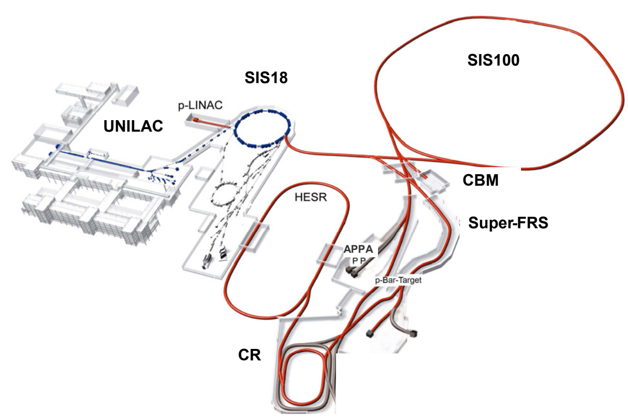


Figure 1: Overview of the FAIR accelerator facility.

The accelerator facility is complemented by a system of storage rings. The collector ring (CR) main task is stochastic cooling of radioactive ion or antiproton beams from the production targets. In addition, this ring offers the possibility for mass measurements of short-lived ions, by operating in isochronous mode. The high-energy storage ring (HESR) is optimized for antiprotons of energy up to 14 GeV. This ring will operate with an internal target and associated detector set-up (PANDA). This unique combination of accelerators and storage rings

ISBN 978-3-95450-118-2

# TECHNOLOGICAL CHALLENGES FOR HIGH-INTENSITY PROTON RINGS*

Y. Yamazaki
Facility for Rare Isotope Beams, Michigan State University, East Lansing, MI 48824, U.S.A.

*Abstract*

High-intensity, pulsed proton accelerators have been and will be requested by a wide variety of scientific fields and industrial and medical applications, for example, pulsed spallation neutron sources and neutrino sources. We will focus our discussion on the proton rings with a pulse length of a few micro second and a beam power of MW, but will make a brief comparison with CW machines. The pulsed accelerators may be used for boosting injectors to higher-energy accelerators, like a neutrino factories. At first, we will discuss on the space-charge force which limit the stored charges in a ring together with the negative-ion injection scheme. The pulsed spallation neutron sources are classified into two schemes. One is the combination of a full-energy linac and an accumulation ring (AR) exemplified by SNS and LANSCE. The other is that of a low-energy linac and a Rapid-Cycle Synchrotron (RCS) exemplified by J-PARC RCS and ISIS. In general, pros and cons of accelerator schemes are dependent upon the technological development results. Pros and cons of AR versus RCS will be discussed on the basis of recent technological developments and beam experiment data together with the future perspectives for MW-class machines.

## INTRODUCTION

In order to understand why high-intensity proton accelerators are requested by so many fields of science and industrial acceleration, the multi-purpose J-PARC project [1, 2] can be used as one example. Here, J-PARC stands for Japan Proton Accelerator Research Complex, which is Joint Project of High-Energy Accelerator Research Organization (KEK) and Japan Atomic Energy Agency (JAEA). The J-PARC comprises a 400-MeV linac (at present, 180 MeV and the upgrade to 400 MeV is ongoing), a 3-GeV Rapid-Cycling Synchrotron (RCS) and a 50-GeV (at present, 30 GeV) Main Ring (MR) Synchrotron. The 1-MW, 3-GeV beams are used for materials and life science, while the several 10 GeV beams from the MR are used for nuclear and particle physics experiment. In future, the linac will be further upgraded to 600 MeV for the basic Research and Development of the Accelerator-Driven nuclear waste transmutation System (ADS).

The reason why the high-intensities are required is that the number of the secondary particles per second to be utilized is proportional to the proton beam power, if the beam energy exceeds the threshold to produce those specific secondary particles. The high beam power is thus requested, while the radioactivity is also proportional to the beam loss power. This is the reason why the beam power front of the "pulsed" protons had been located approximately at 100~200 kW (CW proton beam power was already 1 MW as shown in the next section), before the Spallation Neutron Source (SNS) [3, 4] and J-PARC were in operation. In order to increase the beam power from 100~200 kW to 1 MW, the SNS and J-PARC had to reduce the beam loss rate by one order of magnitude.

It should be noted that the number of the secondary particles "per pulse" is crucial for some important experiments rather than the averaged one. As such, high intensity (or high power), which is a product of beam energy and beam current, is not sufficient for specifying accelerator performance. Time structure and emittances (brightness if the current divided) are other important factors [5]. For the pulsed beams with a pulse length of 1 μs, which is widely required for the neutron science experiments, the beams are accumulated in a ring and then fast extracted. Here, the beams are accelerated by the RCS rings for J-PARC and ISIS (this is not an acronym) [6], while they are extracted immediately after stored in Accumulator Ring (AR) for SNS and Los Alamos Neutron Science Center (LANSCE) [7]. The discussion of pros and cons of these two schemes (RCS and AR) is one of the main parts of this paper. Designed parameters are listed in Table 1 together with the achieved ones. It is also emphasized that availability, stability, reproducibility and cost belong to another category of the important machine "performance", in particular, the former three being vital for maximizing the scientific outputs.

We start the discussion from the CW proton ring accelerators for achieving the high intensity proton beams, and then proceed to pulsed accelerators. Here, space charge force plays an important role in giving rise to the beam loss, limiting the beam power. On the basis of these results, the pros and cons of the RCS scheme and AR scheme will be discussed. Since the highly rapid, high energy RCS requires high field gradient RF system, the discussion is then focused on that in the following section, and summarized by showing the future prospect.

* Work supported by the U.S. Department of Energy Office of Science under Cooperative Agreement DE-SC0000661
#Yamazaki@frib.msu.edu

ISBN 978-3-95450-118-2

# TECHNICAL CHALLENGES IN MULTI-MW PROTON LINACS*

V. Lebedev#, FNAL, Batavia, IL 60510, USA

*Abstract*

The intensity frontier research is an important part of modern elementary particle physics. It uses proton beams to create secondary beams consisting of, but not necessary limited to, neutrinos, muons, kaons and neutrons. Deferent experiments require different time structure of proton beams but all of them require the beam power of about or exceeding 1 MW. In addition, powerful proton linacs can find an application in accelerator driven nuclear reactors and transmutation of radioactive waste. Recent advances in the superconducting RF technology make a multi-MW power level economically acceptable. This paper discusses main physics and technical limitations determining ultimate parameters of such accelerators, their structure and performance.

## INTRODUCTION

There are four main applications where MW scale linacs are used or planned to be used. They are: (1) accelerators supporting the intensity frontier research in high energy physics (SPL [1], Project X [2,3], PSI cyclotron [25]), (2) spallation neutron souses (SNS [4], ESS [5], CSNS [6]), (3) accelerators for accelerator driven nuclear power reactors (MYRRA [7], Indian ADS [8], China ADS [9]), and (4) accelerators for nuclear physics (FRIB [10]). Of the aforementioned machines only the SNS is operational. Others are at the design or conception phases. However, all of them use or plan to use superconducting (SC) accelerator cavities. CEBAF commissioned in 1996 [11] is based on the 1 MW recirculating electron linac which is the first MW scale SC linac. Since that time its average accelerating gradient was increased from ~5 to ~7.5 MV/m. The SNS commissioned in 2007 [4] is the first MW scale proton (actually $H^-$) accelerator. It is based on the experience and technology developed for CEBAF, and presently it is still the only MW scale proton SC linac. Its average accelerating gradient is ~13 MV/m [4]. The recent progress in development of superconducting acceleration cavities is to a large degree based the ILC research [12]. That allowed increasing the accelerating gradient of pulsed machines to well above 30 MV/m. Introduction of SC technology made linacs with MW scale power economically viable and created opportunities which otherwise could not be achieved with normal conducting linac technology.

The proton linacs can be separated into 2 groups: pulsed linacs and continuous wave (CW) linacs. Linacs of the first group are usually used for injection into circular machines and use $H^-$ for the strip injection to the ring. However the ESS will operate in the long pulse regime and accelerate protons. Linacs of the second group usually use protons. However the Project X is based on a CW linac but still uses $H^-$; a small fraction of those is to be strip-injected into a circular machine for further acceleration. That makes $H^-$ the preferred choice.

A typical layout of a proton linac includes a warm frontend and a main SC accelerator. Normal conducting acceleration for CW machine would result in large power consumption and/or reduced accelerating gradient increasing machine cost. Due to more efficient acceleration the energy of transition from warm to SC part is usually higher for pulsed linacs. Below we will consider main physical and technical limitations for such linacs. For illustration we will be using the SNS, ESS and the Project X. The latter compared to other projects is the most advanced and complicated machine.

The Project-X, a multi-MW proton source, is under development at Fermilab. The Project X configuration is shown in Figure 1. It enables a world-leading program in neutrino physics and a broad suite of rare decay experiments. The facility is based on a 3-GeV 1-mA CW superconducting linac which beam is RF separated to support simultaneous operation of a few experiments [3]. A small fraction of the beam is sent to the 8 GeV pulsed linac operating at 10 Hz repetition rate with about 5% duty cycle. After acceleration to 8 GeV the beam is strip-injected to the Recycler and then sent to the Main Injector for further acceleration. A bunch-by-bunch chopping of CW beam is performed at low energy. It allows one to set a desired time structure for each of 3 GeV experiments and to remove unwanted bunches for the beam directed to a ring. Left untouched these bunches would come to the boundaries of RF buckets and would result in a beam loss.

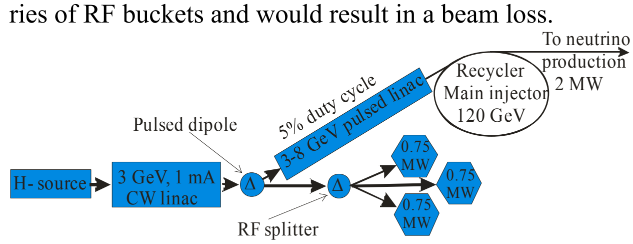


Figure 1: Project X configuration.

## WARM FRONTEND LIMITATIONS

A typical scheme of warm frontend is presented in Figure 2. It includes: ion source, low energy beam transport (LEBT), radio-frequency quadrupole accelerator (RFQ), medium energy beam transport (MEBT) and normal conducting part of the linac. The latter is usually not present in CW machines due to high power and low efficiency required for operation.

Presently a machine performance is usually not limited by ion source current or its phase density even in the case of $H^-$ ion source. The volume-cusp ion source developed by TRIUMF [13] is capable of generating a 15-mA DC beam with 0.12 mm mrad normalized rms emittance. The

*Work supported by Fermi Research Alliance, LLC, under Contract No. DE-AC02-07CH11359 with the United States Dep. of Energy
#val@fnal.gov

ISBN 978-3-95450-118-2

# INTENSE-BEAM ISSUES IN CSNS AND C-ADS ACCELERATORS

Shinian Fu, Jingyu Tang, Sheng Wang, Zhihui Li, Jun Peng, Fang Yan, Shouxian Fang
Institute of High Energy Physics, Beijing 100049, China

*Abstract*

In 2011 construction of two intense-beam accelerators were launched for China Spallation Neutron Source (CSNS) project and China Accelerator Driven System (C-ADS) project. CSNS uses a pulsed accelerator with an $H^-$ linac and a proton rapid cycling synchrotron, and C-ADS has a CW proton linac with superconducting cavities. In both cases, the beam power is high and beam loss control is a key issue in beam dynamics. Beam emittance growth and beam halo formation must be carefully studied in beam dynamics and well controlled in machine design. This paper will present a brief introduction to the physics design of the two intense-beam accelerators, especially on the issue of beam instability. In their linac design equapartitioning focusing scheme is adopted to avoid coupling instability. Some beam halo formation experimental results due to mismatching will be compared with simulations. Beam halo generation due to the quench of superconducting cavity and magnet is investigated in detail and compensation scheme is also proposed. Some code development are presented.

## INTRODUCTION

High intensity proton accelerators have majorly two important applications in China at present: one is for China Spallation Neutron Source and another is for China Accelerator Driven System[1]. The both projects have been formally launched in 2011. The two accelerators impose a great challenge to Chinese accelerator community in terms of not only key technology, but also beam dynamics.

The CSNS is designed to accelerate proton beam pulses to 1.6 GeV kinetic energy at 25 Hz repetition rate, striking a solid metal target to produce spallation neutrons The accelerator provides a beam power of 100 kW on the target in the first phase and then 500 kW in the second phase by increasing the average beam intensity 5 times while raising the linac output energy. A schematic layout of CSNS phase-1 complex is shown in Figure 1. In the phase one, an $H^-$ ion source produces a peak current of 25 mA $H^-$ beam. RFQ linac bunches and accelerates it to 3 MeV. DTL linac raises the beam energy to 80 MeV. After $H^-$ beam is converted to proton beam via a stripping foil, the RCS accumulates and accelerates the proton beam to 1.6 GeV before extracting it to the target. Phase-I has a budget of $260 M for construction of the accelerator, the spallation neutron target and 3 neutron spectrometers. Its site is at Dongguan, south part of China. The local government will support free land, additional budget of $57M, infrastructure, dedicated high-way and power transformer station. The project is expected to be accepted for user operations in the first half of 2018.

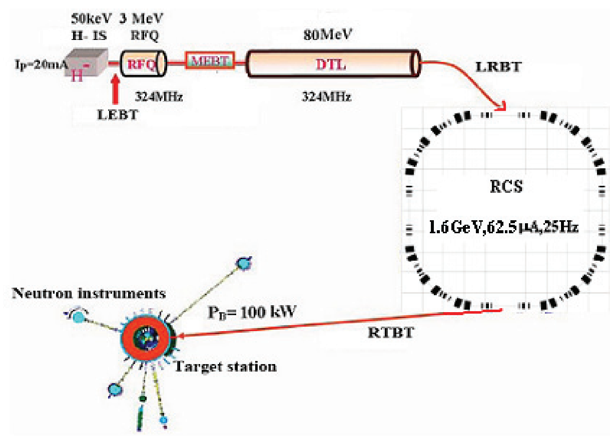


Figure 1:Schematic layout of CSNS facility.

In 2011 a Chinese roadmap for long-term development of ADS was proposed by Chinese Academy of Sciences. It outlines a three-step plan with a small test setup, an experimental facility and a demonstration facility in a period from 2011 to 2032，as plotted in Figure 2.

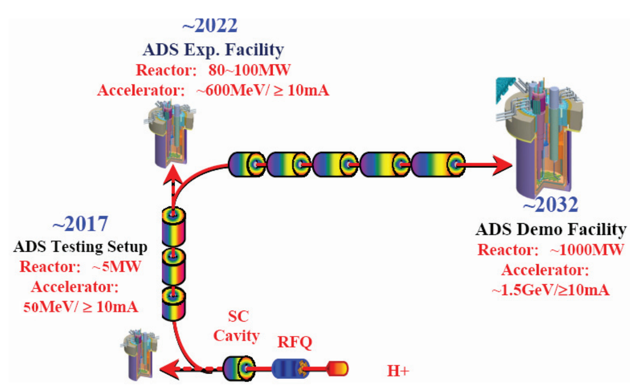


Figure 2: Roadmap of ADS development in China.

The C-ADS proton linac will operate in CW mode with a high average current of 10mA. Superconducting cavity is the best option, except for the front-end. In our preliminary design the 1.5 GeV linac consists of two injectors, two spoke cavity sections and two elliptical cavity sections. In operation, only one injector runs and another is hot standby for a high reliability which is a key requirement for the target and reactor.

ISBN 978-3-95450-118-2

# CHALLENGES IN BENCHMARKING OF SIMULATION CODES AGAINST REAL HIGH INTENSITY ACCELERATORS

I. Hofmann, GSI-HI-Jena, 64291 Darmstadt, Germany


*Abstract*

Benchmarking of simulation codes for linear or circular accelerators involves several levels of complexity, which will be revisited and discussed in this talk. We first give some examples of how simulation codes have been validated towards the goal of gaining confidence about the underlying physics mechanisms. Besides such physics validation a bigger issue has been to feed codes with an accurate enough model of the real machine. We address these questions by discussing several examples of benchmarking efforts, their achievements as well as the limits and difficulties that have been encountered.


## INTRODUCTION

Benchmarking of simulation codes for high-intensity linear accelerators or synchrotrons is necessary in order to raise confidence in predictions on beam loss and beam quality for new projects like the FAIR-project [1], C-ADS and C-SNS [2], ESS [3], IFMIF [4] and others; or to explain observations and possibly improve the performance of running high intensity machines in different laboratories (like SNS [5], J-PARC [6] or the CERN injectors into to LHC [7]). The main efforts of code validation in this field have started in the late 1990's with the coming of the SNS and at the same time the steadily increasing performance of computers.

A few remarks on the historical evolution in this field may be appropriate. The main step of development needed for high intensity accelerators simulation has been the particle-in-cell (PIC) technique. Actually PIC simulation was already developed in the 1960's primarily for fluid dynamics, plasma physics and magnetohydrodynamics. Already in the 1970's PIC codes were commonly used to model plasmas in all fusion laboratories around the world. Major challenges in this new approach have been short wavelength fluctuations in density and electromagnetic fields and the need to overcome limitations from unphysical fluctuations. Progress has been tremendous, and as of today the largest plasma or fluid PIC simulations are done with up to $10^{10}$ particles using as many as $10^5$ processors.

In accelerator physics PIC codes came into practice with about 15 to 20 years of delay - mostly because there was no need. In the 1970's primarily single particle dynamics was used. Coulomb interaction was gradually introduced as binary interaction between particles, and limited to a few thousand simulation particles. In the 1980's the first PIC simulations were started in a number accelerator labs, partly driven by the idea of using accelerators as drivers for inertial fusion. A full transition to PIC codes occurred nearly everywhere in the late 1990's. Although intense beams have something in common with (un-neutralized) plasmas, the challenges in PIC simulation for accelerator beams have been very different from those of plasmas or fluids: internal collective effects are weak, and the main challenge is the interacting with the surrounding structure and the proper modelling of it.

## THE BENCHMARKING "PROBLEM"

With the enormously grown capabilities in computer simulation expectations have grown to use these codes for reliable predictions and even for improvements of accelerators. It is often overlooked that codes can only be a simplified model of reality, but we have practically unlimited information about this model. The problem of the experiment, on the other hand, is a different one. The experiment is a perfect model, but information on the physics in it is always very limited due to diagnostics limitation. This makes it so difficult to bring the two approaches to some level of mutual agreement. The inherent dilemma in code benchmarking crystallizes in the following observation [8]: "No one believes the simulation results, except the one who performed the calculations, and everyone believes the experimental results, except the one who performed the experiment." Clearly, in most eyes the experimentalist has a strategic advantage as the real world stands behind him.

In order to overcome this difficulty it has been accepted that benchmarking of simulation should be seen on basically two levels not to be mixed up: code verification and code validation.

### *Code Verification*

The task is to verify that a computer code represents the intended conceptual model: multi-particles with smoothed space charge forces, idealized magnets and cavities etc.. At this level codes can be compared with analytical models (important also for modelling of experiments) to verify the accuracy of a code with regard to an idealized model accelerator. The basic questions are "Is my code doing what it is written for? Is the algorithm programmed correctly? Is the grid resolution of my Poisson solver consistent with some criteria?"

### *Code Validation*

The goal is to validate a code as sufficient to describe certain experiments - the emphasis is on "certain". Therefore it should not be claimed that the code is validated - it is only a particular calculation or application, which has been validated. Questions are: "Is my code good enough to make predictions for the real machine? Do I have the same



ISBN 978-3-95450-118-2

# BEAM LOSS MECHANISMS IN HIGH INTENSITY LINACS

M.A. Plum, Oak Ridge National Laboratory, Oak Ridge, TN, USA

*Abstract*

Beam loss is a critical issue in high intensity linacs, and much work is done during both the design and operation phases to keep the loss down to manageable levels. Linacs for $H^-$ ion beams have many more loss mechanisms compared to $H^+$ (proton) linacs. Interesting $H^-$ beam loss mechanisms include residual gas stripping, $H^+$ capture and acceleration, field stripping, and intra-beam stripping (IBSt). Beam halo formation, and ion source or RF turn on/off transients, are examples of beam loss mechanisms that are common for both $H^+$ and $H^-$ accelerators. The IBSt mechanism has recently been characterized at the Oak Ridge Spallation Neutron Source, and we have found that it accounts for most of the loss in the superconducting linac. In this paper we will detail the IBSt measurements, and also discuss the other beam loss mechanisms that are important for high intensity linacs.

## INTRODUCTION

Beam loss is a critical issue in high intensity linacs, and much work is done during both the design and operation phases to keep the loss down to manageable levels. A generally accepted rule of thumb is to keep the loss to less than 1 W/m to allow for hands-on maintenance. For example, the SNS linac output beam power is ~1 MW today, and we plan to increase the power to its design value of 1.4 MW over the next few years, and then later to ~3 MW. The fractional loss per meter should then be less than $3x10^{-7}$.

In general, beam loss in $H^-$ linacs is more difficult to manage than $H^+$ linacs due to the greater number of loss mechanisms, including residual gas stripping, $H^+$ capture and acceleration, field stripping, and intra-beam stripping (IBSt). Mechanisms such as beam halo formation, and ion source or RF turn on/off transients, can cause loss in both $H^+$ and $H^-$ linacs.

At SNS, we have recently discovered [1] that IBSt is the cause of most of the beam loss in the superconducting linac. In this paper we will first detail the IBSt measurements at SNS, then discuss other loss mechanisms important to SNS and other high-intensity linacs.

## INTRA-BEAM STRIPPING

In the SNS linac [2], the $H^-$ ion beam is first accelerated to 2.5 MeV by an RFQ, then to 87 MeV by a Drift Tube Linac (DTL), to 186 MeV by a Coupled Cavity Linac (CCL), and finally to 1000 MeV by a Superconducting Cavity Linac (SCL). The SCL has a beam aperture of 76 mm diameter, which is quite large compared to the warm linac (DTL + CCL) aperture of 25 and 32 mm diameter respectively. Due to this large aperture, particle tracking simulation codes predicted zero beam loss in the SCL. Additionally, the vacuum levels in the SCL are very low due to the cryogenic pumping. Therefore, prior to commissioning the beam loss was anticipated to be negligible.

However, as we started to increase the beam power it became clear that the beam loss in the SCL was not negligible. The measured fractional loss per meter was ~$3x10^{-7}$, which, although it meets the value required for hands-on maintenance, was nevertheless a puzzle. The beam loss was eventually lowered by a factor of about two by empirically lowering the SCL quadrupole gradients by up to 40%. This is counterintuitive, since lowering the gradients increases the beam size, which makes it more likely for beam halo to strike the beam pipe walls.

In 2010 a possible explanation of intra-beam stripping (IBSt) was proposed by V. Lebedev [3]. In this beam loss mechanism, interactions of the $H^-$ particles within a beam bunch cause electrons to be stripped off, converting a portion of the particles to $H^0$, which are then lost due to lack of focusing and acceleration. The reaction rate is proportional to the particle density squared, so this explains why the loss is reduced as the beam size is increased. Further measurements showed that the fractional loss is also reduced by lowering the ion source current, in a parametric manner consistent with IBSt. Yet these data could not unambiguously prove that IBSt was the dominant loss mechanism. In 2011 an experiment was conducted that showed that IBSt is in fact the dominant mechanism.

### *The IBSt Experiment*

A thin 5 μg/cm$^2$ carbon stripper foil was inserted just downstream of the RFQ to create a proton beam that has nearly identical beam dynamics properties to the $H^-$ beam. This foil gives a stripping efficiency of ~99.98%, and a kinetic energy loss of just 0.6 keV (to be compared to the beam energy spread from the RFQ of ~12 keV). Beam scattering increases the emittance by ~12%, and the beam duty factor limit to avoid damaging the foil is about 45 μs per second, which is sufficient to accurately characterize the beam loss.

To accelerate the proton beam, all the RF cavity phases were shifted 180 deg. To focus the beam it is not practical to reverse the polarities of all the quadrupole magnets, so instead the magnets in the beam transport line between the RFQ and DTL where adjusted to swap the Twiss parameters of the horizontal and vertical planes at the entrance of the DTL. Therefore, starting from the beginning of the DTL, the beam dynamics of the proton beam are nearly identical to those of the $H^-$ beam.

Consistency checks were performed using the four-wire-scanner emittance station at the exit of the SCL. As expected, the Twiss parameters of the horizontal and



ISBN 978-3-95450-118-2

# BUNCH-BY-BUNCH BEAM LOSS DIAGNOSTICS WITH DIAMOND DETECTORS AT THE LHC

M. Hempel*, CERN ,Switzerland and DESY ,Germany and
Brandenburg University of Technology, Germany
T. Baer, CERN, Switzerland and University Hamburg, Germany
S. Bart Pedersen, B. Dehning, E. Effinger, A. Lechner, R. Schmidt, CERN, Switzerland
E. Griesmayer, CERN, Switzerland and CIVIDEC Instrumentation, Austria
W. Lohmann, DESY and Brandenburg University of Technology, Germany

*Abstract*

A main challenge in the operation with high intensity beams is managing beam losses that imply the risk of quenching superconducting magnets or even damage equipment. There are various sources of beam losses, such as losses related to injection, to beam instabilities and to UFOs (Unidentified Falling Objects). Mostly surprising in the first years of LHC operation was the observation of UFOs. They are believed to be dust particles with a typical size of $1-100\,\mu$m, which lead to beam losses with a duration of about ten revolutions when they fall into the beam. 3600 BLMs (Beam Loss Monitors) are installed around the LHC ring, allowing to determine the accurate location of UFOs. The time resolution of the BLMs is $40\,\mu$s (half a turn revolution). A measurement of the beam losses with a time resolution better than the bunch spacing of $50\,$ns is crucial to understand the loss mechanisms. Diamond sensors are able to provide such diagnostics and perform particle counting with ns time resolution.

In this paper, we present measurements of various types of beam losses with diamond detectors. We also compare measurements of UFO induced beam losses around the LHC ring with results from MadX simulations.

## INTRODUCTION

The Large Hadron Collider is operated in 2012 with a stored beam energy of $130\,$MJ. An energy deposition of only a few $\mathrm{mJ/cm^3}$ is sufficient to quench a superconductive magnet. Also damage of material is possible in case of high beam losses. Therefore, it is important to detect and measure all beam losses and dump the beam in case of adverse beam conditions [1]. The focus of this paper is on beam loss measurements during injection, beam dump, beam instabilities and scattering processes with dust particles, so called UFOs. The beam losses are measured with ionization chambers and diamond detectors. The time resolution of ionization chambers is $40\,\mu$s (the LHC revolution period is $89\,\mu$s). If the beam losses measured by an ionization chamber exceeds a predefined threshold, the beams are dumped. A bunch-by-bunch beam loss information with an operational bunch spacing of $50\,$ns is not possible with ionization chambers. Diamond detectors have a time resolution of $1\,$ns and are therefore capable to distinguish the beam losses of individual bunches [2]. Two diamond detectors are installed in the beam cleaning region (IR7, one of eight regions of the LHC). In this region collimators jaws are positioned to 4-5 sigma from the beam center, the cleaning region is the global aperture limitation of LHC. All major beam losses are detectable there [3]. The diamond detectors are connected to an oscilloscope that allows triggering on certain beam loss events and post mortem analysis. In the following, beam loss measurements with diamond detectors in IR7 are presented.

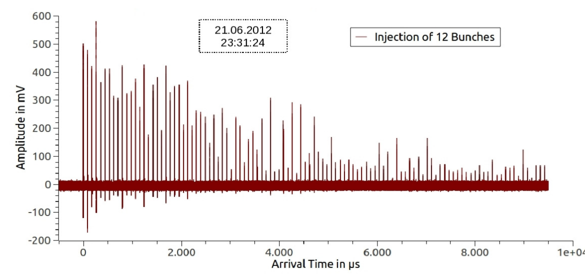


Figure 1a: Measurement of beam losses during injection of 12 bunches for beam 1 into the LHC. Signal amplification: $40\,$dB. The injection process leads to beam losses during $10\,$ms ($\sim$110 turns) and is decreasing after some turns.

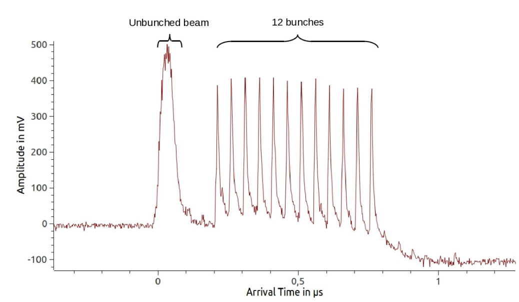


Figure 1b: Zoom into beam losses directly after injection. The measured beam losses are due to unbunched beam and 12 injected bunches with a spacing of $50\,$ns.

* contact: maria.hempel@cern.ch

ISBN 978-3-95450-118-2

# A METHOD TO MEASURE THE INCOHERENT SYNCHROTRON FREQUENCIES IN BUNCHES

Oleksandr Chorniy, Hansjörg Reeg
GSI, Planckstr. 1, 64291 Darmstadt, Germany

*Abstract*

The method of measuring the incoherent synchrotron frequencies in a stationary bunch is presented. It can be shown that by measuring the local current at a fixed coordinate in RF bucket the corresponding incoherent synchrotron frequency can be obtained. Test calculations were done using simulation data where longitudinal space charge effects were included. The incoherent frequencies obtained with the method are in a good agreement with theory. In real experiment, the incoherent frequencies were determined from bunch profiles recorded in the SIS18 with low intensity beam at injection energy. Bunch profiles were measured with a new Fast Current Transformer which has a relatively broad frequency range. The profiles were recorded using 8 bit resolution oscilloscope. The frequency spectra of the local current fluctuations at different longitudinal positions were obtained numerically. The strongest lines in these spectra were at positions of theoretically expected incoherent frequencies. In this paper the method is described in details, the comparison of incoherent frequencies obtained from the simulation and measurement data with theoretical predictions is shown.

## INTRODUCTION

The longitudinal motion of particles in bunched beam can be described using frequency domain. The main characteristics of bunched beam in frequency domain are:

- the coherent frequencies describe the oscillations of the longitudinal bunch shape
- the incoherent frequency $\omega_s(\hat{\phi})$ as function of the particle oscillation amplitude; it is a characteristic of a single particle in the longitudinal phase space
- the particle distribution over the incoherent frequencies $\psi(\omega_s)$

Schottky noise measurements is the non-destructive technique for the measurement of the frequency characteristics in beam [1]. The main application of Schottky diagnostics is the measurement of the particle momentum distribution in coasting beams. In bunched beams, the longitudinal density fluctuations from stationary bunch contains an information on the incoherent and coherent frequencies. Using standard Schottky diagnostics, the coherent frequencies can be clearly observed in the spectrum of the bunched beam [2]. But both particle distribution and the incoherent frequencies is difficult to extract from the bunched beam Schottky noise spectrum.

In a simple way the incoherent frequencies inside RF bucket can be measured with a longitudinally miss-matched bunch [3]. If initially matched bunch is shifted on the distance $\phi_x$ with respect to the RF bucket center then this bunch starts to perform the dipole oscillations. If the longitudinal bunch length is small then the bunch dipole frequency is equal to the incoherent frequency $\omega_{s_x}$ of a single particle with oscillation amplitude of $\hat{\phi}_x = \phi_x$. By measuring the bunch dipole frequency with different $\phi$ the incoherent frequency $\omega_s$ as function of single particle oscillation amplitude $\hat{\phi}$ can be found.

For long bunches the method described above will not work properly since the range of particle oscillation amplitudes inside the bunch is comparable with an initial dipole offset. In the case of long bunches a Beam Transfer Function (BTF) method can be employed [4]. The BTF method is based on the measurements of longitudinal bunch response due to tiny forced perturbations of RF bucket. Analytically, the bunch response is defined throw the dispersion relation. This dispersion relation includes both the particle distribution over the incoherent frequencies and the incoherent frequency as function of the single particle oscillation amplitude. As a non-destructive method, there is "peak detection" technique where the noise produced by the peak value of the longitudinal bunch profile is measured [5]. The frequency spectrum of the peak detector signal contains information about particle distribution and the incoherent frequencies. In both methods one quantity can be extracted if the other is known.

For low intensity beams, if the RF waveform is well defined the incoherent frequencies can be easily calculated. For high intensity beams, longitudinal space charge will modify the effective RF voltage seen by the beam and the incoherent frequencies can differ from the low intensity case. This so-called potential well distortion can be calculated only if the effect of longitudinal space charge is well defined.

Using and extending the theoretical concept given in [5], we propose a method which allows to obtain the incoherent frequencies without knowledge of space charge parameters and without knowledge about the distribution function. It is based on Fourier analysis applied to recorded data.

## NOISE SPECTRUM OF THE LOCAL CURRENT

In the longitudinal phase space confined by stationary RF bucket the particles moves along a certain orbits as it is shown in Fig. 1. The longitudinal phase space is repre-



ISBN 978-3-95450-118-2

# INTENSE HEAVY-ION BUNCHES IN DUAL-HARMONIC RF SYSTEMS*

M. Mehler, O. Kester, Goethe Universität Frankfurt, Frankfurt am Main, Germany
O.Boine-Frankenheim, Technische Universität Darmstadt, Darmstadt, Germany
O. Chorniy, GSI Helmholtzzentrum für Schwerionenforschung GmbH, Darmstadt, Germany

*Abstract*

For the synchrotron's SIS-18 and SIS-100 (FAIR) a dual-harmonic RF system with the harmonic numbers $h_1$ = 2, $h_2$ = 4 and $h_1$ = 10, $h_2$ = 20 respectively is planned. Such systems flatten the bunch form and increase the bunching factor $B_f$ therefore reducing the transverse space charge force. For high currents cavity beam loading and potential-well distortion will deform the flattened bunch shape and lead to phase shifts. Optimized settings for the difference between the two RF phases and for the synchronous phase of the main RF harmonic is an option to reduce these effects. In this contribution we will analyse the effect of optimized RF voltage amplitude settings to the matched bunch distribution in a dual-harmonic system for SIS-100 parameters and its influence to the optimized phase difference.

## INTRODUCTION

Different waveforms and the stability of coherent synchrotron oscillations of Gaussian heavy ion distributions under space charge (SC) are described in [1] and [2]. There is shown that it reduces the RF voltage amplitude below transition energy and that it leads to loss of Landau damping. It is shown that beam loading (BL) caused by the real part of the impedance of the RF cavities can deform bunch shapes by energy loss to wake fields. This slows down the ions so that they center oneself at the back of the distribution.

The resistive part of any impedance in the synchrotron is responsible for the losses leading to phase shift and bunch form deformation by potential-well distortion (PWD) [3] both in single and dual-harmonic RF systems. This adds up to the BL of the RF cavities in the synchrotron SIS-100. The phase shift and beam distribution deformation can be described by the Haissinski equation [3] for Gaussian longitudinal ion distributions. The phase shift of a single harmonic RF system can be corrected by giving the RF voltage a synchronous phase $\Phi_{S1}$ as during acceleration. The beam distribution deformation cannot be corrected; it yet increases because of the accelerating bucket form.

This proceeding will concentrate on the description of the correction of phase shift and bunch form deformation caused by PWD in dual-harmonic RF systems. In [4] has been shown that for quality factors above about Q = 0.4 it is necessary to find an alternative method like an additional small RF voltage [3] or dual-harmonic RF systems with $\alpha \neq 0.5$. Here the behaviour of the $\alpha$-factor and the connected correcting phases over the quality factor Q below transition energy has been investigated also in comparison with the results for a constant $\alpha$-factor.

* Work supported by HGS-HIRe for FAIR

## PHASE SHIFT- AND BUNCH FORM DEFORMATION CORRECTION

For correcting phase shift and bunch form deformation a dual-harmonic RF system has to be applied as described by equation 1 where $\alpha = \frac{V2}{V1}$ and $\frac{h_2}{h_1} = 2$. $V_1$ and $V_2$ are the RF voltage amplitudes and $h_1$ and $h_2$ are their harmonic numbers. It reduces the SC effect by ion bunch flattening and increasing of $B_f$ and makes it possible to countervail for the ion beam distribution deformation by adjusting the right phase difference between main and second RF harmonic $\Delta\Phi$ [4] as long as the quality factor Q of the impedance is low (broadband impedance). The phase shift correction is done as in a single harmonic RF system by adjusting the synchronous phase $\Phi_{S1}$ to the main harmonic.

$$\begin{aligned} V_{RF} =& V_1(sin\Phi - sin\Phi_{S1} - \alpha(sin(\Phi_{S2}+ \\ & \frac{h_2}{h_1}(\Phi - \Phi_{S1}) + \Delta\Phi) - sin\Phi_{S2})) \\ \Delta\Phi =& \Phi_2 - \Phi_{S2} - \frac{h_2}{h_1}(\Phi - \Phi_S) \end{aligned} \tag{1}$$

In Figure 1 the red dashed curve shows the dual-harmonic beam distribution without PWD and SC impedance $X_{SC}$ (defined in [5]) with the $1\sigma$-bunch length of the main harmonic of 0.7 rad at injection energy (200 MeV/u) with $\alpha = 0.5$. The blue curve gives an example for an $U^{28+}$ beam distribution deformation with the quality factor of the impedance Q = 0.1. Only PWD was observed with $N_b = 7.5 \times 10^9$ ions. Only PWD means that it was supposed that $X_{SC}$ = 0. The beam interacts with the shunt impedance $R_{Sh}$ of the longitudinal part of the resistive impedance (equation 2; $\omega_{RF}$: resonance frequency of the impedance). The black line shows the result of the analytical solution for the slope at the potential free area of the dual-harmonic RF system using equation 3. It can be derived from the reduced Haissinski equation for the potential free region in a barrier bucket RF system because the potential free region in a dual-harmonic system is similar to this.

$$\begin{aligned} Z_{Sh||} &= \frac{R_{Sh}}{1 + iQ(\frac{\omega}{\omega_{RF}} - \frac{\omega_{RF}}{\omega})} \\ Z_{Sum||} &= Z_{Sh||} - iX_{SC} \end{aligned} \tag{2}$$

ISBN 978-3-95450-118-2

# NUMERICAL CALCULATION OF BEAM COUPLING IMPEDANCES FOR THE SIS-100 SYNCHROTRON FOR FAIR*

U. Niedermayer# and O. Boine-Frankenheim
Technische Universität Darmstadt, Institut für Theorie Elektromagnetischer Felder (TEMF), Schlossgartenstraße 8, 64289 Darmstadt, Germany

*Abstract*

The transverse impedance of kicker magnets is considered to be one of the main beam instability sources in the projected SIS-100 at FAIR and also in the SPS at CERN. The longitudinal impedance can contribute to the heat load, which is especially a concern in the cold sections of SIS-100. In the high frequency range, time domain codes are commercially available to calculate the impedance but they become inapplicable at medium and low frequencies. We present the ongoing work of developing a Finite Integration (FIT) solver in frequency domain which is based on the Parallel and Extensible Toolkit for Scientific computing (PETSc) framework in C++. The code is applied to an inductive insert used to compensate the longitudinal space charge impedance in low energy machines. Another application focuses on the transverse impedance contribution of a ferrite kicker with inductively coupled pulse forming network (PFN) and frequency dependent complex material permeability. In future we plan to confirm our simulations with dedicated wire or coil bench measurements.

## INTRODUCTION

For the SIS100 synchrotron which will be built in the framework of the FAIR project, especially the coasting beam and the high intensity proton bunch are susceptible to impedance driven coherent transverse instabilities. Since SIS100 will contain ferrite kickers in cryogenic ($<$ 20 K) sections, the beam induced heat load (as also recently reported on LHC-kickers) is an important issue. In the relevant frequency range of several kHz up to the beam pipe cutoff, impedance sources are mainly given by the thin stainless steel beam pipe [1] and ferrite components. Broadband cavities dominate the longitudinal impedance [2]. Slightly below the cutoff frequency, cross-section changes such as collimators might have an impact. Additionally to the necessary ferrite kickers and their supply networks, also an inductive ferrite insertion to compensate the negative inductive longitudinal space charge impedance has been proposed. We will focus on this insert which serves as a test case for the code discussed in this paper. Nonetheless, the main application of the code will be the transverse impedance of SIS100 kicker modules.

Usually coupling impedances are defined as the Fourier transform of the wake function which can be calculated by time domain (TD) codes such as CST Particle Studio [3]. At low frequencies, which become more important for large hadron synchrotrons, this technique is inapplicable due to the necessary large wake length (frequency resolution limitation by Küpfmüller's uncertainty principle [4]).

The following will give a definition of the coupling impedances directly in frequency domain (FD). Underlined symbols emphasize complex variables. This also serves to distinguish between TD and FD. The beam with total charge $q$ in a synchrotron is modeled as a disc with radius $a$ of uniform surface charge density $\sigma$ traveling with velocity $v$. The transverse displacement $d_x$ of the beam (i.e. a coherent dipole oscillation) is approximated to first order by

$$\sigma(\varrho,\varphi) \approx \frac{q}{\pi a^2}\left[\Theta(a-\varrho)+\delta(a-\varrho)d_x\cos\varphi\right] \quad (1)$$

where $\Theta$ is the unit step and $\delta$ is its generalized derivative. The beam current density in frequency domain is

$$\underline{J}_{s,z}(\varrho,\varphi,z;\omega) = \int_{-\infty}^{\infty} v\sigma(\varrho,\varphi)\delta(z-vt)e^{-i\omega t}\mathrm{d}t \quad (2)$$

$$= \sigma(\varrho,\varphi)e^{-i\omega z/v} =: \underline{J}_{\parallel} + \underline{J}_{\perp} \quad (3)$$

where $\underline{J}_{\parallel}$ and $\underline{J}_{\perp}$ are the monopole and dipole components, as in Eq. (1), respectively. The coherent force due to beam induced electromagnetic fields acting back on the beam is described by the coupling impedance [5]

$$\underline{Z}_{\parallel}(\omega) = -\frac{1}{q^2}\int_{\mathrm{beam}} \underline{\vec{E}}\cdot\underline{\vec{J}}_{\parallel}^{*}\mathrm{d}V \quad (4)$$

$$\underline{Z}_{\perp,x}(\omega) = -\frac{v}{(qd_x)^2\omega}\int_{\mathrm{beam}} \underline{\vec{E}}\cdot\underline{\vec{J}}_{\perp}^{*}\mathrm{d}V. \quad (5)$$

The electric field $\underline{\vec{E}}$ is to be calculated from Maxwell's equations. Instead of the cosine distribution for dipolar excitation in Eq. (1) one can also use a twin wire approximation, as described in [6].

## INDUCTIVE INSERT

The longitudinal space charge impedance [7]

$$\underline{Z}_{\parallel}^{SC}(\omega,\beta) = -i\omega\frac{\mu_0 g l}{4\pi\beta^2\gamma^2} \quad (6)$$

constitutes a major fraction of the imaginary part of the longitudinal impedance in SIS100. This leads to a RF-potential-well distortion and to a net decrease of the RF-voltage (decrease of bucket height). We will discuss a tubu-

* Work supported by GSI
#u.niedermayer@gsi.de

ISBN 978-3-95450-118-2

# PLANNING FOR EXPERIMENTAL DEMONSTRATION OF TRANSVERSE EMITTANCE TRANSFER AT THE GSI UNILAC THROUGH EIGEN-EMITTANCE SHAPING

C. Xiao, O. Kester, Institute of Applied Physics, Goethe-University of Frankfurt a.M, Germany
L. Groening, GSI Helmholtzzentrum für Schwerionenforschung, Darmstadt, Germany

*Abstract*

The minimum transverse emittances achieved in a beam line are determined by the two transverse eigen-emittances of the beam. Without coupling, they are equal to the transverse rms-emittances. Eigen-emittances are constants of motion for all symplectic beam line elements. To allow for rms-emittance transfer, the eigen-emittances are changed by a non-symplectic action to the beam, preferably preserving the four-dimensional rms-emittance.

Unlike emittance swapping, the presented concept will allow the transformation of a beam of equal rms-emittances into a beam of different rms-emittances while preserving the four-dimensional rms-emittance. This contribution will introduce the concept for eigen-emittance shaping and rms-emittance transfer at an ion beam line. The actual work status towards the experimental demonstration of the concept at the GSI UNILAC is presented.

## INTRODUCTION

For injection of beams into circular machines with different horizontal and vertical emittance acceptances, the injection efficiency can be increased if these beams are flat. However, beams provided from the linear accelerator are generally round, and the horizontal and vertical emittances are quite equal.

Round-to-flat transformation requires a change of the beam eigen-emittances by a non-symplectic transformation [1]. Such a transformation can be performed by placing a charge state stripper foil inside a longitudinal field region as proposed in [2]. Inside such a solenoidal stripper, the transverse inter-plane correlations are created non-symplectically. Afterwards they are removed symplectically with a coupling correction section. The new set-up providing round-to-flat transformation is shown in Fig. 1. Such a emittance transfer section is proposed to be integrated into the existing beam line between the UNILAC [3] and the SIS synchrotron.

## EMITTANCE

The four-dimensional symmetric beam matrix $C$ contains ten unique elements, four of which describe the coupling. The rms-emittances, $\varepsilon_x$ and $\varepsilon_y$, are defined as the square roots of the determinants of the on-diagonal submatrices. If one or more of the elements of the off-diagonal

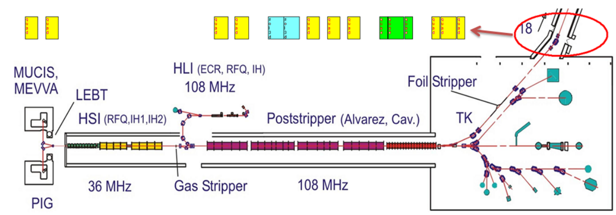


Figure 1: Conceptual layout of the transverse emittance transfer section in the GSI UNILAC.

submatrix is non-zero, the beam is $x$-$y$ coupled. Diagonalization of the beam matrix yields the beam eigen-emittances, $\varepsilon_1$ and $\varepsilon_2$, and the values are calculated as:

$$\varepsilon_1 = \frac{1}{2}\sqrt{-tr(CJ)^2 - \sqrt{tr^2(CJ)^2 - 16|C|}} \qquad (1)$$

$$\varepsilon_2 = \frac{1}{2}\sqrt{-tr(CJ)^2 + \sqrt{tr^2(CJ)^2 - 16|C|}} \qquad (2)$$

The four-dimensional matrix $J$ is the skew-symmetric matrix with non-zero entries on the block diagonal of form. Eigen-emittances are invariant under symplectic transformations, and the eigen-emittances are equal to rms-emittances when the inter-plane correlations are zero.

## BEAM TO BE STRIPPED

Multi-particle beam dynamics simulations have been done using the TRACK code [4]. The uncoupled particle distribution at the entrance of this beam line is concluded from beam experiments and plotted in Fig. 2.

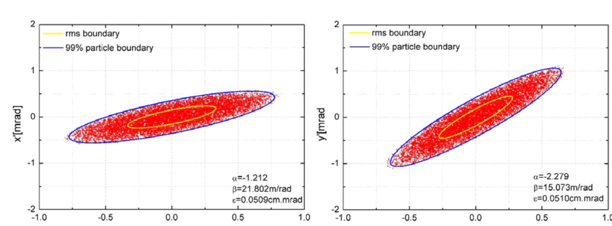


Figure 2: The particle distributions at the entrance of beam line.

The subroutines of the stripper in the TRACK code are based on the SRIM code [5]. The three-dimensional field of



ISBN 978-3-95450-118-2

# HIGH INTENSITY PROTON FFAG RING WITH SERPENTINE ACCELERATION FOR ADS

E. Yamakawa*
Graduate school of Engineering, Kyoto University, Japan
J.-B. Lagrange, T. Uesugi, Y. Kuriyama, Y. Ishi, Y. Mori
Kyoto University Research Reactor Institute, Kumatori, Japan

*Abstract*

In order to produce high intensity proton beam for ADS, a new type of fixed rf acceleration scheme, so-called serpentine acceleration, is examined in scaling FFAG. Longitudinal hamiltonian for scaling FFAG is first derived analytically. Then the features of serpentine acceleration in longitudinal phase space are studied. Ring design for ADS is finally shown.

## INTRODUCTION

High beam power accelerator to produce intense secondary particle beams are desired for Accelerator Driven System (ADS) [1]. Linear accelerators have been considered as a proper candidate so far. An alternative candidate is Fixed-field alternating gradient (FFAG) accelerator [2]. There are two types of FFAG; non-scaling type and scaling type. Scaling FFAG ring is composed of non-linear magnetic fields so that the betatron tune is constant for every particle momentum, contrary to the non-scaling FFAG accelerator.

In order to obtain large current beam, in FFAG accelerators, the acceleration scheme with fixed rf frequency has been proposed. In scaling FFAG, the stationary bucket acceleration [3, 4] has been considered. In this scheme, however, the total acceleration energy gain is limited by the bucket height. In order to make a large bucket height, the acceleration in the relativistic energy region is preferable. On the other hand, in non-scaling FFAG, to minimize orbit shifts during acceleration, the parabolic variation in orbit length with energy is created by the appropriate selection of parameters. At the bottom of the parabola, the momentum compaction approaches zero. Furthermore, for relativistic particles with the parabolic variation in orbit length, time of flight is also approximately parabolic. Therefore, the decreased variation in orbital period allows to operate a fixed rf frequency acceleration scheme with an appropriate selection of rf frequency and a high enough rf voltage. This new type of fixed rf frequency acceleration scheme is called serpentine acceleration [5, 6].

For both types of FFAG accelerators, only relativistic energy particles are suitable for a fixed rf frequency acceleration. However, if serpentine acceleration is applied to scaling FFAG, high-power beam can be also obtained even in the non-relativistic energy region. In this paper, the longitudinal hamiltonian in scaling FFAG with fixed rf frequency is derived analytically first [7]. Then the preliminary ring design of proton driver for ADS based on serpentine acceleration is also presented.

* yamakawa@post3.rri.kyoto-u.ac.jp

## LONGITUDINAL HAMILTONIAN IN SCALING FFAG WITH FIXED RF FREQUENCY

In cylindrical coordinates, the magnetic field in scaling FFAG in the mid-plane has the form:

$$B_z(r, z=0) = B_0\left(\frac{r}{r_0}\right)^k, \tag{1}$$

where $r$ is the radial coordinate with respect to the center of the ring, $B_0$ is the magnetic field at $r_0$, $k$ is the geometrical field index, and $z$ is the vertical coordinate. The closed orbits for different momenta $P$ are given by

$$r = r_0\left(\frac{P}{P_0}\right)^{\frac{1}{k+1}}, \tag{2}$$

where $r_0$ is the radius of the closed orbit at the momentum $P_0$.

In longitudinal particle dynamics with constant rf frequency acceleration in the scaling FFAG, the phase discrepancy $\Delta\phi$ per revolution is written by

$$\Delta\phi = 2\pi(f_{rf}\cdot T - h), \tag{3}$$

where $h$ is the harmonic number, $f_{rf}$ is the rf frequency and $T$ is the revolution period of a non-synchronous particle. Then Eq. 3 becomes

$$\frac{\Delta\phi}{2\pi} = \frac{hT}{T_s} - h, \tag{4}$$

where $T_s$ is the revolution period of a synchronous particle. Equation 4 is also expressed with another description based on Eq. 2 as follows;

$$\begin{aligned}\frac{T}{T_s} &= \frac{r}{r_s}\Big/\frac{P/E}{P_s/E_s} \\ &= P_s^{1-\alpha}\frac{E}{E_s}P^{\alpha-1},\end{aligned} \tag{5}$$

where $r_s$ is the reference radius, $\alpha$ is the momentum compaction factor and $E_s$ is the reference energy at the reference radius $r_s$. Combining Eq. 4 and Eq. 5, the phase difference $\Delta\phi$ becomes

$$\Delta\phi = 2\pi h\left[\frac{P_s^{1-\alpha}}{E_s}EP^{\alpha-1} - 1\right]. \tag{6}$$



ISBN 978-3-95450-118-2

# BEAM STACKING FOR HIGH INTENSITY PULSED PROTON BEAM WITH FFAG

Y. Ishi*, J.-B. Lagrange, T. Uesugi, Y. Kuriyama, Y. Mori,
Kyoto University Research Reactor Institute, Kumatori, Japan

*Abstract*

The reuirement of extremely high intensity pulsed proton beam with low spill rate has apeared from users in the field of spallation neutron source. To realize the beam satisfies this condition, beam stacking at extraction orbit in FFAG ring has been considered. Feasibility studies of rf stacking using the KURRI FFAG main ring are under consideration. Prior to these studies, beam simulations have been done.

## INTRODUCTION

As a candidate of high intensity proton driver of spallation neutron source, potentially, an FFAG accelerator has advantage in terms of high repetition rate such as 100 - 1000 Hz. However, some users desire low spill rate ( $\sim$10 Hz ) for the experiments e.g. neutron radiography using TOF which needs to get rid of contamination from the pulse of different timing. FFAG rings can provide long interval pulse for users, while the machine operation itself is kept at high repetition rate by using rf stacking after acceleration[1]. This scheme reduces space charge effects at injection energy. For the machine, charge in each bunch can be reduced by high repetition rate. In the high energy region i.e. outer radius, accelerated beams are stacked and circulating around until necessary amount of charge is accumulated. For users, highly compressed beam with long time interval can be delivered. Schematic diagram of this methos is shown in Fig. 1.

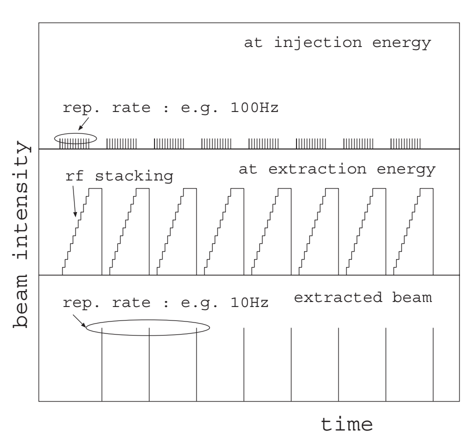


Figure 1: Schematic diagram of rf stacking at extraction energy.

* ishi@.rri.kyoto-u.ac.jp

## SIMULATION STUDIES OF RF STACKING

To confirm the feasibility of rf stacking at extraction energy, simulation studies have been carried out. The model machine used in this study simulates the KURRI FFAG main ring[2], in which the real beam studies are planned. The machine parameters are summarized in Table 1.

Table 1: Machine Parameters used in the Simulations

| | |
|---|---|
| field index $k$ | 7.7 |
| kinetic energy $T$ | 11 - 150 [MeV] |
| momentum $p$ | 144 - 551 [MeV/$c$] |
| circumference $C$ | 28.8 - 33.6 [m] |
| momentum compaction factor $\alpha$ | 0.115 |
| rf voltage $V_{\mathrm{rf}}$ | 8 [MV] |
| rf frequency $f_{\mathrm{rf}}$ | 1.6 - 4.4 [MHz] |
| harmonic number $h$ | 1 |

### *RF Acceleration Scenario*

Beam accelerations have been simulated according to the scenario shown in Figs. 2, 3 and 4. In the real machine operation, we use similar scenarios in which synchronous phase $\phi_s$ and rf voltage are fixed at 30 degree and 4 kV respectively during all the acceleration period. On the other hand, in the scenario used in this simulation study, $\phi_s$ is dropped off linearly from 30 to zero degree when the energy of the beam is between 145 and 150 MeV for soft-landing. The rf voltage is also reduced in this region so that the bucket area $A_B$ is constant in order to make momentum spread small at the end of acceleration. The bucket area is the phase-space area enclosed by the separatrix, i.e.

$$A_B = 16\sqrt{\frac{eV_{rf}}{2\pi\beta^2 E|h|\eta}}\alpha(\phi_s)\frac{\beta^2 E}{\omega_0}, \tag{1}$$

where $E$ is the total energy of the beam particle, $\eta$ is the slippage factor, $\omega_0$ is the revolution frequency and $\alpha(\phi_s)$ is the ratio of the bucket area to the stationary bucket. Here we use approximated expression of $\alpha(\phi_s)$, i.e.

$$\alpha(\phi_s) = \frac{1-\sin(\phi_s)}{1+\sin(\phi_s)}. \tag{2}$$

ISBN 978-3-95450-118-2

# 1-MW BEAM OPERATION SCENARIO IN THE J-PARC RCS

H. Hotchi#, H. Harada, N. Hayashi, M. Kinsho, P.K. Saha, Y. Shobuda, F. Tamura, K. Yamamoto, M. Yamamoto, and M. Yoshimoto, J-PARC, JAEA, Tokai, Ibaraki, 319-1195, Japan
Y. Irie, KEK, Tsukuba, Ibaraki, 305-0801, Japan

*Abstract*

The injection energy of the J-PARC RCS will be upgraded from 181 MeV to 400 MeV in the 2013 summer-autumn period. With this upgraded injection energy, we are to aim at the 1 MW design output beam power. In this paper, we discuss beam dynamics issues for the 1 MW beam operation and their possible solutions.

## INTRODUCTION

The 3-GeV Rapid Cycling Synchrotron (RCS) of the J-PARC has two functions as a proton driver to produce pulsed muons and neutrons at the Materials and Life Science Experimental Facility (MLF) and as an injector to the following 50-GeV Main Ring Synchrotron (MR), aiming at 1 MW output beam power which is the highest level in the world.

As shown in Fig. 1, a $H^-$ beam from the linac is delivered to the RCS injection point, where it is multi-turn charge-exchange injected through a carbon stripper foil. The RCS accelerates the injected protons up to 3 GeV with a repetition rate of 25 Hz. Most of the time, the 3 GeV beam from the RCS is transported to the MLF, while only a portion of the RCS beam (typically four pulses every several seconds) is transported to the MR, where the beam destination is switched pulse-by-pulse by employing a pulse dipole magnet installed downstream of the RCS extraction section.

The current injection energy is 181 MeV. With this injection energy, the RCS first aims at providing more than 300 kW output beam power. The linac will be upgraded in the 2013 summer-autumn period; the output energy will be improved to 400 MeV with the addition of an annular coupled structure (ACS) linac, and the maximum peak current will be increased from 30 to 50 mA by replacing the front-end system (ion source and rf quadrupole linac). After that, we are to aim at our final goal of the 1 MW design output beam power.

The J-PARC beam commissioning began in November 2006 from the linac to the downstream facilities. The RCS was beam commissioned in October 2007. Following the initial beam tuning [1], the RCS was made available for user operation in December 2008 with an output beam power of 4 kW. Since then, the RCS beam power ramp-up has proceeded well. The major beam loss issues observed in high-intensity beam trials of up to 420 kW have been solved so far [2]. In this process, the output beam power for the routine user program has been increased to 280 kW to date.

Thus, now the RCS is in transition from the initial commissioning phase to the final stage aiming at the 1 MW output beam power. Our efforts hereafter will be focused on establishing the 1 MW design beam operation.

In this paper, we discuss beam dynamics issues for the 1 MW beam operation and their solutions aiming for beam loss reduction, better operational flexibility, and high-quality (low-halo/tail) output beam, on the basis of numerical simulations with a 3-dimentional particle tracking code "Simpsons". As described in [2], this numerical simulation well reproduces beam loss patterns and behaviors of transverse and longitudinal beam profiles measured so far. The same manner was applied to the present 1 MW beam simulation with the injection energy of 400 MeV.

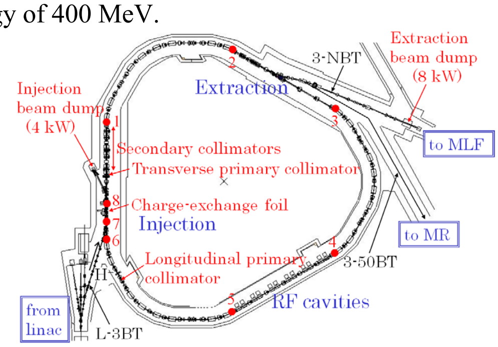


Figure 1: Schematic of the RCS.

## BEAM LOSS EXPECTED FOR 1 MW BEAM OPERATION

The most important issues in increasing the output beam power are the control and minimization of beam loss to keep machine activation within the permissible level. There are many sources of beam loss, in which the most critical one is the space charge effect in the low energy region. It generally imposes a major performance limit on high-power proton synchrotrons. To alleviate this, the RCS adopts transverse and longitudinal injection painting technique.

The major beam loss issues observed in high-intensity beam experiments of up to 420 kW with the injection energy of 181 MeV have already been solved; the large beam loss of 18% observed at the injection energy region for a 420 kW intensity beam was well reduced to less than 1% by transverse and longitudinal injection painting [2]. In the transverse painting, here, 100π-mm-mrad ($\varepsilon_{tp}$) correlated painting was employed. On the other hand, in the longitudinal painting [3,4], the momentum offset injection of −0.2% ($\Delta p/p$) was applied in combination with superposing the second harmonic rf with an amplitude of 80% ($V_2/V_1$) of the fundamental one. As an additional control in the longitudinal painting, the linear phase sweep from −100 to 0 degrees ($\varphi_2$) of the second

#hotchi.hideaki@jaea.go.jp



ISBN 978-3-95450-118-2

# SIMULATION OF LONGITUDINAL BEAM INSTABILITY CAUSED BY HOMs

P. Cheng, Z.H. Li, J.Q. Wang, J.Y. Tang, IHEP, Beijing, China

*Abstract*

Superconducting cavities are employed in C-ADS linac to accelerate 10 mA CW proton beams from 3.2 MeV to 1.5 GeV. High order modes in superconducting cavities are found by using the simulation tools CST and HFSS, then power dissipation caused by HOMs have been investigated, it is indicated that the Qext should not go beyond $10^7$ in order to limit the additional heat load. Beam instabilities caused by high order modes in elliptical cavity sections are investigated using the code offered by Dr. Jean-Luc Biarrotte (CNRS, IPN Orsay, France). Beam errors, linac errors and high order modes frequency spread are investigated in detail. It shows that the monopole modes do not affect the proton beam critically and need no HOM couplers if high order modes frequency spread is more than 100 kHz.

## INTRODUCTION

Beam instabilities caused by high order modes are concerned using code bbusim. It was first offered by Jean-Luc Biarrotte (CNRS, IPN Orsay, France). We did some modification to adapt for the C-ADS real situation. Based on these simulation and analysis, machine specific HOM damping requirements can be defined.

## LONGITUDINAL INSTABILITY SIMULATION

The introduction of basics of high order modes excitation and beam interaction are based on [1-4]. Our code was written by matlab. Simulation results can be obtained by tracking the energy and time error of the particles at the linac end. Lately some modifications were carried out to adapt to the C-ADS real lattice and to understand the instabilities growth. We have also improved the code to reduce the simulation time and memory consuming.

### *Longitudinal Model and Input Parameters*

A drift-kick model was used in the simulation. As [5] refers, in this model the cavities are compressed to a plane located at the cavity mid-plane, where particle cavity interaction takes place instantaneously. Drifts are spaced between the cavities. The drift lengths are not identical, which are based on the real linac layout.

Results attained from the main linac of C-ADS simulation are set as the input parameters. They are listed in Table 1. The beam current is set to <Ib>=100mA as a safety margin, which corresponds to 10 times the nominal current. The accelerator is operated in a CW motion. The linac consists of two sections. In the medium beta section ($\beta g$=0.63), the RF frequency is 650 MHz, twice the bunch frequency, as well as the high beta section ($\beta g$=0.82). The layout of these two sections are shown in Figure 1 and 2. Bunch noises, such as arrival time errors, energy errors and charge jitters are also considered as the input parameters. All these noise is set as Gaussian distributed.

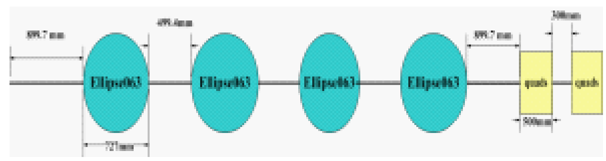

Figure 1: Schematic layout of one cell of the Elliptical063 section.

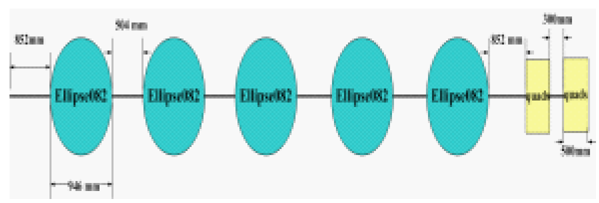

Figure 2: Schematic layout of one cell of the Elliptical082 section.

Table 1: Beam Input Parameters. The Variation Values are Assumed Based on Projects-X and SPL

| Parameter | Value | σ | |
|---|---|---|---|
| Input Energy | 170 | 0 | MeV |
| Accelerating Phase | actual RF phase | 0.1 | deg |
| Beam Current | 100 | 1% | mA |
| Duty Factor | 100 | | % |
| Cavity Numbers | 131 | | |
| HOM Frequency | 1950/1787.5 /1414.6 | 0.1/1 | MHz |

## SIMULATION RESULTS

We separate the simulation into three main parts.

Firstly a center HOM frequency <fH> falling on the machine line is discussed, which is assumed to 1950 MHz, corresponding to 6 times the fundamental mode frequency of 325 MHz. The influence of bunch noise,



ISBN 978-3-95450-118-2

# BEAM LOSSES DUE TO THE FOIL SCATTERING FOR CSNS/RCS*

M.Y. Huang#, N. Wang, S. Wang, S.Y. Xu
Institute of High Energy Physics, Beijing, China

*Abstract*

For the Rapid Cycling Synchrotron of China Spallation Neutron Source (CSNS/RCS), the stripping foil scattering generates the beam halo and gives rise to additional beam losses during the injection process. The interaction between the proton beam and the stripping foil was discussed and the foil scattering was studied. A simple model and the realistic situation of the foil scattering were considered. By using the codes ORBIT and FLUKA, the multi-turn phase space painting injection process with the stripping foil scattering for CSNS/RCS was simulated and the beam losses due to the foil scattering were obtained.

## INTRODUCTION

CSNS is a high power proton accelerator-based facility [1]. The accelerator consists of an 80MeV $H^-$ linear accelerator which is upgradable to 250MeV and a 1.6GeV RCS which accumulates an 80MeV injection beam, accelerates the beam to the designed energy of 1.6GeV and extracts the high energy beam to the target. Its beam power is 100kW and capable of upgrading to 500kW. The design goal of CSNS is to obtain the high intensity, high energy proton beam with a repetition rate of 25Hz for various scientific fields [2].

For the high intensity proton accelerators, injection via $H^-$ stripping is actually a practical method. In order to control the strong space charge effects which are the main causes of the beam losses in CSNS/RCS, the phase space painting method is used for injecting the beam of small emittance from the linear accelerator into the large ring acceptance [3].

Beam losses in an accelerator can be divided into two categories: controlled beam losses and uncontrolled beam losses [4]. In high power accelerator, one potential source of the uncontrolled beam losses is the stripping foil scattering of the $H^-$ ions. When the $H^-$ beam traverses the stripping foil, most of the particles $H^-$ are converted to $H^+$, and the others are converted to $H^o$ or unchanged [5][6]. The interaction of the $H^-$ beam with the stripping foil can induce the beam losses. By using the codes ORBIT [7] which is a particle tracking code for rings and FLUKA [8] which is a code for calculations of particle transport and interactions, the multi-turn phase space painting injection process with the stripping foil scattering for CSNS/RCS can be simulated and the beam losses due to the foil scattering can be calculated.

*Work supported by National Natural Science Foundation of China (Project Nos. 11175020 and 11175193)
#huangmy@ihep.ac.cn

## FOIL SCATTERING

Change exchange phenomena gives rise to capture or loss of electrons by the fast moving ions traverse a material [6]. For CSNS, when the $H^-$ beam traverses the carbon stripping foil, there are six charge exchange processes: three are electron loss reactions and three are electron pickup reactions [9]. For energies above 100keV, the cross sections for electron pickup are very small and can be neglected. Therefore, the remained particles after foil stripping are $H^-$, $H^o$ and $H^+$, as shown in Fig. 1.

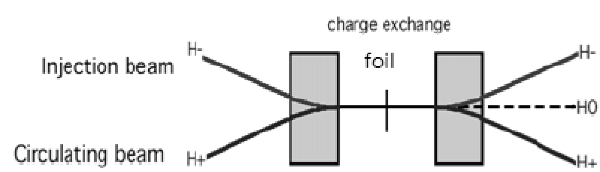


Figure 1: Stripping foil scattering.

During the injection process, the foil scattering can generate the beam halo and result in additional beam losses. The stripping foil scattering had been studied in detail for J-PARC and it can be found that the foil scattering was the main cause of beam losses in the injection region [10]. Therefore, the beam losses due to the foil scattering for CSNS also need to be studied in detail. Table 1 shows the beam parameters for 80MeV injection and 250MeV injection.

Table 1: Beam Parameters for 80 MeV Injection and 250 MeV Injection

| Injection | 80MeV | 250MeV |
|---|---|---|
| Injection beam power/kW | 5 | 80 |
| Average injection current/μA | 62.5 | 312.5 |
| Turn number of injection | 200 | 403 |
| Foil thickness/(μg/cm$^2$) | 100 | 240 |

## A SIMPLE MODEL OF THE FOIL SCATTERING

In order to obtain a preliminary judgment of the beam losses due to the foil scattering, in this section, a very simple model of the stripping foil scattering is adopted, and then simulated by the code FLUKA. A preliminary result of the beam losses can be obtained. The simple model will be used for J-PARC to check its accuracy firstly, and then used for CSNS to calculate the beam losses in the injection region.

Suppose the particle beam is uniform distribution and hitting on the stripping foil vertically. The detector is



ISBN 978-3-95450-118-2

# TEST SYSTEM AND CHARACTERISTICS STUDIES OF FERRITE CORES FOR THE CSNS RCS RF SYSTEM*

H. Shi[#], H. Sun, W. Long, W. L. Huang, X. Li, J. Y. Tang and C. L. Zhang,
Institute of High Energy Physics (IHEP), Beijing 100049, China

*Abstract*

A two-ring ferrite test system for ferrite-loaded cavities of Rapid Cycling Synchrotron (RCS) of China Spallation Neutron Source (CSNS) has been developed. By this system, the RF characteristics of full-sized ferrite cores of RCS cavities have been studied. On dc bias current, the swept frequency range and thresholds of High Loss Effect (HLE) have been presented. On ac bias current of 25 Hz, although the shunt impedance of the cores satisfies the CSNS cavity, comparing with the dc bias, more power dissipation and more required bias current have been observed because the induced magnetic anisotropy of the ferrite cores disappears. Consequently, it is important to evaluate the dynamic features of the cores with 25 Hz bias current for designing the cavities, the power supplies and the bias current sources.

## INTRODUCTION

The Rapid Cycling Synchrotron (RCS) of the China Spallation Neutron Source (CSNS) is a high intensity proton accelerator, and the RF system will have 8 ferrite-loaded coaxial resonant cavities. The gap voltage and RF frequency vary according to the beam dynamic designing parameters in the 20 ms accelerating period of 40 ms cycle. The frequency is from 1.02 to 2.44 MHz and the total voltage is from 21 to 165 kV. Each cavity includes two very similar resonators and each resonator is loaded by 28 pieces of ferrite rings, and the two accelerating gaps are parallel-connected. The shunt impedance of the cavity in 25 Hz repetition frequency is required about 400~1500 Ω, so 30~110 Ω per core is required. In order to acquire the characteristics of the cores on ac bias current with full RF power, a two-ring ferrite test cavity [1] has been developed by the CSNS RCS RF system and the LLRF control system has also been included for precise and efficient test. In this paper, the test system has been introduced, and the ac bias test results are presented and compared with the dc bias test results.

## MEASUREMENT APPARATUS

The Ferroxcube T500/250/25-4M2 has been adopted by CSNS, which is one of soft ferrite and has the feature of fast recovery after magnetic bias. 3 kW valve power supply could drive the two cores far above the realistic magnetic flux densities.

### *Two-ring Test Cavity*

Figure 1 shows the diagram of the two-ring test cavity. Full sized rings lay in separate annular RF cavities, electrically in parallel; bias current counter-couples so as to cancel induction between the bias and RF current paths. The cavity was resonant over the frequency range of 1.02~2.44 MHz by the use of two rings of capacitors one in each RF cavity, together with permeability ($\mu'$) tuning of the ferrite. Temex Ceramics RF power capacitors of 1000 volt peak RF voltage rating were used and the total value is 171 nF. The resonant RF current $I_{rf}$ was sampled by a Pearson model 411 current transformer, and RF voltage $U_{rf}$ was sampled by a Tektronix P5100 probe in the coaxial RF feed line.

Figure 2 is a photograph of the test system. The RF power was supplied to the cavity through the coaxial RF feeder, and no matching circuit was needed because of the impedance transformer connecting between 3 kW valve power supply and test cavity, which could satisfy 30~200 Ω variable load. A bias power supply provided the direct current and 0~25 Hz alternating current up to 3200A. The test system also included the LLRF control box and some test instruments.

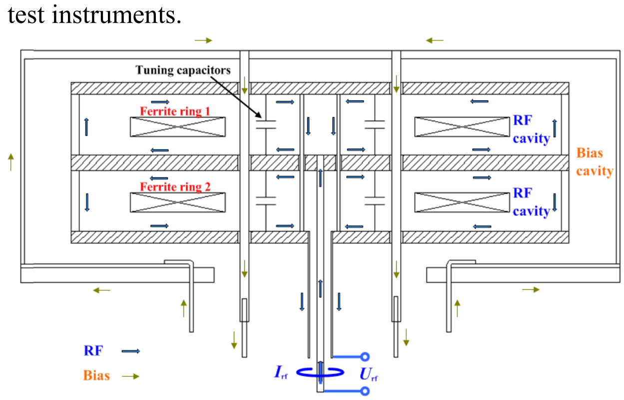


Figure 1: Diagram of two-ring test cavity.

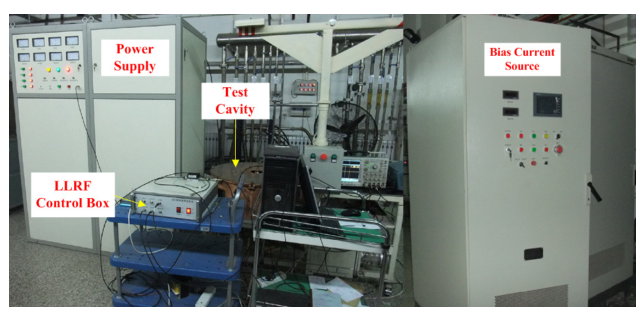


Figure 2: Photograph of the test system.

### *Equivalent Circuit*

Figure 3 shows the equivalent circuit of the test system, where, $C_g$ is the total resonant capacitor, $L_1$ and $L_2$ are the inductance of two cores in the RF cavities.

In resonance, the shunt impedance of the cavity can be expressed as



ISBN 978-3-95450-118-2

# THE STUDY ON MEASURING BETA FUNCTIONS AND PHASE ADVANCES IN THE CSNS/RCS

Y.W. An, S. Wang#, IHEP, Beijing 100049, P.R.C.

*Abstract*

As a key component of the China Spallation Neutron Source (CSNS) Project, the Rapid Cycling Synchrotron (RCS) will accumulate and accelerate the proton beams from 80MeV to 1.6GeV for extracting and striking the target with a repletion rate of 25Hz. To check linear optics and locate the quadruple errors, beta function plays an important role in beam diagnostics of a particle accelerate system. The Independent Component Analysis (ICA) is a robust beam diagnosis method by decomposing the samples recorded by turn by turn BPMs (beam position monitors) into the independent components which represent the inherent motion of the beam. The beta functions and phase advances can be derived from the corresponding independent components. Because the linear part of the space charge gives a defocusing effect to the beam, beta function variation will be induced. We find that the ICA method can measure beta functions with a reasonable tolerance under the conditions of strong space charge effects.

## INTRODUCTION

The CSNS accelerator consists a low energy H- Linac and high energy RCS. A 4-fold symmetry structure with 16 triplet cells is adopted for the lattice design of RCS. In one super-period, there are 8 turn-by-turn beam position monitors (BPMs) located near quadruples for better understanding the beta functions of the RCS Lattice, and the main parameters of RCS are shown in Table 1 [1].

Table 1: Main Parameters of RCS

| Parameters | Units | Values |
|---|---|---|
| Circumference | m | 227.92 |
| Inj. Energy | MeV | 80 |
| Ext. Energy | GeV | 1.6 |
| Repetition Rate | Hz | 25 |
| Average current | μA | 62.5 |
| Quadruples | | 48 |
| Dipoles | | 24 |
| Nominal Tunes(H/V) | | 4.86/4.78 |
| Maximum β | m | 12/26 |
| BPM | | 32 |

#wangs@ihep.ac.cn

Measuring beta functions is a critical issue for many synchrotrons to understand the linear Optics of the Lattice. With turn-by-turn BPMs installing in lots of synchrotrons, getting the beta functions from the samples recorded by turn-by-turn BPMs is becoming more and more popular. Independent components analysis (ICA) is a data mining method that can provide the independent components (also called ICs) which represent the inherent property of the samples data. ICA is first introduced in the accelerator by the team of Professor S.Y. Lee [2] and then applied to many accelerators.

## DATA ACQUISITION

In order to get the samples from turn-by-turn BPMs, RF kicker or pinger is often used to excite betatron oscillation. The beam emmittance will be diluted in the case of pinger, because pinger is a pulsed magnet and the field variation is non-adiabatically. However, the field of RF kicker can be ramped up or down with a sine curve slowly [3], and the beam emmitance can be preserved.

Let's define $\omega_0$ is the orbital angular frequency, and $\omega_m$ is the RF kicker frequency, and $\nu_m = \omega_m / \omega_0$ as the modulation tune. When the fractional part of the modulation tune equals that of tune of the transverse motion, or the sum of two fractional parts equals one, the coherent betatron oscillation can be excited. Figure 1 shows the driven oscillation excited by RF Kicker with the amplitude of 0.2mrad. The RF kicker is switched off when the beam oscillation reaches proper amplitude, and the data of the free oscillations are stored for ICA processing. The first 200 turns is the rise time, and the latter 800 turns is free oscillation after excitation. The RF kicker works at a repetition rate of 449 kHz, which means $\nu_m$=0.14, corresponding to the beam angular frequency of 3.212 MHz in the beam energy of 80 MeV.

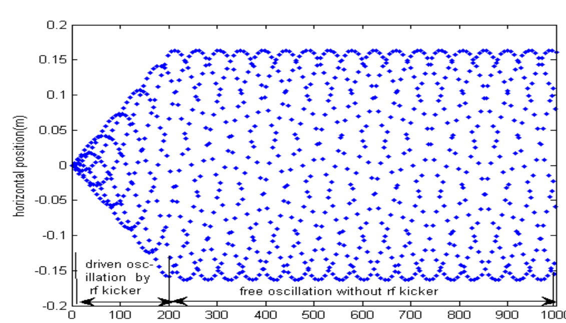


Figure 1: Driven betatron oscillation with RF kicker and free betatron oscillation without RF kicker.



ISBN 978-3-95450-118-2

# THE DESIGN STUDY ON THE LONGITUDINAL BEAM DYNAMICS FOR CSNS/RCS*

N. Wang, Y.S. Yuan, S. Wang, S.Y. Xu, M.Y. Huang, Y. Li, IHEP, Beijing, China

*Abstract*

Rapid Cycling Synchrotron (RCS) is the key part of China Spallation Neutron Source (CSNS) accelerators. The RCS accumulates and accelerates 80 MeV beam from linac to 1.6 GeV. The particle number is 1.56e13 for each pulse, with repetition rate of 25 Hz. In the RCS, longitudinal beam dynamics plays a crucial role in achieving high intensity beam with low beam loss. Longitudinal parameters are studied and optimized for efficient RF trapping of the beam in the longitudinal phase space. Beam performance is investigated by particle tracking simulations. Beam dynamic issues related to the high order mode induced by the RF generator are studied with a new developed code. Primary study on the adoption of dual harmonic cavity for higher beam power is also addressed.

## INTRODUCTION

The accelerator complex of the CSNS consists of an 80 MeV Linac and 1.6 GeV RCS [1]. The RCS lattice has a four fold structure with four straight sections dedicated to beam injection, transverse beam collimation, extraction, and RF systems [2]. Eight RF cavities with harmonic number of 2 will be adopted in the RCS. Seven RF cavities provide total RF voltage of 165 kV, with one additional cavity for redundancy. Dual harmonic cavities will be added in the future upgrade for higher beam power. The layout of the RF cavities around the ring is shown in Fig.1. The physical aperture of the RCS is designed with momentum acceptance of 1%.

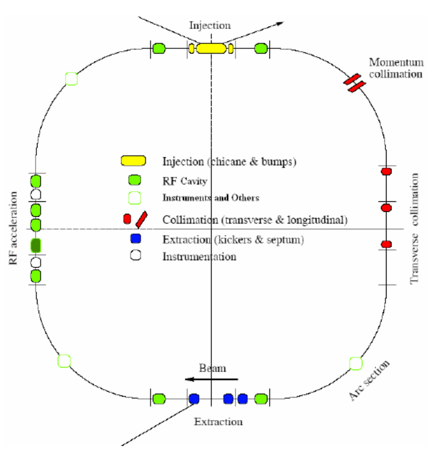


Figure 1: Schematic view of the layout of the RF cavities in the RCS.

In the physical design of the RCS, the longitudinal beam dynamics design and study are crucial for achieving high beam power. Many woks have been done to optimize the RF voltage and phase curves [3]. The related parameters are carefully studied to obtain high transmission efficiency and to decrease the beam loss due to space charge effect [3-5].

In this paper, the design of the longitudinal beam dynamics is first described, and the simulation results of multi-particle tracking are also presented. Then, beam dynamics under the influence of the high order mode induced by the RF generator are investigated. Finally, the design of dual harmonic RF for higher beam power is studied with a new developed code. The main parameters used in the studies are listed in Table 1.

Table 1: The Main Parameters of CSNS RCS

| Parameters | Symbol, unit | Value |
|---|---|---|
| Injection energy | $E_{inj}$, GeV | 0.08 |
| Extraction energy | $E_{ext}$, GeV | 1.6 |
| Circumference | $C$, m | 228 |
| Beam population | $N_p$, $\times 10^{13}$ | 1.56 |
| Harmonic number | $h$ | 2 |
| Repetition frequency | $f_0$, Hz | 25 |
| RF frequency range | $f_{rf}$, MHz | 1.022 ~ 2.444 |

## LONGITUDINAL BEAM DYNAMICS DESIGN

The main function of the RF system in the RCS is to provide acceleration voltage for the circulating beam. The key issues of longitudinal beam dynamics design are keep efficient longitudinal RF trapping during injection and to provide enough RF bucket to keep low loss during the acceleration. As space charge is the dominant origin of beam loss and emittance growth in low energy rings, large bunching factor is preferred to alleviate the space charge effect. Meanwhile, the variation of the RF voltage or phase should not be too steep considering the provision of the RF cavities.

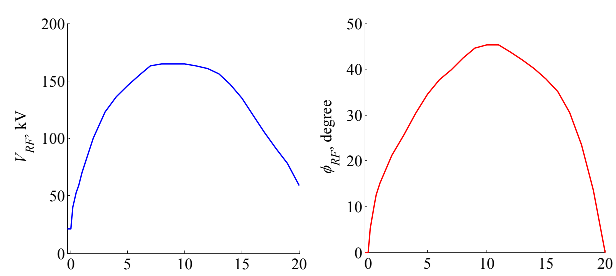


Figure 2: The RF voltage and phase pattern in one RF cycle.

#wangn@ihep.ac.cn

ISBN 978-3-95450-118-2

# MEBT2 PHYSICS DESIGN FOR THE C-ADS LINAC

Zhen Guo, Huiping Geng, Jingyu Tang, Zhihui Li, IHEP, Beijing, China

*Abstract*

The C-ADS linac is composed of two parallel injectors and a main linac, a section of Medium Energy Beam Transport (MEBT2) is designed to guide and match beams from the two injectors to the main linac. The two injectors are hot-spare for each other in order to meet the requirement of very high availability and reliability. At 10 MeV and 10 mA, with strong space charge effects and bending sections, it is found that MEBT2 design is a real challenge.. It is difficult to obtain satisfactory longitudinal matching without bunchers in the bending section, whereas bunchers in a bending section destroy usual achromatism conditions. A special design with bunchers inside the bending section is proposed, which can maintain the achromatism. The online and offline operation modes for each injector have been considered in the MEBT2 design. The multi-particle simulations have also been given.

## LAYOUT DESIGN FOR MEBT2

The C-ADS accelerator is a CW proton linac and uses superconducting acceleration structures except the RFQs, the design specifications for the proton beam are shown in Table 1[1]. The C-ADS linac requires two injectors as each of them is a hot-spare of the other [1]. As this is a high-intensity beam, the physics design of the MEBT2 is tightly constrained by the requirement of very strict control over beam loss and emittance growth. Due to relatively low beam energy of 10 MeV and high intensity of 10 mA, space charge forces are strong here. To avoid significant emittance growth, it is preferred to design a lattice with more-or-less uniform focusing [2]. However, a minimum separation in the transverse space between the two injectors requires a bending section for each branch. It is not easy to maintain the focusing uniformity together with an achromatic bending. A larger bending angle is favored to give more installation space for the injectors, but it increases the difficulty to obtain a good performance in beam dynamics with high-intensity. At the moment, a trade-off design defines 2.4 m for the minimum translational separation between the two injectors. Hence an anti-symmetric bending section of 20° is employed here. Once in the straight main linac tunnel, the elements are common for operating any injector.

The most difficult problem in designing MEBT2 is the longitudinal matching. On the one hand, even at the energy of 10 MeV the required RF voltage for the bunchers is quite high, On the other hand, the RF voltage may be somewhat too low for adopting a superconducting structure and a superconducting cavity together with its cryomodule will take large longitudinal space that is not desired in the MEBT2 design. To solve this problem, we have investigated the possibility to use room-temperature cavities in 650 MHz by taking the advantage of higher focusing gradient with higher RF frequency. However, the study shows that in the CW mode a cavity in 650 MHz even with a half voltage is more difficult to cool than the one in 325 MHz. Therefore, we decide just to use more cavities of 325 MHz when higher voltage is needed.

Table 1: Specifications of the Required Proton Beams for C-ADS

| Particle | Proton | |
|---|---|---|
| Energy | 1.5 | GeV |
| Current | 10 | mA |
| Beam power | 15 | MW |
| RF frequency | (162.5)/325/650 | MHz |
| Duty factor | 100 | % |
| Beam Loss | <1 | W/m |
| Beam trips/year | <25000<br><2500<br><25 | 1s<t<10s<br>10s<t<5m<br>t>5m |

For the positions of the room-temperature bunchers, it is a critical issue in the MEBT2 design. With a long drift distance and in the presence of space charge force at 10 mA, the debunching process is very strong. It is found that it is difficult to obtain satisfactory longitudinal matching without bunchers in the bending section. Then we consider designing the bending section with two or more bunchers inside, the condition of maintaining the achromatism will be discussed below.

The bending section consists of three parts: the first bend magnet, the beam line between the two bending magnets which comprises quadrupoles and bunchers and the second bending magnet. Their transfer matrixes can be expressed as

$$B = \begin{pmatrix} B_{11} & B_{12} & 0 & 0 & 0 & B_{16} \\ B_{21} & B_{22} & 0 & 0 & 0 & B_{26} \\ 0 & 0 & 1 & B_{34} & 0 & 0 \\ 0 & 0 & 0 & 1 & 0 & 0 \\ -B_{26} & -B_{16} & 0 & 0 & 1 & B_{56} \\ 0 & 0 & 0 & 0 & 0 & 1 \end{pmatrix}$$

$$R = \begin{pmatrix} R_{11} & R_{12} & 0 & 0 & 0 & 0 \\ R_{21} & R_{22} & 0 & 0 & 0 & 0 \\ 0 & 0 & R_{33} & R_{34} & 0 & 0 \\ 0 & 0 & R_{43} & R_{44} & 0 & 0 \\ 0 & 0 & 0 & 0 & R_{55} & R_{56} \\ 0 & 0 & 0 & 0 & \boldsymbol{R_{65}} & R_{66} \end{pmatrix}$$

ISBN 978-3-95450-118-2

# DYNAMICS OF PARTICLES IN A TILTED SOLENOIDAL FOCUSING CHANNEL *

Hongping Jiang, Shinian Fu
Institute of High Energy Physics, Chinese Academy of Sciences, Beijing 100049, China

*Abstract*

We use the paraxial ray approximation equations to analysis the dynamics of particles in a tilted solenoidal focusing channel. In this case, the particles' initial canonical angular momentum is nonzero, so we need to add the term of centrifugal potential to the dynamics equation of particles. And in the dynamics equation this centrifugal potential term is nonlinear, which results in the emittance growth. In practice, we also need to consider the spherical aberration's effect on emittance growth and the linear part of the space-charge force of a Kapchinskij-Vladimirskij [1] distribution beam in the dynamics equation of particles.

## INTRODUCTION

Building a high quality transport line is recognized as one of critical issues in the low energy section of a high intensity RF linac. For an RF linac front end used in ADS and Project X, which employs superconducting spoke-type cavities, it was found that solenoid-based lenses can provide the needed focusing[2],[3][4]. The solenoid-based lenses are assembled and aligned in the cryomodules. The level of acceptable misalignment established for HINS linac is 0.3mm lateral and 5 mrad tilt [3], the alignment and assembly in the cryomodules are difficulty. Beam emittance can grow, if the beam passes a solenoid-based focusing lens off-centre. So we analyse the dynamics of particles in a tilted solenoid-based focusing channel.

## DYNAMICS OF PARTICLES

In the paraxial approximation the radial equation for a particle in a solenoidal focusing magnetic field reads [5]

$$\frac{d^2r}{ds^2}+k_0^2r-\frac{p_\theta^2}{m^2c^2\gamma^2\beta^2r^3}=0. \qquad (1)$$

$s$ is the coordinate along the beam axis, $r$ is the particle radius, and $k_0^2=\frac{q^2B_0^2}{4m^2c^2\beta^2\gamma^2}$ is the focusing strength parameter, $p_\theta=\gamma mr^2\dot{\theta}+qrA_\theta$ is the canonical angular momentum of the particle, where $B_0$ is the magnetic field on the beam axis, $\beta c$ is the axial velocity of particles, $c$ is the speed of light in vacuum, and $q$, $m$, and $\gamma=(1-\beta^2)^{-1/2}$ are, respectively, the charge, mass, relativistic factor of beam particles, $\dot{\theta}$ is the azimuthal velocity of particle, $A_\theta$ is the azimuthal part of vector potential of the field in cylindrical coordinates.

For the sake of simplicity we usually consider that the canonical angular momentum is zero, ($p_\theta=0$), and the last term in the paraxial radial equation vanishes ($\frac{d^2r}{ds^2}+k_0^2r=0$), this equation is quite familiar to us. But if we take the errors of alignment into account, the canonical angular momentum is not zero, in this case, we must turn to the Equation (1), not the equation we usually used.

Considered a solenoidal focusing channel is tilted, scaled of$\varphi_0$, we can get the expression of the canonical angular momentum

$$p_\theta=\gamma\beta cmr_0\varphi_0cos\left(\theta_0\right). \qquad (2)$$

$r_0$ and $\theta_0$ are the particles' initial value of radius and azimuth. The value of canonical angular momentum is relative not only with the tilted angle$\varphi_0$ also with the particles' initial conditions ($r_0$,$\theta_0$). Substituting Eq. (2) into the Eq. (1) gives the radial equation

$$\frac{d^2r}{ds^2}+k_0^2r-\frac{\left(\varphi_0r_0cos\left(\theta_0\right)\right)^2}{r^3}=0. \qquad (3)$$

When the canonical angular momentum is different from zero, the last term adds an effective repulsive core or a centrifugal potential, and is a defocusing force. In this case, the particle never crosses the axis ($r\neq 0$).
We rewrite the radial equation as follow

$$\frac{d^2r}{ds^2}+k^2r=0. \qquad (4)$$

$k^2=k_0^2-\frac{(\varphi_0r_0cos(\theta_0))^2}{r^4}$ is the focusing strength parameter including the nonlinear defocusing part from the initial canonical angular momentum. In order to ensure the beam is good focused, we should have perfect alignment, in the ideal case, the tilted angle should be zero. From the formula we can evaluate the tilted angle $\varphi_0$ by seeing the $-\frac{(\varphi_0r_0cos(\theta_0))^2}{r^4}$ as a perturbation of the focusing strength, when the particles radius is larger than 1mm ($r\geq 1$mm, we consider the repulsive core radius is about1$mm$). For simplicity, we select the particles' initial conditions ($r_0=1$mm$,\theta_0=0$) as representative. $k_0^2$ is about $10^{-4}$ mm$^{-2}$, we need $-\frac{(\varphi_0r_0cos(\theta_0))^2}{r^4}$ is smaller than $10^{-6}$mm$^{-2}$, that means the tilted angle $\varphi_0$ is about 1mrad.

*E-mail: jianghp@ihep.ac.cn

ISBN 978-3-95450-118-2

# ERROR ANALYSIS AND CORRECTION SCHEME IN C-ADS INJECTOR-I*

Cai Meng, Jingyu Tang, Zhihui Li
Institute of High Energy Physics, Chinese Academy of Sciences, Beijing 100049, China

*Abstract*

C-ADS Injector-I is a 10-mA 10-MeV CW proton linac. It uses a 3.2-MeV normal conducting 4-Vane RFQ and 12 superconducting single-spoke cavities. According to the detailed sensitivity analysis of alignment and RF errors, the error tolerance of both static and dynamic ones for Injector-I is presented. The simulation results show that with the errors there are beam losses, the residual orbit is too large, which will produce significant emittance growth, so that the correction is necessary for Injector-I. After detailed numerical studies, a correction scheme and monitor distributions are proposed. After correction the rms residual orbit can be controlled within 0.4 mm and RMS emittance growth can be controlled within 10%, but it still has $1.7\times10^{-6}$ beam loss, which comes from the RF errors and small longitudinal acceptance. To minimize beam loss, the causes of beam loss have been studied and a short period Injector-I lattice with larger longitudinal acceptance have been designed with good error tolerance performance. According to detailed analysis and simulations, as a consequence, longitudinal emittance control and longitudinal distribution control as well as large longitudinal acceptance are the key to minimize beam losses and emittance growth in low energy section.

## INTRUDUCTION

The C-ADS project is a strategic plan to solve the nuclear waste problem and the resource problem for nuclear power plants in China [1]. For the C-ADS accelerator that is a CW proton linac, it uses superconducting acceleration structures except the RFQs. The C-ADS linac consists of two injectors and a main linac section, as shown in Fig.1.

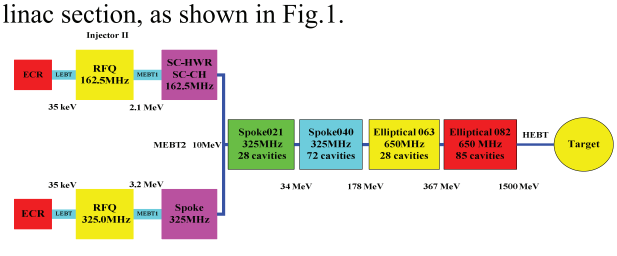


Figure 1: Layout of the C-ADS driver accelerator.

Two identical injectors will be operated in the mode of one as the hot-spare of the other. However, two different injector schemes are shown in Fig.1, and this means that in the early developing phase two different approaches of injector will be developed in parallel by two different teams. C-ADS Injector-I [1] is a 10-mA 10-MeV CW proton linac. It uses a 3.2-MeV normal conducting 4-Vane RFQ and 12 superconducting single-Spoke cavities. This paper will report error analysis and correction scheme in Injector-I including MEBT-1 and spoke cavity section.

## SIMULATIONS CONSIDERING DIFFERENT SOURCES OF ERROR

All the devices having electromagnetic field influence over the beam have installation errors including translational errors and rotation errors, and also field errors. We can classify the possible sources of error into four groups [2]:

- Translational errors: affect all the elements of the accelerator system.
- Rotation errors (pitch/yaw/roll): affect all the elements of the accelerator system.
- Field errors: affect the field level as well as the phase of an accelerating cavity and the field of magnets.
- BPM uncertainty: affect the correction effects

As RMS residual orbit reflects beam loss and emittance growth to some extent [1], it can be considered a criterion to evaluate the influence of errors without correction schemes. The sensibilities of different static errors in Injector-I, such as solenoid displacements, solenoid rotations, spoke cavity displacements, and spoke cavity rotations have been studied.

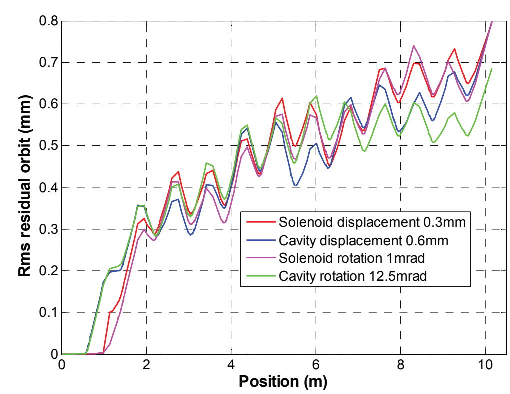


Figure 2: Comparison on rms residual orbit among different error types in Injector-I.

It is found that the rms residual orbit is approximately proportional to the magnitudes of four errors. The sensitivity comparison is shown in Fig.2, which shows the downward importance for the errors: solenoid rotation, solenoid displacement, spoke cavity displacement and spoke cavity rotation. About the rms emittance growth, the spoke cavity displacements have the most important influence and the RF errors have also significant influence. Following the preliminary error study and technical feasibilities, Table 1 shows the initial error definitions for the error studies [3-6].

*Work supported by the China ADS Project (XDA03020000)
E-mail: mengc@ihep.ac.cn

ISBN 978-3-95450-118-2

# LOCAL COMPENSATION-REMATCH FOR MAJOR ELEMENT FAILURES IN THE C-ADS ACCELERATOR

B. Sun, F. Yan, Z.H. Li, J.Y. Tang, IHEP, Beijing, China

*Abstract*

In order to achieve the required reliability and availability for the C-ADS accelerator, a fault tolerance design is pursued. The effects of cavity failure in different locations have been studied and the schemes of compensation by means of local compensation have been investigated. After one cavity failure, by adjusting the settings of the neighbouring cavities and the focusing elements we can make sure that the Twiss parameters and energy are approximately recovered to that of the nominal ones at the matching point. We find that the normalized RMS emittance and emittances including 99.9%and 100% particles have no obvious growth after applying the compensation with the RMS rematch in each section of the main linac. However, the compensation with the TraceWin code doesn't consider the phase change during the cavity resetting. A code based on MATLAB is under developing to compensate the arrival time at the matching point, and shows its effectiveness.

## INTRODUCTION

The extremely high reliability and availability are considered to be the most important characteristics for the C-ADS accelerator [1]. Besides all the hardware is operated with conservative performance and redundancy, it is also important to have fault-tolerant capabilities in the physics design [2, 3]. Anyway, no matter how we improve the hardware's reliability performance, it should be expected to meet some failures of important devices with a much lower frequency. The accelerator design has to deal with these situations. In the following, we will discuss how to compensate the failures of two kinds of major components: superconducting resonators and transverse focusing elements including solenoids and quadrupoles.

## LOCAL COMPENSATION FOR RF CAVITY FAILURES

Several factors may cause the failures of RF cavities: RF power source, coupler, LLRF, cavity mechanic tuning, etc. If a cavity fails and nothing is done, the whole or part of the beam may be lost in the downstream linac. The reason is that the phase slip caused by the velocity change will make the beam center phase to exceed the longitudinal acceptance of the downstream acceleration section. The best way to deal with this kind of failures is to readjust the setting of the neighbouring cavities to regain the nominal velocity, and to rematch the transverse focusing at the same time as the RF cavities also affect the transverse focusing. At SNS, it is the usual operation to adjust some downstream SC cavities when one fails. However, it takes some minutes to make the adjustment and the beam should be cut off during the tuning. For C-ADS, the beam stop time should be controlled within a few seconds and it is better to make the compensation by just involving only a few neighbouring cavities. In this way, more cavity failures in different locations can be compensated independently and efficiently [4].

### *Compensation in the Spoke021 Section*

As mentioned above, the cavity failure may lead to beam loss especially in the low energy section. Taking the cavity failure in the Spoke021 section as an example, the local compensation method for the failure of the first cavity in the Spoke021 section is shown in Fig.1, two bunchers in the MEBT2 [5]are used to rematch, and they can be adjusted together with the other neighbouring cavities.

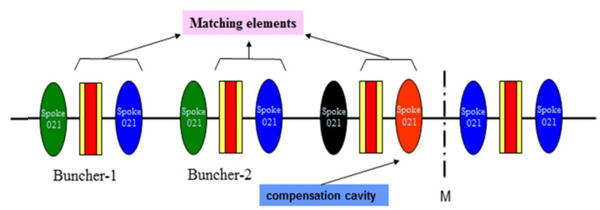


Figure 1: Local compensation method (The blue ellipses stand for cavity, the red squares for solenoids, the black ellipse for the failed cavity, the orange ellipse for major compensation cavity and M stands for the matching point).

If nothing is done for the cavity failure, the large phase slip will lead to beam loss and phase oscillation in both transverse and longitudinal planes (see Fig. 2).

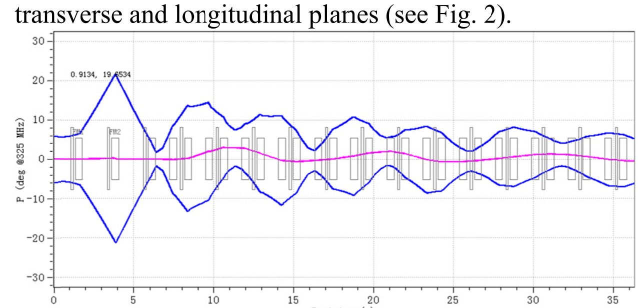


Figure 2: Longitudinal envelope evolution after the cavity failure.

Meanwhile, the beam halo emittance growths are evident in both the longitudinal and transverse planes, as shown in Fig. 3. As the field of the first cavity is quite low, about 0.66 of the nominal value due to the limitation of 90° phase advance in the longitudinal plane, we can compensate the failure by changing the voltage of the second cavity in the same cell and the synchronous phase of the bunchers in MEBT2 from -90° to -70° (see Table 1).



ISBN 978-3-95450-118-2

# PHYSICS DESIGN FOR THE C-ADS MAIN LINAC BASED ON TWO DIFFERENT INJECTOR DESIGN SCHEMES*

Fang Yan, Zhihui Li, Cai Meng, Jingyu Tang,
Institute of High Energy Physics, Chinese Academy of Science, Beijing, 100049, China

*Abstract*

The China ADS (C-ADS) project is proposed to build a 1000-MW Accelerator Driven sub-critical System around 2032. The accelerator will work in CW mode with 10 mA in beam current and 1.5 GeV in final beam energy. The linac is composed of two major sections: the injector section and the main linac section. There are two different schemes for the injector section. The Injector-I scheme is based on a 325-MHz RFQ and superconducting spoke cavities of same RF frequency and the Injector-II scheme is based on a 162.5-MHz RFQ and superconducting HWR cavities of same frequency. The two different designs for the main linac have been studied according to the different beam characteristics from the injector designs.

## INTRODUCTION

The China ADS project is proposed to build a 1000-MW Accelerator Driven sub-critical System around 2032. The driver accelerator will work in CW mode, with a beam of 1.5 GeV in final energy and 10 mA in beam current. The C-ADS linac includes two major sections: the injector section and the main linac section. According to the very strict requirements of high reliability and availability for the ADS application [1], the C-ADS linac adopts two parallel injectors design, with one as the hot-spare of the other. Another redundancy or fault-tolerance design is the application of the so-called local compensation method in the main linac part which allows failures of key components such as cavities and focusing elements. The injectors accelerate the proton up to 10 MeV and the main linac boost the energy from 10 MeV up to 1.5 GeV, and a section of beam line named MEBT2 [2] is applied to transfer and match the beam from the two injectors to the main linac. The general layout of the linac is shown in Figure 1.

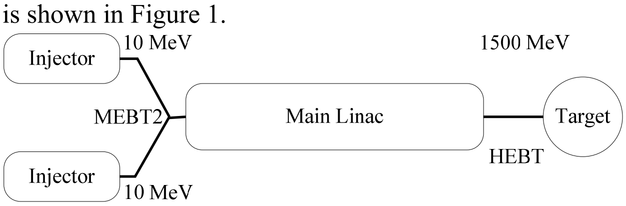


Figure 1: Layout of the C-ADS linac.

At present, two different design schemes for the injectors are proposed [3, 4], with Scheme I based on 325 MHz and Scheme II based on 162.5 MHz. For both design schemes, the injector is composed of an ECR ion source, a LEBT, a RFQ, a MEBT1 and a superconducting section. There will be a matching section – MEBT2 to transfer the beam from any of the two injectors to the main linac. The beam parameters at the exit of the injectors for the two schemes are listed in Table 1.

Table 1: Beam Parameters at the Exit of the Injectors

| Parameters | Scheme I | Scheme II |
|---|---|---|
| Frequency /MHz | 325.0 | 162.5 |
| α /x/y/z | -1.21/-1.19/0.10 | -0.34/-0.37/0.27 |
| β /x/y/z / mm/pi.mrad | 2.43/2.34/1.03 | 0.82/0.84/2.08 |
| $\varepsilon_t$ /mm.mrad | 0.20 | 0.32 |
| $\varepsilon_l$ /mm.mrad | 0.17 | 0.37 |

The beam parameters at the exit of the two injector design schemes are quite different. The difference on the Twiss parameters is not so important for the design of the main linac, since the MEBT2 will match the beam to the main linac. But the differences on bunch frequency and emittances will affect the structure of the main linac significantly. With same beam current, the different bunch frequency means different bunch intensity and different space charge effect. This will ask for different lattice structures to obtain a stable beam dynamics design. The frequency jump in the front of the main linac will ask for a larger longitudinal acceptance and cause potential troubles in longitudinal beam dynamics. The different emittance means difference in the acceptance and in the ratio of longitudinal and transverse phase advances. This paper will present the design considerations of the main linac based on two injector design schemes.

## GENERAL CONSIDERATIONS ON THE MAIN LINAC DESIGN

In order to satisfy the rigorous demands on the accelerator stability and reliability, over-design, redundancy and fault tolerance strategies are implemented in the basic design. The fault tolerant design in the main linac is guaranteed by means of the local compensation and rematch method [5], which is effective only for a linac composed of short independently powered cavities. To cover the whole energy range of from 10 MeV to 1.5 GeV in the main linac section, we need at least four types of superconducting cavities. After optimization, we have chosen two single-spoke cavities working at 325 MHz with geometry betas of 0.21 and 0.40, respectively, and two 5-cell elliptical cavities working at 650 MHz with geometry betas of 0.63 and 0.82, respectively. The acceleration efficiencies of the four cavities and their effective energy ranges are shown in Figure 2. The effective energy ranges for the four types of cavities are all shifted to the lower energy to accommodate the special phase advance law required by the stable beam dynamics. The parameters of the cavities are listed in Table 2. For

*Work supported by Advanced Research Project of CAS
# yanfang@ihep.ac.cn



ISBN 978-3-95450-118-2

# RADIATION SAFETY SYSTEM FOR PKUNIFTY PROJECT *

J. Zhao#, W.W.Wen, Q.F. Zhou, H.Li , Y.R. Lu, S.X. Peng, Z.Y. Guo, J.E. Chen
State Key Lab of Nuclear Physics and Technology, Peking University, Beijing, P.R.China

*Abstract*

PKUNIFTY (Peking University Neutron Imaging FaciliTY) , which is based on a 2 MeV RFQ accelerator-driven compact neutron sourse with an expected fast-neutron yield of $2.9*10^{12}$n/s via the deuteron-beryllium reaction, has been operated this year. A radiation safety system for PKUNIFTY, that protects personnel from radiation hazards has been built and run since last year, is described. It consists of a shielding optimized with Monte-Carlo simulation, a dose interlock system, an alternative interlock with another 4.5MV tandem accelerator facility, and a video monitoring system. The dose of supervision area is less than 0.5μSv/h during beam operation.

## INTRODUCTION

A thermal neutron imaging facility, Peking University Neutron Imaging FaciliTY (PKUNIFTY), which is based on a compact accelerator-driven neutron source, has been constructed and operated in Peking University this year[1]. A total view is shown in Fig.1. It consists of a $D^+$ ion injector, a 201.5 MHz mini-vane four-rod radio frequency quadruples (RFQ) accelerator and a high energy beam transport (HEBT). The accelerated $D^+$ ions are used to produce neutrons by D-Be reaction. The deuteron beam energy is designed as 2MeV and the rated average beam current is 4mA, which gives a fast neutron yield of $2.9*10^{12}$ n/cm2/s [2]. In addition, the Be(d,n) reaction gives a high γ yield.

The purpose of the radiation safety system of the PKUNIFTY is to protect personnel from neutron and γ radiation hazards. It consists of a shielding optimized with Monte-Carlo simulation, a dose interlock system, an alternative interlock with another 4.5MV tandem accelerator facility, and a video monitoring system. The dose interlock system protects operators from strong radiation. It prevents the application of high voltage power supply for the extraction of D+ ion source unless the door to interlocked area is closed and secure. The video monitoring system provides an additional safety measure. Operators in the control room can monitor the beam line area visually. When they find any exception of human accesses, they can shut down the facility manually.

This paper describes in detail the shielding design of PKUNIFTY, dose interlock system, and alternative interlock with another accelerator facility.

## SHIELDING DESIGN

The RFQ accelerator and the target of PKUNIFTY were installed together in an existing neutron experiment hall, of which the wall is made of 1.5m thick concrete. And a lot of electronic devices of the accelerator were installed beside the beam line. The shielding should protect these devices from radiation damages. The reference [3] shows some ordinary electronic devices can work properly when the device's cumulative fast neutron flux below $10^{11}$-$10^{12}$ n/cm$^2$ and cumulative γ dose below $10^3$ Gy. We designed the shield as summing our electronic devices can work in the similar situation.

Consider a simplified model, in which the moderator and reflector are surrounded by a layer of lead and a layer of boron doped PE, the ion beam tube and collimator are omitted, Monte-Carlo simulations of the shielding configuration indicate that an inner 8cm thick lead layer in conjunction with an outer 42cm thick boron doped PE layer is adequate for radiation protection. In this case the neutron flux will be attenuated by an order of magnitude of $10^{-9}$, and the γ-ray dosage out side the shielding will be less than 1mSv/h. With 250 working days the dose is much lower than 1mSv, which is the dose limit for public

Figure 1: A total view of PKUNIFTY

*Work supported by NSFC 10735020 and NBRP No.2010CB833106
# zj@pku.edu.cn



ISBN 978-3-95450-118-2

# DESIGN OF THE MEBT1 FOR C-ADS INJECTOR II

Huan Jia#, Youjin Yuan, Mingtao Song, Yuan He, Cheng Luo, Xiang Zhang, Shichun Huang
Institute of Modern Physics, CAS, China

*Abstract*

The MEBT1 of Chinese ADS Injector II[1] is described. It transports a 2.1MeV, 10mA CW proton beam through a series of 7 quadrupoles and two buncher cavities from the RFQ to the superconducting (SC) DTL. For emittance preservation, a compact mechanical design is required. Details of the beam dynamics and mechanical design will be given.

## INTRODUCTION

The Chinese ADS project is planned to have a 10mA, 1.5GeV CW proton beam for nuclear waste transmutation. Superconducting linac is the major choice in the case. As one of the demonstration of the techniques for C-ADS linac, the Injector II with energy up to about 10MeV is being constructed in IMP independently [1].

A proton ion source provides a 35KeV beam that is matched with a two solenoid LEBT into a 4 meter-long 162.5MHz RFQ and transported by 2.7 meter-long MEBT1 to the first solenoid inside the first cryomodule. The beam will then be accelerated to 10MeV by 16 162.5MHz SC HWR cavities in two cryomodules. The beam will be matched from RFQ into the acceptance of DTL by MEBT1.

In addition, diagnostic devices are supplied to monitor the beam quality during operation and to enable tuning of the MEBT1 itself.

## BEAM DYNAMICS

Due to the requirement of CW operation mode at 10mA, MEBT1 obeys the following design principles [2].

a) minimum beam loss
b) avoiding too large or too small envelope
c) phase space matching and emittance control
d) sufficient beam diagnostic devices
e) scraping beam halo
f) performance/cost evaluation

The major consideration in designing MEBT1 is to reduce the emittance growth. In a high current machine, the emittance growth is normally caused by linear and/or nonlinear coupling or strong space charge effects. In MEBT1, 4 quadrupoles (Q1-4) lie upstream to form an approximately symmetric beam. And 3 quadrupoles (Q5-7) lie downstream to form a symmetric waist in front of the SC DTL. The solenoids in crymodules require symmetric input beam to reduce emittance growth due to coupling of horizontal and vertical motion.

Two bunchers are used to match longitudinal twiss parameters. Room temperature quarter-wave-cavity (QWR) is employed as buncher.

Beam diagnostic box lies between Q4 and Q5, measuring the emittance and bunch length. BPM, wire scanner and scraper are distributed between the quadrupoles in MEBT1.The mechanical layout of the MEBT1 is shown in Fig. 1.

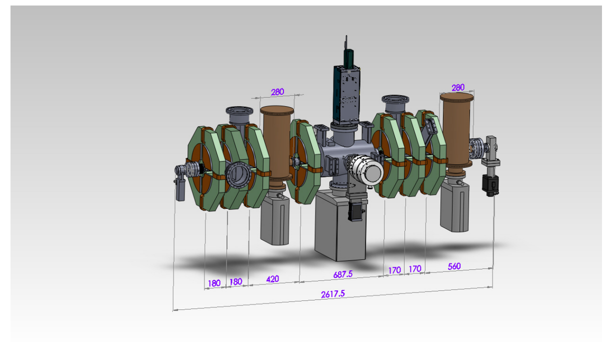


Figure 1: Mechanical layout of the MEBT1.

Figure 2 shows the trace3D simulation of the MEBT1, with beam transversal and phase spread envelopes(1.5cm and 90 degree full scale). The initial emittances are 5$\varepsilon_{rms}$ [3].

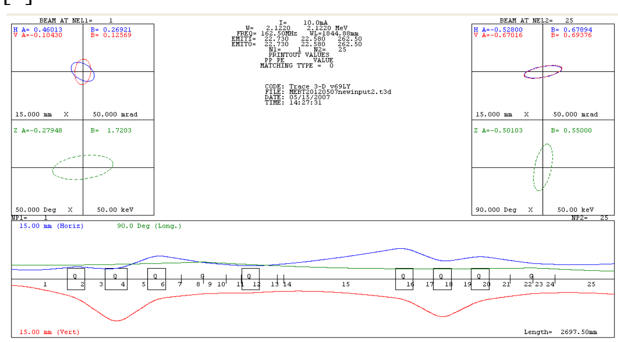

Figure 2: Beam envelopes in MEBT1 by Trace3D.

### *PIC Simulation*

The PIC simulation of MEBT1 with space charge effect is done by Track code, employing the beam distribution from RFQ by Parmteqm, the 3D magnetic field distribution of quadrupoles from Opera and the electro-magnetic RF field of bunchers from CST. For inspection of the field leakage between adjacent quadrupoles, 3 quadrupoles are calculated together. The simulation result is shown in Fig. 3.

The PIC simulation results shows that rms emittance growth in MEBT1 is below 3%. Table 1 shows the normalized rms emittance before and after MEBT1 by Track.

To optimize the matching between MEBT1 and SC DTL, the acceptance of SC DTL section[4] is compared with the emittance at MEBT1 exit. Figure 4 shows that the emittance and acceptance are well matched.

*jiahuan@impcas.ac.cn

ISBN 978-3-95450-118-2

# STUDY OF NON-EQUI-PARTITIONING LATTICE SETTINGS AND IBS EFFECTS FOR J-PARC LINAC UPGRADE

Y. Liu[#], M. Ikegami, KEK/J-PARC, Tokai, Japan

*Abstract*

For the upgrade of J-PARC LINAC from 190MeV to 400MeV the annular coupled structure (ACS) was applied with frequency jump from 324MHz to 972MHz. Equi-partitioning (T=Tx/Tz=1) and envelope-keeping lattices (T=0.3) are studied for the structure and frequency transition. IBS loss rate at this ~110m part is as high as $4\times10^{-5}$ for EP setting, which can be mitigate to 1/3 with non-EP setting with T=0.3. But at the same time obvious emittance exchange were found. The transverse emittance increases by 50%, with no particle loss found in million-macro-particle simulation. The present work is enough to show the problem and possible directions for the solutions.

## INTRODUCTION

For the coming upgrade of J-PARC[1], the power of linac will be greatly increased. This may open many interesting questions. For instance, for efficient acceleration from 190MeV to 400MeV the annular coupled structure (ACS) was applied with frequency jump from 324MHz to 972MHz. Upstream part of J-PARC linac before frequency jump is set with the equi-partitioning (EP) condition [2], which prevents from the coherent resonances. If EP condition is kept for the downstream part, due to the frequency jump, the transverse focusing should also "jump" with shrink of envelop. This affects the interactions between particles, including the intra-beam stripping (IBS) effect [3] in the H- beam by increasing the loss rate.

In order to clarify the "reciprocal" relation between EP-keeping and IBS loss mitigating here, the temperature ratio between transverse and longitudinal planes, the T ratio, is used as a knob to explore the lattice parameter space.

In this paper T-ratio is defined as "Tx" over "Tz", which is convenient because the longitudinal lattice is normally already decided by the best acceleration efficiency.

Two examples are studied with T ratio of 1 and 0.3, i.e. keeping the EP condition or keeping the transverse envelop. The latter shows mitigation of IBS loss rate per unit length to 1/3, from 0.13W/m to 0.043W/m at the design duty cycle of 2.5%, while the simulation shows obvious emittance exchange from longitudinal plane to transverse ones at the upgraded peak current of 50mA.

Lattice Studies

The settings of transverse-longitudinal EP and EP-like lattice are obtained with smooth approximation with axis symmetry (2D). With given longitudinal phase advance, rms matching conditions at both planes and the given T ratio, the envelope of both planes and transverse phase advance are solved, for the 72 DTL cells (38, 21,13 for DTL 1-3), 32 SDTL cells and 42 ACS cells.

Normalized emittance $\varepsilon_x$=0.21, $\varepsilon_z$=0.30 π mm mrad, peak current of 50mA are applied in the calculation, based on the new RFQ design (J-PARC RFQ3).

The settings are done with T=$T_x/T_z$ ranged from 0.2 to 2, according to about 60% and 130% of the quadrupole gradient for T=1. The results are shown in Fig.1, on the tune diagram (Hofmann Chart) for $\varepsilon_x/\varepsilon_z$=0.7.

Settings for weaker focusing for upstream DTL and SDTL cells are not shown due to aperture limit for the practical usage.

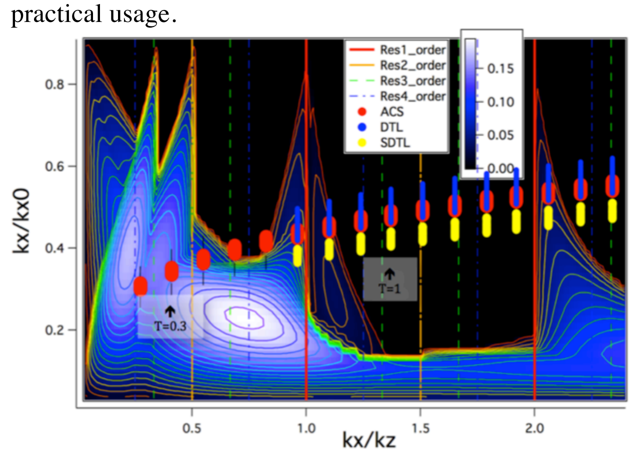


Figure 1: Analytical results of lattice exploring for J-PARC LINAC, on tune diagram for $\varepsilon_x/\varepsilon_z$ = 0.7, T-ratio ranged 0.2-2.0.

The envelope calculated for different T for ACS part is shown in Fig. 2, for choosing envelope transition for the frequency jump.

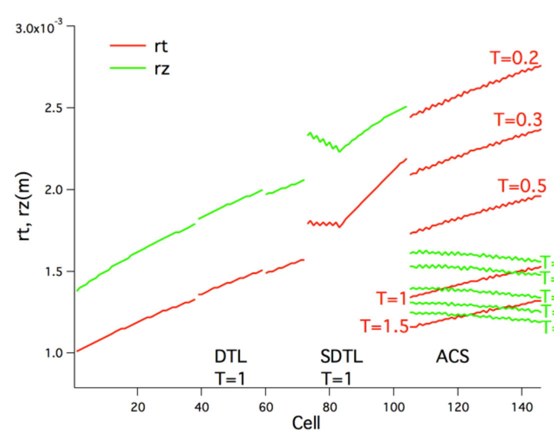


Figure 2: Transverse and longitudinal envelope for EP and EP-like settings, with smooth approximation.

The calculation for the lattice setting using smooth approximation is verified with envelope calculations with linear transfer maps with periodical matching with and



ISBN 978-3-95450-118-2

# OPTIMIZATION OF THE SUPERCONDUCTION SECTION OF INJECTOR II FOR C-ADS*

Shuhui Liu, Zhijun Wang, Yuan He, Insititute of Modern Physics, China

*Abstract*

The China Accelerator Driven System (C-ADS) project which includes a high current SC proton linac is being studied under Chinese Academy of Science [1]. Injector II, one of parallel injectors, is undertaken by Institute of Modern Physics (IMP). The lattice design of Injector II has been done. While in most case, the elements, such as SC cavities and SC solenoids, have different weight to the final beam parameters. What is more, in the real operation process of the machine, the optimized mode is hard to find. In the paper, Latin sampling method specified in DAKOTA code combined with TRACK [2] is adopted to build hundreds of virtual machines to analyse the sensitivity of the SC section and to find optimization operation mode.

## INTRODUCTION

C-ADS project, which is a strategic way to solve the nuclear waste problem and the resource problem in China energy development, is being studied in CAS. It aims to accelerate a 10mA proton beam up to 1.5GeV. It operates in a continuous wave mode (CW). Injector II is under design and built by IMP. Injector II consists of ion source, LEBT, RFQ, MEBT and superconducting accelerating section. The layout of the Injector II is shown in the Figure 1.

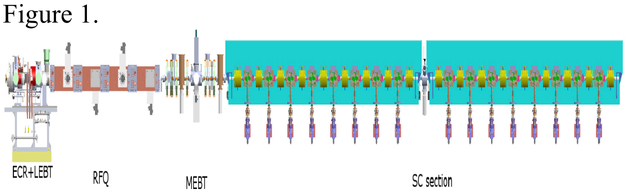


Figure1: Layout of the Injector II.

## BEAM DYNAMICS OF SUPERCONDUCTING SECTION

The SC accelerating section in injector II will accelerate proton from 2.1MeV to 10MeV. In a present work, the design of the superconducting option, using low-$\beta$ half-wave resonators (HWR) at 162.5 MHz has been investigated. There are sixteen cavities and eighteen solenoids included in the superconducting section separated by two cryomodules. Figure 2 shows the lattice structure of superconducting section. The main parameters of the design results are listed in Table1.

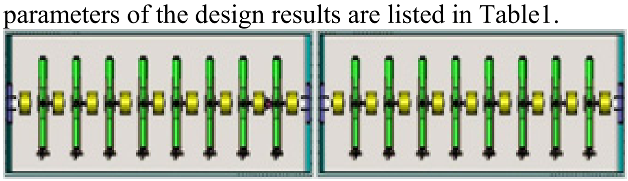

Figure 2: Lattice structure of superconducting section.

Table1: The Main Parameters of the Design Results

| Parameters | Value | Unit |
|---|---|---|
| Particle type | proton | |
| Operation frequency | 162.5 | MHz |
| Beam current | 10 | mA |
| Beam kinetic energy | 10 | MeV |
| Growth of RMS $\varepsilon$ t | 1.7 | % |
| Growth of RMS $\varepsilon$ l | 4 | % |
| Number of cavities | 16 | |
| Number of solenoids | 18 | |

The beam dynamic simulation of superconducting section has been done. In the simulation, the beam current is 10mA.The beam loss is not observed from simulation results.

### *The Phase Advance and the Envelope along the SC Section*

In the simulation, the phase advance should be as smooth as possible along the SC section in order to maintain the stability of beam. Figure 3 shows the phase advance at zero current in each focusing period.

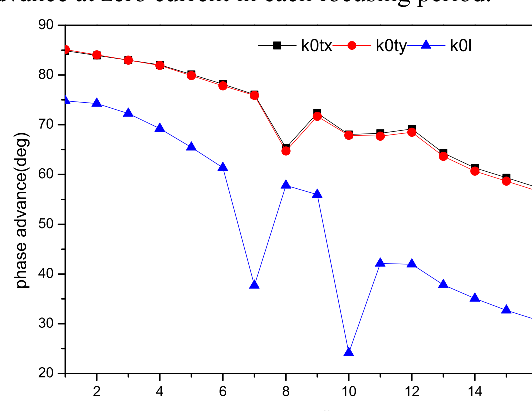


Figure3: Transverse and longitudinal phase advance of each period at zero current.

As can be seen from Figure 3, there are a few of jumps at the location of the transition section. This is because the matching between the two cryomodules. The cavities and solenoids next to the transition section are used as the matching element.

Figure 4 presents the beam envelope along the SC section. The smoothness of the envelope shows good match between the cryomodules.

*Work supported by National Science Foundation of China (Grant No.11079001)

ISBN 978-3-95450-118-2

# ERROR AND TOLERANCE STUDIES FOR INJECTOR II OF C-ADS

Wangsheng Wang, Yuan He, ZhiJun Wang, Insititute of Modern Physics, China

*Abstract*

The proposed Accelerator Driven System (ADS) driver linac is being designed in Institute of Modern Physics (IMP). The driver linac is designed to work at rf frequency 162.5MHz and accelerate proton to final beam energy of 10MeV/u. Because of the high final beam power (100 kW) specified for the linac operation, beam loss must be limited to avoid radiation damage. Misalignment and rf error analysis for cavities and focusing elements after RFQ were performed, and correction schemes developed using the computing code TRACK. The simulation results are presented, and the misalignment and rf error specifications are given for the ADS Linac.

## INTRODUCTION

Recent in these years the China Accelerator Driven System (C-ADS) is proposed and used for future fusion reactors. It is planned to build and test a demonstrator accelerator at full beam current 10mA at 10 MeV/u. In the initial stage, the two demonstrating front-ends operating in CW mode are being designed in IMP and IHEP independently. The front-end in IMP consistes of a ECR ion source (35KeV/u), a low energy beam transport (LEBT), a 162.5MHz 4-vane RFQ for bunching and pre-accelerating to 2.1MeV/u, a medium energy transport (MEBT), and the sc linac section (see Fig. 1). The MEBT, consisting of 7 quadrupoles and 2 bunchers, converts the beam output from RFQ to a symmetric beam in x and y directions in order to matching the sc linac. There are two cryomodules in the sc linac section based on independently phased superconducting (SC) 162.5MHz half-wave resonator cavities (HWR) and SC solenoids.

The error study simulations for the above front-end after RFQ are presently being performed in IMP. We present the results of the simulations performed with the ANL code TRACKV39. The code enables precise calculating of particle tracking, taking into account realistic 3D fields of the accelerating and focusing elements and also effects of space charge. We utilize the linux version of TRACKV39 to simultaneously run the simulations on 100 cpus of the cluster [1].

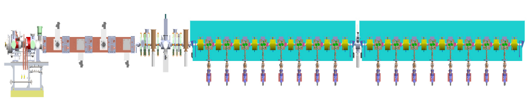


Figure 1: Layout of the C-ADS driver linac.

## ERROR STUDY STRATEGY

Before dealing the different types of error, it is important to remark that two families of errors have to be coped for [2]:

- static errors: the effect of these errors is detected and corrected. The strategy of the correction scheme is established to correct these errors (see below). For an error of amplitude A, the value has a uniform probability to be between −A and +A.
- dynamic errors: these errors are not corrected. They are induced by the vibrations of the RF field or mechanical vibrations from the environment. For an error of rms amplitude σ, a Gaussian distribution truncated at ±3σ is used for them.

The goal of the error study is two-fold: define the alignment and RF error tolerances of the linac, to be built in 2013, and examine the robustness of the linac design as a whole. The RFQ design has already been decided upon and the RFQ is now being built. The beam distribution used at the input of the MEBT accounts for the RFQ output, which has an energy of 2.1 MeV/u and its normalized RMS emittance is estimated to be $\varepsilon_x = \varepsilon_y =$ 0.32 mm.mrad and $\varepsilon_z$ = 0.31 mm.mrad. The average current over the RF pulse is 10 mA and this is the intensity used in the error study simulations as it is the meaningful value for space charge effects.

This analysis is done in two stages [3]. First, the sensitivity of the linac to one single error is determined in order to evaluate the individual contribution and fix an acceptable limit on each type of error. Then, all errors are combined simultaneously to verify the set of tolerances determined previously and estimate the overall degradation of the beam properties.

We have applied 5 possible alignment errors and 4 RF errors to any active element. The alignment errors are sketched in Fig. 2. They include transverse position errors which represent the distance between the centre of the element and the ideal centre of the beam line in the two transverse planes; and angle errors which represent the 3 angles between the ideal beam line reference and the reference system of the element. For magnets these values are referred to the magnetic centre i.e. they represent the 3 angles between the ideal beam line reference and the system in which the magnet is a perfect quadrupole.

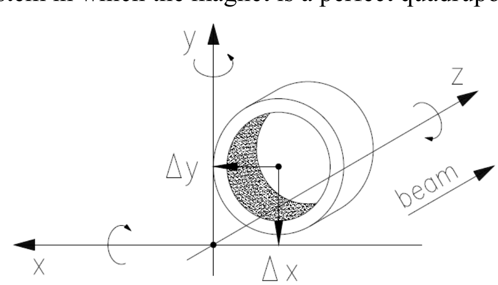


Figure 2: Sketch showing the alignment errors applied to the quadrupoles [4].

We have applied static/dynamic gradient errors to the focusing elements: they represent the percentage deviation from the nominal field. For cavities static/dynamic phase errors are also applied, in degrees.

ISBN 978-3-95450-118-2

# MEDIUM ENERGY BEAM TRANSPORT DESIGN UPDATE FOR ESS

I. Bustinduy*, O. González, A. Ghiglino, I. Rodríguez,
J.L. Muñoz, A. Zugazaga, F.J. Bermejo
ESS-Bilbao, Spain
R. Miyamoto, B. Cheymol, M. Eshraqui, J. Stovall
ESS, Sweden

*Abstract*

The major challenge of this part of the accelerator is to keep a high quality beam, with a pulse well defined in time, a low emittance and a minimized halo, so that the beam losses downstream the linac be limited and the overall ESS reliability be maximized. In order to minimize beam loss at high energy linac, and the consequent activation of components, a fast chopping scheme is presented for the medium energy beam transport section (MEBT). The considered versatile MEBT is being designed to achieve four main goals: First, to contain a fast chopper and its correspondent beam dump, that could serve in the commissioning as well as in the ramp up phases. Second, to serve as a halo scraping section by means of various adjustable blades. Third, to measure the beam phase and profile between the RFQ and the DTL, along with other beam monitors. And finally, to match the RFQ output beam characteristics to the DTL input both transversally and longitudinally. For this purpose a set of ten quadrupoles is used to match the beam characteristics transversally, combined with three 352.2 MHz *buncher* cavities, which are used to adjust the beam in order to fulfill the required longitudinal parameters.

## INTRODUCTION

Along the different designs for high-intensity linear accelerators, the MEBT emerges as one of the critical stretches through the accelerator in terms of losses, emittance increase and halo formation. With the purpose of minimizing emittance growth along this section due to the effects of spatial charge, at least the following two conditions must be satisfied: supplying a solid cross focalization and avoiding sharp changes in focalization strength. To this end, a compact quadrupole with a length of 70 mm is being designed. In addition, some of these quadrupoles, whose field gradients vary between 9 and 30 T/m, are expected to incorporate correcting dipoles in order to minimize any beam misalignments (see Table 1).

Table 1: MEBT Operation Parameters

| Parameter | Value |
|---|---|
| Input Energy | 3 MeV ($\beta$ =0,0798) |
| Total Current | 50 mA |
| Particle | protons ($H^+$) |
| Number de quadrupoles | 10 |
| Min./Max quadrupole gradients | 9–30 T/m |
| Number of *buncher* cavities | 3 |
| Frequency | 352.2 MHz |
| Peak power per cavity | 14 kW |
| Effective Voltage (EoTL) | 150 kV |

## LAYOUT

The layout (Fig. 1) is being designed to achieve four main goals: First, to contain a fast chopper and its correspondent beam dump, that could serve in the commissioning as well as in the ramp up phases. Second, to serve as a halo scraping section by means of various adjustable blades. Third, to measure the beam phase and profile between the RFQ and the DTL, along with other beam monitors. Finally, to match the RFQ output beam characteristics to the DTL input both transversally and longitudinally. Figure 3 shows the realistic RFQ output distribution used in the simulations, the emittance increase along the MEBT, obtained with TRACEWIN, prior to any collimation scheme is $\Delta\epsilon_{xx'}$=17.2%, $\Delta\epsilon_{yy'}$=14.8%, $\Delta\epsilon_{zz'}= - 1.5\%$; keeping the halo parameter <1.4 for all planes (see Fig. 2); with a negligible 0.05% of cumulative losses along the line. When the collimation scheme is applied $\Delta\epsilon_{xx'}$=14.1%, $\Delta\epsilon_{yy'}$=10%, $\Delta\epsilon_{zz'}=-1.8\%$, while cumulative losses stay below an acceptable 1.3%.

The presented layout *S0Q10R3C4*[1] constitutes a relatively compact design (∼3600 mm). It comprises a fast chopper structure, beam dump and provides the separation for the required diagnostics. Similarly to CERN, J-PARC and SNS designs, this fast chopper complements to the LEBT pre-chopper, and will be used to sharpen the beam edges produced by the slow-chopper during rising and falling times (∼10 ns). Eliminating thus, the partially chopped beam that passes through the RFQ [1]. Fundamentally, the chopping structure is based on the Linac4 design. It consists of an electrostatic traveling wave deflector together with a beam dump for dissipating the sectioned beam current, with the goal of reducing beam losses that will occur at higher energies.

* ibon.bustinduy@essbilbao.org

[1] 0 solenoids, 10 quads, 3 bunchers, 4 collimators



ISBN 978-3-95450-118-2

# BEAM POSITION MONITOR SYSTEM OF THE ESS LINAC

H. Hassanzadegan, A. Jansson, A. J. Johansson
European Spallation Source ESS AB, Lund, Sweden

*Abstract*

The pulsed ESS Linac will include about 100 BPMs, mostly with a European XFEL style button design, 6 BPMs with a special design for the Medium Energy Beam Transport, as well as 8 compact-size BPMs foreseen for the Drift Tubes. The required accuracy and resolution of the position measurement are 100 µm (rms) and 20 µm (rms) respectively with the 50 mA 2.86 ms nominal pulse. In addition to the position measurement, the BPM system needs to measure the beam phase in the nominal pulse as well as several diagnostics pulse modes with a minimum duration and intensity of 5 µs and 5 mA respectively. After a study of the possible electronics platforms, MTCA.4 is now considered as the main prototyping platform for the high performance sub-systems at ESS. It is foreseen to prototype a Rear Transition Module for IQ-based RF signal measurements intended for both the BPM and LLRF systems. The requirements and specifications of the BPM system are presented and the plan for the continuation of the project is described in this paper.

## INTRODUCTION

The 352.21 MHz and 704.42 MHz pulsed ESS Linac will include in total about 140 BPMs of various types. In addition to the transversal beam position, the BPMs shall be able to measure the beam phase for energy calculations based on time-of-flight measurements. Furthermore, the BPM system needs to measure the beam position and phase in several diagnostics pulse modes with a minimum duration and intensity of 5 µs and 5 mA respectively. Table 1 summarizes the main specifications of the BPM system.

Table 1: Main BPM System Specifications

| Parameter | Value | Unit |
|---|---|---|
| Position measurement accuracy | 100 | µm (rms) |
| Position measurement resolution | 20 | µm (rms) |
| Phase measurement accuracy | 1 | ° (rms) |
| Phase measurement resolution | 0.2 | ° (rms) |
| Phase measurement range | ±180 | ° |
| Measurement range (w.r.t. beam pipe) | 50 | % |
| Electronics response time | < 1 | µs |
| ADC sample rate | 10-100 | MSPS |
| Refresh rate (end user) | 14 | Hz |

It is planned to use a single type of electronics for all the BPMs. Therefore, the design of the front-end electronics should be flexible so that it can be adapted to all types of the BPM detectors through minor modifications. The electronics should have a large dynamic range and a high bandwidth, so that the BPM system gives useful results, even when the pulse amplitude and duration are decreased to minimum values.

The BPM front-end will include a fast analogue front-end, where the BPM signals are picked up by some sensitive electronics, level-adjusted, down-converted (to be confirmed), filtered and conditioned. The signals are then digitized and fed into an FPGA for position, phase and intensity calculations, linearization, memory read/write etc. The BPM electronics will be integrated into the future EPICS control system.

## CONCEPT

Following a study of the available electronics platforms and as part of an electronics standardization strategy, MTCA.4 is considered as the main candidate for the high performance electronics at ESS, including the BPM and LLRF systems. The main reasons for choosing MTCA.4 against other platforms include: timing and synchronization resources, possibility of using a Rear Transition Module (RTM), high redundancy/availability and future support. Figure 1 shows a simplified schematic view of the BPM system, which is currently being prototyped at ESS. The induced voltages on the buttons are transferred by four coaxial cables to the MTCA.4 crate, to be located in the future ESS Klystron gallery. The crate houses several electronic modules such as a RTM performing the required analogue signal processing, a digital board for ADC sampling and digital signal processing, a CPU running under Linux where EPICS drivers for the electronic cards will be installed, a MicroTCA Carrier Hub (MCH) managing the crate and handling the interconnection among the modules, a timing module providing the required timing and synchronization signals and finally, the infrastructure modules such as power and cooling.

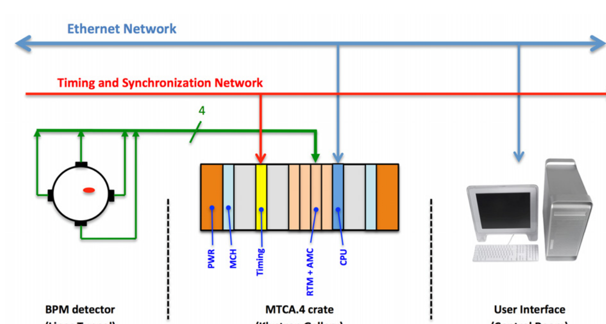


Figure 1: Simplified schematic of the BPM system including the detector, MTCA.4 crate and the terminal.



ISBN 978-3-95450-118-2

# HIGH ENERGY TESTS OF ADVANCED MATERIALS FOR BEAM INTERCEPTING DEVICES AT CERN HIRADMAT FACILITY

A. Bertarelli, R. Assmann, E. Berthome, V. Boccone, F. Carra, F. Cerutti, A. Dallocchio, S.D.M. Dos Santos, P. Francon, L. Gentini, M. Guinchard, N. Mariani, A. Masi, P. Moyret, S. Redaelli, CERN, Geneva, Switzerland
L. Peroni, M. Scapin, Politecnico di Torino, Turin, Italy

*Abstract*

Predicting by simulations the consequences of LHC particle beams hitting Collimators and other Beam Intercepting Devices (BID) is a fundamental issue for machine protection: this can be done by resorting to highly non-linear numerical tools (Hydrocodes). In order to produce accurate results, these codes require reliable material models that, at the extreme conditions generated by a beam impact, are either imprecise or non-existent.

To validate relevant constitutive models or, when unavailable, derive new ones, a comprehensive experimental test foreseeing intense particle beam impacts on six different materials, either already used for present BID or under development for future applications, is being prepared at CERN HiRadMat facility.

Tests will be run at medium and high intensity using the SPS proton beam (440 GeV). Material characterization will be carried out mostly in real time relying on embarked instrumentation (strain gauges, microphones, temperature and pressure sensors) and on remote acquisition devices (Laser Doppler Vibrometer and High-Speed Camera). Detailed post-irradiation analyses are also foreseen after the cool down of the irradiated materials.

## THERMALLY INDUCED DYNAMIC PHENOMENA

The interaction of energetic particle beams with matter provokes dynamic responses in the impacted element [1]. Several parameters can affect intensity and time scale of the response: deposited energy, maximum energy density, interaction duration and strength of the impacted material are the principal ones.

Three regimes are identified at increasing deposited energy, namely Elastic Stress Waves, Plastic Stress Waves and Shock Waves.

### *Elastic Wave Regime*

- Waves propagate at elastic sound speed
- Negligible change of density
- Can be treated with implicit FEM codes [2] and with analytical tools [3]

### *Plastic Wave Regime*

- Wave velocity lower than elastic sound speed
- Limited change of density
- Can be treated with implicit FEM codes [4]

### *Shock Wave Regime*

- Shock waves appear above a critical pressure
- Waves propagate at velocity higher than elastic sound speed
- Significant change of density
- Special explicit, non-linear numerical tools required: Hydrocodes

## HYDROCODES

As opposed to a standard, implicit FEM code, hydrocodes usually rely on complex material constitutive models, able to encompass a much larger range of densities and temperatures, including changes of phase. Strength and failure models are also more complicated, as they take into account effects of strain rate, temperature, density change etc.

### *Equations of State*

An Equation of State (EOS) is integrated in the hydrocode to model the behaviour of materials under any state and condition. It provides the evolution of pressure as a function of density, temperature and internal energy. Most used analytical EOS are Shock, Tillotson and Mie-Gruneisen, however their application is limited since analytical modelling can describe only a single phase region of the EOS [5].

### *Strength Models*

To model the behaviour of materials in the extreme conditions due to shock wave propagation, an advanced yielding criterion is needed. The model must take into account, in addition to strain, the strain rate and the temperature. Most used models are Johnson-Cook [6], Steinberg-Guinan [7] and Johnson-Holmquist [8].

### *Failure Models*

On the same basis, dynamic failure models must take into account many factors such as strain, strain rate, temperature, maximum and minimum pressure, fracture toughness. In addition, failure criteria also depend on the type of failure and on the mesh used for the simulation.

## NUMERICAL SIMULATIONS OF ENERGY BEAM IMPACTS

Analyses methods for complex components under extreme conditions have been developed in recent years at CERN and Politecnico di Torino, partly in the frame of the European Collaboration for Accelerator Research and



ISBN 978-3-95450-118-2

# AN EXPERIMENT ON HYDRODYNAMIC TUNNELLING OF THE SPS HIGH INTENSITY PROTON BEAM AT THE HiRadMat FACILITY

J. Blanco Sancho, CERN-AB, Geneva, Switzerland and
Ecole Polytechnique Federale de Lausanne, Lausanne, Switzerland
F. Burkart, N. Charitonidis, I. Efthymiopoulos, D. Grenier, C. Maglioni,
R. Schmidt, C. Theis, D. Wollmann, CERN-AB, Geneva, Switzerland
E. Griesmayer, CIVIDEC Instrumentation, Wien
N.A. Tahir, GSI, Darmstadt, Germany

*Abstract*

The Large Hadron Collider (LHC) and the future linear colliders operate with very high energy stored in the beams (in the order of several hundred MJoules for LHC) or very high power (for linear colliders). Beam sizes are small, for the LHC down to 10 µm, for linear colliders below one µm. It is important to understand the damage potential of such high energy beams to accelerator equipment and surroundings. What are the consequences of a full LHC beam impact in material, e.g. in case the extraction kickers for the beam dump would deflect the beam with wrong angle?

Simulations have shown that in case of an impact of the full LHC beam onto a solid copper target the beams can penetrate up to 35 m [1] as compared to 140 that is the typical penetration length for 7 TeV protons (hydrodynamic tunneling). For this simulation, a typical Gaussian transverse intensity distribution with $\sigma = 0.2\,\mathrm{mm}$ was assumed. The total number of protons per beam is $3 \times 10^{14}$ that corresponds to an amount of energy of $362\,\mathrm{MJ}$, sufficient to melt $500\,\mathrm{kg}$ copper. Calculations of the impact of dense high intensity proton beams into material have been presented in several papers [1, 2, 3, 4].

How confident are we in these simulations? This paper introduces an experiment designed to reproduce the hydrodynamic tunneling effect that is predicted by simulations and describes the layout of the experiment and the instrumentation. The experiment was performed at the High Radiation to Materials (HiRadMat) facility at the CERN-SPS from the 22nd of June 2012 to the 12th of July 2012.

Results consistent with tunneling of protons in matter are presented. However, further analysis, new simulations with parameters similar to those in the experiment and post-mortem inspection are required to precisely evaluate the tunneling depth and propagation speed.

## MOTIVATION

Extensive simulation studies of the full impact of the ultra-relativistic proton beam generated by the Large Hadron Collider (LHC) on solid targets of different materials of interest have been carried out over the past years. The response of a solid copper cylindrical target that was facially irradiated by one LHC beam along the axis was simulated. These simulations were done using a two-dimensional hydrodynamic computer code, BIG2 [5]. The energy deposition of the 7 TeV/c protons in copper was calculated with the FLUKA code [6] assuming solid target density. This data was used as input to the BIG2 code. This study showed that the high pressure produced in the deposition region after energy deposition by only 100 proton bunches generated a radially outgoing shock wave that led to a substantial reduction in the density at the center. In practice, the protons in subsequent bunches will penetrate much deeper into the target. It was predicted that the LHC protons can penetrate between 10–40 m in solid copper.

The experimental verification of the numerical simulations is very important from the machine protection point of view. However, this is not possible with the LHC beam. Already in 2005, a beam impact experiment [7] was performed in the CERN-SPS TT40 extraction line. Up to $8 \times 10^{12}$ protons were shot onto a target and the onset of damage was measured. FLUKA simulations and experimental observations agreed, however these results cannot be extrapolated to LHC regime since the beam intensity was far below the onset of hydrodynamic tunneling.

For this purpose, an experiment was performed at an experimental facility named HiRadMat [8] (High Radiation Materials). To assist designing of suitable experiments, extensive numerical simulations of heating of solid copper cylinders using the SPS beam were performed [1]. Hydrodynamic tunneling effect is also clearly observed in these simulations. Confirmation of the existence of this phenomenon in the HiRadMat experiments will partially validate the simulations for the LHC beam.

The experimental main objective is to reproduce the hydrodynamic tunneling effect observed in simulations. Further objectives are to measure density, temperature and shock waves during the beam-target interaction. However, the success of the experiment was not linked to the operation of the detectors since a thorough investigation of the target after the experiment will show if there was hydrodynamic tunneling. The additional information gathered with the instrumentation will improve the understanding of the experiment.

## SPS-HIRADMAT

The HiRadMat facility is dedicated to beam shock impact experiments. It is designed to allow testing of acceler-

ISBN 978-3-95450-118-2

# EXPERIMENTAL VERIFICATION FOR A COLLIMATOR WITH IN-JAW BEAM POSITION MONITORS

D. Wollmann*, O. Aberle, R.W. Aßmann, A. Bertarelli, C. Boccard, R. Bruce, F. Burkart, M. Cauchi, A. Dallocchio, D. Deboy, M. Gasior, R. Jones, V. Kain, L. Lari, A. Nosych, S. Redaelli, A. Rossi, G. Valentino, CERN, Geneva, Switzerland

*Abstract*

At present the beam based alignment of the LHC collimators is performed by touching the beam halo with the two jaws of each device. This method requires dedicated fills at low intensities that are done infrequently because the procedure is time consuming. This limits the operational flexibility in particular in the case of changes of optics and orbit configuration in the experimental regions. The system performance relies on the machine reproducibility and regular loss maps to validate the settings. To overcome these limitations and to allow a continuous monitoring of the beam position at the collimators, a design with in-jaw beam position monitors was proposed and successfully tested with a mock-up collimator in the CERN-SPS. Extensive beam experiments allowed to determine the achievable accuracy of the jaw alignment for single and multi-turn operation. In this paper the results of these experiments are discussed. The measured alignment accuracy is compared to the accuracies achieved with the present collimators in the LHC.

## INTRODUCTION

To intercept unavoidable losses of particles from the beam halo into the superconducting magnets the LHC has a powerful collimation system with 44 moveable collimators per beam [1, 2, 3]. The beam-based alignment of the LHC collimators is performed by touching the beam halo with the two jaws of each device and recording beam losses with the beam loss monitor (BLM) installed at the device [4]. This requires dedicated fills at low intensities that are done infrequently because the procedure is time consuming [5]. The introduction of a semi-automatic set-up procedure and constant improvements in the algorithms allowed to significantly reduce the set-up time in 2011 and 2012 compared to the first manual set-up in 2010 [6, 7]. To guarantee the validity of the set-up and therefore a sufficient cleaning, strict requirements for long term orbit stability have to be fulfilled.

To overcome these limitations a new collimator design with in-jaw beam position monitors was proposed and preliminary beam tests were successfully carried out with a mock-up collimator in the CERN-SPS [8, 9]. A sketch of the mock-up jaw with the BPM buttons in the beginning (upstream) and end (downstream) of the jaw is depicted in Figure 1. Figure 2 shows one BPM button in the upstream taper of the jaw during laboratory measurements. A BPM-based alignment, where it is not necessary to touch the beam with the collimator jaws, would allow a fast and non destructive beam-based collimator set-up, which would reduce the need for special fills with intensity constraints. In addition it would allow to continuously monitor the beam offsets in the collimators with a much better resolution than currently possible with the standard LHC BPMs, as the distance between buttons and beam would be much smaller and there would be no need for interpolating the orbit from the closest BPMs. The collimators could follow orbit drifts without overhead and give, therefore, more flexibility for local orbit changes, which are regularly required around the experimental insertions. Furthermore, the margins between collimator families could possibly be reduced, which would eventually allow smaller beam sizes at the experimental IPs, which means an increased luminosity.

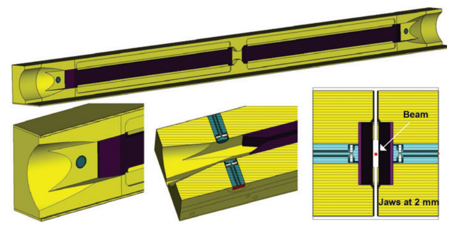


Figure 1: A view of a single jaw and cross-sections of the mock-up collimator with in-jaw BPM buttons [10].

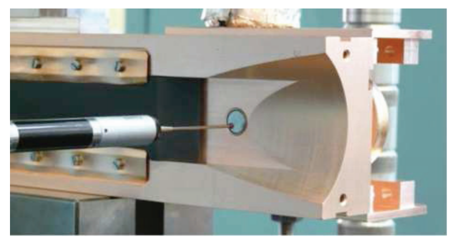

Figure 2: View of the BPM button in the taper at the beginning of the jaw during laboratory measurement of the button position [9].

Because of the promising results of the first beam tests in the SPS, presented in [8], an advanced mechanical design and a production prototype have been developed at CERN [11]. The first collimators with in-jaw beam position monitors will be installed in the period 2013-2014, when the LHC will not be operating because of upgrades and maintenance, into the experimental regions starting

* daniel.wollmann@cern.ch



ISBN 978-3-95450-118-2

# EXPERIMENTAL RESULTS OF BEAM HALO AT IHEP *

H.F. Ouyang#, J. Peng, T. Huang, J. Li, T.G. Xu, IHEP, CAS, Beijing 100049, China

*Abstract*

Space-charge forces acting in mismatched beams have been identified as a major cause of beam halo. In this paper, we describe the beam halo experimental results in a FODO beam line at IHEP. With this beam transport line, experiments are firstly carried out to determine the main beam parameters at the exit of a RFQ with intense beams, and then the measured beam profiles at different positions are compared with the multi-particle simulation profiles to study the formation of beam halo. The maximum measured amplitudes of the matched and mismatched beam profiles agreed well with simulations. Details of the experiment will be presented.

## INTRODUCTION

High-power and high-intensity proton beams are becoming more and more widely applied in the related fields such as neutron spallation source, accelerator driven sub-critical system (ADS) for transmutation of nuclear waste, etc. One of the important characteristics of high-intensity beams is the existence of halo and its hard unavoidability. Because the halo particles tend to be lost easily on the walls of the beam line structures and induce unwanted radioactivity, the interest in understanding the beam halo formation has increased.

Space-charge forces acting in mismatched beams have been commonly identified as a major cause of beam halo. It is found that the mismatch can produce coherent oscillations of the RMS beam size. Individual beam particles interact with the time-varying space charge field due to the beam density oscillation in the beam core, acquire enough transverse energy and then become parts of the halo [1]. In order to understand this process, large numbers of theoretical literature [2] have evolved and large numbers of computer simulations have been carried out [3]. However, few beam experiments have been done, owing in part to the fact that few intense proton beams with the required intensity exist [4]. Fortunately, by making use of the available intense proton beams from a radio frequency quadrupole (RFQ) accelerator designated for ADS study at the Institute of High Energy Physics (IHEP), we have set up a 28-quadrupole beam transport line as the platform to study the beam halo experimentally. It is the first domestic beam line dedicated for the halo study of high intensity proton beam.

## THE BEAM HALO EXPERIMENT TRANSPORT LINE

The 28-quadrupole beam transport line is installed after a 325MHz RFQ with intense beams. The output energy and the design beam current for this RFQ are 3.5MeV and 50mA, respectively. The purpose of this transport line is the experimental study of the beam halo formation. The schematic layout of this transport line is shown in Fig. 1. In this line, the first four quadruples are used to establish match or mismatch conditions for the halo formation, the last 24 quadruples are used to constitute a period FODO lattice. The quadrupole magnets are spaced 19cm each other so that the beam diagnostic devices can be mounted between them. In Table 1, the quadrupole magnet length, gradient and the beam pipe diameter are given. The matched RMS beam radius foreseen is about 0.15cm, while the beam pipe diameter is designed to 3.6cm, which is more than 10 times the RMS beam size.

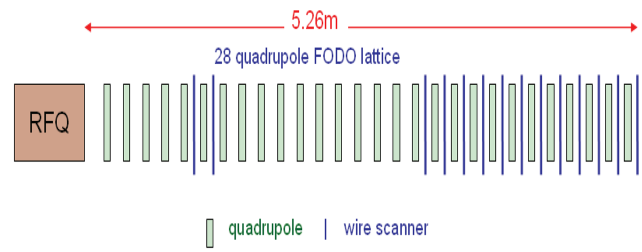


Figure 1: Layout of the beam halo experiment transport line.

Table 1: Parameters of the Experiment Transport Line

| Q magnet number | 1 | 2 | 3 | 4 | 5-28 |
|---|---|---|---|---|---|
| Max gradient (T/m) | 30 | 30 | 30 | 30 | 30 |
| Magnet length (cm) | 10.5 | 10.5 | 10.5 | 10.5 | 7 |
| Beam pipe diameter (cm) | 3.6 | 3.6 | 3.6 | 3.6 | 3.6 |

In the transport line, an array of up to fourteen scanners is used to monitor the beam profiles over the whole line. Each scanner consists of a 32 micron diameter carbon filament for the measurement of the dense beam core and a pair of 1.5mm thick plate scraper for the measurement of the low density halo region. The beam profile scanner can provide intensity measurements over a dynamic range of about $10^5$. The philosophy for scanner locations is the following: the first group of two scanners located after Quadrupole 5 and 6 are used to measure the X and Y beam distribution at the exit of the RFQ respectively and provide a critical initial condition on the halo evolution. As we know, for the matched beam, the beams evolve and form an envelope oscillation with a same period as the LATTICE, but the RMS mismatched beams evolve and form a long period envelope oscillation in a linear focusing beam transport line. Although the oscillation

*Work supported by NSFC (91126003) and State Key Development Program of Basic Research of China (2007CB209904)
#ouyanghf@ihep.ac.cn

ISBN 978-3-95450-118-2

# CERN HIGH-POWER PROTON SYNCHROTRON DESIGN STUDY FOR LAGUNA-LBNO NEUTRINO PRODUCTION

R. Steerenberg, M. Benedikt, I. Efthymiopoulos, F. Gerigk, Y. Papaphilippou, CERN, Geneva, Switzerland

*Abstract*

Within the LAGUNA-LBNO project, CERN has started a high-power proton beam production design study for producing neutrinos. This study foresees a staged approach starting with a study to evaluate the feasibility of a CERN SPS accelerator intensity upgrade to increase the beam power from the existing 500 kW, presently available to CNGS, to 750 kW.

The final stage consists of a conceptual design study for a 30 – 50 GeV, 2 MW protons synchrotron, with the LP-SPL as injector. This paper will provide an overview of the project and then concentrates on the preliminary ideas for the HP-PS.

## THE LAGUNA-LBNO PROJECT

LAGUNA-LBNO [1][2], which is a European FP7 design study, stands for Large Apparatus studying Grand Unification and Neutrino Astrophysics and Long Baseline Neutrino Oscillations and aims at answering fundamental questions on particle and astroparticle physics by developing the next generation of very large volume underground detectors, used to detect besides cosmic neutrinos also neutrinos coming from a high-power protons based neutrino production facility at CERN.

The study that runs from 2011 until 2014 investigates in more detail two sites: The shortest baseline from CERN, Frejus at 130 km from CERN and the longest baseline, Pyhåsalmi in Finland at 2300 km. The study is composed of 5 work packages, which are subdivided in tasks.

Table 1: LAGUNA-LBNO WP4 Tasks

| Task | Brief task description |
|---|---|
| 4.1. | Study of impact of CERN SPS accelerator intensity upgrade to neutrino beams. |
| 4.2. | Assessment of intensity upgrade of CNGS facility. |
| 4.3 | Conceptual design of the CN2PY neutrino beam. |
| 4.4 | Feasibility study of a 30 - 50 GeV High-Power PS. |
| 4.5 | Definition of the accelerators and beam lines layout at CERN. |
| 4.6 | Study the magnetic configuration for the LAGUNA detector. |
| 4.7 | Definition of near detector requirements and development of conceptual design. [1)] |

[1)] The University of Geneva is responsible for this task.

CERN is responsible for work package 4, Long base line neutrino beam prospects and scenarios for detector magnetization, and thus leads the task on the feasibility study of a 30–50 GeV High-Power Proton Synchrotron (HP-PS). This is intended to be the high-power and high-energy proton source for the CERN to Pyhåsalmi (CN2PY) facility, which itself is a task within WP4. The tasks within WP4 are summarized in Table 1.

## HIGH BEAM POWER FACILITIES

The majority of the operational high proton beam power facilities are low energy facilities that produce intense beams in combination with high repetition rates.

SNS, in Oak Ridge USA, delivers about 1 to 1.4 MW beam power, through a LINAC and proton accumulator, at 1 GeV to a spallation target with a 60 Hz repetition rate. Increasing the energy out of the LINAC by 30% to 40% and intensifying the peak current from the $H^-$ LINAC by approximately 50%, should bring the beam power up to 3 MW [3].

ISIS, at RAL in Oxfordshire UK, uses a similar production scheme with a LINAC, accelerating $H^-$ ions up to 70 MeV followed by an RCS that increases the beam energy up to 800 MeV at a rate of 50 Hz, delivering 0.2 MW beam power [4]. An upgrade to a beam power of about 1 MW, using a new 3.2 GeV RCS has been studied, but more ambitious upgrades into the range of 2 – 5 MW beam power have been addressed too [5]. In many of the options discussed, the energy of the RCS is a main parameter together with an increase in beam intensity to reach higher beam powers.

However, few facilities produce high beam power with lower repetition rate and higher energies.

J-PARC [6][7], in Tokai-Mura Japan, is providing besides a high-power beam at 3 GeV, for neutron production, also a high-power and high-energy beam for the hadron hall experiments or the neutrino production for the T2K experiment. The LINAC currently operates at 180 MeV with a beam current of about 30 mA. A nominal LINAC energy of 400 MeV and a beam current of 50 mA, together with the 25 Hz RSC at 3 GeV, should provide a beam power of about 1 MW. The Main Ring that is currently operating at 30 GeV instead of the nominal 50 GeV should then produce a beam power of 0.75 MW at a rate that lies around 0.3 Hz.

CERN, Geneva Switzerland, produces presently a beam power of 0.5 MW out of the SPS for the neutrino production to Gran Sasso [8]. A 400 GeV proton beam at a maximum repetition rate of 6 seconds produces the high beam power. The LAGUNA-LBNO study addresses a possible upgrade of the beam power up to 0.75 MW, mainly through an increase of the beam intensity, as the repetition rate is already at the limit.



ISBN 978-3-95450-118-2

# QUENCH TESTS AT THE LARGE HADRON COLLIDER WITH COLLIMATION LOSSES AT 3.5 Z TeV

S. Redaelli*, R.W. Assmann, G. Bellodi, K. Brodzinski, R. Bruce, F. Burkart, M. Cauchi, D. Deboy, B. Dehning, E.B. Holzer, J.M. Jowett, L. Lari, E. Nebot del Busto, M. Pojer, A. Priebe, A. Rossi, R. Schmidt, M. Sapinski, M. Schaumann, M. Solfaroli Camollocci, G. Valentino, R. Versteegen, J. Wenninger, D. Wollmann, M. Zerlauth – CERN, Geneva, Switzerland

*Abstract*

The Large Hadron Collider (LHC) has been operating since 2010 at 3.5 TeV and 4.0 TeV without experiencing quenches induced by losses from circulating beams. This situation might change at 7 TeV where the quench margins in the super-conducting magnets are reduced. The critical locations are the dispersion suppressors (DSs) at either side of the cleaning and experimental insertions, where dispersive losses are maximum. It is therefore crucial to understand the quench limits with beam loss distributions alike those occurring in standard operation. In order to address this aspect, quench tests were performed by inducing large beam losses on the primary collimators of the betatron cleaning insertion, for proton and lead ion beams of 3.5 Z TeV, to probe the quench limits of the DS magnets. Losses up to 500 kW were achieved without quenches. The measurement technique and the results obtained are presented, with observations of heat loads in the cryogenics system.

## INTRODUCTION

At the time of this workshop, the LHC has accumulated more than 5 $\mathrm{fb}^{-1}$ at 3.5 TeV and more than 14 $\mathrm{fb}^{-1}$ at 4 TeV, with peak luminosities up to $8\times10^{33}\mathrm{cm}^{-2}\mathrm{s}^{-1}$ (80 % of the design luminosity for 7 TeV) and stored beam energies up to 150 MJ. There has been so far no quench induced by losses of the circulating beams. This is an important achievement indicating an excellent performance of the machine protection systems, which catch promptly abnormal loss conditions, and of the collimation system [1], which ensures in all conditions small losses into superconducting magnets. It remains nevertheless crucial to understand the quench limits to predict the LHC performance at the energy of 7 TeV that will be within reach in 2015.

In this paper, the results of quench tests performed with ion and proton beams at 3.5 TeV are presented [2, 3]. These tests are done by maximizing the beam losses on the primary collimators of the betatron cleaning insertion (IR7) to try and reach the quench limits at the limiting locations where the leakage is maximum. We refer to this type of experiments as "collimation quench tests". The present limits of the LHC collimation system are located at the dispersion suppressors (DSs) of the cleaning insertions. Similar losses occur at the DSs of the experimental insertions from luminosity debris. In parallel to this type of tests, other complementary quench tests are being pursued [4, 5, 6] in order to achieve a more complete understanding of the limits in different loss conditions. The machine configuration and the collimator cleaning are presented and the detail procedure established for these tests is introduced. The achieved results in term of peak loss rates for proton and ion beams are discussed. Finally, some conclusions are drawn.

* Stefano.Redaelli@cern.ch

Table 1: Flat-top Collimator Settings for 2011 Quench Tests

| Collimator type | Plane | Name | Setting [$\sigma$] |
|---|---|---|---|
| Primary cut IR7 | H,V,S | TCP | 5.7 |
| Secondary cut IR7 | H,V,S | TCSG | 8.5 |
| Quartiary cut IR7 | H,V | TCLA | 17.7 |
| Primary cut IR3 | H | TCP | 12.0 |
| Secondary cut IR3 | H | TCSG | 15.6 |
| Quartiary cut IR3 | H,V | TCLA | 17.6 |
| Tertiary cut experiments | H,V | TCT | 26.0 |
| Physics debris collimators | H | TCL | out |
| Primary protection IR6 | H | TCSG | 9.3 |
| Secondary protection IR6 | H | TCDQ | 10.6 |

## MACHINE CONFIGURATIONS AND COLLIMATOR CLEANING

Quench tests at 3.5 TeV were performed at top energy before the start of the betatron squeeze ("flat-top"). Collimator settings in IR3 and IR7 reach their final physics settings. Only tertiary collimators in the experimental regions move during squeeze and collision processes, with little effect on the local cleaning in the DSs of IR7. Performing the tests at flat-top has the advantage to avoid additional loss locations in the experimental regions that appear after squeeze, which would require more preparatory work to set thresholds of the Beam Loss Monitors (BLM) system (see next section). The overall turn–around is also shorter than going through the full operational cycle.

The flat-top settings of the different collimators around the ring are listed in Table 1. The same settings were used for proton and ion beams. The cleaning efficiency of the system is shown in Figs. 1 and 2 for the case of proton and ion beams [1]. The ratio between BLM signals measured around the ring and the one measured at the primary collimators of IR7 during dedicated loss maps is given. Loss maps are performed as a part of the system commissioning [7]: the beam lifetime is artificially reduced to maximize the losses at the primary collimators by crossing the third order resonance in either the horizontal or vertical plane,



ISBN 978-3-95450-118-2

# A TOOL BASED ON THE BPM-INTERPOLATED ORBIT FOR SPEEDING UP LHC COLLIMATOR ALIGNMENT

G. Valentino*, N. Sammut
CERN, Geneva, Switzerland and University of Malta, Msida, Malta
R. W. Assmann, R. Bruce, G. J. Müller, S. Redaelli, B. Salvachua
CERN, Geneva, Switzerland

*Abstract*

Beam-based alignment of the LHC collimators is required in order to measure the orbit center and beam size at the collimator locations. During an alignment campaign in March 2012, 80 collimators were aligned at injection energy (450 GeV) using automatic alignment algorithms in 7.5 hours, the fastest setup time achieved since the start of LHC operation in 2008. Reducing the alignment time even further would allow for more frequent alignments, providing more time for physics operation. The proposed tool makes use of the BPM-interpolated orbit to obtain an estimation of the beam centers at the collimators, which can be exploited to quickly move the collimator jaws from the initial parking positions to tighter settings before beam-based alignment commences.

## INTRODUCTION

In the CERN Large Hadron Collider (LHC), collimators are in place to intercept halo particles before they are deposited in the super-conducting magnets, potentially causing quenches [1]. A collimator consists of two blocks of material (jaws) that have to be positioned symmetrically on either side of the beam for optimum halo cleaning. There are four collimator families for ring cleaning: primary (TCP), secondary (TCSG), tertiary (TCT) collimators and absorbers (TCLA). During operation, each collimator family is positioned at a number of beam sigmas from the beam trajectory, such that all the LHC collimators form a four-stage hierarchy. The collimators are mainly located in two insertion regions (IRs), with off-momentum cleaning performed in IR3 and betatron cleaning done in IR7. The TCTs protect the experimental insertions, while as from the 2012 LHC run the TCLs in IR1 and IR5 capture luminosity debris.

Beam-based alignment of the LHC collimators is required to calculate the settings of all collimators throughout the operational cycle and establish the correct collimator hierarchy for machine protection and maximal cleaning efficiency. The alignment is necessary because, due to small beam $\sigma$ values, the required accuracy to respect the hierarchy is not compatible with typical errors in the orbit, BPM readings, optics and design tolerances. A semi-automatic algorithm [2] allows the jaws to be automatically moved in small steps of 5 $\mu$m to 20 $\mu$m towards the beam until the signal of a Beam Loss Monitor (BLM) positioned downstream of the collimator exceeds a pre-defined threshold. The beam center at the collimator is then determined as the average of the two aligned jaw positions. It is sufficient to perform the alignment of all collimators once a year, except for selected TCTs in the event of an optics or orbit change in the experimental IPs.

* gianluca.valentino@cern.ch

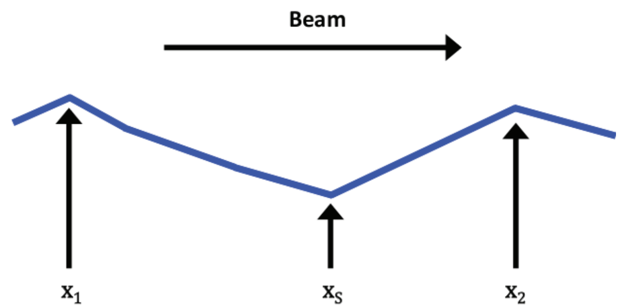


Figure 1: Example of the beam orbit through points 1, S and 2 (from [5]). With BPMs located at point 1 and 2, the objective of the interpolation is to find the orbit at point S.

An approximation to the beam centers at the collimators can be obtained from an interpolation of the orbit measured at specific locations by Beam Position Monitors (BPMs). A BPM consists of four button electrode feedthroughs mounted orthogonally in the beam pipe [3]. These monitors are placed on each side of the warm quadrupoles, providing the minimum configuration that allows a linear interpolation of the closed orbit, dispersion and $\beta$ functions [4].

## BPM-INTERPOLATED ORBIT

An illustrative schema of the LHC beam orbit through various points in a section of the machine is shown in Fig. 1. With BPMs located at point 1 and 2, the orbit at an intermediate point S can be calculated using linear transfer matrices. The interpolation is done per plane and per segment, which is defined as the region between two BPMs. The angle can be calculated from the orbit transfer matrix between a pair of adjacent BPMs. The orbit at point 2 can be established from point 1 using a transfer matrix:

$$\begin{pmatrix} x_2 \\ x_2' \end{pmatrix} = M_{12} \begin{pmatrix} x_1 \\ x_1' \end{pmatrix} = \begin{pmatrix} C_{12} & S_{12} \\ C_{12}' & S_{12}' \end{pmatrix} \begin{pmatrix} x_1 \\ x_1' \end{pmatrix}$$



ISBN 978-3-95450-118-2

# BEAM STABILITY AND TAIL POPULATION AT SPS SCRAPERS

L.Drosdal, K. Cornelis, B. Goddard, V. Kain, M. Meddahi,
B.Mikulec, O.Mete, E. Veyrunes, CERN, Geneva, Switzerland

*Abstract*

Before injection into the LHC the beams are scraped in the SPS to remove the tails of the transverse particle distributions. Without scraping the tail population is large enough to create losses above the beam abort thresholds of the LHC beam loss monitor system when injecting. The scrapers are only effective if correctly set up. This paper shows the results of periodical scraper scans. The beam position and beam size at the scraper is changing with time. The scraper settings hence need to follow accordingly. The scans also give insight into the transverse tail population and could therefore provide useful beam quality diagnostics. The impact on new scraper designs and setting up strategy are discussed.

## INTRODUCTION

The beams produced by the injectors for the LHC can have a large non-Gaussian tail population. These tails must be removed before injection to avoid high losses on the injection elements and later in the LHC cycle on the ring collimators. If these particles are not removed the losses can be high enough to trigger a beam abort in the LHC [1]. The tails are removed in the last LHC pre-injector, the SPS, by means of a horizontal and vertical scraper. Graphite plates are moved close to the beam towards the end of the SPS ramp and scatter the large amplitude particles. The particles are lost in the SPS during the remainder of the ramp.

The 2012 LHC 50 ns full SPS batch consists of 144 bunches with bunch intensities of typically $1.6 \times 10^{11}$ protons. 3 - 5 % of the intensity is scraped off before each LHC injection. The intensity reduction is clearly visible towards the end of the ramp in the SPS, see Fig. 1.

Tests have shown that correct positioning of the scrapers with respect to the beam is essential to control injection losses. Correct positioning implies removing the tails without touching the core of the beam and hence conserving the emittance [2].

During the run of 2012 it was noticed that the scraped intensity can change significantly. This could be due to changes of the beam position at the scraper location, the emittance or the tail population. The strategy of the SPS operations crew was to change the scraper setting to keep the scraped intensity constant. Scraper scans were carried out over the summer 2012 to investigate the sources of the continuous change of scraping conditions. The results are summarized in this paper.

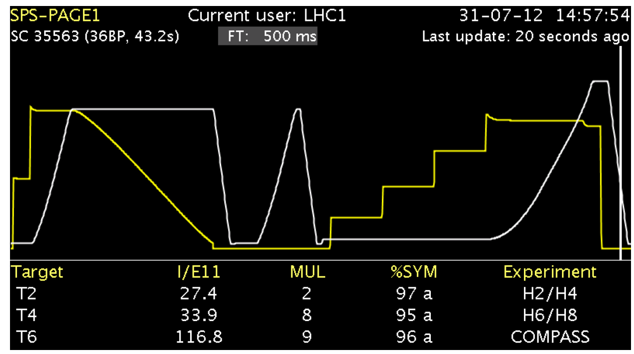


Figure 1: The SPS super cycle configuration during LHC filling. The traces of different magnetic cycles are shown in white. The last one is the LHC cycle. The yellow traces show the intensity of the beam. 4 injections of 36 bunches are required for a full SPS batch of LHC 50 ns beam. The LHC beams are scraped towards the end of the ramp (scraping at 409 GeV) before extraction to the LHC (extraction at 450 GeV).

## SCRAPER SCANS

Because the scraper scans give a detailed description of the beam distribution they can be used as a tool to measure the tail distribution. The beam is scanned by moving the scraper step-wise closer to the beam core and recording the intensity removed by the scrapers. The beam size, $\sigma$, and beam position, $x_0$, with respect to the scrapers can be calculated by Eq. (1) [3].

$$I_1(x) = I_0 e^{-\frac{(x-x_0)^2}{2\sigma^2}} \tag{1}$$

Eq. (1) assumes Gaussian beams, but the scans done reveal that the beams can have large non-Gaussian tails. A double Gaussian function as in Eq. (2) fits the resulting distribution better. The corresponding fit parameters are beam position $x_0$, two beam sizes $\sigma_1$ and $\sigma_2$ for the different Gaussians and the fraction of the amplitudes in each distribution, denoted by $c$.

$$I_2(x) = I_0(1-c)e^{-\frac{(x-x_0)^2}{2\sigma_1^2}} + I_0 c e^{-\frac{(x-x_0)^2}{2\sigma_2^2}} \tag{2}$$

Tails can only be studied if the whole beam is scraped. Each plane has to be scanned separately. To minimize the losses only 36 bunches are used instead of a whole 144 bunch batch. Nevertheless, part of the beam loss monitor system close to the scrapers has to be temporarily masked not to trigger beam aborts in the SPS during the scans.



ISBN 978-3-95450-118-2

# BRIGHTNESS EVOLUTION FOR LHC BEAMS DURING THE 2012 RUN

M. Kuhn (University of Hamburg, Hamburg, Germany), G. Arduini, J.-F. Comblin, A. Guerrero, V. Kain, B. Mikulec, F. Roncarolo, M. Sapinski, M. Schaumann, R. Steerenberg, CERN, Geneva, Switzerland.


*Abstract*

One of the reasons for the remarkable achievements of the LHC is the excellent performance of the LHC injector chain. The evolution of the brightness in the injectors from 2011 to 2012 is discussed and the performance of the LHC in 2012 is shown. During certain run periods, the brightness from the beam provided by the injectors was lower than usual. Some of the issues have been identified so far and will be reported. The latest results on emittance blow-up investigations through the 2012 LHC cycle will also be presented and compared to the 2011 data. Possible implications for LHC upgrade scenarios will be mentioned.


## INTRODUCTION

For achieving high luminosities in a particle collider it is crucial to produce high brightness beams in its injectors and preserve the brightness through the cycle of the collider. The LHC injector produces beams beyond design brightness. The record in 2011 was bunch intensity of $1.5\times10^{11}$ protons per bunch with a transverse normalized emittance of 1.9 µm. These parameters could be even further improved during the 2012 run. The injectors routinely provide bunch intensities of $1.6\times10^{11}$ and emittances of 1.5 µm. The excellent performance of the injectors is one of the main reasons for the outstanding luminosity reach of the 2012 LHC run in proton-proton physics. Despite the lower energy than design (4 TeV in 2012 instead of design energy of 7 TeV) peak luminosities of $7.7\times10^{33}$ cm$^{-2}$s$^{-1}$ could be reached, compared to the design luminosity of $10^{34}$ cm$^{-2}$s$^{-1}$. Table 1 summarizes the LHC 2012 run conditions.

Table 1: LHC Run Configuration 2012

| | |
|---|---|
| Total number bunches for fill | 1374 |
| Max number bunches injected | 144 |
| Bunch spacing [ns] | 50 |
| Intensity/bunch | $1.6\times10^{11}$ |
| Crossing angle (ATLAS, CMS) [µrad] | 290 |
| Number of injections per fill and beam | 12 (+1 pilot) |
| Filling time | ~ 30 min |
| Number collisions (ATLAS+CMS/ALICE/LHCb) | 1368/0/1262 |
| Collision energy per beam | 4 TeV |
| β* (ATLAS, CMS) [cm] | 60 |

Nevertheless the initial brightness from the injectors is reduced in the course of the LHC cycle. This paper discusses the evolution of brightness in the LHC through 2012 and transmission and emittance preservation through the LHC cycle. Possible implications of the findings for the LHC high luminosity upgrade are given.

## BRIGHTNESS EVOLUTION IN 2012

The evolution of beam brightness at the beginning of the LHC collisions and the end of the LHC injector chain, the extraction flattop of the SPS, is shown in Fig. 1. The larger spread on the SPS measurements is due to the few points in the wire scanner profiles and the hence less reliable fit result with the very small beams at SPS extraction energy of 450 GeV. The LHC results are taken from the peak luminosities of one of the high luminosity experiments, CMS. The results from the ATLAS experiment look similar.

Despite the large errors and the spread on the SPS measurements a clear reduction of brightness from SPS extraction to LHC collisions is apparent. On average the brightness is reduced by about 40 %.

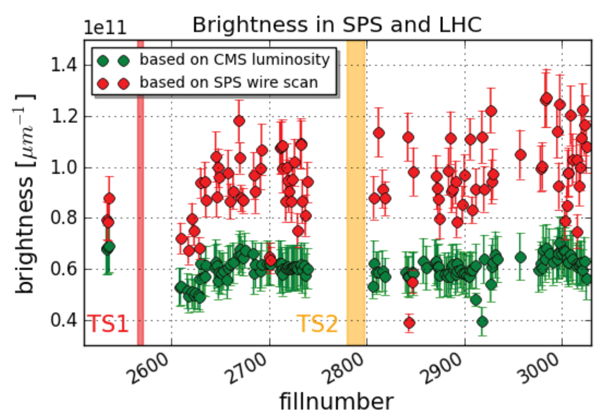


Figure 1: Brightness calculated from instantaneous luminosity in CMS during LHC collisions assuming 15 % error on β* and 5 % error on the crossing angle. The beam intensity measurement was taken from fast Beam Current Transformer (FBCT) in the LHC. For the emittance measurements in the SPS determined with wire scanners an error of 10 % is assumed. The two shaded areas in the plot, TS1 and TS2, indicate the LHC maintenance periods (Technical Stops).

### *Brightness from the Injectors*

To constantly deliver the high performance and to meet the demands for higher and higher bunch intensities of the LHC, the LHC circular injector machines – the PSBooster, the PS and the SPS – have to continuously



ISBN 978-3-95450-118-2

# TUNE SPREAD STUDIES AT INJECTION ENERGIES FOR THE CERN PROTON SYNCHROTRON BOOSTER

B. Mikulec, A. Findlay, V. Raginel, G. Rumolo, G. Sterbini, CERN, Geneva, Switzerland

*Abstract*

In the near future, a new $H^-$ injector, Linac4, will replace the current proton-injector of the CERN Proton Synchrotron Booster (PSB), Linac2. The new charge-exchange injection at 160 MeV will yield higher brightness beams compared to the conventional 50 MeV multi-turn injection of Linac2. To make full use of the higher injection energy, space-charge effects will need to be understood and mitigated to optimize the intensity versus transverse emittance reach. This includes an optimization of longitudinal acceptance and distribution with a two-harmonic rf system, careful selection of the working point to accommodate the large Laslett tune-shift of ≈-0.5 and compensation of resonances within their stopbands. This paper will present calculations of the tune spread, based on measurements of longitudinal parameters and transverse emittances, for energies up to 160 MeV, different bunch densities and varying beam intensities. This should provide valuable information on the expected tune spread after the connection of Linac4 with the PSB and input for the study of resonance compensation techniques.

## INTRODUCTION

The Proton Synchrotron Booster (PSB) located at CERN, Geneva, Switzerland, is currently boosting protons injected by Linac2 from 50 MeV to 1.4 GeV. It is the second accelerator of the LHC injector chain and consists of four superposed rings. Projected LHC beam requirements for the phase after the second long LHC stop currently planned for 2018 identified the PSB injection as first bottleneck many years ago. This led to the design of Linac4, a $H^-$ linear accelerator already being under construction, which will increase $\beta\gamma^2$ by a factor of 2 by increasing the PSB injection energy from 50 to 160 MeV. Moreover transverse phase space painting possible thanks to the $H^-$ charge exchange injection will allow a tailoring of transverse emittances. Space charge effects will on one hand decrease due to the higher energy, but on the other hand much higher beam brightness will be requested by the LHC and other clients. Even longitudinal phase space painting is foreseen to alleviate space charge effects.

This work presents measurements close to the current injection energy and at future Linac4 injection energy, from which the tune spread can be deduced.

## CALCULATION OF THE TUNE SPREAD

The tune spread calculation is based on transverse and longitudinal beam measurements. The horizontal tune spread can be derived from Equation 1 [1].

$$\Delta Q_x = \frac{\lambda_{max} r_p}{2\pi\beta^2\gamma^3} \oint \frac{\beta_x(s)}{\sigma_x(s)[\sigma_x(s)+\sigma_y(s)]} ds \qquad (1)$$

with $\sigma_x(s) = \sqrt{\beta_x(s)\epsilon_x + D_x^2(s)(\frac{\Delta p}{p})^2}$ being one standard deviation of the horizontal beam size and $\sigma_y(s) = \sqrt{\beta_y(s)\epsilon_y}$ one standard deviation of the vertical beam size, as the vertical dispersion is approximately zero in the ring.

$\lambda_{max}$ corresponds to the maximum line density [number of protons/m], $r_p$ to the proton radius, $\beta$ and $\gamma$ to the relativistic factors, $\beta_{x,y}(s)$ to the horizontal/vertical beta functions, $\epsilon_{x,y}$ to the horizontal/vertical physical emittances, $D_x(s)$ to the horizontal dispersion function and $\frac{\Delta p}{p}$ to the rms momentum spread.

For the vertical plane Equation 1 changes as follows:

$$\Delta Q_y = \frac{\lambda_{max} r_p}{2\pi\beta^2\gamma^3} \sqrt{\frac{1}{\epsilon_y}} \oint \frac{\sqrt{\beta_y(s)}}{\sigma_x(s)+\sigma_y(s)} ds \qquad (2)$$

## BEAM PREPARATION

Three different beams have been prepared on PSB ring 2 for the purpose of these measurements with identical magnetic cycle. After injection at 50 MeV the magnetic field is adiabatically ramped up to a 163 MeV flat top and then decelerated back to 50 MeV, where the beam is subsequently lost in the machine (the PSB has no internal dump; see Fig. 1).

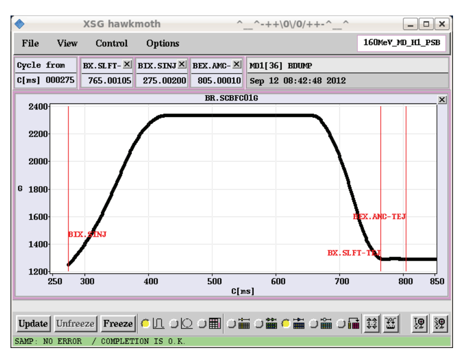


Figure 1: Shown is the B-field of the flat 163 MeV cycle. Injection into the PSB happens at c=275 ms (50 MeV), and usually the beam gets extracted at c=805 ms.

The 3 beams differ only in the longitudinal plane. The PSB has three cavities at its disposal, the main accelerating 2 MHz cavity (C02), a 4 MHz cavity (C04) used to increase the longitudinal acceptance and for double splitting and a

ISBN 978-3-95450-118-2

# COLLIDING HIGH BRIGHTNESS BEAMS IN THE LHC

T. Pieloni, X. Buffat, W. Herr, R. Giachino, E. Metral, G. Papotti, CERN, Geneva, Switzerland

*Abstract*

The CERN-LHC is a high energy particle collider, where intense proton bunches are brought into collision. In order to achieve optimum performance, the bunches must have a high brightness, leading to strong and significant beam-beam effects. Experimental tests during the first two years of its operation have shown that beams with very high brightness can be collided head-on without detrimental effects on the beam dynamics. Such head-on collisions are therefore not expected to limit the LHC performance. Long range beam-beam interactions dominate the adverse effects on the dynamics but can profit from an increased beam brightness, in particular from small emittances. We summarize the experimental results and compare with the theoretical expectations. This allows to optimize the performance for future operation and a definition of promising upgrade scenarios.

## LHC HIGH BRIGHTNESS BEAMS

To deliver the record luminosities achieved this year the Large Hadron Collider injector chain potential for brightness has been exploited during this first part of 2012 physics run. The injector chain has been optimized and can provide the LHC with brighter than nominal beams as already shown in 2011 run. In 2012 run intensities up to $\approx 1.7 \times 10^{11}$ protons per bunch have been delivered and have become operational, to be compared with the $1.15 \times 10^{11}$ ppb in the Design Report [1], for emittances of $\approx 2\ \mu m$ ($3.5\ \mu m$ for nominal LHC parameters). This parameters have been achieved operationally for 50 ns bunch spaced beams. During machine development experiments the beam brightness has been pushed even further colliding single bunches with intensity of $\approx 3.1 \times 10^{11}$ ppb and transverse emittances of less than $2\ \mu m$. With such high brightness beams of course beam-beam effects are pushed to the limits and a careful understanding of the different effects define the optimum choice of parameters to improve performances for the 2012 physics run, for the 7 $TeV$ run and some guidelines for possible upgrade scenarios.

## BEAM-BEAM EFFECTS IN THE LHC

The LHC layout is shown in Fig. 1. The two proton beams collide with a finite crossing angle at four Interaction Regions (IR) where they share a common beam pipe. At the experimental crossing the beams experience head-on collisions in CMS and ATLAS while they collide with a finite offset at LHCb. Several long range interactions are experienced on both sides of the four experiments. During the 2012 run, beams up to 1380 bunches spaced by 50 ns are used. This configuration gives variable number of long range encounters between 30 and 74 maximum (much lower number compared to the nominal 40-120 encounters with a 25 ns beam) depending on the bunch position in the filling scheme.

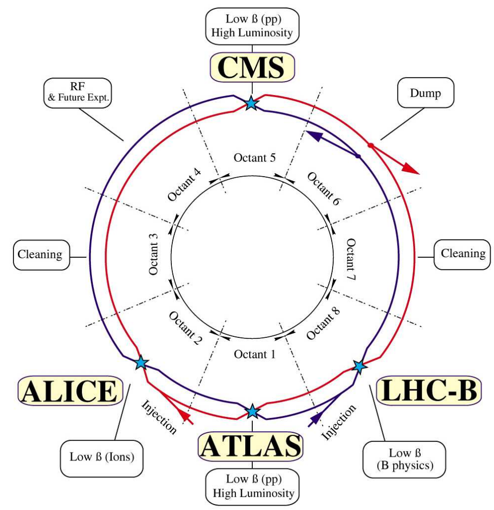


Figure 1: LHC layout.

## HEAD-ON COLLISIONS

Due to the beam filling schemes and the geometry of the different Interaction Points (IPs) the bunches can be classified in different families depending on the number of head-on collisions as well on the number of parasitic long range encounters. The major contribution to beam losses in collision comes from the head-on collisions. For the 2012 run this results in bunch by bunch relative losses as visible in Fig. 2. The red lines in Fig. 2 corresponds to bunches colliding only in LHCb with a transverse offset which cannot be considered as head-on collision as also evident from the small fraction of the losses from this IP. Real head-on collisions occur in ATLAS and CMS from which the biggest contribution to losses come (green lines in Fig. 2). The collision with 4 $\sigma$ in LHCb adds up to the losses for bunches colliding in ATLAS, CMS and LHCb (blue lines in Fig. 2).

### *Head-on Beam-beam Tune Shift*

During 2011 experiments it has been proved that a tune shift of 0.017 per IP can be achieved with single bunch with no evident deterioration of beam parameters neither any dynamics effect [2]. The experiment carried out in 2011 represents still the maximum tune shift reached with very high brightness beams in the LHC. During the 2012 run during regular operation we have tune shift from head-on collisions of $\approx 0.008$ per IP, leading to a total tune shift of the order of $\approx 0.02$ in total.



ISBN 978-3-95450-118-2

# MEASUREMENTS OF THE LHC LONGITUDINAL RESISTIVE IMPEDANCE WITH BEAM

J. F. Esteban Muller*, T. Argyropoulos, T. Bohl, T. Mastoridis, N. Mounet, G. Papotti, B. Salvant, E. Shaposhnikova, D. Valuch, CERN, Geneva, Switzerland

*Abstract*

The resistive part of the longitudinal impedance contributes to the heat deposition on different elements in the LHC ring including the beam screens, where it has to be absorbed by the cryogenic system and can be a practical limitation for the maximum beam intensity. In this paper, we present the first measurements of the LHC longitudinal resistive impedance with beam, done through synchronous phase shift measurements during Machine Development sessions in 2012. Synchronous phase shift is measured for different bunch intensities and lengths using the high-precision LHC Beam Phase Module and then data are post-processed to further increase the accuracy. The dependence of the energy loss per particle on bunch length is then obtained and compared with the expected values found using the LHC impedance model.

## MOTIVATION

The heat load in different elements in the LHC can be a practical limitation for the maximum beam intensity. In particular, the heat load in the injector kickers (MKIs) was excessive for the current nominal intensities and an increase in bunch lengths was required to reduce the heating. This circumstance motivated the study of the longitudinal impedance.

Additionally, very successful electron cloud observations through synchronous phase shift measurements were done in the LHC in 2011 [1]. In some cases, the electron cloud density was so high that it generated particle losses, resulting in a large distribution in bunch lengths and intensities. In that cases, the knowledge of the longitudinal impedance would be very useful in order to take its effect into account to improve the measurements.

## ENERGY LOSS DUE TO RESISTIVE IMPEDANCE

The interaction of the beam with the longitudinal resistive impedance results in an energy loss per particle and per turn that can be written as:

$$U = -q^2 N_b k_{\parallel}, \tag{1}$$

where $q$ is the elementary charge, $N_b$ is the bunch intensity, and $k_{\parallel}$ is the longitudinal loss factor, defined as:

$$k_{\parallel} = \frac{\omega_0}{\pi} \sum_{p=0}^{\infty} \Re\{Z_{\parallel}(p\,\omega_0)\}\, h(p\,\omega_0), \tag{2}$$

where $\omega_0$ is the revolution frequency, $Z_{\parallel}(\omega)$ is the longitudinal impedance, and $h(\omega)$ is the power spectral density of the bunch [2].

The energy loss caused by the impedance is compensated by the RF system by a synchronous phase shift. To achieve this, in the absence of acceleration, the phase shift $\phi_s$ from the synchronous phase should be:

$$\sin\phi_s = \frac{U}{qV}, \tag{3}$$

where $U$ is the energy loss per turn and per particle and $V$ is the RF voltage amplitude.

From Eq. 1 and Eq. 2 it is apparent that the particle energy loss is directly proportional to the bunch intensity and it has also a dependence on bunch lengths through the power spectral density. Combining Eq. 1 and Eq. 3, and for small phase shifts ($\sin\phi_s \approx \phi_s$), we conclude that the synchronous phase shift is proportional to the bunch intensity. We will measure the dependence of synchronous phase on bunch intensity for different bunch lengths to determine the longitudinal resistive impedance of the LHC. This method has been applied successfully in many accelerators at CERN, for example in the SPS [3].

There are two other main sources of beam energy loss in the LHC, the synchrotron radiation and the interaction with an electron cloud, but they can be taken into account. The energy loss per particle by synchrotron radiation does not depend on the total intensity, but on the energy of the particle and its bending radius, resulting in a constant phase offset for any bunch. The electron cloud effect can be avoided by measuring a small number of bunches, as they are not affected by the electron cloud.

## MEASUREMENTS

### *Method*

The synchronous phase shift dependence on bunch intensity was measured for 8 bunches spaced by one ninth of the LHC circumference (9.9 $\mu$s). We chose 8 bunches as a compromise to calculate precisely the dependence and to neglect any interaction between bunches.

Bunch intensities were in the range $0.7 - 2.4 \times 10^{11}$ p, achieved by scraping in the SPS to preserve the longitudinal emittance and distribution, and therefore obtain uniform bunch lengths within the same fill.

Two MD sessions were devoted in 2012 to these measurements, the first one comprising three fills with different injected longitudinal emittances, and the second one in-

* jesteban@cern.ch



ISBN 978-3-95450-118-2

# PROGRESS WITH BUNCH-SHAPE MEASUREMENTS AT PSI'S HIGH-POWER CYCLOTRONS AND PROTON BEAM LINES

R. Dölling, Paul Scherrer Institute, Villigen, Switzerland

*Abstract*

As proposed at HB2010 [1], additional bunch-shape monitors have been installed at the last turns of the Injector 2 cyclotron and at several locations in the connecting beam line to the Ring cyclotron (@72 MeV), as well as behind the Ring cyclotron (@590 MeV). Now at each location in the beam lines, longitudinal-transversal 2D-density distributions of the bunched 2.2 mA proton beam can be taken from four angles of view, each separated by 45°. In addition the monitor in Injector 2 has been upgraded to observe the 13 outermost turns (@57 to 72 MeV), some of them from two or three angles of view. The measurement setup, data evaluation and results are outlined.

## INTRODUCTION

The arrival time of protons, scattered at a 33 um diameter carbon wire under 90° towards a scintillator-photomultiplier (PMT) detector, is measured with respect to the accelerator radio-frequency (50.63 MHz) reference phase. The histogram sampled over a large number of bunches represents the longitudinal density distribution of the bunches at the wire position. Repetition at several transversal positions delivers a two-dimensional (2D) projected profile of the charge density of the bunch.

## NEW DETECTOR SETUP

In the cyclotrons and beam lines (Fig. 1) different detector configurations are used (Fig. 2). Multiple wires provide longitudinal-transversal 2D-density distributions from more than one angle of view.

More relays have been added to the timing circuit described in Ref. [1], allowing the single unit to be used for all detectors.

The time resolution can be determined by measuring the distribution of the differences of arrival times of each proton at two detectors. In contrast to Ref. [2], where the method is based on separate scintillators and PMTs, here both pairs of anodes of a four-anode PMT (Hamamatsu R7600U-200-M4) at a single scintillator are used. (For standard operation all four anodes are combined.) First tests indicate, that the time resolution of the old and new detectors are roughly the same. This is somewhat surprising since more photo-electrons should be created at the PMT anodes due to the truncated-pyramide shape and the higher light yield of the new scintillator (BC418) and the higher quantum efficiency of the new PMT.

The new shape also allows the use of a larger aperture (8 mm x 8 mm) in front of the scintillator. The count rate is consequently increased, and the time for sampling a 2D projected profile at the beam line reduces to typically 6 minutes.

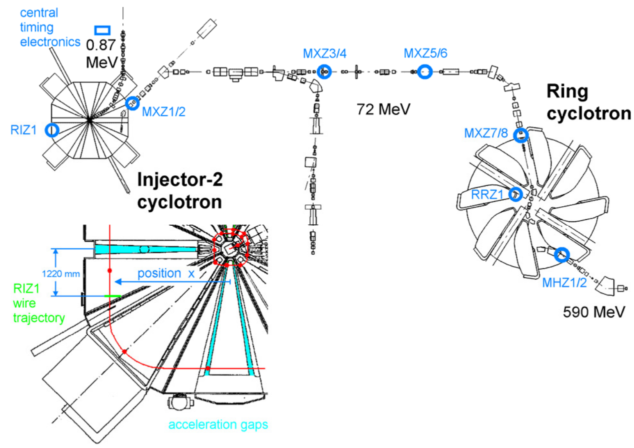


Figure 1: Locations of bunch-shape measurements.

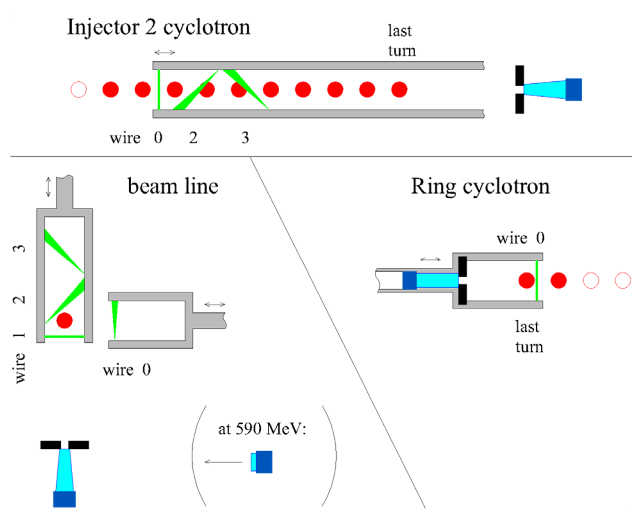


Figure 2: Orientation of beam, wires, drives, scintillators and PMTs (seen in beam direction). Most wires are tilted 45° in beam direction (schematic; the broader printed wire ends are closer to the beholder). Wire centers and scintillator axis are in one plane transversal to the beam. Only in Injector 2 can several wires be in the beam at the same time.

At the 590 MeV location, the deflected protons of 475 MeV are not stopped in the scintillator. Hence, contrary to the situation at 72 MeV, the highest pulses result not from the elastically scattered protons. However, a defined upper pulse height exists, hence allowing the same pulse selection scheme of Ref. [1], which uses only the highest pulses, to be used. Nevertheless, a smaller scintillator (3.7 mm x 3.7 mm x 18 mm) was needed, in order to limit the anode current of the PMT to below critical values.



ISBN 978-3-95450-118-2

# DESIGN OF A PHOTO–DETACHMENT EMITTANCE INSTRUMENT FOR FETS

C. Gabor*, STFC/ ASTeC, Rutherford Appleton Laboratory, Harwell, Chilton Didcot, Oxon, UK
G. Boorman, A. Bosco, Royal Holloway University of London, Surrey, UK
P. Savage, Imperial College of Science and Technology, London, UK
A.P. Letchford, STFC/ ISIS, Rutherford Appleton Laboratory, Harwell, Chilton Didcot, Oxon, UK

*Abstract*

Photo detachment is a possibility to diagnose non-destructively $H^-$ ion beams. For emittance measurements, the produced neutrals are more suitable then the photo-detached electrons. Such a Photo-Detachment Emittance Measurement Instrument (PD–EMI ) is planned for the Front End Test Stand (FETS) at Rutherford Appleton Laboratory (RAL/ UK). FETS comprises a Penning ion source of 60 mA beam current with up to 2 ms pulse length at 50 pps, a Low Energy Beam Transport (LEBT), a four-vane RFQ with 3 MeV and a Medium Energy Beam Transport (MEBT) with a chopper system. The PD-EMI will be integrated at the end of the MEBT to commission the RFQ which is currently under construction. The introduction gives an overview some results reached so far and explains the conceptual design. Beam simulations show how to implement this to the MEBT being under construction. The remaining paper concentrates then on the hardware which is the dipole magnet, the laser and optics. The design and and engineering of the magnet chamber needs special attention to both satisfy beam transportation and diagnostics purpose. First measurements about the laser and its parameters will be presented.

## INTRODUCTION

The papers focus is on the beam instrumentation, its design and engineering to build a non-destructive instrument to measure the beam emittance (PD–EMI ). The main components of such a device are a suitable laser (pulse energy, beam quality), the dipole magnet to separate the neutralized particles from the rest of the $H^-$ beam and the detached electrons and a detector system consisting of a scintillator and an image intensified CCD camera. The particle detector is of no further consideration here but after summarizing the general idea of non-destructively measured emittances utilizing photo-detachment, the magnet, the laser and in particular the vacuum vessel are presented in more detail.

The FETS project aims to demonstrate a fast chopped $H^-$ beam at 3 MeV beam energy with up to 50 pps and 2 ms pulse duration and 60 mA current. For beam diagnostics, that means non-invasive techniques to avoid heat load and activation of mechanical parts such as a slit or wire are most preferred. More information about the test stand itself and its current status can be found in [1].

* christoph.gabor@stfc.ac.uk

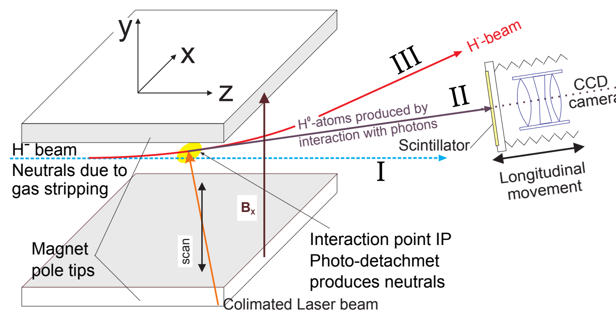


Figure 1: Sketch of the basic idea of the Photo-Detachment Emittance Instrument (PD-EMI). The laser neutralises a small portion of the beam, these particles hit a detector which measures the distribution. Three beamlets can be distinguished; neutrals due to gas stripping, neutrals due to photo-detachment and ions on the reference beam path of the dipole.

### *General Layout*

The basic principle to use photo-detachment for diagnostics is shown in Fig. 1 and described elsewhere in depth [2, 3].

A small portion of the beam gets neutralised with a collimated, i.e. focused laser beam and the produced atoms are detected with a scintillator. If the scintillator is movable and/ or a quadrupole doublet upstream of the magnet varies the focal length, emittance measurements can be done under different for different phase space projections i.e. the transport changes and the beam gets imaged from different angles. This variation of the transport matrix used together with the beam profile and techniques like tomographic image reconstruction (more about Maximum Entropy in [4, 5]) allows to calculate any phase space projections than just $yy'$ [6], only depending how the coordinate system was chosen to extract the profile. If there was no change in the focal length (no change of the sign of $\beta_{\mathrm{twiss}}$) the beam would always be imaged from a similar angle not providing sufficient information for image reconstruction.

This concept of varying the focus for different emittance measurements was developed into a kind of “diagnostics beamline” [7]. The MEBT layout used for these studies was very similar to the ‘baseline’ design published in [8]. Very recently, a new MEBT layout was proposed with the aim of reduced costs, mainly by sparing quadrupols and a buncher cavity [9]. This design is longer (see Fig. 2) than



ISBN 978-3-95450-118-2

# ACCELERATION IN VERTICAL ORBIT EXCURSION FFAGs WITH EDGE FOCUSSING

S.J. Brooks*, RAL, Chilton, OX11 0QX, UK

*Abstract*

FFAGs with vertical orbit excursion (VFFAGs) provide a promising alternative design for rings with fixed-field superconducting magnets. They have a vertical magnetic field component that increases with height in the vertical aperture, yielding a skew quadrupole focussing structure. Edge focussing can provide an alternating gradient within each magnet, thus reducing the ring circumference. Like spiral scaling horizontal FFAGs (but not non-scaling ones) the machine has fixed tunes and no intrinsic limitation on momentum range. Rings to accelerate the 800 MeV beam from the ISIS proton synchrotron are investigated, in terms of both magnet field geometry and longitudinal behaviour during acceleration with space charge. The 12 GeV ring produces an output power of at least 2.18 MW.

## MAGNET FIELD MODEL

The field within the body of a VFFAG magnet is given by $B_y = B_0 \mathrm{e}^{ky}$ on the $x = 0$ mid-plane. The beam travels in the $+z$ direction through the magnet and shifts to height $y = \frac{1}{k} \ln p/p_{\mathrm{inj}}$ as momentum $p$ increases, so the injection orbit is at $y = 0$ and the current windings lie on the $\pm x$ sides of the vertical gap. Optics of a ring with such magnets without edge effects are considered in [1]. At injection, the magnet body has bending field $B_0$ and skew gradient $B_0 k$ (as well as higher multipoles of strength proportional to $B_0 k^{n \geq 2}$), so without edge effects $B_0$ must alternate in sign to provide alternating gradient focussing. $k$ must be constant for the entire ring to satisfy the scaling law

$$y \mapsto y + \Delta y, \qquad (p, \mathbf{B}) \mapsto (p, \mathbf{B})\mathrm{e}^{k\Delta y},$$

which ensures the orbit shape and tunes are preserved during acceleration. Having negative $B_0$ for some magnets produces reverse bends and increases machine circumference for a given field by $\sim$5 times, similar to the circumference factor [2] in horizontal scaling FFAGs.

To represent magnets with edges, the parameter $\tau = \tan\theta_{\mathrm{edge}}$ is introduced, along with a coordinate $\zeta = z - \tau y$ so that the magnet corresponds to the region $0 \leq \zeta \leq L_{\mathrm{mag}}$ for all $y$. Field fall-off is determined by a function $f(\zeta)$ that approaches 1 in the magnet body and 0 outside. Naively one wants a mid-plane field $B_y = B_0 \mathrm{e}^{ky} f(\zeta)$ but to obey Maxwell's equation $(\nabla \times \mathbf{B})_x = 0$, this has to be modified to $(B_y, B_z) = B_0 \mathrm{e}^{ky} \left( f(\zeta) - \frac{\tau}{k} f'(\zeta), \frac{1}{k} f'(\zeta) \right)$. The note [3] derives this formula and the Taylor series extrapolation used to calculate fields for $x \neq 0$. For edge angles, $z \mapsto z + \tau\Delta y$ is added to the VFFAG scaling law to keep $\zeta$ constant (more accurately, this is a rotation of $\tau\Delta y/R$ about the ring centre).

* stephen.brooks@stfc.ac.uk

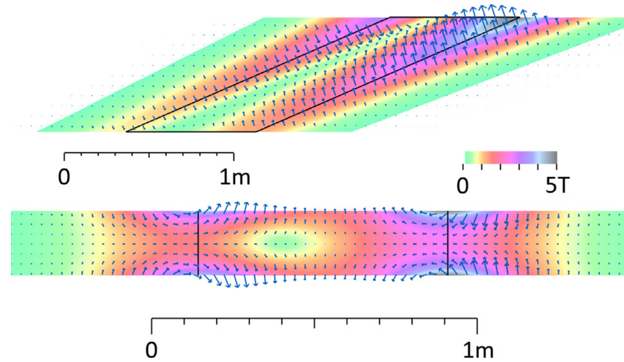


Figure 1: Cross-section of the 5 GeV ring magnet's field in ZY (top) and ZX (bottom) planes.

The resulting field is plotted in Figure 1. The fringe field at the entrance to the magnet has opposite sign to that at the exit, providing alternating gradient focussing without changing the sign of $B_0$. Note that symmetry about the YZ plane forbids conventional quadrupole fields, meaning all focussing is skew apart from the solenoidal component $B_z$.

### *Field Enhancement Factor*

As can be seen in Figure 1, the largest fields are present in the magnet edges and off-plane. The field enhancement factor $\max_z |\mathbf{B}(x, y, z)|/(B_0 \mathrm{e}^{ky})$ is plotted in Figure 2 (at $y = 0$, though by the scaling law it is the same at all $y$).

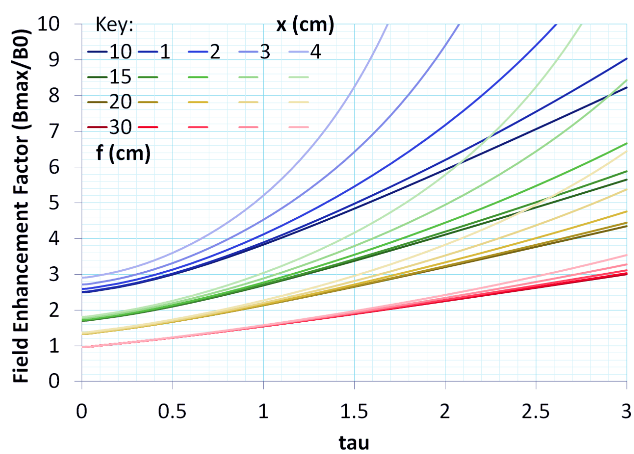


Figure 2: Field enhancements as a function of $\tau$, fringe length ($f$) and distance from mid-plane ($x$) from 0 to 4 cm, in the 3 or 5 GeV magnet design with $k = 2.05\,\mathrm{m}^{-1}$.

Enhancement increases with $\tau$ but is ameliorated by increasing fringe length; it also increases extremely rapidly

ISBN 978-3-95450-118-2

# HIGH-POWER SCALING FFAG RING STUDIES

D. J. Kelliher, S. Machida and G. H. Rees,
STFC Rutherford Laboratory, ASTeC, UK

*Abstract*

High-power FFAG rings are under study to serve as drivers for spallation neutrons, muon production, and accelerator-driven reactor systems. In this paper, which follows on from earlier work [1], a 20 - 70 MeV model for a high-power FFAG driver is described. This model would serve as a test bed to study topics such as space charge and injection in such rings. The design incorporates a long straight to facilitate $H^-$ charge exchange injection. The dynamic aperture is calculated in order to optimize the working point in tune space. The injection scheme is also described. It is planned to experimentally study subjects relevant to high-power FFAGs using the KURRI FFAGs (ERIT and ADSR). Some simulation results of the ERIT FFAG ring are presented including the effects of space charge and foil scattering.

## INTRODUCTION

In FFAG accelerators, the repetition rate is in principle limited only by the available rf voltage. Indeed the potential for FFAGs to accelerate high intensity beams was one of the motivations behind their revival in the 2000's in Japan [2],[3]. Space charge studies are planned, making use of the ERIT ring at KURRI, Japan. Some simulation results of ERIT are shown in the final section of this paper. In order to take the study of various aspects of intense proton beams to the next stage, building a dedicated FFAG may be required. This subject is discussed in the following sections.

## FFAG MODEL

Taking a lead from KURRI, the study takes as its starting point a 100 Hz, 20 MeV, $H^-$ linac injecting into a 20-70 MeV, FFAG, $H^+$ ring . An 8 cell DFD lattice is proposed with cell tunes $\nu_x = 0.401, \nu_y = 0.223$ and $\gamma_t = 2.3368$. The cell tunes are chosen to avoid principal resonances, but may be adjusted following a dynamic aperture survey. The F and D have opposite field directions, so a "return yoke free magnet" is proposed with magnetic shields to reduce end fields as used at KURRI. The edges of the magnet are radial. Each cell is mirror symmetric about the F centre with long drifts at either end.

The initial design work was carried out using a matrix code to model each momentum separately. In order to calculate the optics, the magnets are simulated as dipoles with quadrupole component and finite edge angles. The lattice parameters at injection and extraction used in the matrix code are listed in Table 1. In order to pursue further studies such as a calculation of dynamic aperture, the lattice was simulated by the Zgoubi tracking code.

Table 1: Lattice Parameters at Injection and Extraction

| Parameter | Unit | Injection | Extraction |
|---|---|---|---|
| Short drift length | m | 0.178 | 0.200 |
| Long drift length | m | 1.669 | 1.878 |
| F length | m | 1.450 | 1.632 |
| D length | m | 0.217 | 0.244 |
| D bend angle | rad | - 0.168 | -0.168 |
| F bend angle | rad | 1.120 | 1.120 |
| F, D norm. gradient | $m^{-2}$ | $\pm$ 0.541 | $\pm$ 0.685 |
| Edge field extent | m | 0.034 | 0.030 |
| Mean radius | m | 4.976 | 5.600 |

Table 2: Lattice Parameters in Zgoubi Model

| Parameter | Unit | Value |
|---|---|---|
| Field index | - | 4.345 |
| Reference radius $r_0$ | m | 5.6 |
| D&F Field at $r_0$ | T | -1.078, 0.845 |
| D&F radial extent | rad | 0.044 , 0.291 |
| Edge field extent | m | 0.034 |

In Zgoubi the magnets are simulated as radial FFAGs in which the reference radius $r_0$, field $B_0$, angular extent and field index $k$ need to be specified. The field index is given by $k = g_n * r_m * \rho$ where $g_n$ is the normalised gradient and $r_m$ the mean radius at a particular momentum and $\rho$ is the magnet bending radius. However there are a couple of significant differences between the matrix and Zgoubi models of the magnets.

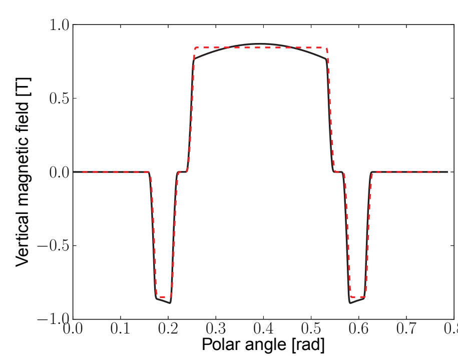


Figure 1: Comparison of vertical magnetic field along the closed orbit at the extraction momentum in one cell between the ASTeC matrix code STRING (black solid) and Zgoubi models (red dash).



ISBN 978-3-95450-118-2

# SPACE CHARGE LIMITS ON THE ISIS SYNCHROTRON INCLUDING THE EFFECTS OF IMAGES

B. G. Pine, C. M. Warsop, ISIS, Rutherford Appleton Laboratory, STFC, UK

*Abstract*

The ISIS synchrotron provides a pulsed, 50 Hz, 800 MeV proton beam for spallation neutron production. Each pulse from the synchrotron contains $\sim 2.8 \times 10^{13}$ protons per pulse (ppp), and at this beam intensity space charge and image forces have a strong effect on transverse beam dynamics. In order to increase intensity in the present machine, and to prepare for possible upgrades running at a higher intensity, studies are underway aimed at understanding the most critical features of such forces and their impact on beam loss. These studies are focused on working point optimisation, including resonances due to space charge and images.

A 2D simulation code, Set, has been developed to improve understanding of transverse dynamics at ISIS, using a particle-in-cell algorithm to include space charge and image forces self-consistently. The ISIS synchrotron has profiled vacuum vessels and RF shields which conform to the shape of the beam envelope, and have a distinctive influence on the beam dynamics. Set is specifically designed to include these image forces. A systematic simulation study of possible working points is presented, along with an assessment of the effect on apertures.

## INTRODUCTION

### *ISIS Accelerators*

The ISIS linac provides $H^-$ ions at 70 MeV for charge-exchange injection into the synchrotron, which then accelerates the protons to 800 MeV. Acceleration is synchronised on the rising edge of the sinusoidal 50 Hz main magnet field. Beam is accelerated using 6 ferrite loaded RF cavities operating at a harmonic number of 2: as a result two bunches are formed in the synchrotron. Bunch shaping is provided with 4 more RF cavities operating at a harmonic number of 4, which have lowered the peak line density and allowed routine operation with beam losses lower than 5%. There are 10 super periods in the synchrotron, which has a circumference of 163 m, with specialised sections for injection, extraction and collimation. Each super period contains 2 trim quadrupoles which allow sensitive manipulation of the working point. The full transverse acceptances are (H, V) = (520 , 430 $\pi$ mm mrad), but the beam is collimated at $\sim 300\,\pi$ mm mrad in each plane. ISIS operates at the highest safe intensity, limited by the control of beam loss.

### *ISIS Upgrade*

A design study is in progress looking at replacing the 70 MeV ISIS linac with a new injector accelerating $H^-$ ions to 180 MeV [1]. This would reduce space charge forces in the synchrotron and enable a higher intensity to be accumulated. In addition, as the new linac will include a beam chopper, beam would be injected directly into the RF buckets in the synchrotron, reducing loss during the bunching process and further increasing the intensity available for acceleration. As a result of these considerations, space charge would be reduced by a factor of 2.6, which suggests that the intensity of $3 \times 10^{13}$ ppp possible with the current linac could be increased to $7.8 \times 10^{13}$ ppp [2]. For the present machine, space charge peaks during the non-adiabatic trapping process ($\sim 1$ ms into acceleration), while in the upgrade design it would do so at the end of injection. At present, and for future ISIS upgrades, space charge and images play a crucial role in loss mechanisms, therefore it is important to understand their influence on beam dynamics. Previous work on transverse dynamics on ISIS has examined the effect of half integer resonance [2, 3], images and closed orbits [4, 5]. Key studies for understanding the current machine [6, 7] and injection upgrade [8, 9] are presented elsewhere.

### *Motivation for a New Working Point Simulation*

ISIS suffers from a resistive-wall head-tail instability when the vertical tune is just below 4 and this could impose intensity limitations when space charge prevents lowering the tune. It will be important to mitigate this instability at higher levels of beam intensity and two options are being considered. One is to remain at the current working point of the machine $(Q_h, Q_v) = (4.31, 3.83)$ but to use an active damping system to control the instability. The other option is to move the vertical working point to a position where the instability is not a concern. Transverse simulations exploring the consequences of moving the working point are the subject of this paper.

Due to the high space charge levels at which the ISIS synchrotron operates, the peak incoherent tune shift in both planes is of the order 0.5. To prevent loss, the coherent quadrupole moments must be kept above the corresponding half integer driving terms. The nearest available vertical working points are below 3.5, or above 4.3, see Figure 1.

One major complication is the structure of the ISIS vacuum vessel, which conforms to the shape of the design beam envelope as determined by the design tunes (4.31, 3.83) and optics. Any changes to the working point alter the shape of the beam inside the beam-pipe and run the risk of reducing useful aperture, or increasing image forces. Figure 2 shows the variation of horizontal and vertical apertures over one super period, compared with the design beam envelopes for a 300 $\pi$ mm mrad test beam.



ISBN 978-3-95450-118-2

# SIMULATION OF INTENSE PROTON BEAMS IN NOVEL ISOCHRONOUS FFAG DESIGNS

S. L. Sheehy*, ASTeC/STFC, Harwell, Oxon, UK
C. Johnstone, Fermilab, Batavia, IL, U.S.A.
M. Berz, K. Makino, Michigan State University, East Lansing, MI, U.S.A.
P. Snopok, Illinois Institute of Technology, Chicago, IL, U.S.A.

*Abstract*

Recent developments in the design of non-scaling fixed field alternating gradient (FFAG) accelerators have been focused on achieving isochronous behaviour with a small betatron tune excursion. These advances are particularly interesting for applications requiring CW beams, such as Accelerator Driven Systems for energy generation or waste transmutation. The latest advances in lattice design have resulted in a 330 MeV to 1 GeV lattice, isochronous to better than +/- 1%. This paper reports on simulations of recent lattice designs incorporating 3D space charge effects.

## INTRODUCTION

New FFAG designs approaching isochronicity give a tantalising possibility of providing CW beams from a strong focusing accelerator. Such an accelerator should be able to support high power beams using a constant RF frequency and fixed field magnets. CW machines have intrinsic advantages in supporting high power beams as they have a much lower peak current than a pulsed or cycling machine. It has also been speculated that due to the strong focusing nature of these accelerators, particular space charge effects may be reduced when compared to a cyclotron [1], particularly at injection where vertical focusing in a cyclotron is typically weak [2].

This work presents two FFAG designs [3], the first is a four cell design which is isochronous to $\pm 3\%$ and the other a six cell design which has now achieved isochronicity to better than $\pm 1\%$. For reasons discussed later, the four cell design is taken to be representative of this type of accelerator in the simulations presented.

### *FFAG Lattice Designs*

The lattice designs presented here are based on the idea of using alternating gradient magnets, incorporating a nonlinear radial field expansion with an appropriate magnet edge angle [4]. This means that the orbit at each momentum can be made proportional to velocity in order to achieve isochronicity and at the same time the betatron tune can be controlled through both edge and weak focusing.

This is in contrast to a classical cyclotron where the main field is predominately the dipole field, which has limitations in adapting the path length to velocity into the relativistic regime. It should be noted that a modern design of a sector cyclotron may in fact look very similar to these recent FFAG designs and in some cases the distinction between the type of accelerator begins to blur [5]. For the purposes of this work we will refer to the designs as FFAGs as this indicates that the lattice design consists of 'F' and 'D' magnets which are opposite in field polarity, meaning that the 'D' magnet provides a reverse bend. Each lattice is completely periodic and in each magnet the radial field has a carefully defined gradient and the magnets have linear edge profiles.

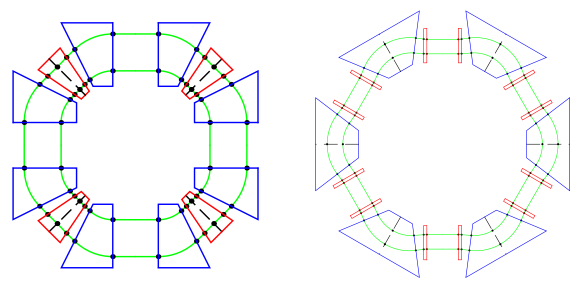

Figure 1: Layout of the 4 cell ring (left) and 6 cell ring (right).

### *4-cell FFAG Design*

The four cell ring is completely periodic and uses a triplet FDF cell structure. A minimum 0.3 - 0.5 m length has been imposed between magnets to prevent end-field overlap and cross talk between magnets. The long straight is 2 m to accommodate injection, extraction and the acceleration cavities.

A four-cell ring periodicity was found to be a strong initial starting point and isochronous to +/-3% over an energy range from 0.25-1 GeV. The ring parameters are given in Table 1. Note that a complete CW accelerator system would likely entail an H- injector. (Use of H- in the lower energy ring permits CW injection into the higher-energy ring through charge-changing or stripping methods.)

### *6-cell FFAG Design*

The six cell ring uses a DFD cell structure, which produces a smaller horizontal beta function and beam size at extraction and is thus preferred. This design is isochronous to +/-1% over its proposed energy range. The choice of a slightly higher injection energy was informed by developments of smaller injector rings, which have a wider range of applications in medical and other areas at 330 MeV rather than 250 MeV.

* suzie.sheehy@stfc.ac.uk

ISBN 978-3-95450-118-2

# BEAM HALO MEASUREMENTS USING ADAPTIVE MASKING METHODS AND PROPOSED HALO EXPERIMENT

H. Zhang, B. Beaudoin, S. Bernal, R. Fiorito, R. Kishek, K. Poor Rezaei, A. Shkvarunets
University of Maryland, College Park, MD 20742, USA

*Abstract*

Beam halo is a common phenomenon in particle beams, especially for modern, advanced accelerators where high beam intensities lead to strong space charge. Halo is generally understood as a population of particles that do, or will, reach large transverse radii relative to a more intense, centralized beam core. It is associated with emittance growth, beam quality degradation and particle loss. The particle-core model is commonly used to describe halo formation as the result of a parametric resonance due to envelope mismatch. Few experiments have been carried out to test this theory. Measurement of beam halo is particularly problematic for faint halos, where light from the intense core obscures the optical image of the halo. In this paper, we review a diagnostic for high-dynamic range halo measurements based on adaptive masking of the beam core. We present the design of an experiment to study halo formation from envelope mismatch for beams spanning a wide range of intensities on the University of Maryland Electron Ring (UMER).

## INTRODUCTION

Modern intense-beam accelerators, where space charge is important, have a wide variety of applications such as spallation neutron sources, rare isotope accelerators, and intense proton drivers for muon and neutrino physics.. A prevalent space charge induced problem is beam halo formation. Halo is generally understood as a population of particles that do, or will, reach large transverse radii relative to a more intense, centralized beam core. It is associated with emittance growth, beam quality degradation and particle loss [1]. Since the density of the halo is often faint compared to the core, it makes particle-in-cell simulation, as well as experimental detection, difficult. Several analytic models such as particle- core model [2] and free energy model [3] are derived either to depict the process of halo formation or to describe the associated emittance growth. Many theory and simulation studies developed these ideas and discussed various mechanisms for halo formation. However, fewer experimental studies have been performed. For example, the LEDA experiment [4] demonstrated agreement with the particle- core model. But unfortunately its propagation length is limited and it is no longer operational. In this paper, we will review a halo diagnostic method with high dynamic range using adaptive mask. Then, we propose a new experiment for testing halo theories.

## BEAM HALO MEASUREMENTS USING ADAPTIVE MASKING METHODS

Comparing with the beam core, the intensity of beam halo is very faint. It can be as low as $10^{-5}$~$10^{-6}$, which is very difficult to detect by normal diagnostic methods because of its low dynamic range. Borrowed from astronomy's idea of coronagraphy, we develop this imaging method using a device called digital micro-mirror-array device (DMD). It successfully masks out the core adaptively and reconstructs the transverse beam distribution with high dynamic range as $10^6$.

We first show the simplified optical design in Fig. 1. In this configuration, we first focus the original beam source onto the DMD surface. The source can be any light source such as fluorescent screen or initiative light sources like OTR and SR. DMD is a commercialized device manufactured by Texas Instrument and widely used in projector and TV industry. It contains 1024*768 tiny mirror, and each mirror can be independent addressable and tilted to two angles. This feature allowed us to use it as spatial filter to redirect the halo image onto the camera while block out the brighter light of beam core (as indicated in the figure with different colors). We applied several compensations to avoid or minimize the effect caused by DMD, such as tilting DMD 45 degree around the optical axis, rotate camera by a scheimpflug angle. The details can be seen in reference [5].

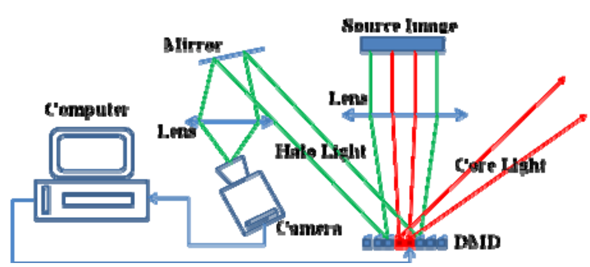


Figure 1: Diagram of adaptive masking method[5].

We have been applied this method at UMER [5], JLab FEL [6] and SPEAR3 [7]. In UMER, we first tested this method using images generated by intercepting the 6 mA, 100 ns, 10 keV beam onto a phosphor screen in UMER. We showed a series of images with different quadrupole strength in the upstream in Fig. 2. The upper halves indicated the beam cores, while the lower ones only displayed the distributions outside with a mask blocking out the beam core. This was the first experimental result to separate the core and halo distributions adaptively, and measure them with normal dynamic range. The combine dynamic range can be as high as $10^5$.

ISBN 978-3-95450-118-2

# A TEST FACILITY FOR MEIC ERL CIRCULATOR RING BASED ELECTRON COOLER DESIGN*

Ya. Derbenev, D. Douglas, A. Hutton, G. Krafft, E. Nissen, Y. Zhang#,
Thomas Jefferson National Accelerator Facility, Newport News, VA 23606, USA

*Abstract*

An electron cooling facility which is capable of delivering a beam with an energy up to 55 MeV and an average current up to 1.5 A at a high bunch repetition rate up to 750 MHz is required for MEIC. The present cooler design concept is based on a magnetized photo-cathode SRF gun, an SRF ERL and a compact circulator ring. In this paper, we present a proposal for a test facility utilizing the JLab FEL ERL for a technology demonstration of this cooler design concept. Beam studies will be performed and supporting technologies will also be developed in this test facility.

## INTRODUCTION

The cooling scheme of MEIC, a medium energy electron-ion collider at JLab [1], requires two electron coolers to achieve the high luminosity goal [2,3]. The first one is a traditional low energy (up to 155 keV) cooler of a DC cooling beam used in the pre-booster synchrotron for assisting ion beam accumulation, and is based on well developed technologies [4]. The other one is used in the ion collider ring and covers a medium energy range up to 55 MeV, thus demanding a new class of technologies including a magnetized photo-cathode SRF gun, an SRF ERL, and a compact circulator ring [3].

Such a design concept of a medium energy electron cooler had been, as a matter of the fact, proposed and studied previously for a hadron-hadron collider (RHIC) [5] or electron-proton/ion colliders (HERA [6] and eRHIC [5]), all based on an ERL, either without [5] or with [7] a circulator ring. These earlier studies were mostly at a conceptual level, with R&D efforts on various key cooler components such as SRF linacs. The cooler facility itself, however, has never been built and tested.

At JLab, we plan to create a test facility for the medium energy ERL Circulator Cooler (ERL-CC) of MEIC in the next three years for a demonstration of the design concept and for technology development. The test facility will be based on the JLab FEL driver ERL for maximum reuse of existing equipment, thus reducing the capital cost, and time to completion. The planed tests will focus on a proof-of-principle (P-o-P) experiment for a circulator cooler ring, and through beam physics studies, will provide an evaluation of its technical merit by examining the reduction of the electron beam current from the photo-cathode gun and the SRF linac. In this paper we will present the proposal of this test facility and discuss the scope and the preliminary plan of the tests and beam studies. We will first briefly summarize the ERL-CC design concept in the next section, followed by a description of the proposed test facility. In the fourth section, we will discuss the required pre-test technology development, and end this paper with an outlook.

* Supported by the U.S. Department of Energy, Office of Nuclear Physics, under Contract No. DE-AC05-06OR23177 and DE-AC02-06CH11357. The U.S. Government retains a non-exclusive, paid-up, irrevocable, world-wide license to publish or reproduce this manuscript for U.S. Government purposes.

# yzhang@jlabl.org

## ERL CIRCULATOR COOLER

As required by the MEIC design, the electron cooler in the collider ring must deliver a cooling beam with a 2 nC bunch charge at a 750 MHz bunch repetition rate. The energy range of this cooler, up to 55 MeV, rules out any electrostatic apparatus which are used in all low energy coolers for accelerating the electron beam. Therefore, the medium energy electron cooler must rely on RF or SRF technology.

Figure 1 illustrates an electron cooler design concept based on an ERL and a compact circulator ring, the two key technologies adopted for overcoming the two critical challenges, namely, a high (up to 81 MW) beam power and an acceptably long lifetime of the photo-cathode gun [3]. A high charge electron bunch from a magnetized photo-cathode injector is accelerated in an SRF linac to energy up to 55 MV and then sent to a compact circulator ring with an optically matched channel for cooling an ion bunch. The photo-cathode injector and SRF linac ensure a high quality of the bunch (small emittance and energy spread). The electron bunch circulates a large number (10 to 100) of turns inside the circulator ring while continuously cooling ion bunches. This circulator ring enables a reduction of the beam current from the cathode and ERL by a factor equal to the number of turns. The cooling bunch then returns to the SRF linac for energy recovery. The recovered energy will be used to accelerate a new electron bunch from the injector.

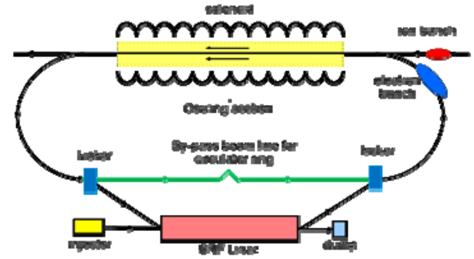

Figure 1: A schematic drawing of an ERL Circulator Ring based electron cooling facility.

ISBN 978-3-95450-118-2

# OBSERVATIONS OF SPACE CHARGE EFFECTS IN THE SPALLATION NEUTRON SOURCE ACCUMULATOR RING*

R. Potts, S. Cousineau and J.A. Holmes, ORNL, Oak Ridge, TN, 37831, USA*

*Abstract*

The Spallation Neutron Source accumulator ring was designed to allow independent control of the transverse beam distribution in each plane. However, at high beam intensities, nonlinear space charge forces can strongly influence the final beam distribution and compromise our ability to independently control the transverse distributions. In this study we investigate the evolution of the beam at intensities of up to ~$8x10^{13}$ ppp through both simulation and experiment. Specifically, we analyze the evolution of the beam distribution for beams with different transverse aspect ratios and tune splits. We present preliminary results of simulations of our experiments.

## INTRODUCTION

The SNS ring compresses a 1 ms beam of up to $1.5x10^{14}$ 1 GeV protons to a short 1 μs pulse for delivery to a liquid mercury target for neutron spallation [1]. Independent control of the transverse beam distributions is desired to facilitate meeting the operational requirements of the SNS liquid mercury target. The target design requirements are that the beam fill a 70 mm by 200 mm spot with a beam profile that is uniform in both transverse planes and has a peak density of less than of $2.6x10^{16}$ protons/m$^2$ for a 1.5 MW beam. It has been previously observed [2] that at high beam intensities the final accumulated beam distributions in each plane depend on the initial distribution in the alternate plane, such that independent control between the planes is lost. However, the effect is only intermittently observed. In other words, we observed space-charge-induced transverse beam coupling for certain beam configurations. We present here current results from experiments and simulations from ongoing efforts to understand transverse space charge coupling in the SNS Accumulator Ring. In this study we investigate the coupling dependence on intensity, tune split, and initial beam distribution for unpainted beams.

Experimental wire scan data was collected during beam development shifts over the past year for various beam configurations. The experimental data was processed and combined with simulations of the experiments using the ORBIT code [3]. In the first section of this paper, we present a summary of the experimental observations. Following this, we discuss our preliminary simulation results and future directions.

* ORNL/SNS is managed by UT-Battelle, LLC, for the U.S. Department of Energy under contract DE-AC05-00OR22725.

## EXPERIMENTAL PARAMETERS

To simplify the beam dynamics, experiments were conducted with flat-topped injection kickers, e.g., no injection painting. The skew quadrupoles throughout the ring were used to nullify any existing lattice coupling. While the nominal beam energy changed from shift to shift, the beam energy was typically on the order of 910 MeV. The nominal betatron production tune of the SNS Accumulator Ring is $\nu_x$ = 6.23 and $\nu_y$ = 6.20. For our experiments, both betatron tunes were varied between 6.15 and 6.25. The nominal production intensity is ~$8x10^{13}$ protons per pulse (ppp) to target. The intensity was varied from ~$2x10^{12}$ ppp to ~$8x10^{13}$ ppp by decimating the beam such that the number of storage turns were the same for all intensities. Profiles were measured for the fully accumulated beam using four wire scanners in the Ring to Beam Target (RTBT) transport line. For our experiments, we formed two types of beams: those that were symmetric, equal aspect ratio, and those that were asymmetric as defined by the beam size at low intensity. Specifically, the symmetric beam had equal beam size in x and y. The asymmetric beams typically had a y distribution that was approximately half-sized compared to the symmetric distribution. The horizontal beam size remained fixed. Coupling was investigated by checking for profile changes in the horizontal plane when the beam distribution was altered in the vertical plane.

### *Dependence on Aspect Ratio and Intensity*

In our experiments, we used decimation, the process of skipping injected pulses during accumulation to achieve a lower intensity beam, to maintain the same beam accumulation scenario while varying the beam intensity. By altering the injection kickers in the vertical plane, we were able to decrease the low intensity vertical beam size by half without changing the horizontal distribution. Figure 1 on the next page shows the horizontal profiles of the beam for the two different beam distributions at three different intensities. The horizontal beam profiles for both distributions are identical at low intensities. As the intensity increased, greater dilution is observed in the symmetric beam cases despite a higher beam density in the asymmetric cases. This is counter-intuitive since one would normally expect that beam density would play a larger role in dilution than beam shape. The fact that the lower density beam suffers more dilution points to another physical process, such as coupling. Furthermore, the observation of higher dilution in symmetric beams is particularly relevant since our production beam configuration is near symmetric, and therefore may also be in a region of high coupling.

ISBN 978-3-95450-118-2

# THE HIGH INTENSITY/HIGH BRIGHTNESS UPGRADE PROGRAM AT CERN: STATUS AND CHALLENGES

S.S. Gilardoni, G. Arduini, T. Argyropoulos, S. Aumon, H. Bartosik, E. Benedetto, N. Biancacci, T. Bohl, J. Borburgh, C. Carli, F. Caspers, H. Damerau, V. Forte, R. Garoby, M. Giovannozzi, B. Goddard, S. Hancock, K. Hanke, A. Huschauer, G. Iadarola, M. Meddahi, G. Métral, E. Métral, B. Mikulec, J.E. Muller, Y. Papaphilippou, S. Persichelli, G. Rumolo, B. Salvant, F. Schmidt, E. Shaposhnikova, R. Steerenberg, G. Sterbini, M. Taborelli, H. Timko, M. Vretenar, R. Wasef, C. Y. Vallgren, C. Zannini, CERN, Geneva, Switzerland
G. Franchetti, GSI, Darmstadt, Germany
A.Y. Molodozhentsev, J-PARC, KEK & JAEA, Ibaraki-ken, Japan
V. Vaccaro, Naples University Federico II, Napoli, Italy
M. Pivi, SLAC, Menlo Park, California, USA
M. Migliorati, University of Rome La Sapienza, Rome, Italy

*Abstract*

The future beam brightness and intensities required by the HL-LHC (High-Luminosity LHC) project and for possible new neutrino production beams triggered a deep revision of the LHC injector performances. The analysis, progressing in the framework of the LHC Injectors Upgrade (LIU) project, outlined major limitations mainly related to collective effects - space charge in PSB and PS, electron cloud driven and TMCI instabilities in the SPS, longitudinal coupled bunch instabilities in the PS for example - but also to the existing hardware capability to cope with beam instabilities and losses. A summary of the observations and simulation studies carried out so far, as well as the future ones, will be presented. The solution proposed to overcome the different limitations and the plans for their implementation will be also briefly reviewed.

## INTRODUCTION

The LHC upgrade foreseen for the high-luminosity run, planned after 2020, requires a vigorous upgrade for the injectors that will be realized in the framework of the LHC Injectors Upgrade (LIU) project. The new beam requirements, presented in Table 1 [1, 2], imply an increase of the beam brightness delivered by the injectors by about a factor of two. This could be realized only thanks to a series of major changes in all the machines of the injector complex plus the introduction of the new Linac4. In the following sections the main challenges related to the production of the high-brilliance 25 ns bunch spacing LHC beam are presented. The details on the hardware changes foreseen for the different machines can be found in [3] and in the references therein. The last section of this paper deals with new requirements for proton beams arising from the new proposals of short and long baseline neutrino experiments, requesting a beam power from the SPS up to 750 kW.

### *25 ns Bunch Spacing Production Schemes*

The production of the 25 ns bunch spacing beam, which remains the baseline for the upgrade, is realized as follows. The Linac2 fills each of the 4 PSB rings at 50 MeV (kinetic E) on $h = 1$. Each PSB bunch, in total 4, is transferred to the PS on $h = 7$ and after 1.2 s, the PS receives two other PSB bunches. On the 1.4 GeV (kinetic E) PS injection flat bottom, the 6 bunches are triple split. The resulting 18 bunches are accelerated up to 26 GeV/c where two consecutive longitudinal splittings produce the final bunch spacing of 25 ns creating a batch of 72 bunches. Prior to the transfer to the SPS, the bunches are rotated in the longitudinal plane to reduce the bunch length to about 4 ns. Up to four consecutive batches of 72 bunches are then injected in the SPS at 26 GeV/c, and accelerated to 450 GeV/c prior to extraction to the LHC [4, 5]. The longitudinal emittance is increased in the PS and SPS to reduce longitudinal instabilities, whereas transverse scraping is done in the SPS before reaching the extraction energy to eliminate tails.

Different challenges are related to the aforementioned production scheme. The first limitation is due to the high intensity injected in PSB, since every PSB bunch is split in the PS 12 times to obtain finally 72 bunches. Clearly, space-charge induced transverse blow up might spoil the small emittance delivered by the Linac during the injection process [6]. The second limitation is produced by the existing PSB injection process based on transverse painting, resulting in a linear correlation between transverse emittances and beam intensities (constant brightness). Both issues should be overcome with the Linac4, that will deliver 160 MeV (kinetic E) $H^-$ to the PSB instead of protons at 50 MeV. The third limitation is due to the long waiting time of the first batch of 4 bunches on the PS injection flat bottom: the large vertical space-charge tune shift of the order today of -0.28 and in the future required to be as high as -0.34 might cause transverse emittance blow up due to resonance crossing. The reduction of the space-charge tune shift to more acceptable values will be realised thanks to the increase of the extraction energy from the PSB from



ISBN 978-3-95450-118-2

# SPACE CHARGE EFFECTS IN ISOCHRONOUS FFAGS AND CYCLOTRONS*

T. Planche†, Y.-N. Rao, R. Baartman, TRIUMF, Vancouver, Canada

*Abstract*

Effects of space charge forces on the beam dynamics of isochronous rings will be discussed. Two different kinds of phenomena will be introduced through a brief review of the literature on the topic. The first one is a consequence of the very weak vertical focusing found in the low energy region of most cyclotrons. The space charge tune shift further reduces the vertical focusing, setting an upper limit on instantaneous current. The second one arises from the fact that longitudinal phase space is frozen in isochronous rings. This leads to effects of space charge forces which are very peculiar to isochronous machines. We will present the simulation tools being developed at TRIUMF to study these effects.

## LITERATURE REVIEW

In this section we present an overview of current knowledge concerning the effect of space charge in isochronous accelerators through a review of the major contributions to that field over the last forty years.

### *Transverse Space Charge Effects*

In cyclotrons at low energy, the vertical focusing comes mostly from the azimuthal dependence of the magnetic field, through edge focusing. In compact cyclotrons, where the radius of the injection orbit is comparable to the magnet gap, the azimuthal field dependence is smoothed out, leading to a very weak vertical focusing (vertical tune $\nu_z \ll 1$). The circulating current is then ultimately limited by the defocusing effect of space charge forces. The current limit is reached when the vertical focusing nearly vanishes, leading to beam losses on the vertical apertures.

This effect is well-known in the synchrotron theory as the space charge driven incoherent tune shift. In the case of non-relativistic particles, a number of textbooks give the following formula [1]:

$$\Delta(\nu_z^2)_{SC} = -\frac{2}{\pi}\frac{NRr_p}{\beta^2\gamma^3 B_f}\left[\frac{1}{b(a+b)} + \frac{\epsilon_1}{h^2}\right], \qquad (1)$$

where $N$ is the number of particles and $B_f$ is the bunching factor, $R$ is the orbit radius, $r_p$ is the classical proton radius ($1.54 \times 10^{-18}$ m), $\beta$ and $\gamma$ are relativistic factors, $a$ and $b$ are the horizontal and vertical beam half-size, resp., $h$ is the metal chamber half-height, and $\epsilon_1$ is the Laslett image coefficient, $\simeq 0.2$ for parallel plates.

The $\beta^{-2}$ factor in Eq. 1 reflects the strong energy dependence of the incoherent tune shift. One way to push further away this current limitation is to increase the injection energy. This is the reason why high-current cyclotrons use external ion sources capable of producing beams of a few hundred keV (300 keV at TRIUMF, 870 keV at PSI). Using even higher injection energy is in principle possible. One major drawback of this approach is that, for a given beam current, increasing the beam energy means increasing the beam power. For high-current machines, even a small fraction of beam loss at injection can lead to high-density power deposited onto the central region.

Another way to overcome this limitation is simply to increase the vertical focusing. This second approach, however, comes necessarily at the expense of the compactness of the machines. This is because, in the absence of radial field dependence, a strong vertical focusing is only possible if the particles experience strong azimuthal variation of the magnetic field.

Typically, cyclotrons in the 10's of MeV range are made as compact as possible to reduce cost. As a result, injection energy is a few 10's of keV and the first few turns have radius comparable to the magnet gap or smaller and there is no magnetic focusing. Use is made of rf focusing: injecting on the falling side of the waveform results in vertical focusing. Roughly, the contribution to $\nu_z^2$ is proportional to $\cos\phi$ where the energy gain is proportional to $\sin\phi$. The result is that along the bunch, the head has $\nu_z \approx 0$ and the tail has $\nu_z \approx 0.1$ to $0.2$. As current is raised, space charge begins to progressively "eat" the head of the bunch [2].

### *Longitudinal-transverse Effects*

The absence of longitudinal focusing in isochronous accelerators, as in synchrotrons at transition, gives rise to a very peculiar effect of longitudinal space charge forces.

Detailed studies of this phenomenon were carried out by M.M. Gordon [3]. The analytical model, assumed a continuous radial beam density (*i.e.* non-separated turns) and led to the prediction of space charge induced energy spread. This study also provides the first experimental evidence of current dependent energy spread, observed at the few $\mu$A level in the MSU cyclotron. Later, W. Joho generalized the description of this phenomenon to the case of separated turns [4].

The space charge induced energy spread has current-limiting consequences when extracting a high-power beam from a cyclotron through a magnetic channel. Through dispersion, this energy spread translates into an increase of the radial size of the beam, compromising the turn separation.

A major milestone in the study of longitudinal space charge effects in the absence of phase stability is the demonstration by W.J.G.M. Kleeven that a charge distri-

* TRIUMF receives federal funding via a contribution agreement through the National Research Council of Canada.

† http://trshare.triumf.ca/~tplanche/HB2012SC

ISBN 978-3-95450-118-2

# PLASMA TRAPS FOR SPACE-CHARGE STUDIES: STATUS AND PERSPECTIVES*

H. Okamoto#, M. Endo, K. Fukushima, H. Higaki, K. Ito, K. Moriya, T. Okano, S. Yamaguchi,
Hiroshima University, Kagamiyama, Higashi-Hiroshima 739, Japan
A. Mohri, Kyoto University, Kyoto 606, Japan

*Abstract*

The beam physics group of Hiroshima University has developed non-neutral plasma traps dedicated solely to a wide range of beam dynamics studies. Those unique experimental tools approximately reproduce, in the laboratory frame, a many-body Coulomb system that is physically equivalent to a charged-particle beam observed from the center-of-mass frame. We have designed and constructed two different types of traps that employ either a radio-frequency (rf) electric quadrupole field or an axial magnetic field for transverse particle confinement. The former type is commonly referred to as a "linear Paul trap (LPT)" and the latter as a "Penning trap". At present, three LPTs and one Penning trap are operational while a new Penning trap for beam halo experiments is under construction. Each of these compact experimental facilities consists of a trap, many power supplies, a vacuum system, a computer control system, etc., and is called "S-POD (Simulator for Particle Orbit Dynamics)". S-POD is particularly useful for fundamental studies of high-intensity and high-brightness hadron beams. We here report on the present status of S-POD and also briefly describe some future plans.

## INTRODUCTION

Recent worldwide demands for high-intensity and high-brightness hadron beams have made it more crucial to understand the mechanisms of the so-called "space-charge effects (SCEs)". Naturally, interparticle Coulomb interactions become stronger as the beam density increases in phase space. The simple single-particle picture is no longer applicable, but instead we have to take the coupled motions of all particles carefully into account. The whole beam is then regarded as an extremely complex nonlinear object rather than a group of many independent particles.

There have been a number of theoretical and experimental studies of SCEs in the past [1,2]. A self-consistent analytic treatment of the collective beam behavior is, however, hopelessly difficult without simplifying assumptions and crude mathematical models. Numerical simulations are very popular these days, but we still need long CPU time for high-precision space-charge simulations even with modern parallel computers. Experimentally, poor controllability of lattice and beam parameters limits systematic SCE studies. Besides, high-power beam losses are not allowed in practice to prevent serious machine damage, while we certainly need intense beams for space-charge experiments and even intentionally make them unstable to identify dangerous parameter ranges. Motivated by these facts, the S-POD project was initiated at Hiroshima University about a decade ago.

S-POD experiments are based on dynamical similarity between non-neutral plasmas in compact electro-magnetic traps and relativistic charged-particle beams in alternating-gradient (AG) focusing channels [3]. Four independent S-POD systems are presently in operation for systematic experimental studies of SCEs. This novel tabletop apparatus enables us to explore diverse beam-physics issues without relying on expensive, large-scale machines. In the following, we outline the recent S-POD status and space-charge experiments in preparation. More detailed information regarding how S-POD works can be found in previous publications [4-6]. Several technical issues required for further improvement of the S-POD performance are also addressed in this paper.

## PRESENT STATUS

### *Paul Traps*

S-POD I, II, and III employ LPTs whose typical operating frequency is around 1 MHz. Figure 1 shows the LPT currently installed in the vacuum chamber of S-POD III. Four electrode rods are symmetrically placed around the trap axis to produce an electric quadrupole field for transverse particle confinement. The rods are axially divided into several pieces (five in Fig. 1), so that we can apply different bias voltages to form axial potential wells. The total length of the LPT in Fig. 1 is only about 20 cm and the aperture size is 1 cm$\phi$. The other LPTs used for S-POD I and II have roughly the same dimension. As the

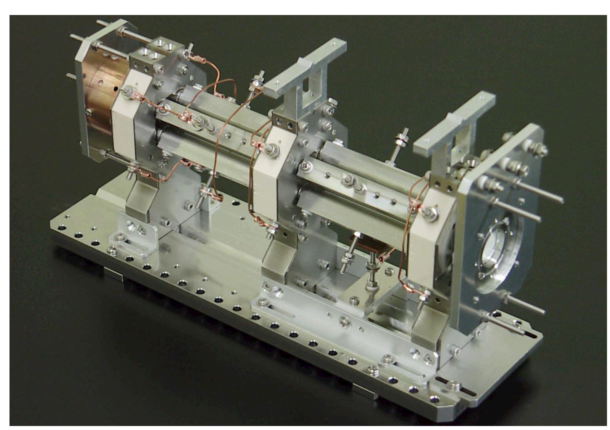

Figure 1: A multi-sectioned LPT for S-POD.

*Work supported in part by a Grant-in-Aid for Scientific Research, Japan Society for the Promotion of Science.
#okamoto@sci.hiroshima-u.ac.jp

ISBN 978-3-95450-118-2

# DYNAMICAL ASPECTS OF EMITTANCE COUPLING IN INTENSE LINAC BEAMS

I. Hofmann, GSI-HI-Jena, 64291 Darmstadt, Germany

*Abstract*

In this paper we use the TRACEWIN code to study in an idealized lattice model the dynamical behavior of non-equipartitioned bunched beams and their approaching equipartition for certain resonance conditions described by stability charts. It is shown that rms emittance transfer on these resonance stop-bands depends on times scales of tune change, whereas regions free from third or fourth order resonances are "safe" and not subject to rms emittance coupling. This provides additional information to support the validity of the stability charts, and as a practically useful design tool for high current linacs.

## INTRODUCTION

One of the important criteria in high intensity linac design is avoidance of emittance transfer between the longitudinal and transverse degrees of freedom. It is commonly accepted that nonlinear space charge is the driving force of emittance coupling, if in addition a resonance condition is satisfied. In order to identify the extended regions in tune space, where coupling could occur, stability charts have been introduced to assist linac design and linac beam dynamics studies [1]. These charts are the result of an analytical self-consistent perturbational analysis of two-dimensional anisotropic beams using Vlasov's equations [2]. Numerous particle-in-cell simulations have been published to support the validity of the charts also for realistic distributions, first in 4D, then in 6D, and by using different simulation codes [3, 4, 5]. An experimental confirmation of the emittance exchange at the "main resonance" $k_z/k_x = 1$ was obtained at the GSI UNILAC [6].

The emphasis of the present study is to illustrate the emittance behavior when tunes cross dynamically regions of tune space, which are characteristic for high current linac design. These simulations with the Tracewin code can be considered as additional check of the validity of the stability charts under tune variation.

## GENERAL REMARKS ON THE STABILITY CHARTS

The definition of the stability charts is to distinguish regions in a suitable representation of tune space, where nonlinear space charge modes are stable, from those where unstable emittance exchange is possible. An example for $\epsilon_z/\epsilon_x = 3$ is shown in Fig. 1. Note that the condition for equipartition (EP) is thus $k_z/k_x = 1/3$, which is indicated by a dotted line. For proper interpretation of the charts a number of observations should be made first.

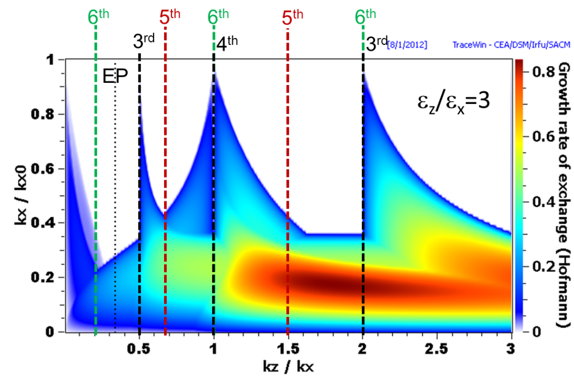


Figure 1: Stability chart for $\epsilon_z/\epsilon_x = 3$ showing stop-bands for $3^{rd}$ and $4^{th}$ order resonances as well as the location of potential $5^{th}$ and $6^{th}$ order resonances (dashed lines).

- *The charts differ essentially from the commonly used tune diagrams of circular accelerators.* The latter only visualize possible resonances with the focusing lattice. They contain no information about real driving terms (strengths) of resonances, and space charge only enters as incoherent "tune footprint". The stability charts, on the contrary, go far beyond and display these driving terms derived from a self-consistent theory (expressed as growth rates and stop-band widths). The choice of a chart with tune depression versus tune ratio is optimum for these internal space charge resonances as the latter characterizes the order of the mode, and the former the width of the associated stop-bands. A third parameter is needed, which is the ratio of emittances. For a dynamically changing emittance ratio it might be expedient to recalculate the charts.

- *The analytical Vlasov theory behind the charts* was developed as theory of resonant instabilities for an initial 2D KV-distribution, but comparison with 3D PIC-simulation has shown that it can be applied equally to realistic beams. For a uniform initial real space distribution all possible modes are present at noise level, from which they may grow at an exponential rate (indicated by the color code). A parabolic initial density profile, instead, contains already a significant space charge octupole and a predicted resonant instability evolves on a shorter time scale.

- *Only resonances up to fourth order* were considered in the Vlasov analysis due to the increasing complexity with order. Theoretically possible resonance lines could be at $k_z/k_x = m/n$, with $m+n$ the order of the resonance. The theoretical location of resonances of



ISBN 978-3-95450-118-2

# STATUS AND RESULTS OF THE UA9 CRYSTAL COLLIMATION EXPERIMENT AT THE CERN-SPS*

S. Montesano†, CERN, Geneva, CH and
W. Scandale, CERN, Geneva, CH, LAL, Orsay, FR, INFN, Roma, IT
for the UA9 Collaboration

*Abstract*

The UA9 experimental setup was installed in the CERN-SPS in 2009 to investigate the feasibility of the halo collimation assisted by bent crystals. Two-millimeter-long silicon crystals, with bending angles of about 150 microrad, are tested as primary collimator instead of a standard amorphous target. Studies are performed with stored beams of protons and lead ions at 270 Z GeV. The loss profile is precisely measured in the area near the crystal-collimator setup and in the downstream high dispersion area. A strong correlation of the losses in the two regions is observed and a steady reduction of dispersive losses is recorded at the onset of the channeling process. The losses around the accelerator ring are also reduced. These observations strongly support our expectation that the coherent deflection of the beam halo by a bent crystal should enhance the collimation efficiency in hadron colliders, such as the LHC.

## INTRODUCTION

In hadron colliders, like the LHC, superconducting magnet technology allows for high-intensity beams necessary to guarantee a large discovery potential. In this situation, the halo particles surrounding the beam core may produce high-power losses. Multi-stage collimation systems are implemented to safely absorb these particles. The primary collimator is the first solid target that repeatedly intercepts the diffusive halo particles, imparting to them random angular kicks by multiple Coulomb scattering. Scattered particles are thus brought into the secondary collimators and into the absorbers. Due to the very low diffusion speed and to the very small impact parameter, halo particles have a finite probability of being back-scattered in the vacuum pipe. This process produces residual losses which are detrimental for both the accelerator and the experimental detectors. Increasing the number of collimation stages improves the collimation performance. In the four-stage LHC setup, a cleaning efficiency of 99.97% is routinely reached [1].

A bent crystal replacing the primary collimator should reduce by an order of magnitude the residual collimation leakage [2, 3]. At a precise orientation of the crystal, impinging particles are trapped between atomic planes and are coherently deflected following the curvature of the lattice (channeling). For the majority of the particles, this deflection happens during the first passage through the crystal. The particles that escape deflection will cross the crystal again and will have an additional probability of being channeled and absorbed in subsequent turns. Due to this process, the impact parameter of the particles with the secondary collimators and the absorbers is considerably increased. Moreover, particles channeled among the crystal planes have fewer encounters with the nuclei of the lattice resulting in a reduced probability of nuclear interactions, of diffractive scattering and, for ion beams, of fragmentation and electromagnetic dissociation events. As a consequence, crystal-assisted collimation should enhance both global and local loss suppression.

The UA9 Collaboration started to investigate crystal collimation in 2009. The single-pass interaction of the beam with the crystal is studied in details at the CERN North Area test beam. In this facility, crystals built with different technologies are tested and characterized in order to select the most suitable ones to the collimation experiment in the CERN-SPS ring. In the SPS the prototype of a crystal-assisted collimation system is implemented. Ad hoc instrumentation is installed to evaluate its collimation capabilities, in comparison with a system based on an amorphous primary target. Using this installation, a reduction of the loss rate close to the primary target has been observed when using a crystal instead of an amorphous material, both for proton [4] and for Pb ion [5] beams. Recently the reduction of the off-momentum halo population has been estimated under the same conditions [6].

## PROTOTYPE SYSTEM IN THE CERN-SPS

The conceptual layout of the UA9 experiment installed in the straight section 5 of the SPS is shown in Fig. 1. The crystal collimation prototype system is composed by the crystal itself and by the absorber. All the remaining equipment is used to study the performance and the properties of the collimation system.

### *Collimation System*

The crystals used by the experiment are mounted on goniometers that allow to align their lattice planes to the incoming halo particles. Each goniometer serves a pair of crystals, installed on two supports that allow horizontal linear movements. The two supports are connected with an aluminum bar. When one of the two crystals is placed at a fixed distance from the beam, it can be rotated in an angular range of tens of mrad by applying a linear movement (1 mm range) to the second one. This rotational movement

* Work supported by EuCARD program GA 227579, in "Collimators and Materials for high power beams" (Colmat-WP) and by LARP.
† simone.montesano@cern.ch

ISBN 978-3-95450-118-2

# EQUIPARTITION, REALITY OR SWINDLE ?

Jean-Michel Lagniel, GANIL, Caen, France


*Abstract*

By way of introduction to a general discussion on space-charge induced energy equipartition (EQP), the following questions will be tackled : Where is the swindle ? Why the formula presently used to define EQP is wrong ? Why energy exchanges can occur although the EQP rule is respected ? Why safe tunings can be found although the EQP rule is not respected ? Why some linac designers nevertheless like to use the EQP rule ?


## THE EQUIPARTITION THEOREM

The EQP theorem, also known as the "equipartition of energy principle", is a fundamental law in classical statistical mechanics. It states that the total energy of a system in thermal equilibrium is shared equally amongst all its energetically accessible independent degrees of freedom. In another way of saying that, the systems relevant of the classical statistical mechanics must distribute their available energy evenly amongst their independent accessible modes of motion when they are reaching a steady state.

For example, for an ideal mono-atomic gas with N "particles" confined in a box (3 translational degrees of freedom only, no rotational and vibrational degrees of freedom), it means that the average kinetic energies in every one of the 3N translational degrees of freedom shall be equal when the system will be in equilibrium.

The EQP theorem is here easily understandable looking to the microscopic level where the energy transfer induced by the collisions between the particles has an equal probability to be done towards the different degrees of freedom.

We must point out here that for this example, the EQP theorem concerns the 3N kinetic energies averaged over time of each one of the N particles

$$\begin{aligned}
&\frac{1}{T}\int_0^T v_{x1}^2\,dt = \frac{1}{T}\int_0^T v_{y1}^2\,dt = \frac{1}{T}\int_0^T v_{z1}^2\,dt = \ldots \\
&= \frac{1}{T}\int_0^T v_{xi}^2\,dt = \frac{1}{T}\int_0^T v_{yi}^2\,dt = \frac{1}{T}\int_0^T v_{zi}^2\,dt = \ldots \\
&= \frac{1}{T}\int_0^T v_{xN}^2\,dt = \frac{1}{T}\int_0^T v_{yN}^2\,dt = \frac{1}{T}\int_0^T v_{zN}^2\,dt \\
&\text{when } T \to \infty \qquad (1)
\end{aligned}$$

For large N systems, (1) leads to equal mean kinetic energies in the x, y and z translational degrees of freedom, the averaging being done over the N particles at a given time

$$\frac{1}{N}\sum_{i=1}^{N} v_{xi}^2 = \frac{1}{N}\sum_{i=1}^{N} v_{yi}^2 = \frac{1}{N}\sum_{i=1}^{N} v_{zi}^2$$

or, written in a simplest form

$$\langle v_x^2\rangle = \langle v_y^2\rangle = \langle v_z^2\rangle \qquad (2)$$

It is important to understand that the equality (2) which describes the macroscopic system behaviour is a consequence of the equality (1) which describes the microscopic behaviour of the systems when the EQP theorem can be applied.

### *EQP Theorem Validity Limit*

The law of equipartition holds only for ergodic systems in thermal equilibrium, the ergodic hypothesis being considered as the basis of the statistical physics and an attempt to provide a bridge between dynamics and statistics. It basically asserts that the state ("trajectory") of an ergodic Hamiltonian system with n degrees of freedom, represented by a point in the 2n-phase space ($q_1$, ..., $q_n$, $p_1$, ..., $p_n$ with $q_i$ and $p_i$ the generalized positions and momenta respectively) will pass equally often on every point of the constant-energy surface in this 2n-phase space during its long term evolution.

The ergodic hypothesis is still one of the most fascinating problems of physics and mathematics, subject of numerous discussions and publications (e.g. [1]) and by far out of the scope of this paper. In order to stick to the question of EQP applicability to our linac beams we will only recall that

*A system is ergodic when the energy surface cannot be divided into finite regions such that, if the initial point in phase-space is located in one such region, the system trajectory remains entirely within that region (John von Neumann*, 1932).

One of the very best descriptions of the Hamiltonian systems behaviour in this context is given in [2]. This paper shows how the complexity of the phase-space trajectories evolves with the nonlinearity level (weak / strong nonlinearity) and with the perturbing forces strength (K) which finally governs the global behaviour of the nonlinear systems :

- Complete integrability without perturbation (K = 0). The particles trajectories in phase space are ordered, their motions are quasiperiodic. The phase space trajectories of the resonant particles are represented by fix points and the non-resonant trajectories by continuous lines.
- KAM integrability for a weak perturbation ($K \to 0$, weakly non-integrable Hamiltonian system). In this first level of disorder in phase space, most of the non-resonant trajectories are only slightly deformed but remains continuous ; then form a "KAM impassable barrier" which limits the accessible domain for the other particles. In the same time, the separatrix associated to the resonances are destroyed, narrow chaotic layers appears (Arnold and Avez, 1968).
- Complete chaos reached when the perturbation is increased ($K \to \infty$). The particle motions are chaotic everywhere in phase space. The dynamics in such conditions becomes so erratic that the notion of phase space trajectory loses its meaning.



ISBN 978-3-95450-118-2

# BEAM LOSS DUE TO FOIL SCATTERING IN THE SNS ACCUMULATOR RING*

J.A. Holmes and M.A. Plum, ORNL, Oak Ridge, TN, 37831, USA*

*Abstract*

In order to better understand the contribution of scattering from the primary stripper foil to losses in the SNS ring, we have carried out calculations using the ORBIT Code aimed at evaluating these losses. These calculations indicate that the probability of beam loss within one turn following a foil hit is ~$1.8\times10^{-8}\tau$, where $\tau$ is the foil thickness in $\mu g/cm^2$, assuming a carbon foil. Thus, for a typical SNS stripper foil of thickness $\tau = 390$ $\mu g/cm^2$, the probability of loss within one turn of a foil hit is ~$7.0\times10^{-6}$. This note describes the calculations used to arrive at this result, presents the distribution of these losses around the SNS ring, and compares the calculated results with observed ring losses for a well-tuned production beam.

## INTRODUCTION

We present here the results of computational experiments aimed at evaluating prompt (within one turn) losses in the SNS ring due to scattering in the stripper foil, and we compare the calculated results with observed ring losses for a well-tuned production beam. We performed the calculations using the ORBIT Code [1]. The calculations consisted of injecting particles into the ring through the stripper foil, tracking them for a single turn, and then analyzing their fate. The injected distribution and location on the foil were taken to be those of the linac beam. Although the actual distribution of foil hits differs from this assumption, due to the circulating beam, the differences are at most a few millimeters or parts of a milliradian and are not considered here. We also made the foil artificially wide to ensure that no injected particles missed the foil. We employed the SNS ring lattice with production tunes $\nu_x = 6.23$ and $\nu_y = 6.20$. The beam energy was taken to be 925 MeV. In order to evaluate the losses, we included a complete set of limiting apertures around the ring. Because we are interested in losses due to foil scattering only, we performed single-particle tracking. Space charge and impedances were ignored. Two alternative settings of the ring injection kickers were used: 1) large kicks to give small betatron oscillations typical of the start of injection, and 2) small kicks to give large betatron oscillations typical of the end of injection.

The ORBIT Code contains four options for treating scattering from carbon stripper foils: 1) transparent foil (ignore scattering); 2) small angle Coulomb scattering only; 3) the full foil model with contributions from small angle Coulomb scattering, Rutherford scattering, nuclear elastic scattering, and nuclear inelastic scattering; or 4) the ORBIT collimation module with an appropriately thin carbon window. Options 3 and 4 contain the same physics [2] and differ only in method of access. Although the physics models in options 3 and 4 are identical, for historical reasons, the small angle Coulomb scattering contribution is formulated differently than in option 2. Option 2 was coded in ORBIT before the development of the collimator model, and it adopted the small angle Coulomb scattering model from the ACCSIM Code [3]. The collimator module uses the small angle and Rutherford scattering formulations presented in the textbook by Jackson [4]. The calculations presented here were carried out alternatively using each of these four methods. We applied both options 3 and 4, rather than simply option 3, as a consistency check and found the results to be in agreement. The assumed density of carbon in all these models is 2.265 $g/cm^3$, consistent with graphite, but because the results are presented for foil thicknesses in units of $\mu g/cm^2$, they are valid for diamond foils also.

Stripper foil model options 2-4 all involve Monte Carlo techniques and the use of random numbers. In its present implementation, we use the computer's clock time to seed the random number generator. Because of this the precise results vary from run to run, but by performing several "identical" calculations, the statistical accuracy of the results can be ascertained. We use $10^7$ macroparticles in the calculations presented here, so that processes of $10^{-6}$ probability should occur ~10 times in our calculations.

## RESULTS

The overall results of the calculations described in Section 1 are presented in Table 1. The first column describes the case. The first three cases assume a foil thickness of 390 $\mu g/cm^2$ and the last three cases assume an artificially high thickness of 18000 $\mu g/cm^2$. This seemingly arbitrary number is the thickness of the original SNS secondary stripper foil and, as such, it has been used in other studies. The 390 $\mu g/cm^2$ results were obtained by averaging over ten runs for each case. For each foil thickness, we present the results for 1) transparent foil (ignore scattering); 2) small angle Coulomb scattering only; and 3) the full foil model with contributions from small angle Coulomb scattering, Rutherford scattering, nuclear elastic scattering, and nuclear inelastic scattering. The performance of the calculations using the ORBIT collimation module, with an appropriately thin carbon window, essentially duplicated the full foil model results. The second and third columns show the number of macroparticles lost due to inelastic nuclear scattering and

* ORNL/SNS is managed by UT-Battelle, LLC, for the U.S. Department of Energy under contract DE-AC05-00OR22725.



ISBN 978-3-95450-118-2

# INJECTION DESIGN FOR FERMILAB PROJECT X*

D.E. Johnson#, C.Y. Tan, Z. Tang Fermi National Accelerator Laboratory, Batavia, IL, 60510 USA


*Abstract*

Fermilab is proposing a staged approach for Project X, a high power proton accelerator system. The first stage of this project will be to construct a 1 GeV continuous wave (CW) $H^-$ superconducting linear accelerator to inject into the existing 8 GeV Booster synchrotron ultimately providing in excess of 1 MW beam power for the Neutrino program out of the Main Injector. We will discuss the current project plans for injection into the Booster and related issues.


## INTRODUCTION

Fermilab accelerator upgrade project called Project X has investigated several different accelerator configurations [1,2] since the initial Proton Driver [3,4] was proposed in 2000. The current base line design configuration [5] consists of a 3 GeV superconducting CW $H^-$ linac providing beam simultaneous to a 3 GeV Experimental Program [6] and a 3-8 GeV pulsed superconducting linac for multi-turn H- injection into the Recycler Ring at 8 GeV. The issues relating to 8 GeV multi-turn injection into the Recycler were discussed at HB2010 [7].

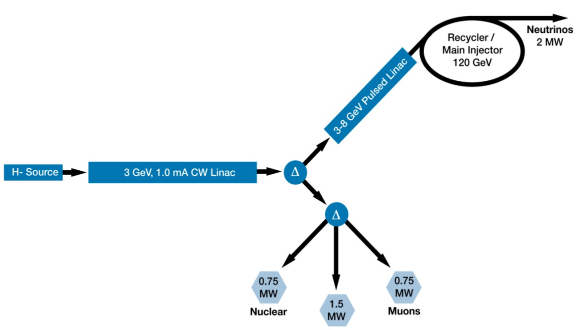


Figure 1: Block diagram of the accelerator configuration in the Project-X reference design.

Although the reference design is still the base line, financial and budgetary constraints led the project to investigate a staged approach which will utilize some of the existing infrastructure [8].

## STAGED APPROACH

The functionality of the reference design can be realized by a set of three stages each capable of increasing the beam power to the long base line neutrino program while supporting a robust experimental program at the 1, 3, and 8 GeV energy ranges. More information about the staging may be found in reference 8. A block diagram of a staged approach is shown in Figure 2 with each of the stages color coded: existing rings in black, stage 1 in blue, 2 in green, and 3 in red. Not shown is the existing 400 MeV linac feeding the Booster. Here, we will concentrate only on Stage 1.

### *Stage 1*

The first stage replaces the existing 400 MeV pulsed Linac with a 1 GeV superconducting CW Linac with an average current of 1 mA. About 2% of the linac beam will be injected into an upgraded 15 Hz Booster accelerator leading to a 50% increase the per pulse proton intensity delivered from the Booster to the Main Injector, thus establishing the potential of delivering up to 1.2MW beam power to the long baseline neutrino experiments. The balance of the linac beam can be delivered to the newly developed Muon campus, providing a factor of ten increase in beam power available to the Mu2e experiment and/or to newly developing programs devoted to nuclear electric dipole moments (edm), ultra-cold neutrons, and possible energy applications [8].

The integration of the new linac into the complex requires the upgrade of the Booster injection system from 400 MeV to 1 GeV, new transport lines, and potentially new civil construction, depending on siting choices.

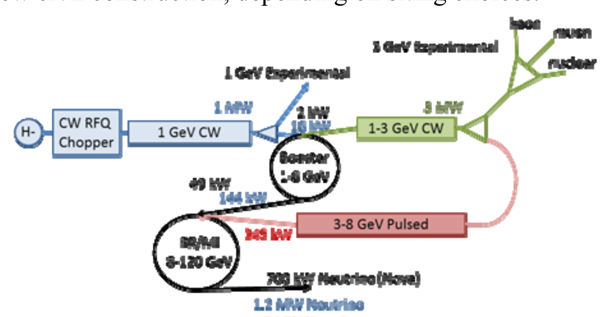


Figure 2: A staged approach for Project X.

## CURRENT BOOSTER CONFIGURATION

The current injections into Booster utilizes a linac pulse length equivalent to 1-10 turns @~2.2 us/turn and does not utilize any transverse phase space painting. The transport line from the linac is "matched to the ring lattice and therefore the linac transverse emittance defines the "base" emittance of the beam in the Booster. Adiabatic capture is utilized. Typical injection intensities are around 5E12 ions/cycle at a 7.5 Hz injection repetition rate corresponding to an injected beam power of 2.4 kW. For the typical carbon foil thickness of ~380 $\mu g/cm^2$, the expected stripping efficiency is 99.9% leaving only 0.1%

*Work supported by US DOE under contract #DE-AC02-07CH11359
#dej@fnal.gov

ISBN 978-3-95450-118-2

# BEAM LOSS CONTROL FOR THE FERMILAB MAIN INJECTOR*

Bruce C. Brown†, Fermilab, Batavia, IL 60510, USA

*Abstract*

From 2005 through 2012, the Fermilab Main Injector provided intense beams of 120 GeV protons to produce neutrino beams and antiprotons. Hardware improvements in conjunction with improved diagnostics allowed the system to reach sustained operation at 400 kW beam power. Losses were at or near the 8 GeV injection energy where 95% beam transmission results in about 1.5 kW of beam loss. By minimizing and localizing loss, residual radiation levels fell while beam power was doubled. Lost beam was directed to either the collimation system or to the beam abort. Critical apertures were increased while improved instrumentation allowed optimal use of available apertures. We will summarize the impact of various loss control tools and the status and trends in residual radiation in the Main Injector.

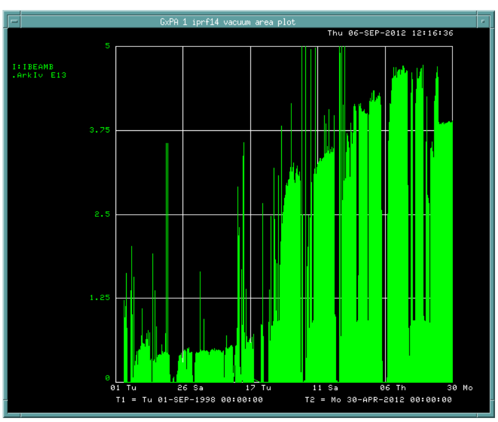


Figure 1: Sampled Intensity per cycle from September 1998 through April 2012.

## PROTONS TO PRODUCE NEUTRINOS AND ANTIPROTONS

On April 30, 2012, the Fermilab accelerator complex began an extended shutdown. This followed seven months after the end of operation for the Tevatron on September 30, 2011 with the accompanying end of antiproton source operation. For the Fermilab Main Injector, this marked $11\frac{1}{2}$ years of commissioning and operation in successively higher intensity operation modes. As the physics program requirements demanded more beam power, limitations in the intensity and beam quality from the Fermilab Booster were overcome by using slip stacking injection[1].This was implemented first for antiproton production and later for neutrino production as well. As intensities increased, a program of monitoring and mitigating losses and residual radiation has controlled the radiation exposure for personnel involved in maintenance and upgrade activities.

Figure 1 illustrates this intensity increase using the number of protons per cycle on a periodic sample of the acceleration cycles. An injection from the Booster is termed a 'batch' with typical intensity of $4–5 \times 10^{12}$ protons and up to 84 rf buckets of beam. Machine commissioning was followed by multibatch operation for a Tevatron fixed target run. In 2001, this transitioned to a Tevatron collider run which utilized a single batch from the Booster for pbar production. Slip stacking injection of two Booster batches for pbar production was developed in 2004. Injecting two batches into buckets of different frequency allows momentum stacking when the buckets slip into alignment and the beam is recaptured in a larger rf bucket. The NuMI beamline for neutrino production was commissioned in 2005 requiring acceleration in each cycle of 5 Booster batches for NuMI in addition to a double batch for pbar production on each cycle (5 plus 2). Slip stacking for increased NuMI beam (9 plus 2) was commissioned in 2007 as was the Main Injector collimation system. At that point intensity was limited by losses in both the Main Injector and the Booster. Collimation, along with improved Booster beam quality, controlled activation and permitted Main Injector intensity per cycle to increase.

Several other features of the Fermilab HEP program are apparent in Fig. 1. Facility upgrades are accomplished using shutdown periods of several weeks. Periods of reduced intensity mark the times required to repair or replace the NuMI horn or target. When pbar production was ended neutrino target intensity limits due to thermal shock could be met by accelerating 9 batches with only three being slip stacked. Reduced per pulse intensity from September 2011 through April 2012 reflects this limitation. The spikes which report exceptionally higher intensity are instrumental. The data uses some of the instrumentation which was replaced by 2007 (see below) and spike above the trend are typically due to instrumentation or data recording errors.

Preparations for the high intensity operation for neutrino production included a program to identify residual radiation issues in the Main Injector tunnel. Exploratory residual radiation measurements in 2004 and 2005 monitored more than 100 locations with more than 20 milliRad/hr residual radiation on contact. By October 2005, a program using a sensitive meter to monitor 127 (later 142) bar-coded locations was initiated[2]. By October 2006, new electronic readout for the beam loss monitors was available[3].

* Operated by Fermi Research Alliance, LLC under Contract No. DE-AC02-07CH11359 with the United States Department of Energy
† bcbrown@fnal.gov



ISBN 978-3-95450-118-2

# THE DESIGN AND COMMISSIONING OF THE ACCELERATOR SYSTEM OF THE RARE ISOTOPE REACCELERATOR – ReA3 AT MICHIGAN STATE UNIVERSITY*

X. Wu#, B. Arend, C. Compton, A. Facco, M. Johnson, D. Lawton, D. Leitner, F. Montes, S. Nash, J. Ottarson, G. Perdikakis, J. Popielarski, A. Rodriguez, M. Syphers, W. Wittmer, Q. Zhao
National Superconducting Cyclotron Laboratory, East Lansing, MI 48824, U.S.A.

*Abstract*

The National Superconducting Cyclotron Laboratory (NSCL) at Michigan State University (MSU) is currently constructing the new rare isotope reaccelerator facility, ReA3. The new facility will provide unique low-energy rare isotope beams by stopping fast rare isotopes in gas stopping systems, boosting the charge state in an Electron Beam Ion Trap (EBIT) and reaccelerating them in a compact superconducting linac [1,2,3]. The rare isotope beams will be produced initially by the existing Coupled Cyclotron Facility (CCF) at NSCL and later by Facility for Rare Isotope Beams (FRIB), currently being designed at MSU [4]. The ReA3 accelerator system consists of a Low Energy Beam Transport (LEBT), a room temperature RFQ and a superconducting linac utilizing superconducting quarter wave resonators. An achromatic High Energy Beam Transport and distribution beam lines towards the new ReA3 experimental area will deliver the reaccelerated rare isotope beams to the multiple target station. Beams from ReA3 will range from 3 MeV/u for heavy nuclei such as uranium to about 6 MeV/u for ions with A<50. The commissioning of the EBIT, RFQ and two cryomodules of the linac is currently underway. The accelerator system design and status of commissioning of ReA3 and future plan will be presented.

## INTRODUCTION

In-flight Particle Fragmentation (PF) method producing fast Rare Isotope Beams (RIBs) has been used at the NSCL (floor plan shown in Figure 1) for nuclear structure and nuclear reaction research with great success since 1989. Heavy ions produced by two ECR ion sources are accelerated by two coupled superconducting cyclotrons (K500 and K1200) to energies up to ~150 MeV/u with beam power of a few kilowatts, and focused onto the production target. The produced RIBs are separated in-flight by the A1900 Fragment Separator, and delivered to multiple fast beam experimental halls for fast RIBs experiments. To meet the strong demands for high quality low energy RIBs from nuclear astrophysics and nuclear physics program [5], significant R&D has taken

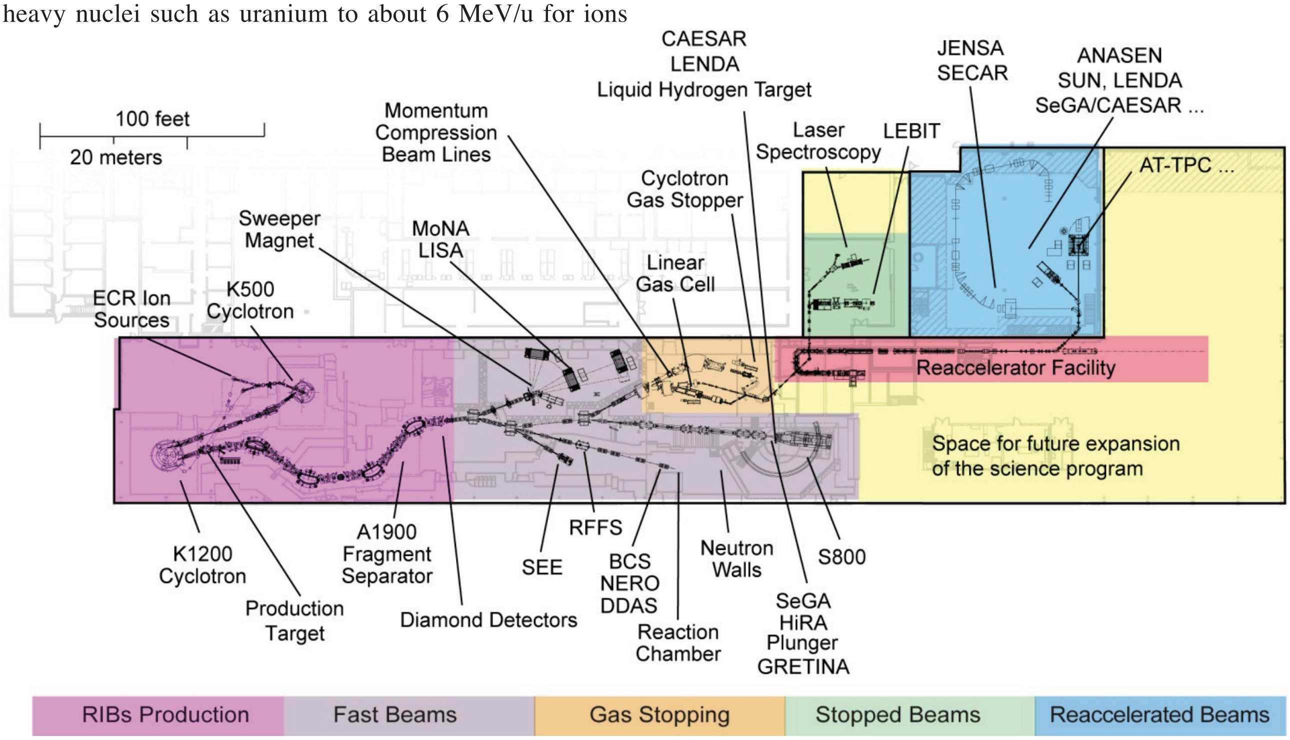


Figure 1: The facility layout of the NSCL.

*Work supported by Michigan State University
#xwu@nscl.msu.edu

ISBN 978-3-95450-118-2

# BEAM DYNAMICS DESIGN OF ESS WARM LINAC

M. Comunian, F. Grespan, A. Pisent, INFN/LNL, Legnaro, Italy
M. Eshraqi, R. Miyamoto, A. Ponton, ESS, Lund, Sweden
R. De Prisco, ESS and Lund University, Lund, Sweden
L. Celona, S. Gammino, L. Neri, INFN/LNS, Catania, Italy
I. Bustinduy, ESS, Bilbao, Spain

*Abstract*

In the present design of the European Spallation Source (ESS) accelerator, the Warm Linac will accelerate a pulsed proton beam of 50 mA peak current from source at 0.075 MeV up to 80 MeV. Such Linac is designed to operate at 352.2 MHz, with a duty cycle of 4% (3 ms pulse length, 14 Hz repetition period). In this paper the main design choices and the beam dynamics studies for the source up to the end of DTL are shown.

## INTRODUCTION

The ESS, going to be built at Lund, will require a high current linac to accelerate protons for the spallation process on which high flux of pulsed neutrons will be generated. The accelerator is 5 MW superconducting proton linac delivering beams of 2.5 GeV to the target in pulses of 2.86 ms long with a repetition rate of 14 Hz [1]. Beam current is 50 mA, 4% duty cycle, which at 352.21 MHz is equivalent to ~ 9×10^8 protons per bunch.

Both hands on maintenance and machine protection set a strict limit on beam losses and have been a concern in every high power linac: Therefore it is crucial, especially for high power accelerators, to design a linac which does not excite particles to beam halo and also minimizes emittance growth. The ESS linac is carefully designed to minimize such effects all along the linac and transfer lines.

In this paper the physical design of ESS warm linac is shown.

## SOURCE AND LEBT

ESS requirements for proton source are quite restrictive, the current required for the ESS facility in the baseline configuration can be satisfied by means of conventional Microwave Discharge Ion Source (MDIS), based on the plasma direct absorption of the pumping electromagnetic waves through the Electron Cyclotron Resonance mechanism.

Considering the experience gained with the already designed and optimized sources at INFN-LNS, the needs of the initial phase of the facility will be fulfilled by using a "conservative" approach, based on a standard MDIS configuration. The second phase requirements are more stringent in terms of currents (up to 90 mA or more), but possible solutions for the source upgrading have been considered already in the design phase, by proposing a new flexible magnetic system. More standard solutions for performance optimization (which do not require any ab-initio design modification) will be implemented, as the alumina tubes introduced into the plasma chamber. Therefore we will not only take care about currents, emittance, efficiency and reliability requirements, but also to a continuous MDIS development [2].

In low energy beam transport of high intensity beams the self-generated repulsion between charged particles can generate a large and irreversible emittance growth, while the optimum matching with the RFQ requires high focussing and low emittance. To reduce this negative effect the space charge neutralization of the beam charge can be done by ionizing the residual gas. Such space charge compensation regime has many similarities to plasma but the electric field produced for example by the pre-chopper introduces many significant variations especially in the transition regimes. In order to preserve the compensation regime from the high electric field located in the extraction system and inside RFQ, a repelling electrode was inserted in the extraction system and in the RFQ collimator. Then, to reduce the longitudinal dimension of the LEBT and to keep free space for the installation of diagnostics, we designed the chopper chamber coupled to the Turbo molecular Pump (TMP) as shown in Fig. 1.

The extraction system has been simulated with AXCEL and the emittance parameters at the position z = 0.14 m has been used as input for the simulation of the LEBT by using the TraceWin code. This software has been chosen because it is able to take into account of space charge along the LEBT and it is able to perform the optimization of the optical element parameters so that we may achieve the RFQ Twiss parameters. Figure 2 shows the beam density obtained in the LEBT by using a space charge compensation value of 98% [3].

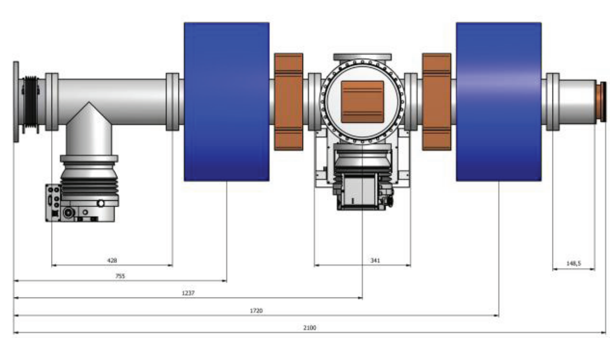


Figure 1: LEBT layout.



ISBN 978-3-95450-118-2

# BEAM DYNAMICS OF THE ESS SUPERCONDUCTING LINAC

M. Eshraqi, H. Danared, R. Miyamoto,
European Spallation Source, Lund, Sweden

*Abstract*

The European Spallation Source, ESS, uses a linear accelerator to deliver the high intensity proton beam to the target station. The nominal beam power is 5 MW at an energy of 2.5 GeV. The superconducting part covers more than 95% of the energy gain and 90% of the length. The beam dynamics criteria applied to the design of the superconducting part of the linac including the frequency jump at a medium energy of 200 MeV as well as the beam dynamics performance of this structure are described in this paper.

## INTRODUCTION

The European Spallation Source, ESS, to be built in Lund, Sweden, will require a high current proton linac to accelerate protons to be used for the spallation process on which high flux of pulsed neutrons will be generated. The accelerator is a 5 MW superconducting proton linac delivering beams of 2.5 GeV to the target in pulses of 2.86 ms long with a repetition rate of 14 Hz [1], [2] corresponding to a duty cycle of 4%. Beam current is 50 mA, which at 352.21 MHz is equivalent to $\sim 9 \times 10^8$ protons per bunch. From $\sim$ 200 MeV onward the acceleration is done at the second harmonic of the front end, 704.42 MHz, to improve the energy efficiency of the linac.

Hands on maintenance and machine protection set strict limits, 1 W/m and 0.1 W/m respectively, on beam losses and have been a concern in every high power linac [3]−[6] , therefore it is crucial, specially for high power accelerators, to design a linac which does not excite particles to beam halo and also keeps the emittance growth to a minimum to avoid losing the particles that otherwise get too close to the acceptance and eventually escape the separatrix. The ESS linac is designed carefully to minimize such effects all along the linac and transfer lines. A recent study relaxed the losses in the low energy part of the linac, mainly in the RFQ and MEBT [7], from the conventional 1 W/m.

The latest design of the linac will be presented here and the 2003 Design Update can be found in Table 1 and reference [1]. In the new design it is foreseen not to exclude the possibility of a potential power upgrade of the linac. One of the scenarios for such a power upgrade would be increasing the power by increasing the energy to 3.5 GeV and/or increasing the current to 100 mA [8].

The beam dynamics of the superconducting linac as well as the handling of the frequency jump will be presented in this paper.

## SUPERCONDUCTING LINAC

The superconducting linac accelerates the beam from 77.5 MeV to 201 MeV using double spoke cavities ($\beta_{opt} = 0.5$) at 352.21 MHz. The phase law in spoke section is adjusted to improve the smoothness and continuity of the phase advance between spokes and medium $\beta$ cavities. This improved smoothness is achieved by ramping the synchronous phase from $-20°$ down to $-33°$ in the last seven periods of the spoke section. The additional effect of this change is improved acceleration in the downstream structure as well as decreasing the range of required power to accelerate the beam in medium $\beta$ cavities.
The five cell elliptical cavities work at twice the frequency and increase the beam energy to 623 MeV using medium $\beta$ cavities ($\beta_g = 0.67$) and then to 2.5 GeV using high $\beta$ cavities ($\beta_g = 0.92$). By increasing the final energy of the spoke section and reducing the geometric $\beta$ of the medium $\beta$ cavities excitation of the Same Order Modes, especially $4\pi/5$, is significantly reduced at the low energy end of medium $\beta$ cavities [9].

The cryomodules of the spoke and elliptical sections house two and four cavities each respectively. The transverse focusing is achieved by normal conducting quadrupole doublets. By adding a diagnostic box in between the quadrupoles as well as vacuum ports a Linac Warm Unit is formed. Each lattice period is composed of a LWU and one cryomodule in the spoke and medium $\beta$ sections, or one LWU and two cryomodules in the high $\beta$ section.

## FREQUENCY JUMP

To allow for larger longitudinal acceptance at low energies and also ease of machining of the components a lower frequency is used at the front end of the ion accelerators. At intermediate energies is beneficial to increase the frequency to one of the higher harmonics of the bunch frequency to

Table 1: ESS Main Parameters

| Parameter | Unit | 2003 (LP/SP)* | 2012 |
|---|---|---|---|
| Ion | – | Proton / $H^-$ | Proton |
| Energy | [GeV] | 1.334 | 2.5 |
| Beam power | [MW] | 5.1 | 5 |
| Repetition rate | [Hz] | $16\frac{2}{3}$ / 50 | 14 |
| Beam current | [mA] | 114 | 50 |
| Beam pulse | [ms] | 2 / 0.48 | 2.86 |
| Duty cycle | [%] | 3.3 / 4.8 | 4 |

* Long pulse / Short pulse.



ISBN 978-3-95450-118-2

# LINAC4 BEAM COMMISSIONING STRATEGY

J-B. Lallement, A.M. Lombardi, P.A. Posocco, CERN, Switzerland


*Abstract*

Linac4 is a 160 MeV H- ion linear accelerator, presently under construction, which will replace the 50 MeV Linac2 as injector of the CERN proton complex [1]. Linac4 is 90 meters long normal-conducting Linac made of a 3 MeV Radio Frequency Quadrupole (RFQ) followed by a 50 MeV Drift Tube Linac (DTL), a 100 MeV Cell-Coupled Drift Tube Linac (CCDTL) and a Pi-Mode Structure (PIMS). Starting in 2013, five commissioning stages, interlaced with installation periods, are foreseen at the energies of 3, 12, 50, 100 and 160 MeV. In addition to the diagnostics permanently installed in the Linac, temporary measurement benches will be located at the end of each structure and will be used for beam commissioning. Comprehensive beam dynamics simulations were carried out through the Linac and the diagnostics benches to define a commissioning procedure, which is summarised in this paper. In particular, we will present a method for emittance reconstruction from profile measurements which keeps into account the effects of space charge and finite diagnostics resolution.


## INTRODUCTION

The commissioning of Linac4 is foreseen in 5 stages at the energies of 3, 12, 50, 100 and 160 MeV corresponding to the commissioning of the different accelerating structures. The measurement of the transverse beam emittance at each energy milestone will be an essential step during the commissioning of the Linac. At low energy (below 12 MeV – DTL tank1), as the beam penetration depth and activation are low, a direct method based on a slit and grid system is preferred. When the beam reaches energies of few tens of MeV the technical realisation of the slit becomes more challenging and therefore indirect methods to measure the emittance are preferred especially for a temporary measurement line. The classical emittance reconstruction technique, based on measuring the beam profile at three different locations [2], is reliable only if the emittance is conserved and there aren't any self-forces acting on the beam in between the 3 monitors. This latter condition is not fulfilled in the energy range 10-100 MeV for a beam which carries about 70 mA of peak current. To compensate for this drawback we have extended the classical method by combining it with an iterative process of multiparticle tracking which starts from upstream the suite of monitors and propagate the beam "forwards" taking into account space charge effects. This very efficient technique, which we call "forward method", is detailed in this paper and applied to the LINAC4 beam.

## THE "FORWARD METHOD"

The forward method is a technique which aims at reconstructing the transverse emittance of a beam of particles at a given location by using information on the beam size measured at three locations downstream. It is assumed that no active elements are located after the point where the emittance is measured. This method consists of two main steps.

### *First Step, the 3 Monitor Method*

The 3 monitor method is now well established and is detailed for sake of completeness. The beam envelope evolution can be represented by the sigma matrix, written as follow, assuming the three planes are uncorrelated.

$$\sigma = \begin{pmatrix} x_m^2 & x_e\, x'_m \\ x'_e x_m & {x'_m}^2 \end{pmatrix} = \epsilon \begin{pmatrix} \beta & -\alpha \\ -\alpha & \gamma \end{pmatrix}$$

If we define a transport matrix R of a beam line going from Z=0 to Z=L as:

$$R = \begin{pmatrix} R_{11} & R_{12} \\ R_{21} & R_{22} \end{pmatrix}$$

The relation between the sigma matrix at Z=0 and Z=L, assuming a constant emittance, is:

$$\sigma(L) = R * \sigma(0) * R^T$$

By introducing a monitor in the beam line, we can measure the first row – first column term and we have therefore the following relation:

$$x_{monitor}^2 = R_{11}^2 \epsilon\beta - 2R_{11}R_{12}\epsilon\alpha + R_{12}^2\epsilon\gamma$$

If we measure the beam sizes at three different locations, we obtain a system of three equations similar to the one above. The transport matrices from reconstruction point to monitors being known, the emittance $\epsilon$, and the Twiss parameters $\alpha$ and $\beta$ can be found by solving the system of 3 equations. This method is fairly accurate if the beam line geometry is well known, the emittance constant and the transport matrix does not depend on the beam input characteristics. In presence of space charge, the latter condition is not satisfied, and this dependence can lead to substantial error in the emittance estimation. This potential error on emittance reconstruction is illustrated by figure 1. It shows, in blue, the horizontal rms beam envelope along the temporary commissioning bench after the 50 MeV DTL in presence of space charge (65 mA peak current). The dashed lines represent the location of the 3 profile monitors. The beam sizes at the location of the monitor are used through the 3 monitor method, and the input beam parameters reconstructed. The red line represents the envelope of the reconstructed beam simulated without space charge, the green line the envelope with space charge. Two information in this graph: first, the difference between the blue and the

ISBN 978-3-95450-118-2

# END TO END BEAM DYNAMICS AND DESIGN OPTIMIZATION FOR CSNS LINAC

J. Peng, H.C. Liu, X.J. Yin, H.F. Ouyang, S.N. Fu, IHEP, Beijing 100049, China

*Abstract*

The China Spallation Neutron Source (CSNS) will use a linear accelerator delivering a 15mA beam up to 80MeV for injection into a rapid cycling synchrotron (RCS). Since each section of the linac was determined individually, a global optimization based on end-to-end simulation results has refined some design choices, including the drift-tube linac (DTL) and the medium energy beam transport (MEBT). The simulation results and reasons for adjustments are presented in this paper.

## INTORDUCTION `

The layout of CSNS linac is sketched in Figure 1. It consists of a 50 keV $H^-$ Penning surface plasma ion source, a 3MeV Radio Frequency Quadrupole (RFQ) accelerator, an 80MeV Alvarez-type Drift Tube Linear Accelerator (DTL) and several beam transport lines. The beam current of the linac is about 15mA with a pulsed beam width about 420 μs and a repetition rate of 25Hz.

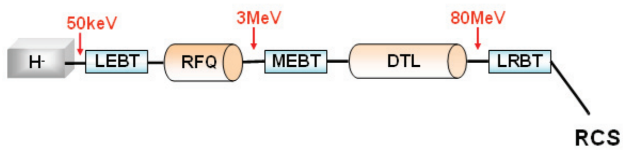


Figure 1: Layout of CSNS linac.

An electrostatic deflector as the pre-chopper, which is installed downstream LEBT, i.e., the entrance of RFQ, is chosen to pre-chop the beam in the rise and fall times of 15~20ns. Four-vane type RFQ is adopted to accelerate the $H^-$ beam from 50keV to 3.0MeV. The length of RFQ is about 3.6m. The RFQ consists of two resonantly coupled sections, and each section includes two mechanical modules connecting together by flange [1].The MEBT is a complex beam transport line. Its main role is to perform transverse and longitudinal matching to the succeeding 324MHz DTL. The MEBT includes ten quadrupole magnets (Q1~Q10) for transverse matching, two 324MHz buncher cavities for longitudinal matching, and various beam diagnostic instrumentations for beam diagnosis. The DTL consists of 4 tanks operating at 324MHz with final output energy of 80MeV. The transverse focusing is arranged in an FFDD lattice utilizing electro-magnet quadrupoles. The line to RCS beam transport line (LRBT) transfers the $H^-$ beam from the linac injector to the RCS ring [2]. The layout here described is the result of several revisions of previous designs [3], the main changes being in the control of beam loss.

## BEAM LOSS STUDY

Each section of CSNS linac has been studied and optimized independently at the beginning of design. After an initial layout of the accelerator is produced, a campaign of end to end simulation is launched with the purpose of identifying bottlenecks, weak points and acceptance limitations. The codes PARMILA [4] and PARMTEQM [5] have been used for these studies. From the results of simulation, we found that the 1$^{st}$ tank of DTL was the weak point and most beam loss happened in it. We simulated the beam transporting through the MEBT and the DTL. The initial distribution at the exit of RFQ is obtained with PARMTEQM. The beam current is 15mA and the duty factor is 1.05%. Considering the machine imperfections, alignment, focusing and RF errors are added in simulations as follows for the quadrupole magnets:

- Transverse displacements: $\delta_{x,y}=\pm 0.1$mm
- Rotations : $\phi_{x,y,z}=\pm 3$mrad
- Integrated field : $\triangle GL/GL=\pm 1\%$

And for the accelerating field:

- Klystron field: $\triangle E_{klys}/E_{klys}=\pm 1\%$
- Klystron phase $\phi_{klys}=\pm 1$deg
- Gap field:: $\triangle E_{gap}/E_{gap}=\pm 1\%$

In 11 out the 100 runs, particles are lost along the linac and most beam loss concentrated in the 1$^{st}$ tank of DTL, where the estimated power lost is higher than the acceptable limit of 1W/m. The excessive beam loss in the 1$^{st}$ tank of DTL is due to small bore radius of the tank, which is only 6mm. There are two reasons for us to underestimate beam size and so choose small bore radius: (1) at the beginning of DTL design, beam parameters at the exit of RFQ are adopted and the emittance growth in the MEBT is ignored, which is more than 20 %, (2) the K-V distribution is adopted as the initial beam distribution rather than more realistic distribution from PARMTEQM. Based on these analyses, we refined the MEBT and DTL designs. In this study we refer to the initial design as the "old" design and the optimized design as the "new" design.

## MEBT OPTIMIZATION

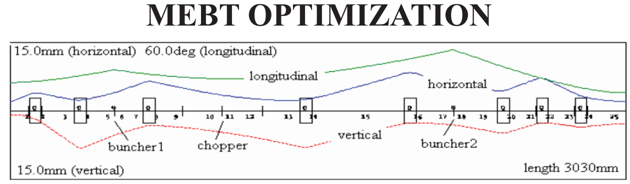


(a) Old design

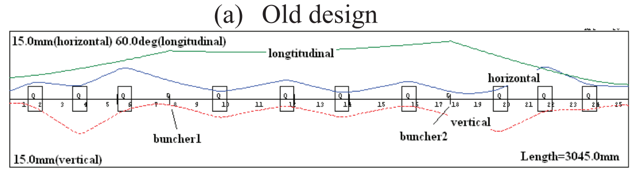


(b) New design

Figure 2: 6σ Beam Envelope in MEBT.



ISBN 978-3-95450-118-2

# BEAM DYNAMICS OF THE 13 MeV/50 mA PROTON LINAC FOR THE COMPACT PULSED HADRON SOURCE AT TSINGHUA UNIVERSITY*

Q.Z. Xing#, X.L. Guan, C. Jiang, C.X. Tang, X.W. Wang, H.Y. Zhang, S.X. Zheng, Key Laboratory of Particle & Radiation Imaging (Tsinghua University), Ministry of Education, Beijing 100084, China
G.H. Li, NUCTECH Co. Ltd., Beijing 100084, China
J. Billen, J. Stovall, L. Young, USA

*Abstract*

We present the start-to-end simulation result on the high-current proton linac for the Compact Pulsed Hadron Source (CPHS) at Tsinghua University. The CPHS project is a university-based proton accelerator platform (13 MeV, 16 kW, peak current 50 mA, 0.5 ms pulse width at 50 Hz) for multidisciplinary neutron and proton applications. The 13 MeV proton linac contains the ECR ion source, LEBT, RFQ, DTL and HEBT. The function of the whole accelerator system is to produce the proton beam, accelerate it to 13 MeV, and deliver it to the target where one uniform round beam spot is obtained with the diameter of 5 cm.

## INTRODUCTION

For the spallation neutron source, the high-current proton accelerator provides one important platform for the multidisciplinary development of condensed matter physics, radiation physics, materials science, aerospace science and life science. One pulsed high-current proton Linac is being built for the Compact Pulsed Hadron Source (CPHS) project at Tsinghua University. With the proton beam bombarding a Beryllium target, the neutron will be generated for the Small Angle Neutron Scattering (SANS) and neutron imaging [1].

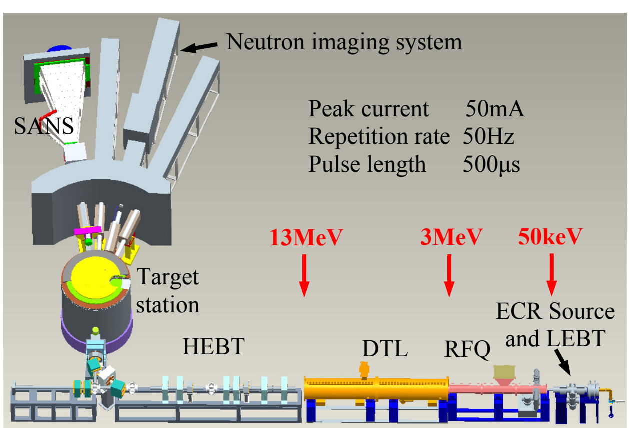


Figure 1: CPHS proton Linac layout.

The function of the whole accelerator system is to produce the proton beam, accelerate it to 13 MeV, and deliver it to the target where one uniform round beam spot is obtained with the diameter of 5 cm. To fulfil this requirement, various codes are adopted to design the Linac and carry out dynamics simulation. The layout of the CPHS proton Linac is shown in Fig. 1. The 13 MeV/50 mA proton linac contains the ECR ion source, LEBT, RFQ, DTL and HEBT. The beam dynamics simulation of the whole accelerator is presented in this paper.

*Work supported by the Major Research plan of the National Natural Science Foundation of China (Grant No. 91126003).
#xqz@tsinghua.edu.cn

## ECR SOURCE AND LEBT

The Electron Cyclotron Resonance (ECR) ion source is adopted to produce the proton beam [2]. After passing through the LEBT, the 50 keV pulsed proton beam (50 Hz/500 µs) is matched to the RFQ ($\alpha$=1.35, $\beta$=7.73 cm/rad). At the entrance of the RFQ, the designed proton beam current is 50 mA with the normalized RMS emittance not larger than 0.2 $\pi$ mm·mrad.

The 50 keV pulsed proton beam (50 Hz/500 µs) is extracted by a four-electrode extraction system, which consists of the plasma electrode, mid-electrode, suppression electrode and extraction electrode. PBGUNS [3] is adopted for design and simulation of the extraction system.

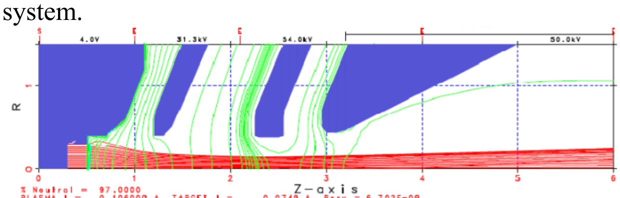


Figure 2: PBGUNS simulation for the LEBT extraction.

To shorten the length of the LEBT, steering magnets are placed inside the two Glaser solenoids. One cone structure (the cone, ACCT and electronic trap) before the RFQ entrance is expected to enhance the proton ratio larger than 85%. The LEBT is designed by PBGUNS and TRACE-3D [4], which agrees well.

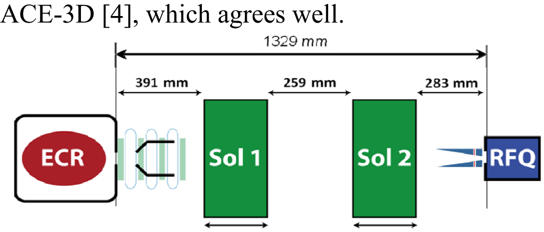


Figure 3: CPHS LEBT configuration.

The beam dynamics from the exit of the ECR source to the entrance of the RFQ is studied by TRACK [5] and TSTEP [6], which can both read the field distribution of



ISBN 978-3-95450-118-2

# RECENT DEVELOPMENTS ON HIGH INTENSITY BEAM DIAGNOSTICS AT SNS*

W. Blokland, ORNL*, Oak Ridge, TN 37831, USA

*Abstract*

The Spallation Neutron Source Ring accumulates 0.6 us long proton bunches of up to 1.5e14 protons with a typical peak current of over 50 Amp during a 1 ms cycle. To qualify the beam, we perform different transverse profile measurements that can be done at full intensity. The electron beam scanner performs a non-interceptive measurement of the transverse and longitudinal profiles of the beam in the ring. Electrons passing over and through the proton beam are deflected and projected onto a fluorescent screen. Analysis of the projection yields the transverse profile while multiple transverse profiles, offset in time, yield the longitudinal profile. Progress made with this system will be discussed as well as temperature measurements of the stripper foil and the target imaging system.

## INTRODUCTION

Up to a thousand proton beam bunches from the linac accumulate in the ring to generate an approx. 645 ns long proton pulse of up to 1.5e14 protons. Figure 1 shows the linac (green), the ring (blue), and the beam on target (red) current waveforms. The linac current is multiplied 100x to make it visible. The process repeats at 60 Hz.

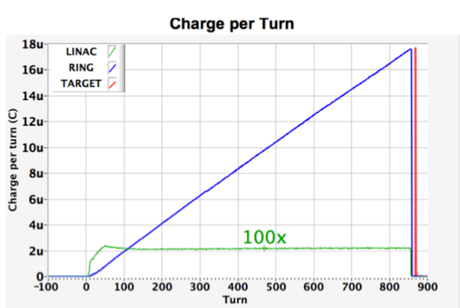


Figure 1: The accumulation of particles in the ring.

The 1 ms long accumulation of bunches in the ring with ever-increasing intensity makes it a challenging environment in which to use an interceptive device to make transverse measurements in the ring. This excludes the use of standard wire scanners at full beam power. Instead, we have one electron scanner for each plane to measure the horizontal and vertical transverse profiles [1,2]. The electron scanner for the vertical profile (horizontally mounted) is shown in Fig. 2.

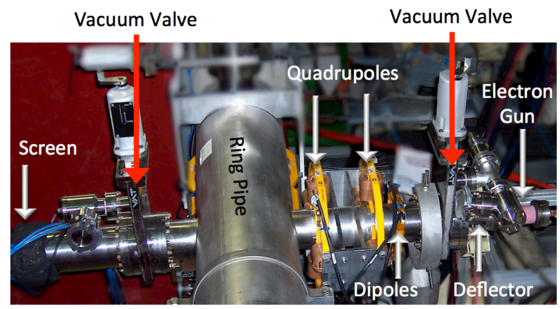


Figure 2: The electron scanner.

The Target Imaging System (TIS) makes the final transverse profile measurement. The system consists of a digital camera viewing the fluorescent coating of Cr:Al2O3 on the target. The light emanating from the coating is directed through mirrors and optical fibers to a low radiation area [3]. The latest installed target is shown in Fig. 3 with a superimposed TIS image.

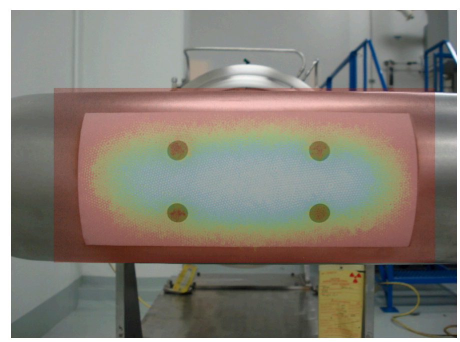

Figure 3: Target vessel with superimposed TIS image.

Another important aspect of the SNS accelerator is the stripper foil [4]. This foil strips the electrons from the $H^-$ beam to implement a charge-exchange injection scheme. The foil must be positioned such that it strips as much of the incoming $H^-$ beam as possible but also such that it minimizes interception of the circulating proton beam. A radiation hard analog video system installed in the tunnel provides foil images at 30 Hz or half the beam rep rate. A new telescope-based Foil Imaging System (FIS) has been installed outside of the tunnel to provide better visibility of the foil and also to make temperature measurements, see Fig. 4.

This paper presents progress made with the electron scanner, the Target Imaging System, and the Foil Imaging System.

* ORNL/SNS is managed by UT-Battelle, LLC, for the U.S. Department of Energy under contract DE-AC05-00OR22725



ISBN 978-3-95450-118-2

# ONLINE MONITORING SYSTEM FOR THE WASTE BEAM IN THE 3-GeV RCS OF J-PARC

P.K. Saha*, S. Hatakeyama, M. Yoshimoto, K. Yamamoto, H. Hotchi, H. Harada and N. Hayashi
J-PARC Center, KEK&JAEA, Tokai-mura, Naka-gun, Ibaraki 319-1195, Japan

*Abstract*

We have succeeded online monitoring of the waste beam of only about 0.4% in the 3 GeV Rapid Cycling Synchrotron (RCS) of Japan Proton Accelerator Research Complex (J-PARC). We use conventional monitors but established efficient measurement technique so as to measure such a waste beam even with sufficient less error. An FFT analysis of the raw signal measured by a current transformer (CT) made it possible to clearly identify the beam signal corresponding to the frequency of the intermediate pulse. The waste beam as a whole was measured to be (0.38±0.03)%. In addition, we also use a multi-wire profile monitor (MWPM) for simultaneous and separate measuring of the partially stripped ($H^0$) and if any un-stripped ($H^-$) components of the waste beam profiles. Analysis of the $H^0$ and $H^-$ beam profiles give quantitative information of the foil degradation, such as foil thinning and pinhole formation, respectively. Both methods already play important roles for the RCS operation so as to directly know the stripper foil condition and would have great importance especially, for high power operation.

## INTRODUCTION

The 3-GeV Rapid Cycling Synchrotron (RCS) of the Japan Proton Accelerator Research Complex (J-PARC) is designed to deliver a high power proton beam of 1 MW to the neutron and muon production target in the Material and Life Science Facility (MLF) as well as to the Main Ring (MR) [1]. The injection energy of RCS is 181 MeV at present and will be upgraded to the design energy of 400 MeV next year, while the extraction energy is 3 GeV [2]. RCS operates with a repetition rate of 25 Hz and will have $8.33\times10^{13}$ particles per pulse (ppp) at 1 MW operation. RCS beam power for the user operation at the latest was nearly 300 kW to both MLF and MR.

The incoming $H^-$ beam from the Linac is converted to a proton beam and injected into RCS during 0.5 ms multi-turn injection period. It is done by a primary stripper foil named 1st foil placed in the middle of injection bump magnets [3]. The primary stripper foil is a double-layer type of the HBC (Hybrid type Boron doped Carbon) foil [4] with a thickness of 200 $\mu$g/cm$^2$ for the present injection and will be changed to 290 $\mu$g/cm$^2$ for 400 MeV injection. By using the cross sections measured in an earlier experiment at 200 MeV and on Carbon targets, the stripping efficiency at present is calculated to be 99.6% [5]. For 400 MeV, the extrapolated cross sections are used and the stripping efficiency is calculated to be 99.7% [6]. The remaining 0.4% or 0.3% of the beams are called waste beams and ideally they are with partially stripped (single electron detachment at the 1st foil) becomes neutral (un-charged) and is called $H^0$ beam, where the un-stripped $H^-$ are expected to be negligibly small. They are further stripped to proton beams by the secondary stripper foils named 2nd and 3rd foils, respectively and transported to the injection beam dump. As the main component of the waste beam is $H^0$, injection dump is also called the H0 dump.

* Electronic address: saha.pranab@j-parc.jp

A proper monitoring of the waste beam is very important and was always an issue since design stage. Because the dump has a capacity of the only 4 kW and thus a little change of the stripping efficiency would increase the waste beam so as to increase the head load on the dump. Unexpected long tail or halo of the injected beam, failure of any related accelerator components for which injected beam misses the 1st foil are also other possible sources for increasing the waste beam. Usually foil lifetime becomes shorter as beam intensity goes higher but a foil might have degradation before complete breaking. A sudden failure certainly reduces accelerator availability as well as raised maintenance issues. Degradation of a foil increases the waste beam and could be a signal of a foil breaking. One can determine a proper foil replacement timing and also can avoid a sudden failure through a reliable measurement of a foil degradation. However, not only because of the small fraction (0.3% $\sim$ 0.4%) but also for the large noise from the nearby complicated injection system the measurement is very difficult. As a result, a little change of the waste beam fraction is further difficult to monitor through any straightforward way even using any sophisticated monitor. In order to overcome these difficulties, we have continued our efforts and recently established a precise method which employs a rather simple principle and does not require any sophisticated monitor or device. The time domain signal of a current transformer (CT) placed near the entrance of the H0 dump is collected by an oscilloscope and then a fast Fourier transformation (FFT) analysis is done. As a result, picking up the amplitude of the power spectrum corresponding to the frequency of the intermediate pulse, which depends on the frequency of the RCS RF system gives the beam signal. Formation of intermediate pulses and the timing relation between the Linac and the RCS can be found in [7]. The waste beam in a realistic condition was measured to be (0.38±0.03)% and was consistent with expectation [8]. Being non destructive, the present method is already in operation for online monitoring of the waste beam during the RCS operation.

We have also extended our effort for measuring $H^0$ and $H^-$ component separately by using a multi-wire profile

ISBN 978-3-95450-118-2

# THE BEAM DIAGNOSTICS OF CSNS

T.G. Xu#, J.N. Bai, C. Chen, L.X. Han, F. Li, P. Li, M. Meng, J.L. Sun, J.M. Tian, A.X. Wang, B. Wang, M.H. Xu, Zh.H. Xu, X.Y. Yang, L. Zeng, IHEP, Beijing, China

*Abstract*

First, the beam diagnostics of CSNS is introduced. Then the progress of CSNS beam diagnostics is described. At last, the next year's plan is predicted.

## INTRODUCTION OF CSNS

China Spallation Neutron Source (CSNS) will be a multi-purpose research centre. It is consisted of an 80 MeV Linac, a 3 GeV Rapid Cycling Synchrotron (RCS), two beam transport lines (LRBT, RTBT), a target and three neutron instruments. The beam power of CSNS is about 100 kW. The main beam parameters which related with beam diagnostics are listed in table 1.

Table 1: CSNS Beam Parameters

| Parameter | Value |
|---|---|
| | Linac+LRBT |
| Particle | $H^-$ |
| Beam energy (MeV) | 0-80 |
| Repetition rate (Hz) | 25 (1) |
| Pulse current (mA) | 15(5) |
| Macro pulse width (μs) | 500(50) |
| Chopped pulse width (ns) | 468 |
| Chopped ratio | 50% |
| RF frequency (MHz) | 324 |
| | RCS+RTBT |
| Particle | proton |
| Beam energy (MeV) | 80-1600(80) |
| Repetition rate (Hz) | 25(single shot) |
| Bunch particles | 7.80E+12 |
| Harmonic | 2 |
| Bunch length (ns) | 500-100 |
| Injection turns | 225 |
| Revolution frequency (MHz) | 0.535-1.232 |

The number in the brackets is the value of the first step of CSNS commissioning [1].

## INTRODUCTION OF CSNS BEAM DIAGNOSTICS

The CSNS beam diagnostics system is a new established system. The members in the group are all freshman. In order to finished the aim of CSNS beam diagnostics, the mature and traditional diagnostics method is firstly chosen. In China, there is not a so large scale proton accelerator. The experience on proton accelerator is absent. So the design of CSNS beam diagnostics is referred mainly from J-Parc [2] [3] and SNS [4].

The each type beam monitor according to different need from each area of CSNS accelerator is listed in table 2 and 3.

Table 2: Linac Section Beam Monitor

| Type | Number | | |
|---|---|---|---|
| | LEBT | MEBT | DTL |
| Beam Current Transformer | 2 | 2 | 3 |
| Beam Position Monitor | | 8 | |
| Beam Loss Monitor | | 3 | 12 |
| Fast Beam Loss Monitor | | | 1 |
| Wire Scanner | | 4 | |
| Phase Detector | | 5 | 3 |
| EMittance system | 1 | 1 | |

Table 3: Ring and Beam Transport Line Beam Monitor

| Type | Number | | |
|---|---|---|---|
| | LRBT | RCS | RTBT |
| Beam Current Transformer | 4 | 2 | 4 |
| Beam Position Monitor | 20 | 35 | 33 |
| Beam Loss Monitor | 28 | 72 | 50 |
| Fast Beam Loss Monitor | 3 | 9 | 2 |
| Wire Scanner | 7 | | 8 |
| Multi-Wire Profile Monitor | 6 | | 2 |
| Phase Detector | 5 | 3 | |
| Wall Current Monitor | 3 | 2 | |
| DCCT | | 1 | |
| Tune system | | 1 | |
| Foil Video System | 1 | | |

### *The Introduction of Each Monitor*

According to the beam structure, the monitor can be divided into two parts. The first part is BR (Before Ring) section which includes FE, DTL and LRBT. They have almost similar beam structure. The beam structure has three layers from time domain viewpoint, the top layer is the macro structure, the middle layer is chopped beam structure, and the bottom layer is the bunch structure with

# xutg@ihep.ac.cn



ISBN 978-3-95450-118-2

# DETECTION OF UNIDENTIFIED FALLING OBJECTS AT LHC

E. Nebot del Busto*, T. Baer, F. Day, B. Dehning, E. B. Holzer, A. Lechner, R. Schmidt, J. Wenninger, C. Zamantzas, M. Zerlauth, F. Zimmermann, CERN, Geneva, Switzerland
M. Hempel, Brandenburg University of Technology , Germany

*Abstract*

About 3600 Ionization Chambers are located around the LHC ring to detect beam losses that could damage the equipment or quench superconducting magnets. The Beam Loss Monitors (BLMs) integrate the losses in 12 different time intervals (from $40\mu s$ to $83.8s$) allowing for different abort thresholds depending on the duration of the loss and the beam energy. The signals are also recorded in a database at 1 Hz for offline analysis. Since the 2010 run, a limiting factor in the machine availability occurred due to unforeseen sudden losses appearing around the ring on the ms time scale. Those were detected exclusively by the BLM system and they are the result of the interaction of macro-particles, of sizes estimated to be 1-100 microns, with the proton beams. In this document we describe the techniques employed to identify such events as well as the mitigations implemented in the BLM system to avoid unnecessary LHC downtime.

## DETECTION AND OBSERVATIONS

The BLM system [1] is responsible for the protection of the LHC magnets against quenches or damage caused by beam losses. About 3600 Ionization Chambers (IC) are situated at likely-loss locations. The electrical signals of the BLM monitors are integrated via current to frequency converter over a period of $40\mu s$, digitized and sent to the surface installation for further treatment. The system keeps a history and computes 12 running sums, which correspond to signals integrated in 12 different time intervals spanning from $40\mu s$ to $83s$. The BLM system will request a beam dump if any of the 12 Running Sums (RS) exceed a set of predefined thresholds [2], that estimate the quench or damage levels for a given energy and loss duration. Furthermore, the BLM system drives the signals recorded in the 12 RSs and corresponding thresholds of all 3600 detectors to both an on-line display for continuous monitoring and to the LHC logging service, where they are stored for offline analysis. Finally, in case of trigger of a beam dump, post-mortem data with information of the losses around the ring during up to 1000 LHC turns are stored.

On the 7th of July of 2010, the BLM system triggered a beam dump as a consequence of unforeseen beam losses in the time range of $\sim 1ms$. A total of 48 similar events have occurred since then, becoming a limiting factor for the operation of the LHC. The cause of these losses is believed to be the interaction of dust particles of sizes 1-100$\mu m$ falling into the beam, the so-called Unidentified Falling Objects (UFOs). In order to accumulate statistics and further understand the behaviour of such events, a systematic search for below threshold UFOs was carried out. The detection algorithm requires two BLMs within a distance of 40m to have a signal larger than $1 \cdot 10^{-4} Gy/s$ in RS04 ($0.640ms$ integration window). In addition, constrains are set in the ratio of signals observed in RS02/RS01 ($80\mu s/40\mu s$) and RS03/RS01 ($320\mu s/40\mu s$) to separate low signal UFOs from noise.

Figures 1 and 2 present a typical longitudinal and temporal profile of a UFO event as observed by the BLM system. The beam losses may be observed in several cells downstream of where the proton-dust originally interacted as well as aperture limitation (i.e collimation areas). The temporal profile follows a gaussian-like distribution, with $\sigma \sim 100\mu s$.

* Eduardo.Nebot.Del.Busto@cern.ch

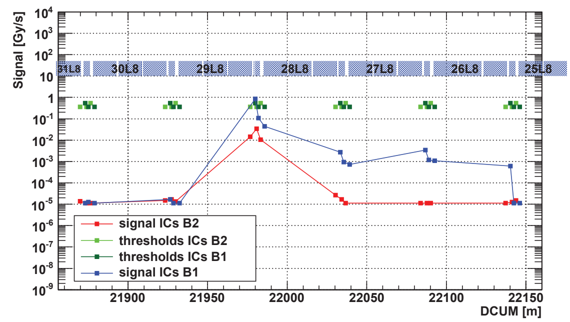


Figure 1: Longitudinal profile of a UFO in the LHC arc.

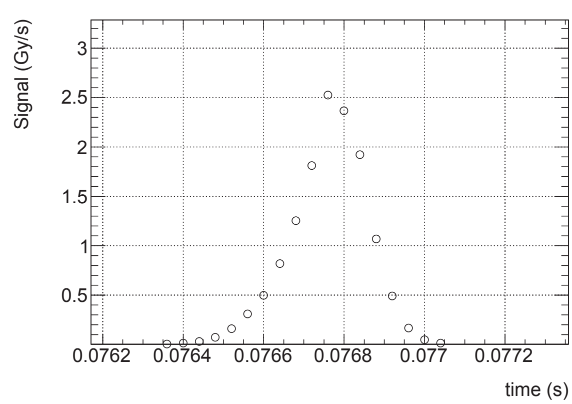


Figure 2: Temporal profile of a UFO in the LHC arc.

ISBN 978-3-95450-118-2

# MEASUREMENTS AND INTERPRETATION OF THE BETATRON TUNE SPECTRA OF HIGH INTENSITY BUNCHED BEAM AT SIS-18 *

R. Singh, O. Boine-Frankenheim, GSI, Darmstadt, Germany and TEMF, TU Darmstadt, Germany
O. Chorniy, P. Forck, R. Haseitl, W. Kaufmann, P. Kowina, K. Lang, GSI, Darmstadt, Germany
T. Weiland, TEMF, TU Darmstadt, Germany

## ABSTRACT

Two independendent tune measurement systems were installed in the GSI heavy ion synchrotron SIS-18. Using these fast and sensitive systems, tune spectra were obtained with high accuracy. Besides the machine tune, the spectra reveal information about the intensity dependent coherent tune shift and the incoherent space charge tune shift. The space charge tune shift is obtained from a fit of the observed shifted positions of the synchrotron satellites to an analytic expression for the head-tail eigenmodes with space charge. Time domain identification of the head tail modes is also performed.

## INTRODUCTION

Accurate measurements of the machine tune and of the chromaticity are of importance for the operation of fast ramping, high intensity ion synchrotrons. In such machines the tune spread $\delta Q_{x,y}$ at injection energy due to space charge and chromaticity can be up to 0.5. In order to limit the incoherent particle tunes to the resonance free region the machine tune has be controlled with a precision better than $\Delta Q \approx 10^{-3}$. In the GSI heavy-ion synchrotron SIS-18 there are currently two betatron tune measurement systems installed. The Tune, Orbit and Position measurement system (TOPOS) is primarily a digital position measurement system which calculates the tune from the measured position [1]. The Baseband Q measurement system (BBQ) concieved at CERN performs a tune measurement based on the concept of diode based bunch envelope detection [2]. The BBQ system provides a higher measurement sensitivity than the TOPOS system. For fast tune measurements using standard pick-ups, external excitation is often applied for measurement of transverse beam signals. The frequency resolution of both systems depend on the time scale of measurement, the tune fluctuations during the measurement and width of tune peak due to non-linearities in the machine. During acceleration, $\Delta Q$ achieved is $\approx 10^{-3}$ limited by length of measurement time window. A higher resolution of $10^{-4}$ is achievable during injection or extraction plateaus where the main limitation is machine non-linearities and long term beam losses.

For low intensities the theory of transverse signals from bunched beams and the measurement principles are well known [3, 4]. In intense, low energy bunches the tune spectra can be modified significantly by the transverse space charge force and by ring impedances. Previously the effect of space charge on head-tail modes had been the subject of several analytical and simulation studies [5, 6, 7, 8, 9]. Recently these effects were observed experimentally at SIS-18 [10, 11, 12, 13].

This contribution aims to complement the previous studies and extract the relevant intensity parameters from tune spectra measurements using the TOPOS and BBQ tune measurement systems. Section  presents the space charge and image current effects on tune measurements and respective theoretical models. Section  report on the experimental conditions and compares the beam excitation mechanisms and measurement systems. Section  presents the experimental results in comparison with the theoretical estimates of the various high intensity effects.

## TUNE SPECTRUM FOR HIGH INTENSITY BEAM

If the transverse signal from a low intensity bunch is sampled with the revolution period $T_s$ then the positive frequency spectrum consists of one set of equidistant lines

$$Q_k = Q_0 + \Delta Q_k, \tag{1}$$

usually defined as baseband tune spectrum, where $Q_0$ is the fractional part of the machine tune, $\Delta Q_k = \pm k Q_s$ are the synchrotron satellites and $Q_s$ is the synchrotron tune. For a single particle performing betatron and synchrotron oscillations, the relative amplitudes of the satellites are [3]

$$| \, d_k \, | \sim | \, J_k(\chi/2) \, | \tag{2}$$

where $\chi = 2\xi\phi_m/\eta_0$ is the chromatic phase, $\xi$ is the chromaticity, $\phi_m$ is the longitudinal oscillation amplitude of the particle and $\eta_0$ the frequency slip factor. $J_k$ are the Bessel functions of order $k$.

At high beam intensities the transverse space charge force together with the coherent force caused by the beam pipe impedance will affect the motion of the beam particles and also the tune spectrum. The space charge force induces an incoherent tune shift $Q_0 - \Delta Q_{sc}$ for a symmetric beam profile of homogeneous density where

$$\Delta Q_{sc} = \frac{q I_p R}{4\pi\epsilon_0 c E_0 {\gamma_0}^2 \beta_0^3 \varepsilon_x} \tag{3}$$

is the tune shift, $I_p$ the bunch peak current, $q$ the particle charge and $E_0 = \gamma_0 mc^2$ the energy. The relativistic parameters are $\gamma_0$ and $\beta_0$, the ring radius is $R$ and the emittance of the rms equivalent K-V distribution is $\varepsilon_x$.

* This work is supported by DITANET (novel DIagnostic Techniques for future particle Accelerators: A Marie Curie Initial Training NETwork), Project Number ITN-2008-215080



ISBN 978-3-95450-118-2

# INSTRUMENTATION DEVELOPMENTS AND BEAM STUDIES FOR THE FERMILAB PROTON IMPROVEMENT PLAN LINAC UPGRADE AND NEW RFQ FRONT-END*

Victor E. Scarpine#, Cheng-Yang Tan, Pat R. Karns, Daniel S. Bollinger, Kevin L. Duel, Nathan Eddy, Ning Liu, Alexei Semenov, Raymond E. Tomlin, and William A. Pellico,
Fermilab, Batavia, IL 60510, USA

*Abstract*

Fermilab is developing a Proton Improvement Plan (PIP) to increase throughput of its proton source. The plan addresses hardware modifications to increase repetition rate and improve beam loss while ensuring viable operation of the proton source through 2025. The first phase of the PIP will enable the Fermilab proton source to deliver 1.8e17 protons per hour by mid-2013. As part of this initial upgrade, Fermilab plans to install a new front-end consisting of dual H- ion sources and a 201 MHz pulsed RFQ. This paper will present beam studies measurements of this new front-end and discuss new beam instrumentation upgrades for the Fermilab linac.

## INTRODUCTION

From its beginning, Fermilab has operated a successful program of supplying high-energy protons to its experimental programs. The present Fermilab proton facility (H- sources, pre-accelerator, linac and booster) has been operational for many years. However, this proton facility will be required to supply protons to the Main Injector and to the 8-GeV physics program until the era of Project X.

To meet these requirements, Fermilab has embarked on the Proton Improvement Plan (PIP) to improve and upgrade the present proton facilities [1]. The specific objectives are to enable proton operation capable of delivering 1.8E17 protons/hour (at 12 Hz) by 2013 and 2.25E17 protons/hour (at 15 Hz) by 2016 while maintaining Linac/Booster availability greater than 85%, maintaining residual activation at acceptable levels, and ensuring a useful operating life through 2025.

The first phase of the PIP is underway. Part of this first phase includes (1) replacing the present H- source and pre-accelerator with a new front-end injector based on a radio frequency quadrupole (RFQ) and (2) upgrading many of the linac beam diagnostics instrumentation. This work will be completed during the present long-term shutdown, which ends spring of 2013.

## NEW LINAC FRONT-END

The present linac front-end consists of dual Cockcroft-Walton pre-accelerators with individual H- ion sources. A 2009 review determined that this Cockcroft-Walton-based front-end is a liability and a large source of linac downtime. The first phase of the PIP project will replace the dual Cockcroft-Walton sources with an RFQ-based front-end. This new front-end injector consists of

- two 35 keV H- magnetron sources on a movable slide;
- a two-solenoid low-energy beam transport (LEBT) with an Einzel lens chopper with a beam current toroid between the solenoids;
- a 201.25 MHz, 750 keV RFQ; and
- a short medium-energy beam transport (MEBT) with a single buncher cavity.

This new front-end will feed beam into the first drift tube linac. Figure 1 shows a rendering of this new front-end injector, while figure 2 shows the actual ion source, LEBT and RFQ portion of the injector system.

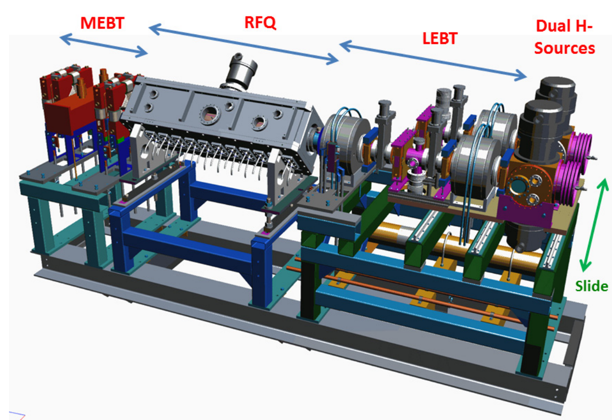


Figure 1: Fermilab's new front-end injector system.

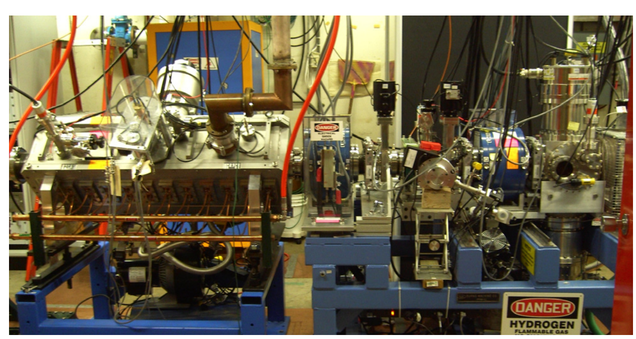


Figure 2: Completed ion source, LEBT and RFQ portion of the front-end injector system assembled in the source testing lab.

*Work supported by U. S. Department of Energy under contract No. DE-AC02-07CH11359.
#scarpine@fnal.gov



ISBN 978-3-95450-118-2

# FNAL PROTON SOURCE HIGH INTENSITY OPERATIONS AND BEAM LOSS CONTROL*

F.G. Garcia#, W. Pellico, FNAL, Batavia, IL 60510, USA


*Abstract*

The 40-year-old Fermilab Proton Source machines, constituted by the Pre-Injector, Linac and the synchrotron Booster, have been the workhorse of the Fermi National Accelerator Laboratory (Fermilab). During this time, the High Energy Physics Program has demanded an increase in proton throughput, especially during the past decade with the beginning of the neutrino program at Fermilab. In order to achieve a successful program, major upgrades and changes were made in Booster. Once again, the Proton Source has been charged to double their beam throughput, while maintain the present residual activation levels, to meet the laboratory Intensity Frontier program goals until new machines are built and operational to replace the Proton Source machines. This paper discusses the present performance of Booster and the plans involved in reaching even higher intensities.


## INTRODUCTION

The Fermilab Booster [1] is rapid cycling synchrotron which accelerates protons from the injection energy of 400 MeV to 8 GeV in 33 msec, at up to 15 Hz. It is 472 m in circumference and has a harmonic number of 84, with 96 combined function magnets distributed on a FDooDFo 24 symmetric lattice period. The Booster frequency changes rapidly through the accelerator cycle, from 37.9 – 52.8 MHz and there are 19 RF cavities in the machine. Early in 2000's the demand for protons increased 12-fold in comparison to the previous 10 years of Booster operations with the beginning of the neutrino program at Fermilab.

Present protons per batch in Booster are 4.5E12 at 7.5 Hz with 90% efficiency and 85% uptime. In the future, the required number of protons to the next generation of neutrino experiments has once again challenged the Proton Source: a factor of 2 more protons from the present running conditions is expected out of Booster. In order to achieve this demand, the number of cycles with beam will be increased rather than the intensity per cycle. Currently the Booster RF cavities do not possess appropriate cooling to run reliably at high repetition rate. Therefore, improvements in both hardware and operational efficiency of the Booster are required in order to have a successful physics program.

Therefore, the Proton Improvement Plan (PIP) [2] was established in 2010. The goal is to deliver 2.25 E17 protons per hour at 15 Hz by 2016. This increase in proton throughput has to be achieved by:

- maintaining 85% or higher availability;
- maintaining the same residual activation in the accelerator components.

*Work supported under DOE contract DE-AC02-76CH03000

#fgarcia@fnal.gov

## PRESENT BOOSTER PERFORMANCE

Figure 1 shows the protons delivered per day and the integrated protons delivered since 1992 up to May 2012.

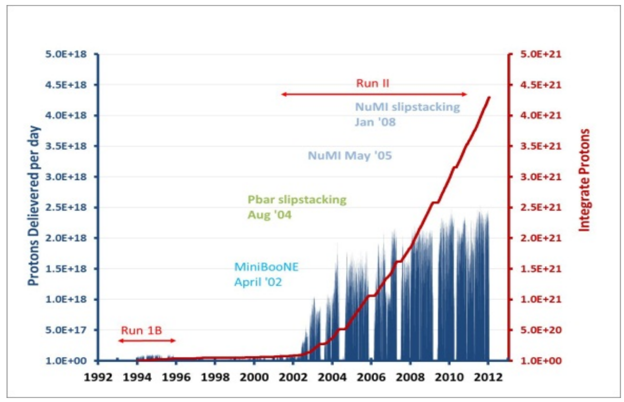


Figure 1: Booster integrated and per day protons delivery for the past 2 decades.

The primary users of the protons were the 8 GeV neutrino experiments at the Booster Neutrino Beam (BNB), whose repetition rate depends on other demands for protons, but typically run at 2 Hz up to 5 Hz. Another major consumer of protons is the 120 GeV neutrino experiments from the Neutrino at the Main Injector (NuMI). In this case, Booster provides 9 batches of 4.5E12 protons per pulse to Main Injector where the batches are slipstacked to generate 300 kW of beam power to the NuMI target.

The major projects that permitted Booster to run at higher intensities are quickly described in the following sections.

### *New Corrector System*

While the main lattice elements of the Booster ramp, the corrector system had historically operated DC. This means that the beam position moved on the order of several millimeters over the acceleration cycle. A multi pole magnet [3] was installed during shutdown periods in 2007 and completed in 2009 in the 48 locations around the ring with each capable of ramping which stabilized the Booster orbit through the accelerator cycle. Some major improvements in beam orbit control were obtained, such as better tune control at high energy, smaller emittance and better orbit coupling correction at high energy.



ISBN 978-3-95450-118-2

# CHARACTERIZING AND CONTROLLING BEAM LOSSES AT THE LANSCE FACILITY*

L. Rybarcyk#, Los Alamos National Laboratory, Los Alamos, NM 87545, U.S.A.

*Abstract*

The Los Alamos Neutron Science Center (LANSCE) currently provides 100-MeV $H^+$ and 800-MeV $H^-$ beams to several user facilities that have distinct beam requirements, e.g. intensity, micropulse pattern, duty factor, etc. Minimizing beam loss is critical to achieving good performance and reliable operation, but can be challenging in the context of simultaneous multi-beam delivery. This presentation will discuss various aspects related to the observation, characterization and minimization of beam loss associated with normal production beam operations in the linac.

## INTRODUCTION

LANSCE is a multi-user, multi-beam facility that produces intense sources of pulsed, spallation neutrons and proton beams in support of US national security and civilian research. It comprises a pulsed 800-MeV room temperature linear accelerator and 800-MeV proton storage ring and has been in operation for over 37 years. It first achieved 800-MeV beam on June 9, 1972. The facility, formerly known as LAMPF, routinely provided an 800 kW beam for the meson physics program. Presently, the LANSCE user facilities include:

- Lujan, which uses the proton storage ring (PSR) to create an intense, time-compressed proton pulse that is used to produce a short pulse of moderated (spallation) neutrons (meV to keV range),
- Proton Radiography (pRad), which provides high resolution, time-sequenced radiographs of dynamics phenomena,
- Weapons Neutron Research (WNR) that provides a source of unmoderated (spallation) neutrons in the keV to multiple MeV range,
- Isotope Production (IPF), which is a source of research and medical isotopes for the US, and
- Ultra-Cold Neutrons (UCN), which is a source of sub-μeV neutrons for fundamental physics research.

A list of beam parameters for present day operation is shown in Table 1.

## ACCELERATOR

The accelerator consists of separate proton ($H^+$) and $H^-$ Cockcroft-Walton based injectors that produce 750-keV beams for injection into the drift tube linac (DTL). Each low energy beam transport (LEBT) contains magnetic quadrupoles for transverse focusing, a single-gap 201.25-MHz buncher cavity for initial bunching of the beam, and

Table 1: Typical Parameters for LANSCE Linac Beams Note: All beams are 800 MeV, $H^-$ except for IPF, which is 100 MeV, $H^+$.

| Area | Rep Rate [Hz] | Pulse Length [μs] | Chopping pattern | Iavg [μA] | Pavg [kw] |
|---|---|---|---|---|---|
| Lujan | 20 | 625 | 290ns/358ns | 100-125 | 80-100 |
| pRad | ~1 | 625 | 60 ns bursts every ~1 μs | < 1 | < 1 |
| WNR (Tgt4) | 40 | 625 | 1 μ–pulse every ~ 1.8 μs | ≤2 | ~ 1.6 |
| UCN | 20 | 625 | Lujan-like to none | < 5 | < 4 |
| IPF | ≤30 in pulsed mode | 625 | NA | 230 | 23 |

an electrostatic deflector for "gating" beam into the linac or inhibiting beam when a fault condition occurs. The $H^-$ LEBT also contains a 16.77-MHz buncher for producing single, high-charge, micropulses and a slow-wave beam chopper for modulating the intensity of the beams. The $H^+$ and $H^-$ beams are merged in a common LEBT that contains a single 201.25-MHz buncher cavity, aka main buncher, which performs the majority of the bunching for the standard linac beams and four quadrupole magnets to achieve the final match into the linac.

The 100-MeV DTL is an Alvarez style 201.25-MHz linac comprised of four independently powered tanks for a total length of 61.7 m. The tanks contain electromagnetic quadrupoles in a FODO lattice. At the beginning of tank 3, the lattice transitions to a quad magnet in every other drift tube.

Following the DTL is a 100-MeV beam transport, aka the Transition Region (TR), which consists of separate paths (chicanes) for the two beam species, that allows for independent matching, steering and phasing of the $H^+$ and $H^-$ beams into the subsequent structure. The split nature of this transport is required in order to have the flexibility necessary to simultaneously achieve proper phasing of both beams into the next linac. The $H^+$ segment of the TR also contains a kicker magnet for extracting 100-MeV beam to IPF. Since there are currently no users of 800-MeV $H^+$ beam, this magnet is operated in DC mode.

Following the TR is the 805-MHz coupled-cavity linac (CCL) that accelerates beams up to 800 MeV. It consists of 44 independently powered modules, which have either two or four tanks, for a total length of 727 m. Each tank

*Work supported by DOE under contract DE-AC52-06NA25396.
#lrybarcyk@lanl.gov

ISBN 978-3-95450-118-2

# BEAM LOSS MITIGATION IN THE OAK RIDGE SPALLATION NEUTRON SOURCE

M.A. Plum, on behalf of the SNS accelerator team,
Oak Ridge National Laboratory, Oak Ridge, TN, USA

*Abstract*

The Oak Ridge Spallation Neutron Source (SNS) accelerator complex routinely delivers 1 MW of beam power to the spallation target. Due to this high beam power, understanding and minimizing the beam loss is an ongoing focus area of the accelerator physics program. In some areas of the accelerator facility the equipment parameters corresponding to the minimum loss are very different from the design parameters. In this presentation we will summarize the SNS beam loss measurements, the methods used to minimize the beam loss, and compare the design vs. the loss-minimized equipment parameters.

## INTRODUCTION

The SNS accelerator complex [1] comprises a 1 GeV linac followed by an accumulator ring, with a design average beam power of 1.4 MW at 60 Hz. The present operating power is ~1 MW. With this high beam power, beam loss control and mitigation is critical. To allow for hands-on maintenance, the beam loss should be less than ~1 W/m. Long-term plans call for increasing the beam power to 3 MW or higher, so this corresponds to a fractional loss of less than $3 \times 10^{-7}$ per meter, which is a very low value compared to previous accelerator systems.

Almost all the 350+ beam loss monitors (BLMs) at SNS are based on ion chambers [2]. Additionally, there are photomultiplier-based neutron detectors and fast BLMs. The neutron detectors are especially important at low beam energies (<100 MeV) where the ion-chamber BLMs have low sensitivity. The signal from each BLM is sampled at typically 100 kHz and the waveforms can be examined and recorded using the accelerator control system. Typical activation measurements are shown in Fig. 1. There are several hot spots spread throughout the complex. The location with the highest activation is just downstream of the charge-exchange-injection stripper foil, caused by the inevitable scattering of the injected and circulating beam by the foil.

## BEAM LOSS MITIGATION

The three main methods used to mitigate the beam loss at SNS are: 1) beam halo/tail scraping, best done at low beam energy; 2) increasing the beam size in the superconducting linac (SCL) to minimize the loss due to intra-beam stripping (IBSt) [3]; and 3) empirical adjustment of the magnet and RF set points.

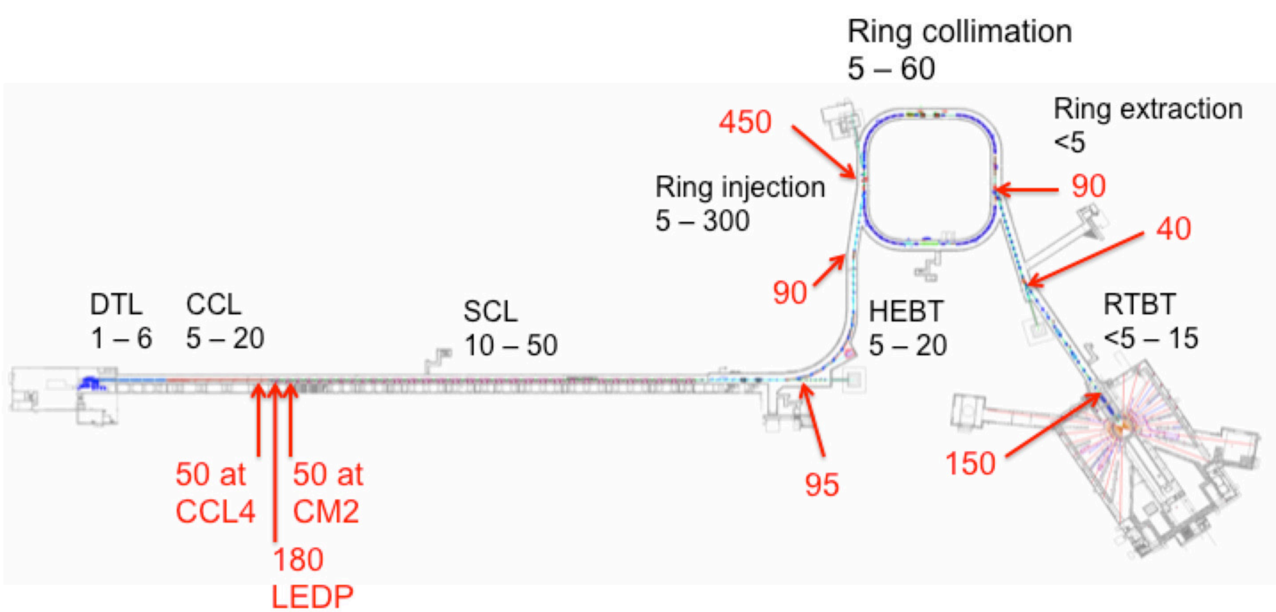


Figure 1: Typical activation levels from 1 MW operations followed by ~48 hours of low-power studies. All numbers are mrem/h at 30 cm from beam line. The numbers in red indicate localized hot spots.



ISBN 978-3-95450-118-2

# BEAM COMMISSIONING PLAN FOR CSNS ACCELERATORS #

Sheng Wang*, Jun Peng, Huafu Ouyang, Shinian Fu
IHEP, Beijing, 100049, China

*Abstract*

The China Spallation Neutron Source (CSNS) is now under construction, and the beam commissioning of ion source will start from the end of 2013, and will last several years for whole accelerators The commissioning plan for CSNS accelerators is presented in the presentation, including the commissioning correlated parameters, beam instrumentation in used commissioning, the goal at different commissioning stages, and some key commissioning procedures for each part of accelerators. The detailed schedule for commissioning is also given.

## INTRODUCTION

The China Spallation Neutron Source (CSNS) is a high intensity proton accelerators based facility [1]. Its accelerator consists of an 80MeV H- linac, an 1.6 GeV Rapid Cycling Synchrotron (RCS) and related beam transport line. The 50keV H- beam is accelerated to 3MeV by RFQ, and the 3MeV beam is matched into Drift Tube Linac (DTL) through Medium Energy Beam Transport (MEBT). The beam is accelerated to 81MeV at the end of DTL. The 81MeV H- beam is transported to the injection point of RCS through Linac to Ring Beam Transport (LRBT) line. By using stripping painting, 81 MeV H- beam is stripped into proton and accumulated in the RCS. The proton beam is accelerated to 1.6GeV at repetition rate of 25Hz. The 1.6GeV beam is extracted in single-turn extraction. The 1.6GeV proton beam is transported through Ring to Target Beam Transport (RTBT) line onto the neutron target. The designed average beam power is 100kW, and is capable of upgrading to 500kW. Figure 1 gives the schematic layout of CSNS, and the Table 1 shows the primary parameters of CSNS.

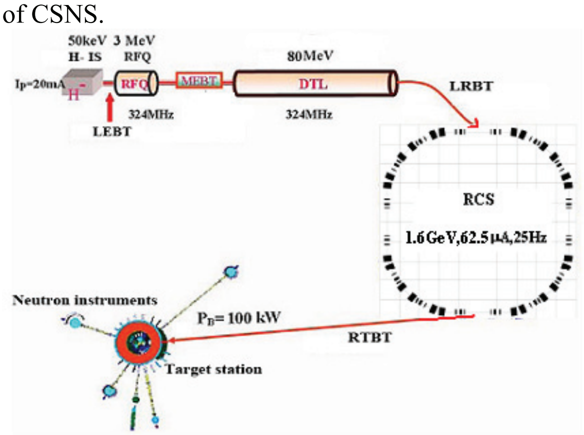


Figure 1: The Schematic Layout of CSNS

Table 1: The Main Parameters of CSNS RCS

| | CSNS | Upgrade |
|---|---|---|
| Beam power (kW) | 100 | 500 |
| Repetition rate (Hz) | 25 | 25 |
| Target number | 1 | 1 |
| Average current (μA) | 62.5 | 312 |
| Proton energy (GeV) | 1.6 | 1.6 |
| Linac energy (MeV) | 80 | 250 |

The construction of CSNS has been started in September 2011. The commissioning will start at the end of 2013. Starting from the ion source, the accelerators will be installed and commissioned sequentially.

## THE COMMISSIONING SCHEDULE AND THE GOAL AT EACH STAGE

According to the commissioning goal, the commissioning can be divided into 3 stages: The first stage is from Oct. 2013 to Aug. 2017, to commission the low intensity beam to the target; The second stage is from Aug. 2017 to Mar .2018 to increase the beam power to 10kW for official acceptance; The third stage is from Mar. 2018 to Mar. 2021 to increase beam power to the design goal of 100kW. The first stage is the most important for the commissioning. In the first stage, the front end, linac, LRBT, RCS, and RTBT will be brought into beam operation, and the primary beam parameters will be characterized with low intensity, and establish and validate the whole commissioning procedures which will be used for the high intensity normal operations. The study of various error effects on the beam, and the dependence of beam performance on various tuning parameters will be done. The study on the beam loss will be done, and the measurement of the beam losses to determine the threshold of beam loss for MPS will be also done at this stage. Table 2 shows the planned commissioning schedule. Table 3 shows the beam dump will be used in the commissioning.

Table 2:. Planned commissioning schedule

| | |
|---|---|
| Front end | Oct.18,2013-Apr.10,2014 |
| RFQ,MEBT,DTL1 | Jun.5,2014-Aug.27,2014 |
| DTL2-4 | Jun.302015-Nov.3,2015 |
| LRBT+Linac | Nov.4,2015-Jan.6,2016 |
| RCS | May13,2016-Mar.2,2017 |
| RTBT | Mar.3,2017-Aug.24,2017 |
| First beam on target | Aug.24, 2017 |
| Beam power to 10kW | Aug.25,2017-Mar.3,2018 |
| Beam power to 100kW | Mar.3,2018-Mar.3,2021 |

#Supported by National Natural Science Foundation of China (11175193)
*wangs@ihep.ac.cn



ISBN 978-3-95450-118-2

# THE RESULT OF BEAM COMMISSIONING IN J-PARC 3-GeV RCS

H. Harada#, H. Hotchi, P.K. Saha, Y. Shobuda, N. Hayashi, K. Yamamoto, M. Yoshimoto, F. Tamura, M. Yamamoto and M. Kinsho, J-PARC/JAEA, Tokai, Japan
S. Kato, Graduate School of Science, Tohoku University, Sendai, Japan
Y. Irie, T. Koseki, K. Satou, Y. Sato and M. Shirakata, KEK, Tsukuba, Japan

*Abstract*

The 3-GeV RCS of J-PARC is a high-power pulsed proton driver aiming at 1 MW output beam power. The RCS was beam commissioned in October 2007. From the results obtained in the beam tuning, we re-optimized the operating point for high-intensity beam, where the RCS has successfully achieved high-intensity beam trials of up to 420 kW by using the painting-injection technique for transverse and longitudinal plane. Then, remaining beam loss was found to be caused by scattering at the charge-exchange foil, and the RCS has successfully localized the loss at the installed injection collimator. Additionally, the RCS has successfully reduced the beam halo of the extracted beam by introducing longer second harmonic RF voltage. This paper will discuss the results of operational parameters away from the design set points, minimization of beam loss, localization of beam loss using new collimator and beam-halo reduction of extracted beam.

## INTRODUCTION

The Japan Proton Accelerator Research Complex (J-PARC) is a multipurpose proton accelerator facility [1,2], comprising a 400-MeV linac, a 3-GeV rapid cycling synchrotron (RCS), a 50-GeV main ring synchrotron (MR), and three experimental facilities that are a meterials and life science experimental facility (MLF), a hadron experimental hall (HD), and a neutrino beam line to Kamioka (NU). In this chain of accelerators, the RCS has two functions as a proton driver to produce pulsed muons and neutrons at the MLF and as an injector to the MR, aiming at 1 MW output beam power.

The RCS was commissioned in October 2007 and the output beam power has been steadily increasing following progressions in beam tuning and hardware improvements. So far, maximum beam powers for user operation and beam tuning (single shot) are 280 kW and 420 kW-equivalent beam, respectively.

Since starting the beam tuning, the RCS has performed optics parameter tuning, measurement of lattice imperfections, transverse painting-injection study, tune survey and so on. In these beam tests, we found several lattice imperfections, and the RCS cannot have large transverse-painting emittance and suppression of large incoherent tune spread. So, operating point for higher output beam power has been re-optimized in order to keep the tune spread away from integer resonance line. In this paper, we present the measured result of lattice imperfections, the beta modulation and the improved operating point.

So far, the RCS has successfully achieved high-intensity beam trials of up to 420 kW at less than 1% by using the painting-injection technique for transverse and longitudinal plane. In this paper, we show the result of measured and numerically simulated beam survival for painting-injection parameters.

The RCS has a high dose rate area at the downstream of charge-exchange foil after routine user operation. We found that the beam losses were caused by large scattering at the foil. From the view point of hardware maintenance, reduction and localization of the beam loss is main key issue. As measure of the issue, we installed the additional collimator in summer 2011. In this paper, we describe the new collimator system and localization results of beam experiments.

As an injector to MR, the RCS has another issue of beam halo reduction. The physical aperture of BT line to neutron target (3-NBT) is 324π mm mrad. On the other hand, the collimator aperture of 3-50BT line is 54π mm mrad. Therefore, it is important to reduce beam halo of extracted beam from RCS. In this paper, we present the result of beam halo reduction by introducing longer second harmonic RF voltage pattern of RCS.

## RESULTS OF BEAM TUNING

### *Lattice property and operating point*

In design stage, we performed thorough investigations of the basic lattice property, looking, in particular, for intrinsic lattice imperfections in the ring, and to find better operating point (6.68, 6.27) for high-intensity beams.

We found several lattice imperfections of the RCS ring in the beam experiments. Such imperfections generally make a distortion of the lattice super-periodicity and drives random lattice resonances. As the result, dynamic aperture and tune ability degrease, especially, they have a significant impact on high intensity operation.

In the RCS, beam injection is performed with a horizontal local bump orbit formed by four sets of rectangular type pulse dipole magnets called shift bump magnets (SB). This method generates edge focus at the entrance or exit of each SB, causing beta function modulation during beam injection. We performed the beta function measurement with/without local injection bump in the ring (the technical details of optics measurement in the RCS are described in [3]) and the measured and calculated beta function are shown in Fig.1. From this

#hharada@post.j-parc.jp

ISBN 978-3-95450-118-2

# IMPEDANCE STUDIES OF 2D AZIMUTHALLY SYMMETRIC DEVICES OF FINITE LENGTH

N. Biancacci (CERN, Geneva; Rome University "La Sapienza", Rome),
V.G.Vaccaro (CERN, Geneva; University Federico II, Naples)
E.Métral, B.Salvant (CERN, Geneva),
M.Migliorati, L.Palumbo (Rome University "La Sapienza", Rome)

*Abstract*

In circular accelerators, the beam quality can be strongly affected by the self-induced electromagnetic fields excited by the beam in the passage through the elements of the accelerator. The beam coupling impedance quantifies this interaction and allows predicting the stability of the dynamics of high intensity, high brilliance beams. The coupling impedance can be evaluated with finite element methods or using analytical methods, such as Field Matching or Mode Matching. In this paper we present an application of the Mode Matching technique for an azimuthally uniform structure of finite length: a cylindrical cavity loaded with a toroidal slab of lossy dielectric, connected with cylindrical beam pipes. In order to take into account the finite length of the structure, with respect to the infinite length approximation, we decompose the fields in the cavity into a set of orthonormal modes. We obtain a complete set of equations using the magnetic field matching and the non-uniform convergence of the electric field on the cavity boundaries. We present benchmarks done with CST Particle Studio simulations and existing analytical formulas, pointing out the effect of finite length and non-relativistic beta.

## INTRODUCTION

The problem of calculating the impedance of finite length devices, in particular simple cavities, has been approached in different ways: it was studied as a field matching problem in [1], and, approximated as a thin insert in [2, 3].

In this application we want to study rigorously the electromagnetic fields by means of the mode matching method [4, 5].

## THEORETICAL BACKGROUND

In this section we will show the expressions for electromagnetic field decomposition in a closed volume. The derived equations are the basis for the mode matching method.

Given a volume $V$, enclosed in an ideal surface $S$, the scattered electromagnetic fields E and H may be decomposed by means of the Helmholtz theorem in summation of irrotational and solenoidal eigenmodes which constitute a complete set. We can write:

$$\bar{E} = \sum_n V_n \bar{e}_n + \sum_n F_n \bar{f}_n, \tag{1a}$$

$$\bar{H} = \sum_n I_n \bar{h}_n + \sum_n G_n \bar{g}_n, \tag{1b}$$

where $\bar{e}_n$ and $\bar{h}_n$ are orthonormal solenoidal eigenvectors and $\bar{f}_n$ and $\bar{g}_n$ irrotational ones. In Table 1 is listed a set of eigenvectors and the relative differential equations and boundary conditions they have to satisfy ($\bar{n}_o$ is the unit vector normal to $S$ pointing internally the volume) [5].

Table 1: Eigenvector equations

| Eigenvector | In volume $V$ | On surface $S$ |
|---|---|---|
| $\bar{e}_n$ | $\nabla \times \bar{e}_n = k_n \bar{h}_n$ | $\bar{n}_o \times \bar{e}_n = 0$ |
| $\bar{f}_n = \nabla\Phi_n$ | $\nabla^2\Phi_n + \mu_n^2\Phi_n = 0$ | $\Phi_n = 0$ |
| $\bar{h}_n$ | $\nabla \times \bar{h}_n = k_n \bar{e}_n$ | $\bar{n}_o \cdot \bar{h}_n = 0$ |
| $\bar{g}_n = \nabla\Psi_n$ | $\nabla^2\Psi_n + \nu_n^2\Psi_n = 0$ | $\partial\Psi_n/\partial n = 0$ |

Since the eigenvectors are determined by the geometry of the structure under study, the problem reduces in finding the coefficients $V_n, I_n, F_n, G_n$. This can be done by imposing the continuity of the em-field on the openings in the surface $S$. It is understood that in this matching one must take into account also the impressed field generated by the sources.

Because of the homogenous boundary condition, which is an intrinsic property of the eigenmodes, it is not possible to perform *tout court* the matching of the electric field.

This difficulty can be surmounted resorting to a procedure which will be described in the sequel.

Let be $\bar{\mathrm{E}}$ the given imposed electric field on the surface $S_0$ . Consider the quantity $\nabla \cdot (\bar{\mathrm{E}} \times \bar{h}_n^*)$ and resort to simple algebra to get the following expression:

$$\nabla \cdot (\bar{\mathrm{E}} \times \bar{h}_n^*) = \bar{h}_n^* \cdot (\nabla \times \bar{\mathrm{E}}) - \bar{\mathrm{E}} \cdot (\nabla \times \bar{h}_n^*)$$

Now into the RHS make use of Maxwell's equation for $\bar{\mathrm{E}}$ and the expression (1a), then integrate in the volume $V$. Applying the divergence theorem and exploiting the orthonormality of the eigenmodes, one may get the following expression:

$$\int_{S_o} (\bar{\mathrm{E}} \times \bar{h}_n^*) \cdot \bar{n}_o dS = -jkZ_o I_n - k_n V_n$$



ISBN 978-3-95450-118-2

# LHC IMPEDANCE MODEL: EXPERIENCE WITH HIGH INTENSITY OPERATION IN THE LHC

B. Salvant, O. Aberle, G. Arduini, R. Assmann, V. Baglin, M.J. Barnes, P. Baudrenghien, A. Bertarelli, C. Bracco, R. Bruce, X. Buffat, F. Carra, G. Cattenoz, F. Caspers, S. Claudet, H. Day, J. Esteban Mueller, M. Garlasché, L. Gentini, B. Goddard, A. Grudiev, B. Henrist, W. Herr, S. Jakobsen, R. Jones, G. Lanza, L. Lari, T. Mastoridis, E. Métral, N. Mounet, A. Nosych, J. L. Nougaret, S. Persichelli, T. Pieloni, A. M. Piguiet, S. Redaelli, F. Roncarolo, G. Rumolo, B. Salvachua, M. Sapinski, E. Shaposhnikova, L. Tavian, M. Timmins, J. Uythoven, A. Vidal, R. Wasef, D. Wollman (CERN, Geneva, Switzerland), A. Burov* (FNAL/LARP), S. White* (BNL/LARP).

*Abstract*

The CERN Large Hadron Collider (LHC) is now in luminosity production mode and has been pushing its performance in the past months by increasing the proton beam brightness, the collision energy and the machine availability. As a consequence, collective effects have started to become more and more visible and have effectively slowed down the performance increase of the machine. Among these collective effects, the interaction of brighter LHC bunches with the longitudinal and transverse impedance of the machine has been observed to generate beam induced heating, as well as longitudinal and transverse instabilities since 2010. This contribution reviews the current LHC impedance model obtained from theory, simulations and bench measurements as well as a selection of measured effects with the LHC beam.

## INTRODUCTION

The quest for higher LHC luminosity has required a significant increase of the proton beam brightness in 2010, 2011 and 2012, as well as a decrease of the β function β* at the interaction points (IP) in 2012 thanks to tight collimator settings [1]. Both number of bunches and bunch intensity were significantly ramped up during these runs, which - together with the smaller collimator gaps of the collimators at collision energy in 2012 - was observed to enhance instabilities and beam induced heating.

The impedance of the LHC was known to be a source for beam instabilities and beam induced heating and estimates of the LHC impedance model have been refined since the first impedance database ZBASE [2, 3].

In this proceeding, the LHC impedance model will be compared to observables obtained from beam measurements before reviewing current beam brightness limitations.

## CURRENT LHC IMPEDANCE MODEL

The current impedance model [3] contains contributions from collimators, beam screens, warm beam pipe and a broadband impedance model described in the design report [4, p.101]. The longitudinal and transverse impedance models are shown in Figs. 1 and 2. It can be noticed that the horizontal and vertical impedances are of similar order of magnitude. Other impedance contributions obtained from 3D simulations of individual devices are planned to be added to the impedance model, but simulating very long wakes for multibunch multiturn macroparticle simulations has proved to be very difficult so far.

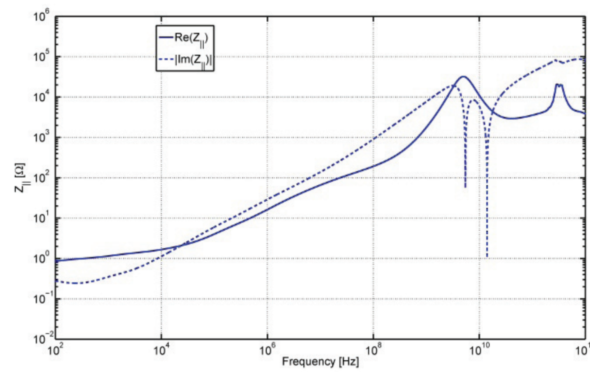


Figure 1: LHC longitudinal impedance model as a function of frequency at injection energy (2012).

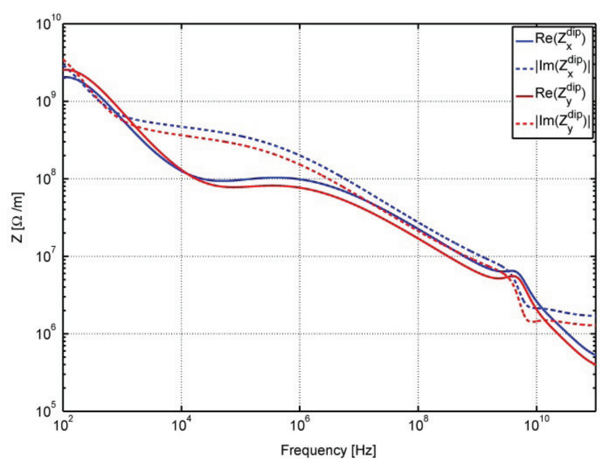


Figure 2: LHC transverse impedance model as a function of frequency at collision energy with squeezed optics (2012).

* Work partially supported by US-LARP.

ISBN 978-3-95450-118-2

# RESISTIVE WALL INSTABILITY IN CSNS/RCS*

Liangsheng Huang, Sheng Wang#, Y. D. Liu, IHEP, Beijing, P. R. China.


*Abstract*

Rapid Cycling Synchrotron (RCS) of the China Spallation Neutron Source (CSNS) is a high intensity proton accelerator, with average beam power of 100kW. The collective effects caused by the coupling impedance may be the limit to beam power. The impedance estimation for components on beam line shows that the resistive wall impedance and its instability are more serious than any others. Based on the impedance budget, the instability is theoretically estimated. A simple resistive wall wake field model is used to simulate the bunch oscillation and obtain the growth time. In this simulation model, the continuous resistive wall wake field is concentrated to one position in the ring and the long bunch is sliced into many micro-bunches. By tracking the dynamics of the macro-bunches, the transverse growth time are obtained. The simulation results are also confirmed the restriction to instability by natural chromaticity.


## INTRODUCTION

The China Spallation Neutron Source (CSNS) accelerators consists of an $H^-$ Linac and a proton Rapid Cycling Synchrotron (RCS), beam transportations, a target station, spectrometers. RCS is designed to accumulate and accelerate proton beam from 80MeV to 1.6GeV. The extracted 100 KW beam strike the neutron target with repetition rate of 25Hz. Due to the high beam intensity, the ratio of beam loss must be controlled to a very low level. The RCS lattice adopt a triplet cell based 4-fold structure[1]. The time of movement for every pulse is about 20 milliseconds.

Considered the upgrading requirement, the impedance budget needs to be meeting the requirement of higher beam current for 500kW beam. Corresponding to 500kW beam power, the physics parameters should be more flexible on the phase of CSNS design. The impedance and instability need to be restricted seriously. With beam current in upgrades, resistive wall instability will be an important commission limitation for CSNS/RCS. Table 1 listed the main parameters of CSNS/RCS.

Table 1: Main Parameters of CSNS/RCS

| Parameters | Values |
|---|---|
| Circumference/m | 227.92 |
| Inj. energy/MeV | 80 |
| Ext. energy/GeV | 1.6 |
| Stainless steel length /m | 140 |
| Average beta function(H/V)/m | 9.5/10.5 |
| Nominal tunes(H/V) | 4.86/4.78 |
| Natural chromaticity(H/V) | -4.64/-8.27 |
| Bunch number | 2 |
| Particles per bunch | 7.8x1012 |

Studies on beam instability due to impedance are the vital work in accelerator physical design, so the impedance calculation and control on vacuum components is one of the important challenges in CSNS project. Impedances of RCS mainly come from resistive wall, RF cavities, and collimators. The estimated impedance values were summarised in Table 2. It is clear that resistive wall is much more serious.

The beam loss in RCS caused by resistive wall may be one of the limits to reach the design beam power. Especially, at the low-energy end of each cycle, the resistive wall instability is much more serious. The detailed study on resistive wall instability in RCS is necessary to the design of accelerator.

According to the analytical formula and impedance model on resistive wall instability, the instability is estimated. Them a simple simulation model is introduced and with the tracking method on macro-particles, the bunch oscillation is simulated. Based on the analytical and simulation results, the way for depressing the resistive wall instability is introduced in the last part of the paper.

Table 2: CSNS/RCS Critical Components Impedance Estimated Value, $n=\omega/\omega_0$, $\omega_0$ is Angular Revolution Frequency

| Component \ Item | Injection longitudinal (Ω/m) | Injection transverse(kΩ/m) | Extraction longitudinal(Ω/m) | Extraction transverse(kΩ/m) |
|---|---|---|---|---|
| Space charge | –j811.45 | –j16.77k | –j96.62 | –j3.30k |
| Resistive wall | $1.68(1+j)/n^{1/2}$ | $36.12(1+j)/n^{1/2}$ | $2.61(1+j)/n^{1/2}$ | $23.23(1+j)/n^{1/2}$ |
| RF cavity | j0.014 | j4.74 | j0.033 | j4.74 |
| Collimator | j0.17 | j0.23 | j0.42 | j0.23 |

* Supported by National Natural Science Foundation of China (11175193)
# wangs@ihep.ac.cn



ISBN 978-3-95450-118-2

# LONGITUDINAL INSTABILITIES IN THE SPS AND BEAM DYNAMICS ISSUES WITH HIGH HARMONIC RF SYSTEMS

E. Shaposhnikova, T. Argyropoulos, T. Bohl, J. E. Muller, H. Timko, CERN, Geneva, Switzerland

*Abstract*

Even after the successful impedance reduction programme which eliminated the microwave instability, longitudinal instability in the SPS is still one of the main intensity limitations. It is observed during acceleration for both single bunch and multi-bunch beams at intensities below the nominal LHC intensity. The thresholds are increased in the new SPS optics with lower transition energy, under intensive study now, but even in this case the 4th harmonic RF system is required for stability of the nominal beams. The upgrade program for both RF systems has started in the SPS to cope with future higher intensity beams required for the High Luminosity LHC. The results of studies of the parameter space required for beam stability are presented and compared with operation modes of double RF systems in other accelerators.

## INTRODUCTION

Already by the end of 2010 LHC beams with both 50 ns and 75 ns spaced bunches became operational and were regularly taken by the LHC. In 2012 the SPS has been able to deliver at top energy (450 GeV) up to four batches of 36 bunches spaced at 50 ns with bunch intensity of $1.6 \times 10^{11}$ and nominal longitudinal (0.5 eVs) and smaller than nominal transverse (2.5 $\mu$m) emittances. The LHC beam at 25 ns bunch spacing with nominal intensity of $1.2 \times 10^{11}$ ppb was also obtained in the SPS a few years ago.

Various LHC upgrade scenarios which are presently under consideration are based on the SPS beam with bunches of $2.2\times10^{11}$ ppb spaced at 25 ns or of $3.6\times10^{11}$ ppb spaced at 50 ns [1]. In both cases the SPS must be able to reliably accelerate much higher beam intensities than achieved so far and therefore significant improvements to the machine performance should be found and implemented on the same time scale as the LHC upgrade. The upgrades foreseen in the SPS are related to the known intensity limitations: beam losses, longitudinal coupled-bunch instabilities, beam loading in the two RF systems as well as heating of different machine elements. The present machine seems to be well scrubbed and no signs of e-cloud instabilities are observed for intensities achieved so far.

## LONGITUDINAL INSTABILITIES

### *Observations*

The longitudinal multi-bunch instability observed during acceleration has the lowest intensity threshold: one batch of 36 bunches at 50 ns spacing with $2 \times 10^{10}$ ppb and nominal injected longitudinal emittances (0.35 eVs) is unstable with the RF feedback, feed-forward and longitudinal damper (low modes) in operation. Possible sources of this instability are the fundamental and HOMs of the main (200 MHz) and high harmonic (800 MHz) RF systems.

As expected from the calculated threshold for the coupled-bunch instability [2], the threshold clearly depends on energy and longitudinal emittance: more dense bunches become unstable earlier in the cycle. A comparison of LHC beams with different bunch spacing $T_b$ shows that the energy threshold scales roughly as $1/E_{th} \sim N_b/T_b$, or with total beam current. Indeed in our measurements the 50 ns beam with a bunch intensity of $N_b = 1.6 \times 10^{11}$ was unstable around 160 GeV/c and the 25 ns beam with $N_b = 1.2 \times 10^{11}$ at 110 GeV/c. Higher intensity 25 ns and 50 ns beams are also at the limit of stability on the 26 GeV/c flat bottom.

On the other hand the instability threshold doesn't depend on the number of batches in the ring, at least for the 50 ns spaced beam (with 250 ns batch gaps), see Fig. 1 (top). This short-range wake is compatible with the main impedances of the 200 MHz and 800 MHz RF systems which have, correspondingly, quality factors of 150 and 300.

One batch consisting of 6 bunches with $N_b = 1.6\times10^{11}$ spaced at 50 ns became unstable over a wide energy range (240-410) GeV/c. Note that these bunches are held by the phase loop and are usually slightly (5%) shorter.

The single bunch instability threshold on the flat top is around $1.1 \times 10^{11}$ and on the flat bottom it is close to $1.3 \times 10^{11}$ in the operational voltage of 2 MV. Injected bunches continue to oscillate during the whole 11 s long flat bottom. The threshold for the loss of Landau damping during the operational cycle [2] calculated using Sacherer' criterion [3] suggests that single bunches should be much more stable on the flat bottom than observed. Measurements on the flat bottom with phase loop on show that this instability threshold strongly depends on the capture voltage. Bunches with this intensity are much more stable in the lower capture voltage of 1 MV, impossible to use in operation with the LHC beam due to beam loading leading to beam losses. Another possible explanation for the low threshold is related to the particular bunch distribution coming from the PS after bunch rotation, see [4], which creates high frequency modulation of the bunch profile.

The LHC beam in the present operation is stabilised by increased synchrotron frequency spread using a 4th harmonic RF system in bunch-shortening (BS) mode (see below) and controlled emittance blow-up, see Fig. 1 (center).



ISBN 978-3-95450-118-2

# HIGH ENERGY ELECTRON COOLING

V.B. Reva, M. I. Bryzgunov, V.M. Panasyuk, V.V. Parkhomchuk, BINP, Novosibirsk, Russia

*Abstract*

The electron cooler of a 2 MeV for COSY storage ring FZJ is assembled in BINP [1]. This paper describes the first experimental results from the electron cooler with electron beam and high voltage. The cooling section is designed on the classic scheme of low energy coolers like cooler CSRm, CSRe, LEIR that was produced in BINP before. The electron beam is transported inside the longitudinal magnetic field along whole trajectory from an electron gun to a collector. This optic scheme is stimulated by the wide range of the working energies 0.025÷2 MeV. The electrostatic accelerator consists of 33 individual unify section. Each section contains two HV power supply (plus/minus 30 kV) and power supply of the magnetic coils. The electrical power to each section is provided by the cascade transformer. The cascade transformer is the set of the transformers connected in series with isolating winding.

## SETUP DESCRIPTION

The schematic design of the setup is shown in Fig.1. The electron beam is accelerated by an electrostatic generator that consists of 33 individual sections connected in series. Each section has two high-voltage power supplies with maximum voltage 30 kV and current 1 mA. The electron beam is generated in electron gun immersed into the longitudinal magnetic field. After that the electron beam is accelerated, moves in the transport line to the cooling section where it will interact with protons of COSY storage ring. After interaction the electron beam returns to electrostatic generator where it is decelerated and absorbed in the collector.

The optics of 2 MeV cooler for COSY is designed close to the classical low-energy coolers. The motion of the electron beam is magnetized (or close to magnetized conditions) along whole trajectory from a gun to a collector. This decision is stimulated by requirement to operate in the wide energy range from 25 keV to 2 MeV. So, the longitudinal field is higher then transverse component of the magnetic fields. The bend magnets and linear magnets of the cooler are separated by a section with large coils for the location of the BPMs, pumps and a comfort of the setup assembling. The length of the linear magnets is defined by the necessity to locate the electrostatic generator outside the shield area of the storage ring.

The vacuum chamber is pumped down by ion and titanium sublimation pumps. The typical diameter of the vacuum chamber is 100 mm and the aperture in the transport channel and cooling section is close to this value. The diameter of the accelerating tube is 60 mm.

## MAGNETIC SYSTEM

The magnetic field in the accelerating tube is taken 500 G and this value is related to the maximum power that can be transfer to a high voltage potential with help of the cascade transformer. The value in the transport channel is located in the range 0.5 kG – 1 kG. The energy 2 MeV is high enough in order to don't have the complete adiabatic motion of the electrons because the magnetic field of the bend elements is chosen to provide the length of bend equal to integer number of Larmour lengths. In such case the kick on entry to bend is compensated by kick on leaving and the excitation of the transverse motion of the electron is small. So, it is convenient to change the longitudinal magnetic field according to the electron momentum. At attainment of the maximum magnetic field the transition to another integer number is implemented.

The magnetic field in the cooling section is taken 2 kG in order to have the maximum Larmour oscillation (~ 10) of the electron during its interaction with ion in order to have the magnetized Coulomb collisions even the highest electron energy 2 MeV.

The transition from accelerating tubes to transport channel is made with 7 coils powered by independent power supplies [2]. The transition from the transport channel to the cooling section is made with 5 coils with small regulation of the longitudinal current with regulated electrical shunt. In this region the magnetic field is strong and the electron motion is close to adiabatic so the matching can be realized by the proper location of these coils in order to minimize the amplitude of the transverse motion.

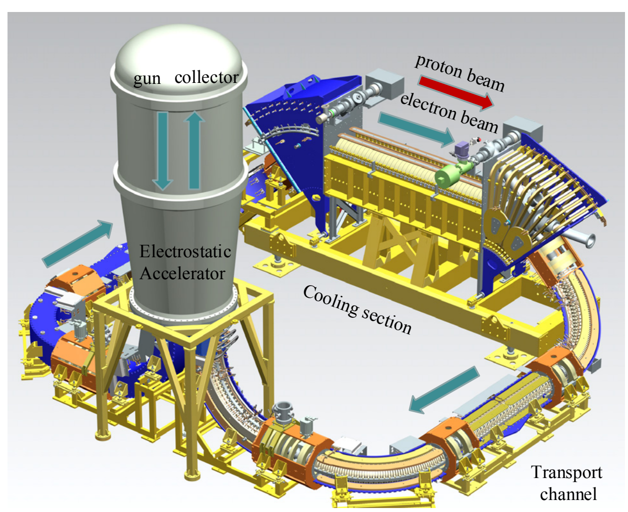


Figure 1: 3D design of 2 MeV COSY cooler.



ISBN 978-3-95450-118-2

# BEAM LOSS AND COLLIMATION IN THE ESS LINAC

R. Miyamoto*, B. Cheymol, H. Danared, M. Eshraqi, A. Ponton, J. Stovall, L. Tchelidze
ESS, Lund, Sweden
I. Bustinduy, ESS-Bilbao, Bilbao, Spain
H.D. Thomsen, A.I.S. Holm, S.P. Møller, ISA, Aarhus, Denmark

*Abstract*

The European Spallation Source (ESS), to be built in Lund, Sweden, is a spallation neutron source based on a 5 MW proton linac. A high power proton linac has a tight tolerance on beam losses to avoid activation of its components and it is ideal to study patterns of the beam loss and prepare beam loss mitigation schemes at the design stage. This paper presents simulations of the beam loss in the ESS linac as well as beam loss mitigation schemes using collimators in beam transport sections.

## INTRODUCTION

The European Spallation Source (ESS) will be a spallation neutron source based on a 5 MW proton linac, planned to be constructed in Lund, Sweden [1]. Design of the linac has been updated under the ESS Accelerator Design Update Project, a collaboration between universities and institutions in five European countries with additional contributions and supports from accelerator laboratories inside and outside of Europe. The project is near the completion and the updated design will be presented in the ESS Technical Design Report, published at the end of 2012 together with a cost report, time schedule and other documents needed for the final approval of the construction of ESS.

Figure 1 shows the schematic layout of the ESS linac [2] which consists of room temperature accelerating structures, an iron source (IS), radio frequency quadrupole (RFQ), and drift tube linac (DTL), and a superconducting linac (SCL), including spoke, medium $\beta$, and high $\beta$ elliptical cavities, together with low, medium and high energy beam transport (LEBT, MEBT and HEBT) sections.

One of the toughest challenges in design and operation of a high power proton linac is to minimize beam losses. *Fast losses* (infrequent, short term, and high power losses mostly from fault scenarios) from a 5 MW proton beam could damage the linac components quite fast [3], and so a machine protection system which detects anomalies in the linac and stops the beam operation is a critical system but is not in scope of this paper. *Slow losses* (continuous and low power losses) which do not damage the components may still produce radioactive nuclei inside the components and prevent hands-on maintenance after a reasonable cooling time. Minimizing the slow losses requires a lot of efforts in various aspects and on-going efforts include 1) identifying the loss limit based on the activation level of components, 2) understanding the correlation between the losses and the beam and lattice conditions, 3) preparing collimators to remove halo particles, and 4) preparing diagnostics devices and strategies. This paper presents status of the efforts 1), 2), and 3).

* ryoichi.miyamoto@esss.se

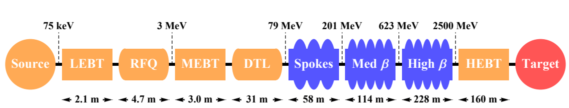


Figure 1: Schematic layout of the ESS linac.

## BEAM LOSS LIMIT IN RFQ AND DTL

A study is conducted to estimate the beam loss limit in the RFQ and DTL which allows the hands-on maintenance by radiation workers after a reasonable cool down time (four hours are assumed) [4] and to re-evaluate the often quoted 1 W/m loss criteria. Two documents [5, 6] specify ionizing radiation does limits for radiation works at ESS but, in the following study, a more restricted limit of CERN for supervised temporary workplace, 15 $\mu$Sv/hr measured 40 cm from an accelerating structure, is used.

The relation between the beam loss and radiation does on the outer surface and at 40 cm from the outer surface are estimated for the RFQ and DTL with MARS code [7]. Figure 2 shows a the DTL model used in MARS where the bottom and top lines are the beam axis and the outer surface of the tank. In the figure, SS and SmCo stand for Stainless Steel and Samarium-Cobalt, constituent of a permanent magnet quadrupole used in the DTL. Dimensions of the drift tube in the figure is adjusted according to the proton beam energy. In the study, the beam loss is modeled as a proton beam incident on a point of the inner wall of the drift tube. The beam loss is often quoted as loss density in units of W/m. A detailed study showed that a point source gives the worst activation both on the outer surface and the 40 cm location compared when the same energy and power of protons are incident on either multiple spots or uniformly on a line [4]. Hence, to make a pessimistic estimate, a point source is assumed. Two cases when the

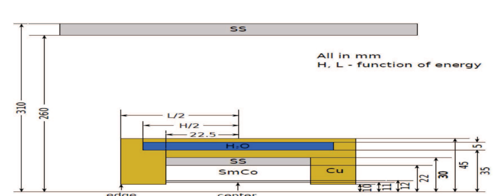


Figure 2: DTL model used in MARS. SS and SmCO stand for Stainless Steel and Samarium-Cobalt.



ISBN 978-3-95450-118-2

# EXTRACTION, TRANSPORT AND COLLIMATION OF THE PSI 1.3 MW PROTON BEAM

D. Reggiani#, Paul Scherrer Institut, 5232 Villigen PSI, Switzerland

*Abstract*

With an average operating beam power of 1.3 MW the PSI proton accelerator complex is currently leading the race towards the high intensity frontier of particle accelerators. This talk gives an overview of the extraction of the 590 MeV beam from the ring cyclotron and its low loss transport to the meson production targets M and E as well as to the SINQ spallation neutron source. Particular regard is given to the collimator system reshaping the beam which leaves the 40 mm thick graphite target E before reaching SINQ. Since 2011, up to 8 second long beam macro-pulses are regularly diverted to the new UCN spallation source by means of a fast kicker magnet. The switchover from the SINQ to the UCN beam line as well as the smooth beam transport up to the UCN spallation target constitute the subject of the last part of the talk.

## INTRODUCTION

The PSI high intensity proton accelerator (HIPA) generates a continuous wave (50.6 MHz frequency) 590 MeV, 1.3 MW beam [1]. A schematic of the accelerator complex is shown in Fig. 1. Protons are provided by an ECR source, brought to 870 keV energy by a Cockcroft-Walton generator and then transferred through a LEBT-section to the 72 MeV injector cyclotron. The medium energy beam is transferred to the 590 MeV ring cyclotron. Losses occurring at the ring extraction are the most common limiting factor for the beam intensity. Indeed, in order to avoid unsustainable machine activation, the extraction losses have to be kept within the lower $10^{-4}$ range. The 1.3 MW beam is transported to a first 5 mm thick meson production graphite target (M) where 1.6% of the beam is lost. A second 40 mm thick graphite target (E) is mounted some 18 m downstream. About 12% of the beam is lost on the target itself while an additional 18% of it is absorbed by a powerful collimator system that reshapes the highly divergent beam and at the same time protects accelerator components from activation. The remaining beam is eventually transported to the SINQ neutron spallation source where it is completely absorbed. In case of a SINQ technical stop, the HIPA facility can still run at about 1 MW beam power (75% of the nominal intensity) thanks to a beam dump installed downstream of target E. A total of seven muon or pion secondary beam lines are located at the meson production targets M and E while SINQ provides neutrons for eighteen beam lines.

In 2011 the UCN neutron source was brought into routine operation at HIPA [2]. This second spallation source runs concurrently to SINQ and is driven by 1.3 MW proton macro-pulses kicked into the UCN beam line with a maximum duty cycle of 1%. The switchover of a megawatt class beam between two beam lines is another unique feature of the PSI high intensity proton accelerator facility.

A crucial issue related to a MW-class acceletator is the machine protection system (MPS). The HIPA-MPS get signal from hundreds of diagnostics devices as well as power supplies and is capable of stopping the beam within 5 ms [3].

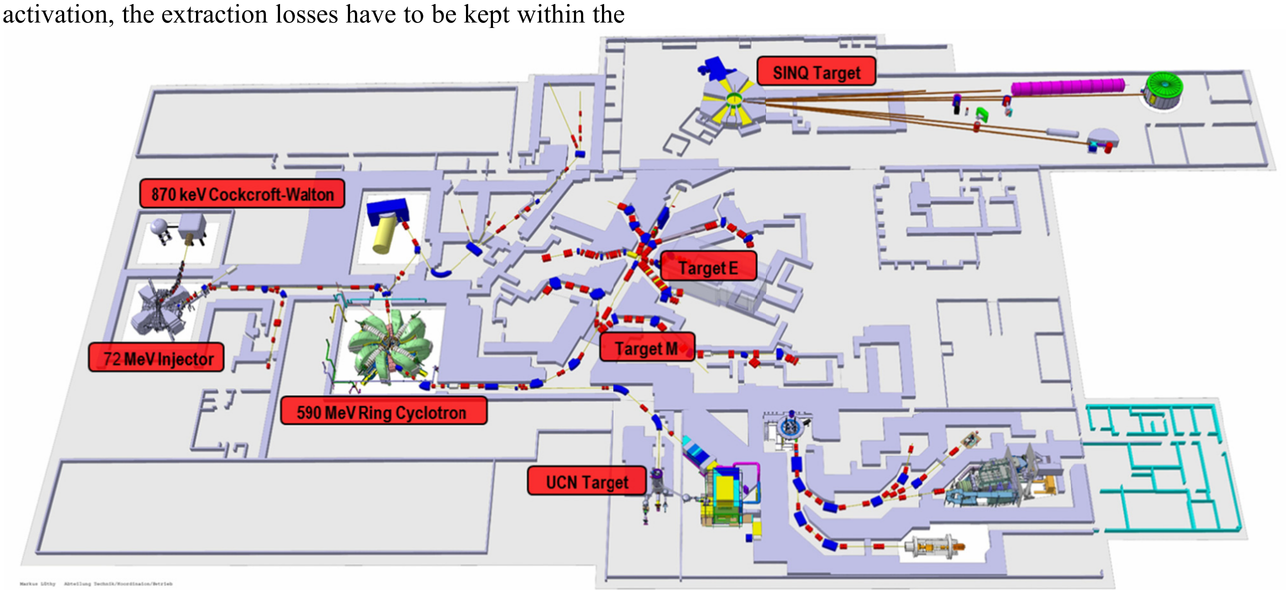


Figure 1: Overview of the PSI high intensity accelerator facility.

#davide.reggiani@psi.ch



ISBN 978-3-95450-118-2

# CURRENT AND PLANNED HIGH PROTON FLUX OPERATIONS AT THE FNAL BOOSTER*

F.G. Garcia#, W. Pellico, FNAL, Batavia, IL 60510, USA

*Abstract*

The Fermilab Proton Source machines, constituted by Pre-Injector, conventional Linac and Booster synchrotron, at Fermi National Accelerator Laboratory (Fermilab) had have a long history of successful beam operations. Built in late 60's, the Fermilab Proton Source began operations early in the 70's and since then it has successful provided protons to support the laboratory physics experiments. During the past decade, Booster performance reached unprecedented proton flux delivery of the order of 1.0–1.1E17 protons per hour, corresponding to 40 kW of beam power while maintained an allowed upper limit of 525 W of beam loss in the tunnel. In order to achieve this historical performance, major hardware upgrades were made in the machine combined with improvements in beam orbit control and operational awareness. Once again, the Proton Source has been charged to double their beam throughput, while maintaining the present residual activation levels, to meet the laboratory Intensity Frontier program goals until new machines are built and operational to replace them. In this paper we will discuss the plans involved in reaching even higher beam throughput in Booster.

## INTRODUCTION

The Fermilab Booster [1] is rapid cycling synchrotron which accelerates protons from 400 MeV to 8 GeV for injection, until recently exclusively into the Main Injector, and for the Booster Neutrino beamline (BNB). It is 472 m in circumference and it operates at a Radio Frequency (RF) harmonic number of 84. The Booster frequency changes rapidly through the accelerator cycle, from 37.9 – 52.8 MHz and there are 19 RF cavities in the machine. Early in 2000's the demand for protons increased 12-fold in comparison to the previous 10 years of Booster operations prompted by the beginning of the neutrino program at Fermilab.

Present protons per batch in Booster are 4.5E12 at 7.5 Hz with 90% efficiency and 85% uptime. In the future, the required number of protons to support the laboratory physics program, until Project X is operational, requires double the proton flux from the present running conditions. Booster is not current capable of running at 15 Hz mainly due to RF power system limitations [2]. In addition, reliability of Booster machine is an issue that has been increasing and will continue to increase with time just as the physics program demands better performance. Improvements in both hardware and operational efficiency of the Booster are required in order to have a successful physics program. Therefore, the Proton Improvement Plan (PIP) [3] was established in 2012. The goal is to deliver 2.25E17 protons per hour at 15 Hz by 2016. This increase in proton throughput has to be achieved by:

- maintaining 85% or higher availability;
- maintaining the same residual activation in the accelerator components.

The primary users of a high-intensity proton beam will continue be to generate neutrinos at the 8 GeV Booster Neutrino beamline and the 120 GeV Neutrino at Main Injector (NuMI) beamline.

## HIGH PROTON FLUX OPERATION

Achieving > 80 kW beam power from Booster will require increasing the repetition rate and/or the beam current per cycle. The ability to increase the Booster beam power by increasing the beam charge per cycle is primarily constraint by beam losses, decreasing Booster overall efficiency and shortfall in beam parameters that are acceptable to be cleanly and efficiently transfer from Booster to Main Injector. Therefore, PIP chose the path to increase the beam throughput by increasing the number of cycles with beam. Figure 1 shows the protons delivered per day and the integrated protons delivered since 1992 up to May 2012.

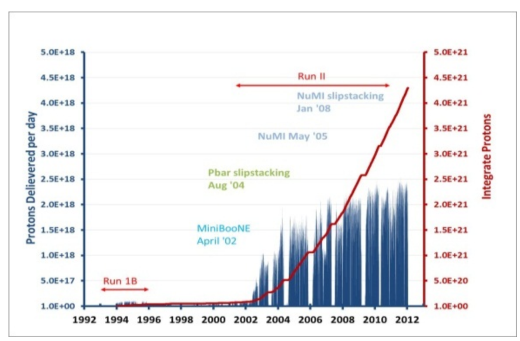


Figure 1: Booster integrated and per day protons delivery for the past 2 decades.

As can be seen, proton flux has seen a rapid increase with each yearly output exceeding the previous. Now Booster faces another challenge after the yearlong 2012 shutdown. The driving force for this long shutdown is to make the necessary Accelerator and NuMI Upgrades (ANU) for the NuMI Off-axis neutrino Appearance (NOvA) experiment [4].

NOvA is expecting up to 700 kW of peak proton power with 4.3E12 protons per batch from Booster delivered to Recycler in 12 spills at 9 Hz, where it will be slip stacked,

*Work supported under DOE contract DE-AC02-76CH03000
#fgarcia@fnal.gov



ISBN 978-3-95450-118-2

# LOW GAMMA TRANSITION OPTICS FOR THE SPS: SIMULATION AND EXPERIMENTAL RESULTS FOR HIGH BRIGHTNESS BEAMS

H. Bartosik, G. Arduini, T. Argyropoulos, T. Bohl, K. Cornelis, J. Esteban Muller, K. Li, A. Yu. Molodozhentsev, Y. Papaphilippou, G. Rumolo, B. Salvant, F. Schmidt, E. Shaposhnikova, H. Timko, CERN, Geneva, Switzerland

*Abstract*

The single bunch transverse mode coupling instability (TMCI) at injection is presently one of the main intensity limitation for LHC beams in the SPS. A new optics for the SPS with lower transition energy yields an almost 3-fold increase of the slip factor at injection energy and thus a significantly higher TMCI threshold, as demonstrated both in simulations and in experimental studies. It is observed furthermore that the low gamma transition optics yields better longitudinal stability throughout the entire acceleration cycle. In addition, simulations predict a higher threshold for the electron cloud driven single bunch instability, which might become an important limitation for high intensity LHC beams with the nominal 25 ns bunch spacing. This contribution gives a summary of the experimental and simulation studies, addressing also space charge effects and the achievable brightness with high intensity single bunch beams.

## INTRODUCTION

Performance limitations for LHC beams in the CERN accelerator complex and their mitigations are studied in the frame of the LHC injectors upgrade (LIU) project, with the goal to reach the beam parameters required for the future high luminosity LHC (HL-LHC). Presently known intensity limitations in the SPS are due to beam loading in the travelling wave 200 MHz and 800 MHz cavities, which requires an upgrade of the RF system, and due to various single and multi bunch instabilities [1]. At injection, the transverse beam coupling impedance drives a single bunch transverse mode coupling instability (TMCI) in the vertical plane. For mitigating longitudinal instabilities, a double harmonic RF system is used for LHC beams where the 800 MHz system serves as Landau cavity in bunch shortening mode. Controlled longitudinal emittance blow-up is performed during the ramp to stabilize the beam at high energies up to the flat top [2]. The performance of future high intensity LHC beams with 25 ns bunch spacing might be furthermore limited by transverse emittance blow-up and transverse instabilities due to electron cloud effects in the main dipole magnets.

For constant longitudinal bunch parameters and a matched RF-voltage, higher intensity thresholds for all of the above instabilities are expected when increasing the slip factor $\eta$. The nominal SPS optics has $\gamma_t = 22.8$. Since the working point in this optics is $(Q_x, Q_y) = (26.13, 26.18)$, it will be referred to as “Q26” optics in the following. LHC-type proton beams are injected with $\gamma = 27.7$ (26 GeV/c), i.e. above transition. By reducing $\gamma_t$, the slip factor is increased throughout the acceleration cycle with the largest relative gain at injection energy. Figure 1 shows $\eta$ normalized to the value in the nominal SPS optics ($\eta_{\gamma_t=22.8}$) as function of $\gamma_t$ for injection energy and for top energy. A significant gain of beam stability can thus be expected for a relatively small reduction of $\gamma_t$, especially in the low energy part of the acceleration cycle.

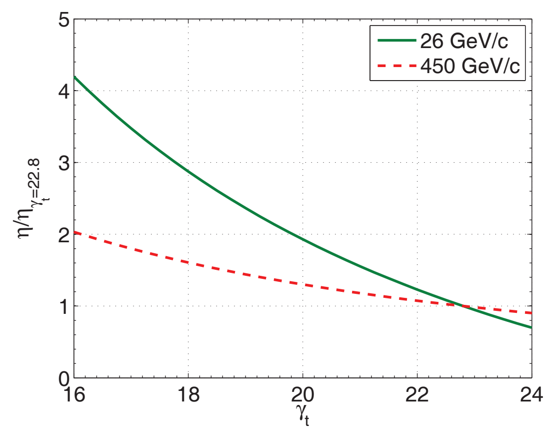


Figure 1: Slip factor $\eta$ relative to the value of the nominal SPS optics (nominal $\gamma_t = 22.8$) as a function of $\gamma_t$. At injection $\gamma = 27.7$ and at extraction $\gamma = 480$.

In a FODO lattice (like the SPS) $\gamma_t$ scales like the horizontal phase advance in the arcs. This is exploited in the “Q20” optics [3], where the working point of the SPS is changed to $(Q_x, Q_y) = (20.13, 20.18)$. As in the nominal optics, the phase advance along the arcs is close to multiples of $2\pi$ and thus the dispersion in the straight sections is small. The transition energy is reduced to $\gamma_t = 18$ in the Q20 optics, which translates to a relative gain of $\eta$ by a factor 2.85 at injection energy and a factor 1.6 at top energy compared to the nominal optics (see Fig. 1). Since the end of 2010, the Q20 optics was successfully tested in a series of machine studies and proved to show the expected gain of beam stability both in the transverse and in the longitudinal plane. An overview of the studies and the present understanding of instabilities in comparison with the nominal SPS optics will be given in the following.

ISBN 978-3-95450-118-2

# OPTICS DESIGN OPTIMIZATION FOR IBS DOMINATED BEAMS

F. Antoniou, H. Bartosik, Y. Papaphilippou, CERN, Geneva, Switzerland
N. Milas, A. Streun, Paul Scherrer Institut, Switzerland
M. Pivi, SLAC, Menlo Park, CA, USA
T. Demma, LAL, Université Paris-Sud, Orsay, France

*Abstract*

Intra-beam scattering is a small angle multiple Coulomb scattering effect, leading to emittance growth. It becomes important for high brightness beams in low emittance lepton rings, but also hadron synchrotrons and ring colliders. Several theoretical models have been developed over the years, however, when the IBS becomes predominant, the divergence between the models becomes important. In addition, the theoretical models are based on the consideration of Gaussian beams and uncoupled transverse motion. Recently, two multi-particle tracking codes have been developed, in order to enable the understanding of the IBS influence on the beam distribution and the inclusion of coupling. The comparison between theoretical models in different lattices and different regimes is discussed here and the bench-marking of the theoretical models with the tracking codes is presented. Finally, first measurement results are presented in low emittance rings and hadron synchrotrons.

## INTRODUCTION

Future $e^+/e$ linear collider damping rings, b-factories, modern high brilliance light sources but also hadron synchrotrons and ring colliders, aim to produce high brightness beams, entering in a regime where collective effects and especially intra-beam scattering (IBS) are predominant.

IBS is a small angle multiple Coulomb scattering effect, which depends on the lattice and the beam characteristics, leading to the diffusion of the six-dimensional phase-space. Several theories and their approximations were developed over the years describing the effect. In this report, the theoretical models of Bjorken-Mtingwa (B-M) and Piwinski (P) and their high energy approximations, Bane and the Complete Integrated Modified Piwinski (CIMP) respectively are used [1–4].

One of the main weaknesses of all theoretical models is the consideration of Gaussian beam distributions whose preservation, especially in strong IBS regimes, is not evident. The generation of non-Gaussian tails and its impact on the damping process can only be investigated with multiparticle algorithms [5, 6]. The bench-marking of these theoretical and numerical models with beam experiments would be the ultimate goal for understanding IBS.

In this report, the IBS effect is studied for three different lattices at different regimes. The CLIC DRs for ultra low emittance beams, the SLS at low energy and high bunch current and the SPS for the ion beams. First measurement results are finally presented and discussed.

## IBS STUDIES FOR THE CLIC DR

The role of the CLIC DRs is to produce the required ultra low emittance at a high bunch intensity and a fast repetition rate, imposed by the luminosity requirements of the collider [7]. They have a racetrack configuration with two arc sections filled with theoretical minimum emittance (TME) cells and two long straight sections filled with superconducting wigglers, which are necessary for the fast damping and the ultra low emittance [7].

The CLIC DR have to deliver a high bunch intensity of $4.1 \times 10^9$ particles with ultra low horizontal and vertical emittances of 500 nm·rad and 5 nm·rad respectively, normalized to the beam energy. What indeed diversifies the required beam characteristics in the DRs is the very small longitudinal normalized emittance of 6 keV·m, which is imposed by the bunch compression requirements of the downstream RTML (Ring To Main Linac) system [7]. The increased beam density of the beam triggers a number of single bunch collective effects with Intrabeam Scattering (IBS) being the main limitation for the ultra low emittance.

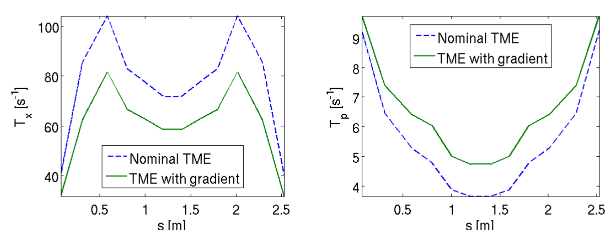


Figure 1: Horizontal (left) and longitudinal (right) growth rate increments along a nominal (blue-dashed) and a modified (solid-green) TME cell.

In the initial design of the CLIC DR [8] the nominal TME cells were used, targeting a very low equilibrium emittance. This was due to the fact that the IBS growth factor of the lattice at that stage of the design was very large ($\sim 6$). One of the first steps in the optimization procedure was to modify the TME cell, using a combined function dipole with a low defocusing gradient, calling this a modified TME cell. The low gradient do not have any impact on the emittance, however, it reverses the vertical beta function at the middle of the dipole, maximizing the vertical beam size at that location where all horizontal and vertical beam sizes and dispersion used to be minimum in the initial design [7]. This reduced the IBS growth factor by a factor of 2. Figure 1 shows the comparison of the horizontal (left) and longitudinal (right) IBS growth rate increments along a TME cell, for a nominal (dashed-blue lines) and a modified



ISBN 978-3-95450-118-2

# CIRCULAR MODES FOR FLAT BEAMS IN LHC*

A. Burov, FNAL, Batavia, IL 60510, USA

*Abstract*

Typically x/y optical coupling is considered as unwanted and thus suppressed; particular exclusions are electron and ionization coolers. Could some special coupled modes be effectively applied for the LHC complex? Apparently, the answer is positive: use of the circular modes [1] in the injectors with their transformation into planar modes in the LHC allows both the space charge and beam-beam luminosity limitations to be significantly reduced, if not practically eliminated.

## PLANAR AND CIRCULAR MODES

Conventional x/y betatron oscillations can be referred to as planar, since in the geometrical 3D space every one of them is seen as a plane, horizontal or vertical. Planar optical modes are described by the conventional Twiss functions; Courant-Snyder invariants and betatron phases are canonical actions and phases for these modes. In more general case, the two transverse degrees of freedom are arbitrary coupled, and their description requires more complicated set of general 4D Twiss functions, which can be taken ether in Edwards-Teng or Mais-Ripken form (see e. g. Ref. [2]). For the coupled case, there are still two Courant-Snyder invariants, expressed as quadratic forms of the 4D phase space vectors. Provided that an optical transformation is linear and symplectic, the two Courant-Snyder invariants are preserved.

An interesting example of fully coupled optics is presented by circular modes, when particles are moving along clockwise or counter-clockwise spirals [1]. These modes are eigenfunctions for rotation-invariant focusing elements, like solenoids and bending magnets with the field index ½:

$$-\frac{\partial B_y}{\partial x}\frac{\rho}{B_y}=\frac{1}{2}.$$

For quadrupole and skew-quadrupole based focusing, optical modes are generally elliptical, being more close to planar or circular in special cases. In principle, there is a direct analogy between light polarization and optics of particles in accelerators: the eigenfunctions are determined by symmetry of the media or focusing. For rotation-invariant matrices, the angular momentum is preserved; thus, the angular momentum $M = xp_y - yp_x$ has to be proportional to a difference of the two circular Courant-Snyder invariants $J_\pm$; in fact, it is just equal to that: $M = J_+ - J_-$. Since the beam emittances are nothing else as averages of the two actions, the beam angular momentum is given by a difference of its two circular emittances: $\langle M \rangle = \varepsilon_+ - \varepsilon_-$. An important aspect of the analogy between light and charged particle optics relates to planar-circular transformations. For charged particle optics, a possibility of this transformation was pointed out in Ref. [3] and practically demonstrated in Ref [4], where it was shown that these *optical adapters* can be implemented by means of skew-triplets. If a beam in a planar state is coming into a planar-to-circular adapter, the outgoing beam would be circular, and vice-versa. If a beam with very different emittances is in a planar state, it is flat. If this beam is transformed into a circular state, it becomes a round vortex, which angular momentum is equal to the larger emittance. Since adapters are based on linear optics, circular-planar transformations preserve the both emittances: $\varepsilon_\pm \leftrightarrow \varepsilon_{x,y}$.

## SPACE CHARGE SUPPRESSION

For planar modes, the space charge tune shift is determined by both emittances, being maximal for a plane of smaller emittance. That is why space charge limitation suggests for the two emittances to be close to each other. For circular modes, the space charge limitation works differently: when the emittance ratio is high, the space charge tune shift is determined by the larger emittance only – even if the smaller emittance goes to zero. Indeed, for the circular beam state, the beam size is determined by the larger emittance, making space charge insensitive to the smaller one. To make this tune shift of a circular beam with two very different emittances identical to the tune shift of a planar beam with two equal emittances, the larger circular emittance has to be two times higher than one of the planar emittances [5].

This property of the circular modes suggests an idea to use them for low-energy accelerators, with the larger emittance determined by the space charge tune shift, and the smaller one can be as small as possible. In this case, the beam brightness can be significantly increased due to reduced value of the smaller emittance. After acceleration to sufficiently high energy, the beam can be transformed into a planar state, becoming flat.

## FLAT BEAMS IN LHC

A flat beam in the collider provides significant advantages, seen in electron machines. A first one relates to the luminosity. Keeping in mind that the space charge requires larger emittance be two times higher than in the conventional planar case, it can be concluded, that luminosity can be increased as soon as the emittance ratio is 4 or higher, being proportional to the square root of the emittance ratio.

Another important benefit of the flat beam is suppression of beam-beam resonances. Indeed, a power of

* FNAL is operated by Fermi Research Alliance, LLC under Contract No. DE-AC02-07CH11359 with the United States Department of Energy



ISBN 978-3-95450-118-2

# ON SCALING PROPERTIES OF THIRD-ORDER RESONANCE CROSSING IN PARTICLE ACCELERATORS*

S.Y. Lee, Indiana University, Bloomington, IN 47405, US
K.Y. Ng, Fermilab, Batavia, IL 60510, US

*Abstract*

The effects of charged particle beams crossing a third-order resonance in an accelerator are studied. A 20% emittance growth or 2.5% of trap-fraction can be used to define the critical or tolerable resonance strength, which is found to follow simple scaling laws vs tune-ramp rate and initial emittance. One scaling law can be derived by solving Hamilton's equations of motion in a perturbative approach. Such scaling laws can be used to evaluate the performance of high power accelerators, such as fixed-field alternating-gradient accelerators (FFAGs) and cyclotrons [6].

## INTRODUCTION

The third-order resonance plays a dominant role in dynamic aperture and may also limit accelerator performance [1, 2, 3, 4]. In particular, the betatron tunes of *non-scaling* FFAGs are designed to ramp through many resonances during the acceleration process. We study here the fractional emittance growth (FEG) and particle trap-fraction after crossing the third-order resonance. Our aim is to derive scaling laws for a tolerable resonance strength. The results will be compared with multi-particle tracking [5]. The model ring used for tracking resembles the Fermilab Booster, which is of circumference 474 m, composed of 24 FODO cells with 24-fold supersymmetry. The betatron functions at the quadrupoles are $\beta_x^F = 40$ m, $\beta_z^F = 8.3$ m, $\beta_x^D = 6.3$ m, $\beta_z^D = 21.4$ m. A sextupole and an octupole are placed at one of the D-quads to generate the third-order resonance strength $G$ and the horizontal detuning $\alpha$. The beam kinetic energy is kept at 1 GeV. The horizontal tune is ramped from $\nu = 6.40$ to 6.28 crossing the $3\nu = \ell$ resonance, while the vertical tune is fixed at 6.45. In general, 5000 macroparticles are used, initially in a 6-$\sigma$-truncated Gaussian distribution of rms emittance $\epsilon_i$.

## HAMILTONIAN AND FIXED POINTS

We start from the Hamiltonian [7]

$$H = \delta I + \frac{1}{2}\alpha I^2 + G I^{3/2}\cos 3\psi \qquad (1)$$

in the horizontal phase space, describing the action $I$ and angle $\psi$ of a particle in the rotational frame of a third-order resonance, where $G$ is the absolute value of the resonance strength and $\delta = \nu - \ell/3$ is the proximity of the horizontal betatron tune $\nu$ to the resonance at $3\nu = \ell$. The Hamilton's equations of motion are

$$\dot{I} = 3GI^{3/2}\sin 3\psi, \quad \dot{\psi} = \delta + \alpha I + \frac{3}{2}GI^{1/2}\cos 3\psi. \qquad (2)$$

When $\alpha > 0$, unstable fixed points (UFPs) are given by

$$\frac{\alpha I_{\rm ufp}^{1/2}}{G} = \mp\frac{3}{4} \pm \frac{3}{4}\sqrt{1-\frac{16\alpha\delta}{9G^2}}, \quad \begin{cases} \delta < 0, \\ 0 \le \delta \le 9G^2/16\alpha, \end{cases}$$

with $\psi_{\rm ufp} = 0, \pm 2\pi/3$ changing to $\pi, \pm\pi/3$ as $\delta$ changing from negative to positive. The stable fixed points (SFPs) are given by

$$\frac{\alpha I_{\rm sfp}^{1/2}}{G} = +\frac{3}{4} + \frac{3}{4}\sqrt{1-\frac{16\alpha\delta}{9G^2}}, \quad \delta \le 9G^2/16\alpha, \qquad (3)$$

with $\psi_{\rm sfp} = \pi, \pm\pi/3$. These are shown in Fig. 1. The total area of the three resonance islands is approximately $\frac{16}{\pi} G^{1/2}|\delta|^{3/4}|\alpha|^{-5/4}$.

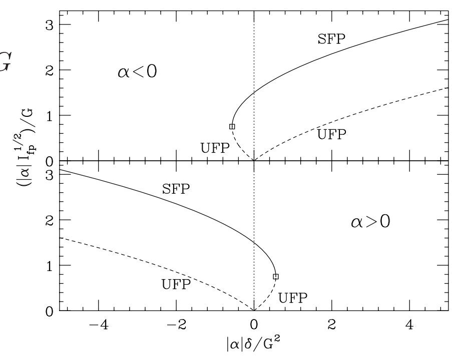


Figure 1: Fixed points $|\alpha| I_{\rm fp}^{1/2}/G$ vs $|\alpha|\delta/G^2$ for $\alpha < 0$ (top) and $\alpha > 0$ (bottom). Bifurcation occurs at $\delta_{\rm bif} = 9G^2/(16|\alpha|)$ and is marked by a rectangle.

## RING BEAM AND ADIABATIC RAMPING

Without loss of generality, we consider only downward ramping of the horizontal tune. As shown in Fig. 1, the resonance islands move outward with increasing size at positive detuning, trapping particles. This is demonstrated by simulating a ring of particles in Fig. 2. It is apparent that the emittance increases without limit. As a result, the resonance crossing effects are characterized by the fraction of particles trapped inside the islands.

On the other hand, with negative detuning, the resonance islands move inward and no particles can be trapped.

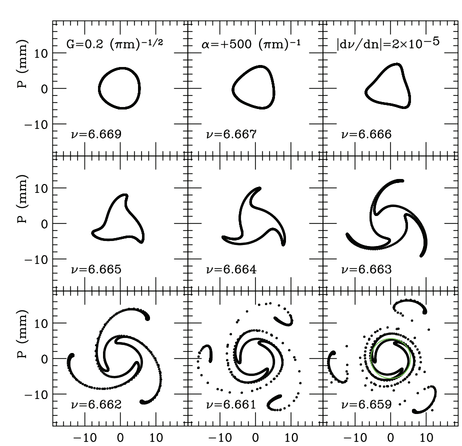


Figure 2: Evolution of a ring of particles showing some captured into resonance islands. Tune-ramp rate is $-2\times 10^{-5}$ at detuning $\alpha = 500$ $(\pi\mathrm{m})^{-1}$ and resonance strength $G = 0.2$ $(\pi\mathrm{m})^{-1/2}$.

* Work supported by the US DOE under contracts DE-FG02-92ER40747, DE-AC02-76CH030000, and the NSF under contract NSF PHY-0852368.



ISBN 978-3-95450-118-2

# PTC-ORBIT STUDIES FOR THE CERN LHC INJECTORS UPGRADE PROJECT

A.Molodozhentsev, E.Forest, KEK, Tsukuba, Japan
G. Arduini, H. Bartosik, E.Benedetto, C.Carli, V.Forte, M.Fitterer, S.Gilardoni, M.Martini, E.Metral, N.Mounet, F.Schmidt, R.Wasef, CERN, Geneva, Switzerland

*Abstract*

The future improvement of the beam brilliance and intensities required in the frame of the LIU (LHC Injectors Upgrade) project triggered a comprehensive study of the combined effects of the space charge and the machine resonances for the CERN synchrotrons, which are the injector chain for LHC. In frame of this report we describe new features of the PTC-ORBIT code which allow the beam dynamics modeling in the LHC injectors in the realistic way taking into account the time variation of the machine parameters during the injection process. The measurements, obtained during recent 'Machine Development' (MD) companies, and simulations for the low-energy high-intensity beams, will be discussed. Finally, basic results obtained in frame of the RCS conceptual design study are summarized.

## INTRODUCTION

According to the LHC upgrade scenario the brightness of the LHC25 beam at the flat top should be increased at least 2.4 times. Such high brightness can be achieved by increasing the number of proton per bunch and at the same time by reducing the transverse beam emittance. This significant improvement of the LHC parameters requires an upgrade of whole LHC injector complex. The major mile stones of this upgrade are (1) improvement of the injection process into PS Booster by using new LINAC4 and (2) increasing the injection energy for PS up to 2GeV.

LINAC4 should replace the existing LINAC2, which deliver the 50MeV proton beam to PS Booster. The 160MeV H-minus beam from LINAC4 will improve the efficiency of the multi-turn injection process. The total particle losses in PS Booster should reach 5% instead of (55-60)%, which are typical for the current machine operation. PS Booster should be able to reach the beam intensity of 35e11ppb with small transverse emittances of 1.9μm (normalized rms value). The current beam intensity and the transverse emittances extracted from PS Booster to fill LHC with the 25nsec bunches are 16e11ppb and 2.5μm, respectively. Increasing the injection energy for the CERN PS machine will allow to use this high performance beam from the PS Booster keeping the vertical space charge tune spread as now in PS.

The novel injection scheme, proposed for the CERN PS Booster by using the 160MeV H-minus beam, allows manipulating with the particle distribution in the transverse and longitudinal plans, providing required transverse beam profiles and bunching factor. As the result, the space charge detuning for the PS Booster beam at the injection energy can be kept less than (-0.4).

The transverse emittance blowup and the particle losses after the upgrade of the LHC Injectors should be not more than 5% for PS Booster and PS. To minimize the particle losses during the injection and acceleration process it is necessary first of all to optimize the 'bare' working point for the required beam parameters. This optimization should be done in combination with appropriate correction schemes to compensate effects of machine resonances.

In frame of this report we will summarize new features of the PTC-ORBIT code which allow the comprehensive modeling of the beam dynamics in the LHC Injectors taking into account the time variation of the machine parameters during the injection process. The measurements, obtained during recent MD companies, and simulations for the low-energy high-intensity beams, will be compared. The multi-turn injection study by using new ability of the code will be presented.

## COMPUTATIONAL TOOL

To reach the required beam parameters a computational model of the machine should be developed taken into consideration all known field imperfections of the machine magnets and alignment errors. The combined PTC-ORBIT(MPI) code [1], developed in the collaboration between KEK (Tsukuba, Japan) and SNS (Oak Ridge, USA), allows creating the common university for the complete 'Normal Form' analysis of the single particle and the multi-particle dynamics, taken into consideration realistic machine imperfections, resonance correction schemes and the collective effects. The code has been used extensively at the early stage of the JPARC Main Ring commissioning process [2]. The combined PTC-ORBIT code is installed and compiled for different multi-processor systems like the KEK supercomputer and the CERN multi-processor cluster.

The bunch length for the CERN Injectors is much more than the transverse beam size, so that the 2.5D model can be used to simulate the space charge effects by the ORBIT part of the combined code. At the space charge nodes, distributed by PTC around the machine, the transverse space charge forces are evaluated as nonlinear kicks using the explicit second-order PIC model and FFT. The particle motion between the 'space charge' nodes is simulated by using the high-order symplectic integrators, implemented in to the PTC code.

ISBN 978-3-95450-118-2

# FRIB ACCELERATOR BEAM DYNAMICS DESIGN AND CHALLENGES*

Q. Zhao#, A. Facco, F. Marti, E. Pozdeyev, M. Syphers, Y. Yamazaki, Y. Zhang, J. Wei, X.Wu,
FRIB/MSU, East Lansing, MI 48824, USA

*Abstract*

The Facility for Rare Isotope Beams (FRIB) will be a new national user facility for nuclear science and applications. This cw, high power, superconducting, heavy ion driver linac consists of a front end to provide various highly charged ions at 0.5 MeV/u, three superconducting acceleration segments connected by two 180° bending systems to achieve a final output beam energy of beyond 200 MeV/u for all varieties of stable ions, and a beam delivery system to transport multi-charge-state beams to a fragmentation target at beam power of up to 400 kW. The linac has an 80.5 MHz base frequency and utilizes four types of low-beta resonators with one frequency transition to 322 MHz after the first segment at beam energy of up to 20 MeV/u, where ion charge states are increased through a stripper. The challenges of beam dynamics design include the simultaneous acceleration of multi-charge-state ion beams to meet beam-on-target requirements, efficient acceleration of high intensity, low energy heavy ion beams, limitation of uncontrolled beam loss to less than 1 W/m, accommodation of multiple charge stripping scenarios, and other characteristic features. We report the recent optimizations on linac lattice, present the results of end-to-end beam dynamics simulations with machine errors, and discuss the simulation of beam tuning and fault conditions.

## INTRODUCTION

The Facility for Rare Isotope Beams (FRIB), baselined as a 7-year, US$680 million construction project, is to be built at Michigan State University under a Cooperative Agreement with the US Department of Energy (DOE) [1]. High availability, maintainability, reliability, tunability, and upgradability are especially required for the FRIB accelerator to operate as a national scientific user facility. Since it received CD-1 (Approve Alternative Selection and Cost Range) from the DOE in September 2010, the facility has achieved a fully developed design capable of producing up to 400 kW of average beam power with energies beyond 200 MeV/u for all stable ion species, and delivering to the final target station a spot size and energy spread consistent with experimental requirements. The project is prepared to establish the performance baseline and the start of conventional facility construction. Space is reserved for potential future enhancements, such as energy upgrades, ISOL targets, and a light ion injector.

The FRIB driver linac is a cw heavy ion machine with high beam power (up to 400 kW). This machine has its unique features compared with high power proton ones. In contrast to high intensity spallation neutron sources and neutrino sources that require pulsed beams, most FRIB experiments will prefer cw beams. By choosing cw acceleration, a low peak beam current (average of < 1 emA) can meet the final beam power of 400 kW. Therefore, the space charge effects are mostly negligible except for the ion source and low energy beam transport. To maximize heavy ion beam intensity on the target, multiple charge states are accelerated simultaneously (e.g. 2 charge states of $U^{33+}$ and $U^{33+}$ before stripping, and 5 charge states of $U^{76+}$ to $U^{80+}$ after stripping). The acceleration of heavy ions is much slower than that of protons due to the low charge-to-mass ratio. But it is feasible to accelerate heavy ions from very low energy (0.5 MeV/u) with low-beta superconducting cavities and focusing solenoids housed in a cryomodule. Two-gap quarter- and half-wave resonators are chosen throughout the entire linac for efficient acceleration. The phase and amplitude of each cavity are independently adjustable, which makes it very flexible and efficient to accelerate varieties of ions with different charge-to-mass ratios. Heavy ions have much larger stopping powers (higher Bragg peaks) than protons, therefore, heavy ion beam losses result in higher power-density in material and tend to damage the surface of beam elements (e.g., niobium cavity) easily. The apertures of the FRIB accelerating

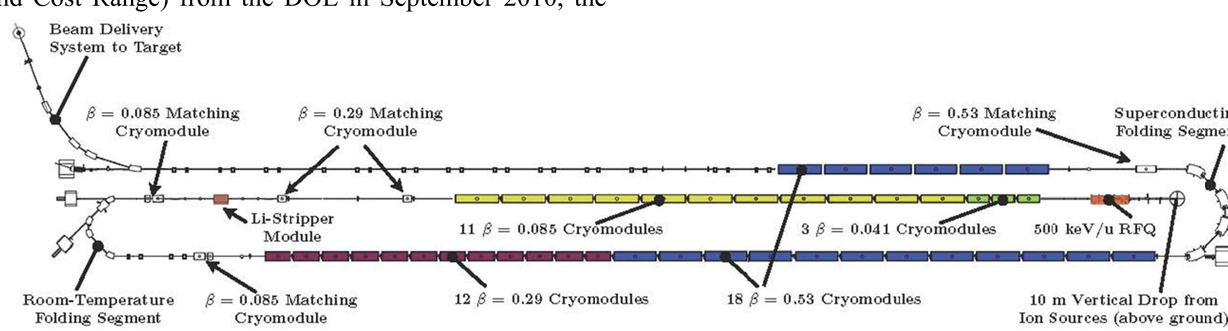


Figure 1: Layout of the FRIB accelerator at tunnel level (above-grade portion of the Front End not shown).

* Work supported by the U.S. Department of Energy Office of Science under Cooperative Agreement DE-SC0000661
# zhao@frib.msu.edu



ISBN 978-3-95450-118-2

# ACCELERATION AND TRANSPORTATION OF MULTIPLE ION SPECIES AT EBIS-BASED PREINJECTOR*

D. Raparia#, BNL, Upton, New York U.S.A


*Abstract*

Electron Beam Ion Source (EBIS)-based preinjector was come into operation in 2010. Since than it has been delivering various ions to NASA Space Radiation Laboratory (NSRL) radiobiology program and Relativistic Heavy Ion Collider (RHIC) physics program. During the Run12, the EBIS-based preinjector provided $U^{39+}$, $Au^{32+}$, and $Cu^{11+}$ ions for the RHIC physics program. The preinjector has delivered beams of $He^{2+}$, $Ne^{5+}$, $Ar^{11+}$, $Ti^{18+}$, $Fe^{20+}$, $Kr^{18+}$, $Xe^{27+}$, and $Ta^{38+}$ for the NASA Space Radiation Laboratory radiobiology program for last three years. The performance and operational experience with multiple ion species of this preinjector is presented.


## INTRODUCTION

In past Tandem Van de Graaff was providing heavy ions for NASA Space Radiation Laboratory (NSRL) radiobiology program and Relativistic Heavy Ion Collider (RHIC) physics program. Tandem preinjector is 40 years old and less flexible, for example it could not provide noble gas ions to NSRL radiobiology program and uranium for RHIC physics program. A new preinjector based on electron beam ion source (EBIS) was come into operation in 2010 [1]. This preinjector can produce ions of any species and able to switch between multiple species in 1 second to simultaneously meet the needs of both science programs. The main parameters for the preinjector are given in Table 1, and the layout of the preinjector is shown in Figure 1.

Table 1: EBIS-Based Preinjector Parameters

| | |
|---|---|
| Ions | He – U |
| Q / m | ≥1/6 |
| Current | > 1.7 emA |
| Pulse length | 10–40 μs |
| Rep rate | 5 Hz |
| Output Emittance | 0.14 pi mm mrad |
| Momentum Spread | ±0.5% |
| Linac output energy | 2 MeV/u |
| Time to switch species | 1 second |

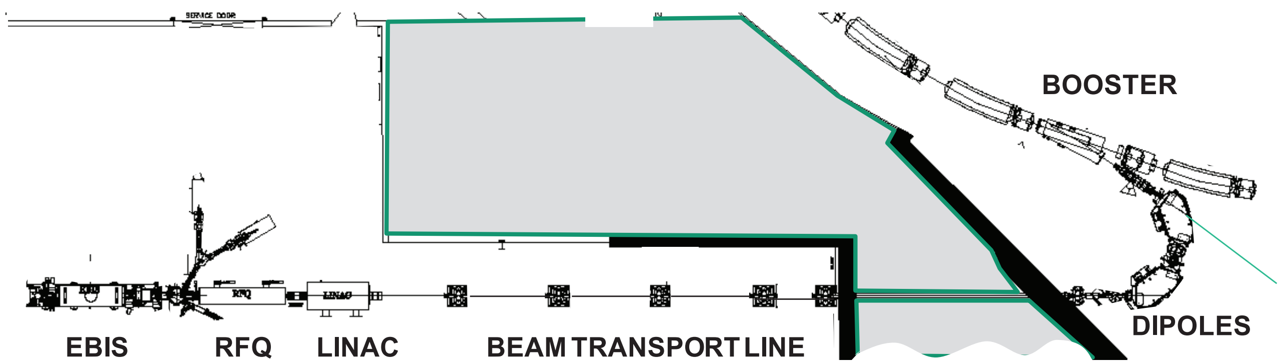


Figure 1: Schematic of the EBIS-based heavy ion preinjector

## EBIS-BASED PREINJECTOR

The preinjector uses an EBIS source, a low energy transport line (LEBT), a Radio Frequency Quadrupole (RFQ), a medium energy transport line (MEBT), a linac and a 37 meter long high-energy transport line (HEBT).

The EBIS has a 5T superconducting solenoid which compresses an electron beam of up to 10A in a ~1.5 m long trap region. Ions of the desired species are injected, held in the trap, and stepwise ionized by the electron beam. When the desired charge state is reached, they are released from the trap in a short pulse.

The source is followed about a meter long low energy transport line (LEBT), which facilitates injection of singly charge ions into the EBIS and transport and match into the RFQ for high charge state ions. Figure 2 shows the functional block diagram of the LEBT.

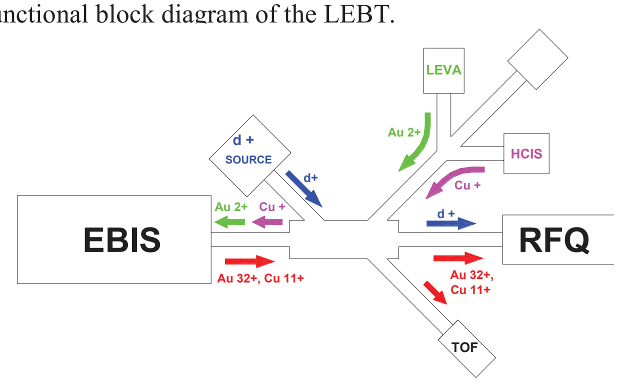


Figure 2: Functional block diagram of the LEBT.

The LEBT contains couple of electrostatic lenses, ~ 100 kV accelerating gap to provide energies of 17 keV/u, a solenoid to focus beam into the RFQ and current monitoring devices. About one-meter free space in the

*Work supported by Brookhaven Science Associates, LLC under Contract No. DE-AC02-98CH10886 with the U.S. Department of Energy, and by the National Aeronautics and Space Administration.
#raparia@bnl.gov

ISBN 978-3-95450-118-2

# PXIE AT FNAL

N.Solyak#, S.Holmes, V. Lebedev, S. Nagaitsev, A.Saini, A. Shemyakin, C. Baffes, A. Chen, Y. Eidelman, B. Hanna, J.-F. Ostiguy, R. Pasquinelli, D. Peterson, L. Prost, G. Saewert, V. Scarpine, D. Sun, V. Yakovlev, Fermilab*, Batavia, IL 60510, USA

*Abstract*

The Project X Injector Experiment (PXIE) [1,2], a test bed for the Project X front end, will be completed at Fermilab at the end of 2016. The goal of this facility is to demonstrate the most challenging technologies proposed for Project X. PXIE will operate at full specified parameters for Project X and should demonstrate upgradability of the front-end for 2 mA operation.

In MEBT section a dedicated chopper will form a 1 mA H- beam with an arbitrary selected bunch pattern from the initially 5 mA 162.5 MHz CW train provided by RFQ. MEBT section will transport and match beam from RFQ to superconducting accelerator, provide enough diagnostics to measure all beam parameters after RFQ and before SRF cryomodules, dump ~80% of the beam after chopping and collimate the beam to minimize beam losses in upstream SRF. This paper presents the PXIE scheme and status of development of its elements, including ion source, LEBT, RFQ, the kickers and absorber, SC cavities and cryomodules, beam extinction experiment and 50 kW beam dump at the end of facility.

## INTRODUCTION

PXIE is a front-end of the Project X. It includes: ions source, Low Energy Beam Transport (LEBT) section with diagnostics and pre-chopper, RFQ, Middle Energy Beam Transport (MEBT) section with bunch-to-bunch chopper, two superconducting cryompodules (HWR and SSR1), beam diagnostics and 50 kW beam dump. The general layout of the PXIE facility is shown in Figure 1. The total length of facility is ~40 m.

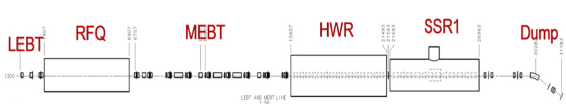


Figure 1: PXIE layout.

These goals of PXIE are:

- reliable operation of 2.1 MeV RFQ in CW regime
- a bunch-by-bunch chopper,
- low-β acceleration in SRF cryomodules.
- small emittance growth during initial acceleration
- good particle extinction for the removed bunches

Bunch by bunch chopper in MEBT section will be able to form arbitrary pattern of the beam structure for multi-user experimental program, by removing up to 80% bunches from 5 mA beam accelerated in RFQ. Layout of PXIE beam optics and transverse and longitudinal 3-sigma envelopes for passing trough beam are shown in Fig. 2 (LEBT and RFQ are not included). In the vertical plane yhe passing trough beam is deflected by two kickers and then returned back to the axis by DC corrector in MEBT section [3].

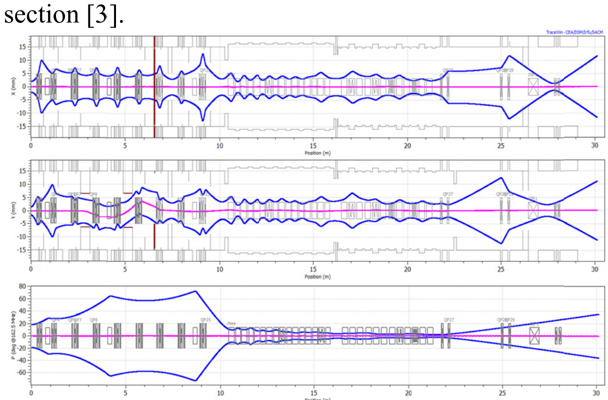

Figure 2: 3-sigma beam envelopes (X, Y and Z-longitudinal bunch phase) in PXIE (after RFQ) for 5 mA.

## ION SOURCE AND LEBT

PXIE ion source should provide $H^-$ source working in DC regime with 5 mA nominal current and possibility to regulate output current in the range of 1-10 mA. PXIE specify voltage 30 kV and lifetime 350 hrs or better. TRIUMF type $H^-$ volume-cusp source produced from D-Pace was purchased and commissioned at TRIUMF and LBNL [4]. The general view of the source and result of emittance measurements in the range of 1-10mA beam current are shown in Figure 3. Measured normalized emittance at the exit of source is current is below 0.12 π·mm·mrad and not sensitive to the output beam current.

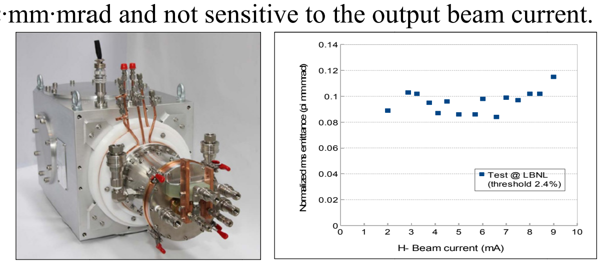


Figure 3: Ion source and emittance vs. beam current.

LEBT original design, proposed by LBNL includes beam emittance diagnostics, pumping, electrostatic chopper and two solenoids to match beam from IS to the RFQ [5]. Switchable bending magnet in this design will bend beam from one of the two ion sources to the RFQ. In current configuration the replacement of the ion source will not disturb operation of the Project X complex. In PXIE we are not planning to use second leg of LEBT with spare source. Beam space charge in LEBT transport line is compensated by neutralized ions. Recently it was proposed to modify this design by adding ion cleaning electrode after bending magnet and extra solenoid as shown in Fig. 4 [6]. The goal of this modification is to

# solyak@fnal.gov

* Operated by Fermi Research Alliance, LLC, under Contract No. DE-AC02-07CH11359 with the United States Department of Energy



ISBN 978-3-95450-118-2

# RFQ BEAM DYNAMICS DESIGN FOR LARGE SCIENCE FACILITIES AND ACCELERATOR-DRIVEN SYSTEMS

Chuan Zhang #
Institut für Angewandte Physik, Goethe-Universität, D-60438 Frankfurt a. M., Germany

*Abstract*

Serving as the front-end of large science facilities and Accelerator-Driven Systems (ADS), the Radio-Frequency Quadrupole (RFQ) accelerator usually needs to reach low beam losses, good beam quality, high reliability, and cost savings such design goals at high beam intensities. To address the challenges for modern RFQs, a special beam dynamics design technique characterized by a reasonable and efficient bunching process with balanced space-charge forces has been developed as an alternative to the classic Four-Section Procedure proposed by Los Alamos National Laboratory (LANL). In this paper, the design studies of some recent RFQ projects will be presented as examples.

## BACKGROUND

Particle accelerators were originally invented and are still being mainly developed as exploring tools for the subatomic world. Since 2000, a new generation of large science facilities based on accelerators has been built, e.g. J-PARC [1], SNS [2], and LHC [3], or proposed, e.g. FAIR [4], FRIB [5], and Project-X [6].

Meanwhile, many other important applications taking advantage of accelerators have been also developed quickly. For instance, nuclear waste transmutation using the ADS technology is now being intensively investigated by the EU and China by means of the MAX [7] and China-ADS [8] projects, respectively.

Generally speaking, the driver accelerators of the above-mentioned projects are all started with an RFQ accelerator, accelerate protons or ions up to several hundreds of MeV/u even several tens of GeV/u through a full linac or a combination of linear and circular accelerating structures, and finally bombard a certain target with the output beam to generate various useful secondary particles, e.g. neutrons and radioactive ions.

To increase the production of secondary particles, naturally one needs to increase the current of the primary beam to the target as well. When circular machines are involved, usually the peak beam intensity $I_{\text{peak}}$ of the driver accelerator has to be high, as the duty cycle (dc) is limited by the rise-time of magnets. In case of a full linac, high dc even Continuous Wave (CW) operation is feasible so that $I_{\text{peak}}$ could be modest.

Therefore, typically modern RFQ accelerators are required to work at high peak beam intensities or at high duty cycles or even in both cases. High $I_{\text{peak}}$ will lead to strong space-charge effects, which is especially serious for the RFQ working with low-velocity beams. In this case, certainly, high inter-vane voltage $U$ is desired for sufficient focusing strength. However, high dc operation prefers low $U$ for reducing sparking risks and cooling difficulties. It can be seen that a big challenge to the beam dynamics design of a modern RFQ is how to reach low beam losses, good beam quality, high reliability, and cost savings such design goals at high beam intensities using modest $U$. It's beyond question that unconventional design and optimization methods have to be developed and applied.

# Chuan Zhang: zhang@iap.uni-frankfurt.de

## DESIGN PROCEDURES

For the RFQ beam dynamics design, the LANL Four-Section Procedure (FSP) [9] is a classic technique, dividing an RFQ into four sequential sections: Radial-Matcher (RM), Shaper (SH), Gentle Buncher (GB), and Accelerator (ACC).

The heart of this method is the GB section originally proposed by Kapchinsky and Teplyakov (K-T), in which the longitudinal small oscillation frequency $\omega_l$ and the geometric length of the separatrix $Z_\psi$ are kept constant in order to maintain a constant beam density for an adiabatic bunching. $\omega_l$ and $Z_\psi$ are determined by Eqs. (1) and (2) [10] with $\varphi_s$ and $\psi$ as the synchronous phase and the phase width of the separatrix, respectively.

$$\omega_l^{\,2} = \frac{\pi^2 qAU \sin(-\varphi_s)}{M\beta^2\lambda^2} \tag{1}$$

$$Z_\psi = \frac{\psi\beta\lambda}{2\pi} \tag{2}$$

$$\tan\varphi_s = \frac{\sin\psi - \psi}{1-\cos\psi} \tag{3}$$

A typical example of the LANL-style design is given in Fig. 1. It's a test design for the FRANZ RFQ [11], a 200mA, CW, proton RFQ planned by Frankfurt University. Clearly, for satisfying the K-T conditions, $\varphi_s$ and the electrode modulation $m$ are changing very slowly in the GB section, especially at the beginning. For avoiding a too long RFQ, the Shaper with a pushed pre-bunching has to be used, which could be an important source of unstable particles. Another distinctive characteristic of the Four-Section Procedure is that the transverse focusing strength $B$ defined by Eq. (4) is kept invariant after the RM section. The idea is to maintain a constant mid-cell aperture $r_0$ and consequently a quasi-



ISBN 978-3-95450-118-2

# USING STEP-LIKE NONLINEAR MAGNETS FOR BEAM UNIFORMIZATION AT IFMIF TARGET*

Z.Yang, J.Y. Tang, IHEP, Beijing, China
P.A. Phi Nghiem, Nicolas Chauvin，CEA-Saclay, France

*Abstract*

Uniform beam distribution and minimum beam halo on target are often required in high intensity beam applications to prolong the target lifetime, ease cooling and obtain better irradiation effect. In this report, step-like nonlinear magnets instead of standard multipole magnets have been studied for the application at IFMIF. Although the preliminary results are still below the very critical requirement of spot uniformity at the IFMIF target, they are quite permissive. The method demonstrates significant advantages over the conventional combination of octupole and duodecapole on very low beam loss, better uniformity and very low cost. Further studies are needed to fully meet the IFMIF specifications.

## INTRODUCTION

For high power hadron beam applications such as spallation neutron sources, material-irradiation studies, and accelerator-driven subcritical system etc., it is important to produce a beam spot at target as uniform as possible to prolong the lifetime of the targets as well as beam windows separating the target environment from the vacuum in the beam transport lines. In a hadron accelerator, there is still a very important halo part in beam distribution which can not be neglected. To produce a uniform spot distribution at target, only methods using non-linear magnets can be considered as other methods such as the scattering method and the scanning method used in hadron therapy are ruled out due to either too large beam loss or harmful time structure.

The SIEEV Department at CEA-Saclay (IRFU/SIIEV) is working on the accelerator design of the IFMIF (International Fusion Materials Irradiation Facility) accelerator. In this typical application based on two high power deuteron beams of 125 mA and 40 MeV, it is important to produce a uniform beam spot at the target as mentioned above. In earlier preliminary studies, a combination of non-linear magnets such as octupoles and dodecapoles has been considered for this purpose.

In this study, step-like field magnets are used to meet the very strict requirements at the IFMIF target. Step-like field magnets were initially proposed for the beam spot uniformization at the ESS targets [1]. They were also applied to the China Spallation Neutron Source [2] and China-ADS project for the same purpose. They are considered to be more effective and cheaper than conventional standard multipole magnets in this kind of applications.

## BASICS

In some cases, the original distribution is not regular, so standard multipole magnets are not effective in the transformation to obtain a uniform beam spot at target. Step-like nonlinear magnets were proposed here to tackle the problem. Instead of twisting the distribution by higher order forces (standard multipole magnets or combined-function magnets) in phase space, the nonlinear magnets of step-like fields (see Fig. 1 and Fig. 2) are used to translate parts of the distribution. This method has a better control over outmost particles, thus is effective to carry out distribution transformation in the case of large beam halo. An example of such magnet with one step is shown in Fig. 2. Multi-step field can be produced by two or three adjoining magnets of one-step.

The step rising in the field of a step-like field magnet can be represented by an approximation:

$$B(x) = \frac{F_S / L}{1 + e^{-b(x - x_0)}} \qquad (1)$$

B, x0 are the parameters for fitting; the field factor f and the distance x0 between the mid-rising and the beam center as well the field sharpness b can be used for the optimization. To improve the sharpness of the step field, another pair of irons and coils with reverse magnetic flux can be nested

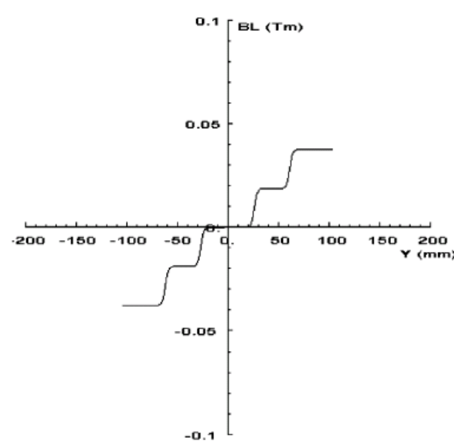


Figure 1: Multi-step magnetic field for the distribution transformation.



ISBN 978-3-95450-118-2

# EFFECT OF SELF-CONSISTENCY ON PERIODIC RESONANCE CROSSING

G. Franchetti*, GSI, Darmstadt, Germany

*Abstract*

In high intensity bunched beams resonance crossing gives rise to emittance growth and beam loss. Both these effects build up after many synchrotron oscillations. Up to now long-term modeling have relied on frozen models neglecting the physics of self-consistency. We address here this issue and present the state of the art of simulations applied to the SIS100.

## INTRODUCTION

The phenomenon of resonance crossing [1, 2, 3] can be induced by space charge in bunched beams [4]. The simulation of the beam evolution when resonance crossing cannot be avoided poses extraordinary challenges for computer modeling of long-term storage. The computation of Coulomb forces, usually performed via particle in cell (PIC) algorithms, unavoidably produces a noise on the macro-particle dynamics. Studies on the effect of this noise [5] have shown that a significant emittance growth can arise from PIC codes.

For short term simulations, where the effects of self-consistency created by space charge (coherent resonances, instability of coherent modes, etc.) are very fast, this noise does not play a role, as it has not time to build up. Different is the case for a beam dynamics that drives an emittance growth after long-term. In particular on the phenomenon of the space charge induced periodic resonance crossing, the extraction of particles from the beam happens slowly, and the small growth rate can significantly be affected by simulation code spurious effect as the noise induced by PIC algorithms.

The level of noise in PIC simulations depends on the number of macro-particles per PIC cell. Statistical fluctuations scale as $1/\sqrt{N_c}$, with $N_c$ the number of macro-particles in a cell. Therefore the reduction of these unwanted effects is obtained by raising the number of macro-particles used to model the bunch. Hence, the prize to pay for controlling the noise is an increased CPU time required to perform the simulations. Therefore simulations on a time scale of $10^5, 10^6$ turns are not feasible with PIC algorithms.

For this reason in the studies performed till now (see for example Ref. [6]) the Coulomb force has been computed by assuming a beam distribution frozen. In this approach a frozen Coulomb force is used for tracking "test" macro-particles in the accelerator structure. This approach relies on the assumption that macro-particle loss is small (maximum of 10%). For beam loss larger than this value, simulation predictions are not reliable.

* g.franchetti@gsi.de

Given the substantial approximation made, benchmarking of code predictions with experiments has been performed. The benchmarking had the purpose of verifying/confirming the underlying mechanism, and to verify the accuracy of code predictions [4, 7].

At practical level the necessity of making beam loss prediction is very important for the SIS100 synchrotron in order to consolidate the effectiveness of resonance compensation schemes [8, 9]. Uncontrolled beam loss is required to be within a 5% budget in order to mitigate a progressive vacuum degradation, dangerous for beam lifetime. Therefore the study of the effect of self-consistency is relevant for the assessment of effective beam loss, crucial quantity in the discussion on the nonlinear components in magnets, residual closed orbit distortion as well as in the resonance compensation strategy.

## LESSONS FROM THE MACHINE EXPERIMENT EXPERIENCE

Two benchmarking campaigns have been performed till now: the first in the CERN-PS in 2003, and later at GSI using the SIS18 in 2008-2010. In both the experiments the lattice was modeled at the best of the available informations. In Fig. 1 we report the main experimental results of the GSI campaigns, and the associated simulation results. Details and discussion of the experiment and its parameters are reported in Ref. [7]. We note that the smaller beam survival is found to be of $\sim 20\%$. The simulations instead show a minimum beam survival of $\sim 50\%$. The discrepancy of these two results is not fully understood. While on one hand it is not clear of whether the machine modeling is complete, on the other hand, the effect of the self-consistency is not included in the simulations as a frozen model is used. In Ref. [7] it was concluded that the discrepancy might be attributed to the incomplete modeling of the self-consistency in the computer code.

## A GLIMPSE TO THE FUTURE

A relevant application of the frozen model is in the FAIR project [10]. The SIS100 will certainly be afflicted by a web of resonances created by superconducting magnet nonlinear components, closed orbits misalignment, and random errors [6]. In Fig. 2a is shown for a possible model of the SIS100 the resonance web, which is formed by integer, half integer, third and forth order normal and skew resonances. These resonances are found via tune scans of the short-term dynamic aperture (1000 turns). Beam survival for several intensities after one second storage are shown in Fig. 2b. The maximum intensity corresponds to $0.625 \times 10^{11}$ ions/bunch, which creates a large tune-shift represented schematically in the picture. The space

ISBN 978-3-95450-118-2

# SIMULATION AND MEASUREMENT OF HALF INTEGER RESONANCE IN COASTING BEAMS IN THE ISIS RING

C. M. Warsop, D. J. Adams, B. Jones, S. J. Payne, B. G. Pine, H. V. Smith, R. E. Williamson, Rutherford Appleton Laboratory, Oxfordshire, UK.

*Abstract*

ISIS is the spallation neutron source at the Rutherford Appleton Laboratory in the UK. Operation centres on a high intensity proton synchrotron, accelerating $3\times10^{13}$ ppp from 70-800 MeV, at a repetition rate of 50 Hz. Present studies are looking at key aspects of high intensity behaviour with a view to increasing operational intensity, identifying optimal upgrade routes and understanding loss mechanisms. Of particular interest is the space charge limit imposed by half integer resonance: we present results from coasting beam experiments with the ISIS ring in storage ring mode, along with detailed 3D (ORBIT) simulations to help interpret observations. The methods for experimentally approaching resonance, and the implications on beam behaviour, measurement and interpretation, are discussed. In addition, results from simpler 2D simulations and analytical models are reviewed to help interpret expected beam loss and halo evolution. Plans and challenges for the measurement and understanding of this important beam loss mechanism are summarised, as are some closely related areas of high intensity work on ISIS.

## INTRODUCTION

### *The ISIS Synchrotron*

The ISIS synchrotron accelerates $3\times10^{13}$ protons per pulse (ppp) from 70-800 MeV on the 10 ms rising edge of the sinusoidal main magnet field. At the repetition rate of 50 Hz this corresponds to a beam power of 0.2 MW. Charge-exchange injection takes place over 130 turns as the high intensity beam is accumulated, with painting in both transverse planes over the collimated acceptances of ~300 π mm mr. The ring has a circumference of 163 m, with a revolution time of 1.48 μs at injection. Nominal betatron tunes are $(Q_x,Q_y)$=(4.31,3.83), but these are varied using two families of 10 trim quadrupoles. A dual harmonic RF system captures and accelerates the un-bunched injected beam, and allows enhanced bunching factors. Peak incoherent tune shifts exceed -0.4 at about 80 MeV during the bunching process. Single turn extraction makes use of a fast vertical kicker at 800 MeV. Main loss mechanisms are associated with non-adiabatic trapping and transverse space charge. The loss associated with half integer resonance is highly relevant for present ISIS operations and proposed upgrades [1].

### *Half Integer Loss and Aims of Study*

The "space charge limit" of a high intensity proton ring is generally expected to be that imposed by the half integer resonance. The inclusion of self-consistency leads to the coherent resonance condition as a basic guideline for designs [2]. For realistic beams however, behaviour leading to loss is more complicated than this simplified model suggests. These studies look at this loss mechanism in more detail.

For a rapid cycling synchrotron (RCS) such as ISIS, half integer resonance is further complicated by addition of longitudinal motion (i.e. 3D dynamics) and fast changes of parameters. To reliably predict the high intensity limit of such machines a deeper understanding is desirable. This paper is part of a programme of study to address these topics, presently working on the simpler case of 2D coasting beams, with plans to study non-accelerated bunched beams next, and finally the full RCS case. A central objective is to perform detailed measurements of the loss processes, allowing benchmarking of codes and theory. This in turn has the potential for more detailed beam optimisations, with perhaps increased beam intensities.

### *ISIS Studies and Present Experiments*

Earlier work has looked in detail at various aspects of half integer resonance in 2D on ISIS: solution of the envelope equation and coherent modes for the large tune-split case [3,4]; comparison with ORBIT simulations, evolution of halo and beam loss near coherent resonance [4,5]; and more recently development of new experiments and more sophisticated simulations to explain them [6,7]. This paper continues the later work where the essential aim is to measure and simulate half integer resonance, and compare with relevant models.

In [7] measurements and simulations of half integer resonance in the ISIS ring were shown to be in agreement with predictions from coherent resonance theory. This gives the following relations for the envelope frequencies (large tune split case, equal transverse emittances):

$$\begin{aligned}\omega_x^2 &= 4Q_{0x}^2 - 5Q_{0x}\Delta Q_{inc} \\ \omega_y^2 &= 4Q_{0y}^2 - 5Q_{0x}\Delta Q_{inc}\end{aligned} \quad \text{with } \Delta Q_{inc} = \frac{r_p N}{2\pi\beta^2\gamma^3\varepsilon}\frac{1}{B} \qquad (1)$$

where: $\omega_{x,y}$ envelope frequencies, $Q_{0x,y}$ zero intensity tunes, $\Delta Q_{inc}$, incoherent tune shift of RMS equivalent KV beam, $r_p$ proton radius, $N$ intensity, $\varepsilon=4\varepsilon_{rms}$, $\varepsilon_{rms}$ RMS emittance, $B$ bunching factor and $\beta, \gamma$ relativistic parameters. From (1) the coherent frequencies as a function of intensity can be calculated, and predict resonance and loss. An example, appropriate for these experiments, is shown in Figure 1: the vertical coherent tune is approaching 7, equivalent to the $2Q_y$=7 line.

In [6,7] work concentrated on the experimental observation of loss as a function of tune and intensity. We now take this a stage further, looking at evolution of



ISBN 978-3-95450-118-2

# LONGITUDINAL BEAM LOSS STUDIES OF THE CERN PS-TO-SPS TRANSFER

H. Timko*, T. Argyropoulos, T. Bohl, H. Damerau,
J.F. Esteban Müller, S. Hancock, E. Shaposhnikova
CERN, Geneva, Switzerland

*Abstract*

Bunch-to-bucket transfer between the Proton Synchrotron (PS) and the Super Proton Synchrotron (SPS) is required before beams can enter the Large Hadron Collider (LHC). The overall beam loss at this transfer is currently around 5–10 %, and is increased for higher intensities or larger longitudinal emittances. Previous attempts to reduce the losses with additional RF voltage from spare cavities in the PS were unsuccessful. In this paper, we modelled the complete PS flat-top bunch splitting and rotation manipulations, PS-to-SPS transfer, and SPS flat bottom using end-to-end simulations. Starting from the measured bunch distributions, the simulations provide an accurate insight into the problem and allow direct benchmarking with experiments. As a result, it was understood and confirmed by measurements that shorter bunches do not necessarily lead to better transmission. The particle distribution in longitudinal phase space at PS extraction should be optimised instead. A significant loss reduction of up to 50 % is expected from simulations; experimental studies are on-going to verify these theoretical findings.

## INTRODUCTION

Different types of studies to optimise the PS-to-SPS transfer of the LHC beam have been on-going for several years now. Initially, the aim of these studies was to reduce the beam loss in the SPS, which was in the range of 10–40 % [1, 2, 3]. Amongst others, it was attempted to optimise the PS bunch rotation [4], which is done just before extraction in order to fit the PS bunches into the SPS bucket, by creating shorter bunches using additional, spare-cavity voltage for the rotation. Shorter bunches were successfully obtained, however, the transmission remained the same and the underlying reason was not understood at that time.

Nowadays, losses are as low as $\sim 5$ % at the current intensity of $(1.6–1.7) \times 10^{11}$ ppb, due to an extensive optimisation of the SPS flat-bottom (FB) RF settings and reduced electron-cloud activity. However, relative losses increase with intensity, so for the future high intensities of the high-luminosity LHC the issue has to be re-considered. Furthermore, a solution which would allow for higher longitudinal emittance is desirable, since both in the PS and the SPS the beam is at the limit of longitudinal stability at the present intensity.

* helga.timko@cern.ch

## SIMULATION AND MEASUREMENT STUDIES

The currently operational LHC-type 50 ns-spaced beam has been modelled with single-bunch simulations using the longitudinal tracking code ESME [5]. The averaged, real bunch distributions measured at the PS flat top (FT) have been sampled with 500 000 macro-particles and tracked over the full chain of PS and SPS RF manipulations including adiabatic voltage reduction, a double splitting, and a bunch rotation in the PS, injection and FB in the SPS. Intensity effects have not yet been taken into account. Furthermore, simulations include an experimentally observed emittance blow-up, which may be attributed to the synchronisation process in the PS (for more details, see [6]).

To verify the predictions from simulations, a series of measurements has been carried out this year with 36 bunches of LHC-type 50 ns-spaced beam. The operational intensity of about $1.6 \times 10^{11}$ ppb (at injection to the SPS) has been used in all experiments, except for measurements investigating intensity dependence. The timings of the PS rotation voltage programme, $t_{40\,\mathrm{MHz}}$ and $t_{80\,\mathrm{MHz}}$ (Fig. 1), have been scanned systematically to find the optimal transmission. To increase the rotation voltage, we investigated two options: operating the spare 40 MHz or the spare 80 MHz cavity.

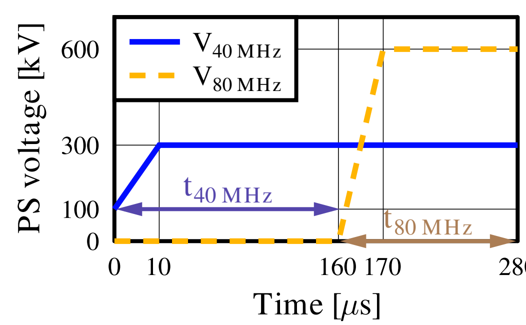


Figure 1: Currently operational PS bunch-rotation voltage programme [4]. The voltage is produced with one 40 MHz and two 80 MHz cavities. A hot spare cavity is available for both the 40 MHz and the 80 MHz RF systems.

Both in simulations and measurements, the bunch length ($4\sigma$) has been obtained from a Gaussian fit to the bunch profiles. Experimentally, the transmission has been determined as the ratio of the bunch intensity at 30 GeV/c (the FB momentum is 26 GeV/c) to the injected intensity, in order to include all losses due to uncaptured particles, also those that occur at the beginning of the acceleration ramp. Simulations took only capture and FB losses into account.

ISBN 978-3-95450-118-2

# ACCELERATION OF HIGH-INTENSITY PROTONS IN THE J-PARC SYNCHROTRONS

M. Yoshii KEK/JAEA J-PARC Center, Tokai, Japan

*Abstract*

The J-PARC consisting of the 181 MeV Linac, the 3 GeV rapid cycling synchrotron (RCS) and the 50 GeV main synchrotron (MR), is the first high intensity proton synchrotron facility to use the high field gradient magnetic alloy (MA) loaded accelerating cavity. MA is a low-Q material. However, because of the high permeability and the high saturation magnetic flux density, the MA cores are the only materials to realize the required gradient. The MA loaded cavity can be considered as a stable passive load. No tuning control is necessary. 11 RF systems are operational in the RCS, and 8 RF systems in the MR. In addition, the RCS RF systems are operated in a dual harmonic mode to perform the acceleration and the longitudinal manipulation of the high intensity beam in the available space in RCS. Beam loading compensation is an important issue. The feed-forward method using the RF beam signals from the wall current monitor has been established. The J-PARC synchrotrons realize stable, reproducible and clean acceleration of high intensity protons. A transition-free lattice and a precise digital timing system asynchronous to the AC-line are the distinctive features, which enable this achievement.

## INTRODUCTION

The J-PARC facility is a versatile science facility using the secondary particles like neutron, neutrino, Kaon, pion, etc. produced by an intense proton beam. The Linac and the RCS run at 25 Hz. The 3 GeV proton beam of $8.3\times10^{13}$ protons per pulse from the RCS, which corresponds to the designed output beam power of 1 MW, is sequentially delivered to the MLF and the MR. Consideration of beam loss during accelerating in the synchrotrons is one of the important issues. The intensity handled at the J-PARC is 100 times higher than the intensity of the KEK-PS that we have ever experienced. A transition free lattice is introduced in designing the two synchrotrons [1]. The Fermi chopper has large rotational momentum inertia. The time-jitter of the extracted proton beam is required to be less than 100 nsec. Scheduled extraction to the MLF from the RCS has been considered, too. To realize the requirements, the J-PARC timing system is based on the 12 MHz precise external clock, which is asynchronous to the 50 Hz AC-line.

The J-PARC beam commissioning has been started with the lower Linac energy of 181 MeV. In case of 181 MeV injection, the output beam power in the RCS is limited to 60%. Until now, a 420 kW equivalent beam was extracted from the RCS as a high intensity trial and the 275 kW beam is steadily delivered to the MLF.

The nominal machine cycle of the MR is 6.0 seconds for the Hadron experiment (SX: slow beam extraction by using a third-integer resonance) and 2.56 seconds for the Neutrino experiment (FX: fast beam extraction by using the fast kicker magnets). The MR cycle for T2K experiments has been set 30 % shorter than the original 3.64 seconds to obtain the maximum output beam power. On 30th May 2012, the number of accelerating particles per pulse exceeded 114 Tera ($114\times10^{12}$) protons at a high intensity trial run. The output beam power corresponds to 213 kW.

* masahito.yoshii@kek.jp

Table 1: Major Parameters

| | 3GeV RCS | MR |
|---|---|---|
| Energy (GeV) | 0.181 – 3 | 3 – 30 |
| $\gamma_t$ | 9.14 | j31.6 *1 |
| Circumference (m) | 348.333 | 1567.9 |
| Intensity (ppp) *2 | $2.5\times10^{13}$ ($8.3\times10^{13}$) | $1.4\times10^{14}$ ($3.3\times10^{14}$) |
| Cycle/period | 25Hz | 2.56 s (FX) 6.00 s (SX) |
| Acc. Voltage (kV) | 400 | 280 |
| RF harmonics | 2 | 9 |
| No. of RF stations | 11 (12) | 9 |
| Voltage per cavity | 45 kV | 45 kV |
| No. of gaps | 3 | 3 |
| Cavity length (m) | 1.996 | 1.846 |
| Q-value | 2 | 22 |
| Cavity Impedance per each gap | 890 Ω | 1100 Ω |

* Numbers in ( ) are the design values.
*1: imaginary energy
*2: (upper) achieved value and (lower) designed value
FX: Fast extraction, SX: Slow beam extraction

## RF SYSTEMS

The RCS and the MR each have a three-fold symmetry lattice. One of three long straight sections is assigned for the location of the RF cavities. There are 12 and 9 spaces for the RF systems of the RCS and the MR, respectively. The beam commissioning has been started at the RCS in 2007 with four RF systems and at the MR in 2008 with the four RF systems and the system has were upgraded every year.

The RF systems for the J-PARC synchrotrons provide a high accelerating gradient (more than 20 kV/m). Magnetic alloy (MA) cores were the only material, which could realize the required accelerating voltages in the



ISBN 978-3-95450-118-2

# LONGITUDINAL SPACE CHARGE PHENOMENA IN AN INTENSE BEAM IN A RING *

R.A. Kishek#, B. Beaudoin, I. Haber, D. Feldman, T. Koeth, and Y.C. Mo, Institute for Research in Electronics & Applied Physics, University of Maryland, College Park, MD 20742, USA

*Abstract*

The University of Maryland Electron Ring (UMER) [1] uses nonrelativistic, high-current electron beams to access space charge phenomena observable in high-intensity hadron beams. The UMER beam parameters correspond to space charge incoherent tune shifts, at injection, in the range of 1-5.5 integers. Longitudinal induction focusing is used to counteract the space charge force at the edges of a long rectangular bunch, confining the beam for 100s of turns. We report on two recent findings: (1) Observation of a space-charge-induced longitudinal multi-streaming instability formed from overlapping bunch ends in a ring. An analytical theory successfully predicts the onset of the instability over a wide range of beam currents and initial pulse lengths. (2) Experimental observations of the formation and propagation of soliton wave trains arising from large-amplitude longitudinal perturbations. Both phenomena are reproduced in WARP [2] simulations.

## INTRODUCTION

Space-charge-dominated beams, in which the strength of space charge-induced expansion exceeds that from beam emittance, differ fundamentally from beams where space charge is merely a perturbation. The former can support a variety of collective modes and longitudinal space charge waves that can result in exotic structures on the beam, such as high-density rings, solitary waves, or beam halo. While some of this physics has had a long history of theoretical study [3-5], limitations of experimental facilities have, until the recent commissioning of UMER, prevented adequate experimental verification. Prior experimental studies of deep space charge suffered from inadequate transport distances, thus constraining them to measuring the initial transients in beam evolution. UMER, by contrast, accesses deep space charge over long transport distances (tune-shifts > 5 for many turns).

This paper reviews two recent studies concerned with the evolution of noisy, or non-smooth, initial distributions. First we discuss the evolution of a space-charge-induced longitudinal multi-streaming instability [6] relevant to multi-bunch injection in a ring. Second, we discuss the formation and propagation of solitons [7] from large amplitude longitudinal perturbations, observed experimentally and reproduced in simulations.

* Supported by the US Dept. of Energy, Offices of High Energy Physics and Fusion Energy Sciences, and by the US Dept. of Defense, Office of Naval Research and the Joint Technology Office.

# ramiak@umd.edu

## EXPERIMENTAL SETUP

Figure 1 illustrates UMER. The UMER ring has 72 quadrupoles and 36 dipoles arranged in 36 FODO cells of period 32 cm. The ring also has three glass gaps for applying longitudinal focusing and acceleration via induction cells. Currently the glass gap at RC4 is used as an induction cell for longitudinal focusing, RC16 for acceleration, and RC10 is used as a wall-current monitor. A 10 keV electron beam is produced from a gridded thermionic gun with a pulse length variable from 25-140 ns. The beam current (0.5-100 mA) and normalized rms emittance (0.3-3.0 μm) are varied by means of an aperture wheel downstream of the anode. The different beam currents enable varying the strength of space charge from the emittance-dominated to the extremely space-charge-dominated.

A single long rectangular bunch is injected through a pulsed dipole into the ring, at a repetition rate of 60 Hz. The bunch circulates until it is totally lost. Application of longitudinal focusing using an induction cell [8] has extended the containment of the bunch to hundreds of turns for the lower-current UMER beams. The pulsed induction “ear fields” keep the beam ends from expanding and indefinitely maintain a rectangular bunch with a flat-top. Development of additional induction modules for the higher current beams is in progress. An extraction section currently in the late design / early construction stage is planned for installation by summer 2013.

## MULTI-STREAM INSTABILITY

Without longitudinal focusing, a bunch freely expands under its space charge self-fields. The expanding bunch ends fill the ring, interpenetrate, and wrap repeatedly [9], leading to a “DC” beam on the peak-to-peak current signal. The striated longitudinal phase space, however, drives a multi-stream instability different from the unbounded volumetric two-stream plasma instability. The same effect can occur in multi-bunch injection schemes in a ring, as predicted theoretically [10].

We have observed this instability experimentally (Fig. 2), and systematically studied it over a wide range of beam parameters. Figure 2 illustrates a typical signature of the instability on the wall-current monitor signal. The peak-to-peak signal dwindles as the beam expands and becomes “DC” at about 7 μs, followed by a damped lower-amplitude re-bunching of the beam. The instability appears at about 16.5 μs as a sharper and more random re-bunching, with higher-frequency content.

We have derived a simple theoretical model that accurately predicts the onset of the instability. The model



ISBN 978-3-95450-118-2

# MEASUREMENT AND SIMULATION OF LUMINOSITY LEVELING IN LHC VIA BEAM SEPARATION*

Stefan Paret†, Ji Qiang, LBNL, Berkeley, USA
Reyes Alemany-Fernandez, Rama Calaga, Rossano Giachino, Werner Herr, Delphine Jacquet, Giulia Papotti, Tatiana Pieloni, Laurette Ponce, Michaela Schaumann, CERN, Geneva, Switzerland
Ryoichi Miyamoto, ESS, Lund, Sweden

*Abstract*

Leveling of the luminosity in LHC by means of separating the beams colliding at an interaction point is examined. An experiment in which the separation of the beams was stepwise increased to up to 2.5 times the beam width is presented. The luminosity at all IPs and emittance of the beams were measured to detect possible side effects of the collision with an offset. Strong-strong simulations that closely follow the experimental setup are discussed and compared with the measurements. Finally, potential alternatives for luminosity leveling are briefly described.

## LUMINOSITY

The high-luminosity upgrade of the LHC aims at increasing the *integrated luminosity* $\int L\mathrm{d}t$ significantly beyond the nominal value [1]. Here $L$ is the *instantaneous luminosity*. For two equal circular beams with Gaussian density profiles colliding head-on, the luminosity (per collision) is given by

$$L_0 = \frac{N^2 f_0}{4\pi\epsilon\beta^*}, \tag{1}$$

where $N$ is the number of particles per bunch, $f_0$ is the revolution frequency, $\epsilon$ is the emittance and $\beta^*$ is the beta function at the interaction point (IP).

The gain in luminosity relies on an increase of the beam intensity and brightness, as well a decrease of the beta function at the IPs. Maximizing the instantaneous luminosity with these parameters is not the target, though. There are several reasons to limit the peak luminosity. One reason is the limited pile-up capacity of the experiments, i. e. the limited number of simultaneous reactions that can be distinguished in the analysis. Another reason is that the luminosity decays the faster the larger the initial luminosity is, due to emittance growth and particle loss.

In order to maximize the integrated luminosity without driving the peak luminosity to extremes, *luminosity leveling* will be employed. Luminosity leveling is a measure to keep the luminosity at a constant value, which is significantly smaller than the potential peak luminosity without

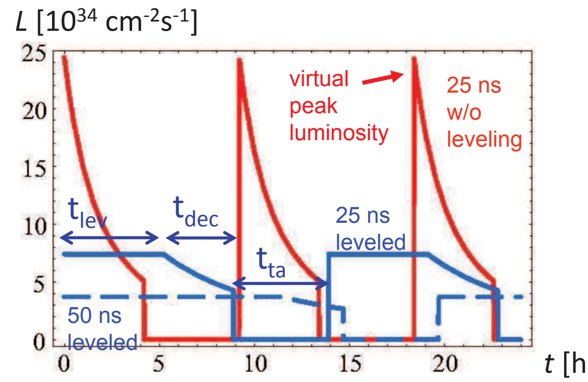


Figure 1: Projected luminosity in the high luminosity LHC as a function of the time. The red line indicates the luminosity that would be yielded without leveling. The solid blue line shows the target course with leveling. The dashed blue line refers to an alternative set of beam parameters also with leveling.

Courtesy O. Brüning [1]

leveling, as long as possible. As Fig. 1 reveals, leveling avoids high pile-ups and slows down the beam degradation thus permitting longer storage times [1]. The leveling ends when the beam deterioration can no longer be compensated ($t_{\mathrm{lev}}$ in Fig. 1). Collisions still go on until the luminosity drops below a threshold which triggers a beam dump ($t_{\mathrm{dec}}$). The time gap for injection and preparation of new beams until collisions can be resumed ($_{\mathrm{ta}}$) is independent of this procedure.

The suppression of the luminosity decay overcompensates the reduction of the peak luminosity. In addition, the increased storage time improves the ratio of the usable time $t_{\mathrm{lev}}$+$t_{\mathrm{dec}}$ to the restoration time $t_{\mathrm{ta}}$. Consequently, the long term integrated luminosity is increased by leveling.

Luminosity leveling requires a reversible reduction of the instantaneous luminosity. Reversibility is essential to compensate the natural luminosity decay. In addition, at LHC the leveling has to be strictly local to match the individual needs of all 4 experiments. Thus only beam optical parameters can be varied for leveling. Another prerequisite for a useful method is a weak to negligible impact on the beam quality.

One lever for luminosity leveling is $\beta^*$, according to Eq. 1. Two other options are a based on a reduction of the

* This work was partially supported by the U. S. LHC Accelerator Research Program and the National Energy Research Scientific Computing Center of the U. S. Department of Energy under contract No. DE-AC02-05CH11231

† sparet@lbl.gov

ISBN 978-3-95450-118-2

# INJECTION AND STRIPPING FOIL STUDIES FOR A 180 MeV INJECTION UPGRADE AT ISIS

B. Jones, D.J. Adams, M.C. Hughes, S.J.S. Jago, H.V. Smith, C.M. Warsop, R.E. Williamson
ISIS, STFC, Rutherford Appleton Laboratory, UK

*Abstract*

The Rutherford Appleton Laboratory (RAL) is home to ISIS, the world's most productive spallation neutron source. ISIS has two neutron producing target stations (TS-1 and TS-2), operated at 40 Hz and 10 Hz respectively with a 50 Hz, 800 MeV proton beam from a rapid cycling synchrotron (RCS), which is fed by a 70 MeV $H^-$ drift tube linac.

The multi-turn charge-exchange injection process used on ISIS has been the subject of a programme of detailed studies in recent years including benchmarked simulations and experiments. More recently, these studies have been expanded as plans for upgrading ISIS have focussed on replacement of the 70 MeV linac with a new, higher energy injector and a new synchrotron injection straight. Whilst much of these studies have been reported elsewhere, this paper presents a summary of the programme with some further details.

## INTRODUCTION

The ISIS spallation neutron source now accelerates up to $3\times10^{13}$ protons per pulse (ppp), cycling at 50 Hz corresponding to a total beam power of 0.2 MW which is split 40 pulses per second (pps) to TS-1 and 10 pps to TS-2. Fig. 1 is a schematic of the facility.

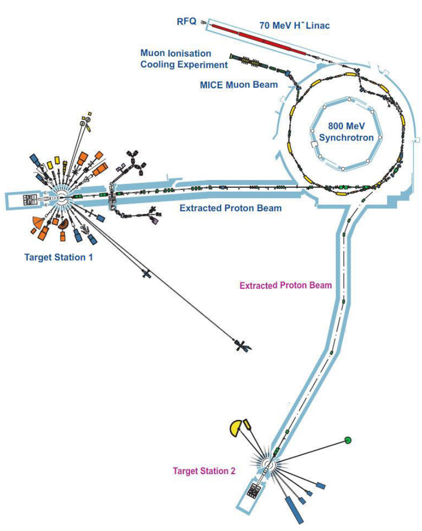


Figure 1: ISIS schematic layout.

With the successful operation of higher power spallation sources at J-PARC and SNS, a number of upgrade routes for ISIS are being studied. The favoured option is the addition of a 3.2 GeV RCS initially fed by bucket-to-bucket transfer from the existing 800 MeV RCS to provide ~1 MW. The later addition of a new 800 MeV linac would raise beam power further to the 2-5 MW range. Present studies, however, focus on replacement of the 70 MeV linac with a new ~180 MeV injector and new injection region of the RCS. The combined effects of reduced space charge and an optimized, chopped injection scheme could enable operation at 0.5 MW. This upgrade addresses reliability and obsolescence issues with the present linac and would provide a corresponding scaling in power for later upgrades.

## 70 MEV INJECTION

The 202 MHz, 70 MeV injector provides a 200 µs, 25 mA $H^-$ beam pulse. This beam is accumulated in the synchrotron over ~130 turns from 400 µs before the sinusoidal main magnetic field reaches its minimum. A 50 µg/cm$^2$ aluminium oxide foil is used to strip the $H^-$ to $H^+$ at injection with ~97 % efficiency. The 550 W waste beam of $H^0$ and $H^-$ is collected by a 40 mm long water-cooled graphite dump. Circulating beam is bumped towards the foil, located on the inside of the synchrotron, during injection by four serially powered injection dipoles. The dipoles bend the 70 MeV beam by 45 mrad creating a ~67 mm deflection at the foil. This bump is established and stabilised before injection begins and collapses over 100 µs after injection ends to limit foil recirculation to ~30 per proton.

Anti-correlated transverse painting is employed to reduce space charge forces within the beam. Horizontal painting makes use of the changing dispersive closed orbit during injection; as the main magnetic field falls the dispersive closed orbit moves away from the foil thus painting from a small to large emittance. Beam is painted vertically by moving the injection point; a single dipole magnet in the injection transfer line with a falling current is used to paint from a large to small emittance.

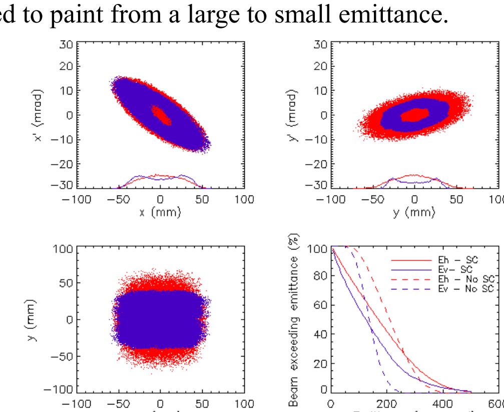


Figure 2: ORBIT simulations: Phase space, real space and emittance occupancy at 0 ms with (red) and without (blue) space charge.



ISBN 978-3-95450-118-2

# COLLIMATION OF ION BEAMS*

I. Strasik#, O. Boine-Frankenheim, GSI Helmholtzzentrum für Schwerionenforschung, Darmstadt, Germany

*Abstract*

The SIS 100 synchrotron as part of the FAIR project at GSI will accelerate various beam species from proton to uranium. An important issue is to minimize uncontrolled beam losses using a collimation system. An application of the two-stage betatron collimation concept, well established for proton accelerators, is considered for the fully-stripped ion beams. The two-stage system consists of a primary collimator (a scattering foil) and secondary collimators (bulky absorbers). The main tasks of this study are: (1) to specify beam optics of the system, (2) to calculate dependence of the scattering angle in the foil on the projectile species, (3) to investigate importance of the inelastic nuclear interactions in the foil (4) to calculate momentum losses of the primary ions in the foil and (5) to estimate dependence of the collimation efficiency on the projectile species. A concept for the collimation of partially-stripped ions is based on the stripping of remaining electrons and deflecting using a beam optical element towards a dump location.

## INTRODUCTION

Various beam dynamics processes can cause that particles enter into unstable orbits with large betatron amplitudes which leads to beam halo formation and emittance growth [1, 2]. The main reasons for halo formation are space charge, mismatched beam, nonlinear forces, RF noise, magnet errors, scattering, resonances, beam-beam effects and electron clouds [1, 2]. Beam halo is one of the reasons for uncontrolled beam-loss interacting with accelerator structures. Uncontrolled beam loss causes the following problems: vacuum degradation due to desorption process, superconducting magnets quenches, activation of the accelerator structure, radiation damage of the equipment and devices [1]. The main purpose of the collimation system is to remove the halo, consequently to reduce above mentioned problems and to provide a well defined and shielded storing location for the beam losses.

The halo collimation system in future SIS 100 synchrotron of FAIR (Facility for Antiproton and Ion Research) must be capable to collimate various ion species from proton up to uranium [3]. The situation is even more complicated due to operation with partially- (e.g. $^{238}U^{28+}$) and fully- (e.g. $^{40}Ar^{18+}$) stripped ions. In case of the proton and light-ion beams the collimation system is required in order to limit the residual activation of accelerator components. A tolerable level of uncontrolled beam-losses is 1 W/m for protons [4]. The tolerable losses for other ion species are estimated in Ref [5]. In case of the heavy ions the main issue is the vacuum degradation due to desorption [6] as well as the radiation damage [7].

*Work supported by BMBF and EU program EuCARD, WP8, ColMat

#i.strasik@gsi.de

For proton and light fully-stripped ion beams a well established two-stage betatron collimation system [8-11] was adopted for transverse collimation in SIS 100. The collimation concept for the partially-stripped heavy ions is rather different. It is based on the change of the charge state of the halo particles using a stripping foil. Consequently the stripped ions can be deflected toward a dump location using a beam optical element.

## TWO-STAGE BETATRON COLLIMATION

The two-stage collimation system consists of: a) a primary collimator (a thin foil) which scatters the halo particles and b) secondary collimators (bulky blocks) which are necessary to absorb the scattered particles (secondary halo) [8-11]. It is not desirable to intercept the halo particles directly by the secondary collimators. For this reason they are located further from the beam envelope than the primary collimator by a so-called "retraction distance", $\delta = n_S/n_P - 1$, where $n_P$ and $n_S$ are the normalised apertures of the primary and secondary collimators, respectively. Optimal phase advances for maximum collimation efficiency at certain values of $n_P$ and $n_S$ can be calculated using the formulas:

$$\mu_{S1} = \arccos\frac{n_P}{n_S} \qquad \mu_{S2} = \pi - \mu_{S_1}, \tag{1}$$

where $\mu_{S1}$ and $\mu_{S2}$ is the phase advance between the primary – 1st secondary and primary – 2nd secondary collimator, respectively.

Detailed beam-optics specifications of the two-stage collimation system in 1D and 2D are derived by Trenkler and Jeanneret [8, 9] and Seidel [10].

### *1D Optics*

In order to specify the two-stage collimation system we use normalized particle coordinates $X$ and $X'$:

$$\begin{pmatrix} X \\ X' \end{pmatrix} = \frac{1}{\sigma_x}\begin{pmatrix} 1 & 0 \\ \beta_x & \alpha_x \end{pmatrix}\begin{pmatrix} x \\ x' \end{pmatrix} \qquad \sigma_x = \sqrt{\beta_x \varepsilon_x}, \tag{2}$$

where $x$ and $x'$ are the coordinates in the horizontal plane, $\alpha_x$ and $\beta_x$ are the Twiss parameters and $\varepsilon_x$ is the beam emittance in the $x$ transverse plane. Transport of the particles in the normalized phase space from the primary collimator to the secondary collimators can be calculated using the $2\times2$ transfer matrix $M$:

$$\begin{pmatrix} X_S \\ X'_S \end{pmatrix} = M\begin{pmatrix} X_P \\ X'_P \end{pmatrix} \qquad M = \begin{pmatrix} \cos\mu_S & \sin\mu_S \\ -\sin\mu_S & \cos\mu_S \end{pmatrix}, \tag{3}$$

ISBN 978-3-95450-118-2

# BEAM HALO DYNAMICS AND CONTROL WITH HOLLOW ELECTRON BEAMS*

G. Stancari†, G. Annala, A. Didenko, T. R. Johnson, I. A. Morozov, V. Previtali, G. Saewert, V. Shiltsev, D. Still, A. Valishev, L. G. Vorobiev, Fermilab, Batavia, IL 60510, USA
D. Shatilov, BINP, Novosibirsk, Russia
R. W. Assmann‡, R. Bruce, S. Redaelli, A. Rossi, B. Salvachua Ferrando, G. Valentino, CERN, Geneva, Switzerland

*Abstract*

Experimental measurements of beam halo diffusion dynamics with collimator scans are reviewed. The concept of halo control with a hollow electron beam collimator, its demonstration at the Tevatron, and its possible applications at the LHC are discussed.

## INTRODUCTION

Beam quality and machine performance in circular accelerators depend on global quantities such as beam lifetimes, emittance growth rates, dynamic apertures, and collimation efficiencies. Calculations of these quantities are routinely performed in the design stage of all major accelerators, providing the foundation for the choice of operational machine parameters.

At the microscopic level, the dynamics of particles in an accelerator can be quite complex. Deviation from linear dynamics can be large, especially in the beam halo. Lattice resonances and nonlinearities, coupling, intrabeam and beam-gas scattering, and the beam-beam force in colliders all contribute to the topology of the particles' phase space, which in general includes regular areas with resonant islands and chaotic regions. In addition, various noise sources are present in a real machine, such as ground motion (resulting in orbit and tune jitter) and ripple in the radiofrequency and magnet power supplies. As a result, the macroscopic motion can acquire a stochastic character, describable in terms of diffusion [1, 2, 3, 4, 5].

In this paper, we first address the issue of obtaining experimental data on the dynamics of the beam halo. It was shown that beam halo diffusion can be measured by observing the time evolution of particle losses during a collimator scan [6]. These phenomena were used to estimate the diffusion rate in the beam halo in the SPS at CERN [7], in HERA at DESY [6], and in RHIC at BNL [8]. A much more extensive experimental campaign was carried out at the Tevatron in 2011 [9] to characterize the beam dynamics of colliding beams and to study the effects of the novel hollow electron beam collimator concept [10]. Recently, the technique was also applied to measure halo diffusion rates in the LHC at CERN [11]. These measurements shed light on the relationship between halo population and dynamics, emittance growth, beam lifetime, and collimation efficiency. They are also important inputs for collimator system design and upgrades, including new methods such as channeling in bent crystals or hollow electron lenses.

In the second part of the paper, we discuss the novel concept of hollow electron beam collimation (HEBC), and how it affects halo dynamics. The results of experimental studies at the Fermilab Tevatron collider are briefly reviewed, with an emphasis on the effect of the hollow electron beam on halo diffusion in the circulating beam. We conclude with a summary of recent research activities aimed at a possible application of hollow beam collimation at CERN.

## BEAM HALO DIFFUSION

As discussed in the introduction, particle motion in an accelerator at the microscopic level is in general very rich. Two main considerations lead to the hypothesis that macroscopic motion in a real machine, especially in the halo, will be mostly stochastic: (1) the superposition of the multitude of dynamical effects (some of which stochastic) acting on the beam; (2) the operational experience during collimator setup, which generates loss spikes and loss dips that often decay in time as $1/\sqrt{t}$, a typically diffusive behavior.

### *Experimental Method*

A schematic diagram of the apparatus is shown in Fig. 1 (top). All collimators except one are retracted. As the jaw of interest is moved in small steps (inward or outward), the local shower rates are recorded as a function of time. Collimator jaws define the machine aperture. If they are moved towards the beam center in small steps, typical spikes in the local shower rate are observed, which approach a new steady-state level with a characteristic relaxation time (Fig. 1, bottom). When collimators are retracted, on the other hand, a dip in losses is observed, which also tends to a new equilibrium level. By using the diffusion model presented below, the time evolution of losses can be related to the diffusion rate at the collimator position. By independently calibrating the loss monitors against the number of lost particles, halo populations and collimation efficiencies can also be estimated.

* Fermilab is operated by Fermi Research Alliance, LLC under Contract No. DE-AC02-07CH11359 with the United States Department of Energy. This work was partially supported by the US LHC Accelerator Research Program (LARP).

† stancari@fnal.gov
‡ Present address: Deutsches Elektronen-Synchrotron (DESY), Hamburg, Germany.



ISBN 978-3-95450-118-2

# LONG BASELINE NEUTRINO EXPERIMENT TARGET MATERIAL RADIATION DAMAGE STUDIES USING ENERGETIC PROTONS OF THE BROOKHAVEN LINEAR ISOTOPE PRODUCTION (BLIP) FACILITY*

N. Simos#; J. O Conor; BNL, Upton, NY 11973, USA,
P. Hurh, N. Mokhov; FNAL, Batavia, IL 60510, USA
Z. Kotsina, Democritos National Center for Scientific Research, Greece

*Abstract*

One of the future multi-MW accelerators is the LBNE Experiment where Fermilab aims to produce a beam of neutrinos with a 2.3 MW proton beam as part of a suite of experiments associated with Project X. Specifically, the LBNE Neutrino Beam Facility aims for a 2+ MW, 60-120 GeV pulsed, high intensity proton beam produced in the Project X accelerator intercepted by a low Z solid target to facilitate the production of low energy neutrinos. The multi-MW level LBNE proton beam will be characterized by intensities of the order of 1.6 e+14 p/pulse, σ radius of 1.5-3.5 mm and a 9.8 μs pulse length. These parameters are expected to push many target materials to their limit thus making the target design very challenging. To address a host of critical design issues revealed by recent high intensity beam on target experience a series of experimental studies on radiation damage and thermal shock response conducted at BNL focusing on low-Z materials have been undertaken with the latest one focusing on LBNE.

## INTRODUCTION

High-performance targets under consideration to intercept multi-MW proton beams of a number of new particle accelerator initiatives depend almost entirely on the ability of the selected materials to withstand both the induced thermo-mechanical shock and simultaneously resist accumulated dose-induced damage which manifests itself as changes in material physio-mechanical properties.

One of the future multi-MW accelerators is the LBNE Experiment where Fermilab plans to produce a beam of neutrinos with a 2.3 MW proton beam as part of a suite of experiments associated with Project X. Specifically, the LBNE Neutrino Beam Facility aims for a 2+ MW, 60-120 GeV pulsed, high intensity proton beam produced in the Project X accelerator intercepted by a low Z solid target to facilitate the production of low energy neutrinos. The multi-MW level LBNE proton beam will be characterized by intensities of the order of 1.6 e+14 p/pulse, σ radius of 1.5-3.5 mm and a 9.8 μs pulse length. These parameters are expected to push many target materials to their limit thus making the target design very challenging. Recent experience from operating high intensity beams on targets have indicated that several critical design issues exist namely thermal shock, heat removal, radiation damage, radiation accelerated corrosion effects, and residual radiation within the target envelope. A series of experimental studies on radiation damage and thermal shock response conducted at BNL and focusing on low-Z materials have unraveled potential issues regarding the damageability from energetic particle beams which may differ significantly from thermal reactor experience.

To address irradiation damage from energetic particles proton a wide array of materials considered to support high power experiments have been studied extensively using the BNL 200 MeV proton beam of the Linac and utilizing the target station of the Linear Isotope Producer (BLIP) where 20-24 kW of proton beam power (~110 μA current) are effectively used to irradiate target materials under consideration [1]. Of interest to the LBNE operating with 120 GeV protons are low Z target materials and their operational life that is expected to be limited by irradiation damage. Instead of extrapolating from thermal neutron damage experience accumulated in fission reactors damage from the energetic protons at BNL Linac was sought to deduce target lifetime estimates. Based on first principles of energetic particle interaction with matter, it is anticipated that the damage to these sought low Z materials will be greater at these MeV proton energy levels than the 120 GeV of the LBNE beam.

Extensive simulations performed by MARS15 indeed revealed that for the NuMI/LBNE experiment operating at 120 GeV with beam σ = 1.1mm and 4.0e20 protons/year is expected to see peak damage in graphite of ~0.45 dpa while for the BLIP configuration with a beam energy of 165 MeV and σ = 4.23mm and 1.124e22 protons on target/year the expected damage of 1.5 dpa. Guided by these analytical predictions on carbon materials of interest the equivalent damage of LBNE operations at the 700 kW level may be achieved with ~7-8 weeks irradiation using the BNL 181 MeV Linac proton beam and ~5mm sigma.

The main objectives of the irradiation experiment were to (a) assess the effect that the operating environment has on the onset and acceleration of structural degradation of graphite and carbon composites when exceeding certain fluence levels of energetic protons that are far lower than the thermal neutron fluences, (b) the role of irradiation temperature in restoring damage induced by the irradiating beam and (c) the variability in damage experienced by different grades of graphite with distinct polycrystalline structure as well as other materials such as carbon and h-BN that exhibit lattice similarities.

*Work supported by the U.S. Department of Energy.
#simos@bnl.gov

ISBN 978-3-95450-118-2

# UNDERSTANDING ION INDUCED RADIATION DAMAGE IN TARGET MATERIALS*

M. Tomut#, GSI Helmholzzentrum für Schwerionenforschung, Darmstadt, Germany
C. Hubert, TU Darmstadt, Germany

*Abstract*

Successful operation of next generations of radioactive beam facilities depends on the target survival in conditions of intense radiation field and thermo-mechanical solicitations induced by the driving ion beam. Material property degradation due to ion- beam induced damage will limit target lifetime, either by affecting target performance or, by reducing the material resilience. Similar problems are faced by beam protection elements at LHC. Understanding the mechanism of radiation damage induced by ion beam in these materials provides valuable knowledge for lifetime prediction and for the efforts to mitigate performance degradation. On their way through the target material, energetic heavy ions induce a trail of ionizations and excitations, resulting in formation of ion tracks consisting of complex defect structures. This work reports on the ion-induced structural and thermo-mechanical property degradation studies in high power target materials.

## ION- INDUCED RADIATION DAMAGE IN TARGET MATERIALS

The development of high-power heavy ions accelerators poses new challenges to materials that have traditionally served in the nuclear field. Targets, key accelerators components have to perform in severe radiation conditions, experiencing dimensional and structural changes, stresses and severe degradation of properties that control thermal-shock and fatigue resistance. Carbon remains the best choice for high temperature and high dose applications due to the low energy deposited by the primary heavy ion beam, scaling with the atomic number of the target material.

Fine-grained isotropic graphite and carbon-carbon composites have been selected for manufacturing the production target and beam protection elements at the planned Super-FRS fragment separator [1] at FAIR, at FRIB, at LHC and at neutrino facilities. Failure criteria due to irreversible ion-beam induced damage are related to dimensional changes, embrittlement and to degradation of thermal conductivity, leading to increased thermal stresses. To get an estimate for the critical doses, both simulations and experiments are needed.

Samples of high-density, fine-grained, isotropic graphite were exposed to $^{197}$Au and $^{238}$U ions, at the UNILAC linear accelerator at GSI, Darmstadt, at energies close to Bragg peak, for maximum efficiency of cylindrical damage trails formation. [2]. Irradiated carbon materials present evidence of dimensional changes, induced stress and hardening.

Dimensional changes have been investigated using a Dektak 8, Veeco profilometer. Previous studies have shown that this technique allows a relatively simple, non-destructive test of the sensitivity of a given material to ion-induced damage. The samples were polished to optical quality and partially covered during the irradiation using a thick Al mask. The mean height of the step between pristine and irradiated area has been determined by averaging several individual scans.

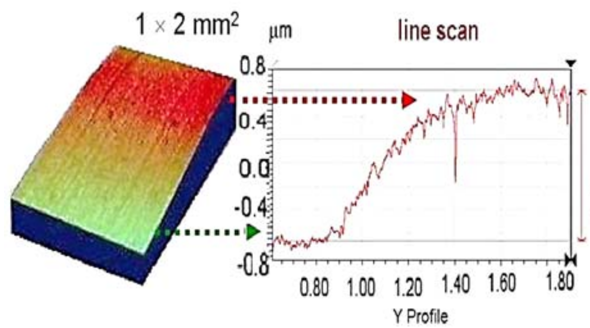


Figure 1: Profilometer mapping at the transition from non-irradiated (front) to irradiated (back) area of a masked polycrystalline graphite sample exposed to $10^{13}$ $^{238}$U ions/cm$^2$ (11.1 MeV/u). Selected scan displays a step height of 1.3 µm.

Isotropic graphite shows a remarkable resistance to defect production as indicated by the low values of dimensional changes at fluences of up to $10^{12}$ U ions/cm$^2$. In the range of $10^{12}$ to $10^{13}$ U ions/cm$^2$ swelling increases steeply. At fluences of $10^{13}$ U ions/cm$^2$, ion tracks having a diameter of about 3 nm start to overlap. At this fluence the measured out-of-plane swelling is 1.3 ± 0.1 µm, 1% of the range (120 µm) of the ions (Figure 1). Profilometer mapping of the surface of samples irradiated with $10^{13}$ U ions/cm$^2$ reveals crack formation. We also observe a significant bending of this sample due to a strong in-plane stress which develops at the interface between the swollen, irradiated layer and the non-irradiated substrate.

Irradiation induced deformation due to stresses at the interface between irradiated and non-irradiated material has been investigated as a function of fluence. Thin cantilever samples of high density graphite were exposed to GeV heavy ions. The ions are stopped at a depth representing one tenth of the thickness of the sample, inducing strong stresses at this interface and determining the bending of the sample. The radius of curvature was

* Work supported by EU, EUCARD contract No. 53102
# m.tomut@gsi.de



ISBN 978-3-95450-118-2

# BEAM-BEAM EFFECTS IN RHIC*

Y. Luo, M. Bai, W. Fischer, C. Montag, S. White,
Brookhaven National Laboratory, Upton, NY 11973, USA

*Abstract*

In this article we review the beam-beam effects in the polarized proton runs in the Relativistic Heavy Ion Collider (RHIC). The operational observations, limitations, and the next luminosity goal are presented and discussed. With an upgraded polarized proton source, the proton bunch intensity will be increased from $1.7 \times 10^{11}$ up to $3.0 \times 10^{11}$. To accommodate the large beam-beam tune spread in the current tune space between 2/3 and 7/10 and to compensate the nonlinear beam-beam resonance driving terms, head-on beam-beam compensation with electron lenses (e-lenses) is to be installed.

## INTRODUCTION

RHIC consists of two superconducting rings, the Blue ring and the Yellow ring. They intersect at 6 locations around the ring circumference. The two beams collide at two interaction points (IPs), IPI6 and IP8. Fig. 1 shows the layout of RHIC. RHIC is capable of colliding heavy ions and polarized protons (p-p). The maximum total beam-beam parameter for 2 IPs was 0.003 in the 100 GeV Au-Au collision and 0.017 in the 250 GeV p-p collision. In this article we only discuss the beam-beam effects in the p-p runs.

The main limitation to the beam lifetime in the RHIC p-p runs are the beam-beam interactions, the nonlinear magnetic field errors in the interaction regions (IRs), the nonlinear chromaticities with low $\beta^*$s and the machine and beam parameter modulations.

The working point in the RHIC p-p runs is chosen to provide a good beam-beam lifetime and to maintain the proton polarization during the energy ramp and physics stores. The nominal working point $(Q_x, Q_y) = (28.695, 29.685)$ is constrained between 2/3 and 7/10. 7/10 is a 10th order betatron resonance and also a spin depolarization resonance. Experiments and simulations have shown that the beam lifetime and the proton polarization are reduced when the vertical tune of the proton beam is close to $7/10$ [1].

Figure 2 shows the proton tune footprint including beam-beam interactions. The proton bunch intensity is $2.0 \times 10^{11}$ and the 95% normalized transverse emittance (6 times the rms normalized emittance $\epsilon_{\rm n,rms}$) is $15\pi$ mm.mrad leading to a beam-beam parameter of 0.02. From Fig. 2, there is not enough tune space to hold the large beam-beam tune spread when the proton bunch intensity is larger than

* This work was supported by Brookhaven Science Associates, LLC under Contract No. DE-AC02-98CH10886 with the U.S. Department of Energy.

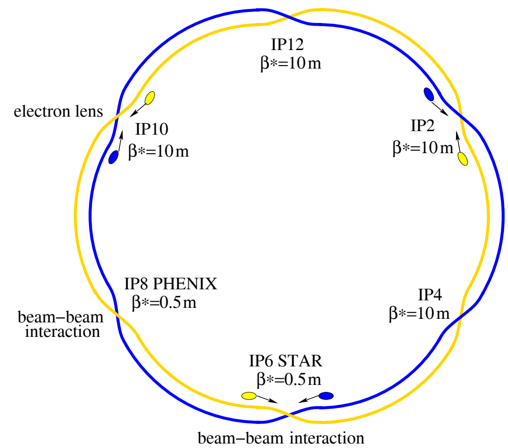


Figure 1: Layout of RHIC. Two beams collide at IP6 and IP8. The e-lenses are to be installed close to IP10.

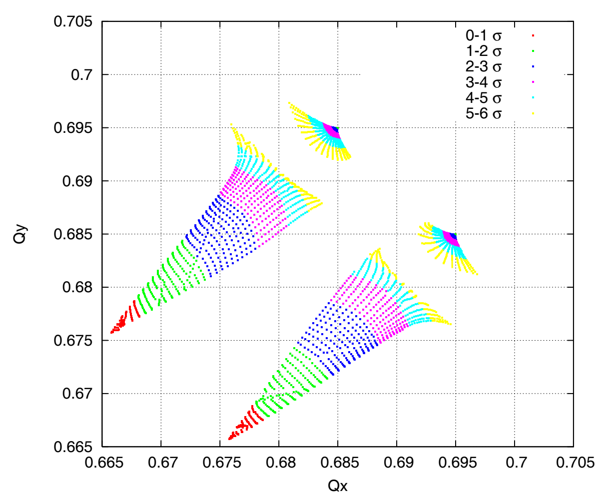


Figure 2: Tune footprints without and with beam-beam. In this calculation, the bunch intensity is $2.0 \times 10^{11}$.

$2.0 \times 10^{11}$ [2]. Simulations and experiments have been continuously carried out to explore new tune spaces.

## OBSERVATIONS

### *Previous p-p Runs*

The luminosity in the p-p collision is given by

$$L = \frac{N_{\rm p}^2 N_{\rm b} \gamma f_{\rm rev}}{4\pi \epsilon_{\rm n,rms} \beta^*} H(\frac{\beta^*}{\sigma_l}). \quad (1)$$

Here $N_{\rm p}$ is the proton bunch intensity, and $N_{\rm b}$ the number of bunches, $\gamma$ the Lorentz factor, $f_{\rm rev}$ the revolution frequency. $\epsilon_{\rm n,rms}$ is the rms normalized emittance and $\sigma_l$ the



ISBN 978-3-95450-118-2

# EFFECTS OF MAGNETIC FIELD TRACKING ERRORS AND SPACE CHARGE ON BEAM DYNAMICS AT CSNS/RCS*

S. Y. Xu#, S. Wang, N.Wang
Institute of High Energy Physics (IHEP), Beijing, 100049, China

*Abstract*

The Rapid Cycling Synchrotron (RCS) is a key component of the China Spallation Neutron Source (CSNS). For this type of high intensity proton synchrotron, the chromaticity, space charge effects and magnetic field tracking errors can induce beta function distortion and tune shift, and induce resonances. In this paper the combined effects of chromaticity, magnetic field tracking errors and space charge on beam dynamics at CSNS/RCS are studied systemically.

## INTRODUCTION

The China Spallation Neutron Source (CSNS) is an accelerator-based facility. It operates at 25 Hz repetition rate with the design beam power of 100 kW. CSNS consists of a 1.6-GeV Rapid Cycling Synchrotron (RCS) and an 80-MeV linac. RCS accumulates 80 MeV injected beam, and accelerates the beam to the design energy of 1.6 GeV, and extracts the high energy beam to the target. The lattice of the CSNS/RCS is triplet based four-fold structure. Table 1 and Fig.1a show the main parameters for the lattice [1] [2].

The preferred working points of CSNS/RCS are (4.86, 4.78) which can avoid the major low-order structure resonances. But because of the chromatic tune shift, space-charge incoherent tune shift and the tune shift caused by magnetic field tracking errors between the quadrupoles and the dipoles, some structure resonances are unavoidable. The chromaticity, space charge effects and magnetic field tracking errors can also induce beta function distortion, and influence the transverse acceptance and the collimation efficiency of the collimation system. In such a situation, a clear understanding of the effects of magnetic field tracking errors, space charge, and the chromaticity on beam dynamics at CSNS/RCS is an important issue.

In this paper the effects of chromaticity, magnetic field tracking errors and space charge on beam dynamics at CSNS/RCS are studied systemically. 3-D simulations are done introducing magnetic field tracking errors and space charge effects. The combined effects of chromaticity, magnetic field tracking errors and space charge on the beam dynamics for CSNS/RCS are discussed.

## EFFECTS ON LATTICE

The natural chromaticity of the CSNS/RCS lattice is (-4.3, -8.2), which can produce the tune shift of (±0.04, ±0.08) for the momentum spread of $\Delta p/p=\pm 0.01$ (The momentum aperture of the collimator is $\Delta p/p=\pm 0.01$). The dependence of the Beta functions on the momentum spread along a super-period without chromatic correction is shown in Fig. 1b.

Table 1: Main Parameters of the CSNS/RCS Lattice

| | |
|---|---|
| Circumference (m) | 227.92 |
| Superperiod | 4 |
| Number of dipoles | 24 |
| Number of long drift | 12 |
| Total Length of long drift (m) | 75 |
| Betatron tunes (h/v) | 4.86/4.78 |
| Natural Chromaticity (h/v) | -4.3/-8.2 |
| Momentum compaction | 0.041 |
| RF harmonics | 2 |
| Injection energy (MeV) | 80 |
| Extraction energy (MeV) | 1600 |
| RF Freq. (MHz) | 1.0241~2.444 |
| Accumulated particles per pulse | $1.56\times 10^{13}$ |
| Trans. acceptance (μπm.rad) | >540 |

In the case of uniform distribution in transverse direction, the incoherent tune shift due to space charge effects can be expressed as:

$$\Delta\upsilon = -\frac{r_p N}{2\pi\varepsilon\beta^2\gamma^3 B_f} \tag{1}$$

where $r_p=1.53\times10^{-18}$m is the classical proton radius, N is the accumulated particles, $\varepsilon_{rms}$ is the un-normalized emittance, $B_f$ is the longitudinal bunching factor, β and γ are the relativistic Lorentz factors. For CSNS/RCS, the longitudinal bunching factor, just after the injection painting, is about 0.32. With the energy of 80MeV, the space charge induced incoherent tune shift is about 0.2 for the case ε =350πμm.rad, which is the acceptance of the primary collimators. For the actual beam, which deviates from the uniform distribution, the incoherent tune shift for the particles in the beam core may be much greater than 0.2.

*: supported by National Natural Sciences Foundation of China (No. Y2113A005C)
#: xusy@ihep.ac.cn



ISBN 978-3-95450-118-2

# DUAL-HARMONIC ACCELERATION STUDIES AT CSNS RCS

J.F. Chen, X.Y. Zhang, J.Y. Tang#, IHEP, Beijing, China

*Abstract*

Dual harmonic acceleration is proposed to alleviate the space charge effects in the RCS (Rapid Cycling Synchrotron) at the upgrading stages of the CSNS (China Spallation Neutron Source). Different dual harmonic acceleration schemes have been studied by using a self-made parameter calculation code – RAMADH and the simulation code – ORBIT. Both complete and partial coverage of the dual harmonic RF system along the acceleration cycle have been considered. The injection by combining beam chopping and off-momentum is used in the macro-particle tracking simulations by ORBIT. In addition, a new idea that unlocks the RF frequency and the magnetic field in the injection period is found very useful in obtaining a good longitudinal painting.

## INTRODUCTION

The under-construction CSNS is a large scientific facility based on a high-power proton accelerator complex mainly consisting of an H- linac and an RCS. It is designed to provide a proton beam power of 100 kW in the first phase (CSNS-I) with the upgrading capability to 500 kW in the second phase (CSNS-II) [1, 2]. As shown in Table 1, the accelerator is designed to accelerate proton beams to 1.6 GeV in kinetic energy at a repetition rate of 25 Hz. To meet the requirements for the CSNS-II, the output energy of linac is improved from 80 MeV to 250 MeV and a dual-harmonic RF system in the RCS is applied to alleviate the space charge effect at low-energy phase. Besides, at CSNS-I the partial dual-harmonic acceleration which uses a spare cavity in all eight cavities for higher-frequency component is also taken into consideration [3]. The basic parameters of CSNS RCS are listed in Table 1.

Table 1: Basic Parameters of the CSNS RCS

| **Project phase** | **I** | **II** |
|---|---|---|
| Beam power /kW | 100 | 500 |
| Ring circumference /m | 228 | 228 |
| Curvature of bending magnet /m | 8.021 | 8.021 |
| No. of RF cavities | 8 (h=2) | 8 (h=2)+ 3(h=4) |
| Injection energy/MeV | 80 | 250 |
| Extraction energy /GeV | 1.60 | 1.60 |
| Protons per pulse /$10^{13}$ | 1.56 | 7.8 |
| Repetition rate /Hz | 25 | 25 |

The RF pattern plays an important role in the dual-harmonic acceleration. It not only decides the quantities of the required higher-harmonic cavities, but also affects the operation cost. In addition, it affects the achievable beam loss rate and eventually the beam power in the RCS to a large extent. Therefore, the design of good RF programs is a key point here, especially for CSNS-II where the RF program is expected to provide a large bunching factor at low-energy stage and a large bucket area in later stages.

Two codes are used in studying the dual-harmonic acceleration. One is a self-make calculation code — RAMADH, which bases on a single-harmonic acceleration code — RAMA [4]. The other is a 3D simulation code — ORBIT, which is applied to inject and trace micro-particles [5, 6]. Some related calculation and simulation results with the two codes will be presented in this paper. Besides, a new idea — stationary-bucket injection method that releases the RF frequency from the synchronization with the changing magnetic field in the injection period is found very useful in obtaining a good longitudinal painting. The feature is also added in the ORBIT code.

## DUAL-HARMONIC ACCELERATION

Two bunches are accelerated at the CSNS-I by a single harmonic ($h$=2) RF system. At the upgrading phase, CSNS-II, a second harmonic ($h$=4) RF system will be added to the existing fundamental one to increase trapping efficiency and improve bunching factor or bucket area for more stable beam dynamics. This dual-harmonic RF system is defined by:

$$V = V_1\left[\sin\phi - \delta\sin(2\phi+\theta)\right] \tag{1}$$

where $V_1$ is the amplitude for the harmonic $h$=2, $\delta V_1$ $(V_2)$ is the amplitude for the harmonic $h$=4, $\phi$ is the RF phase and $\theta$ is the phase between the first ($h$=2)and second ($h$=4) harmonic waveforms.

Bucket area and bunching factor are the most important parameters in designing the dual-harmonic RF patterns which are the results of weighing the two parameters in the course of acceleration.

### *Bucket Area*

In the longitudinal phase space expressed by $(\phi, \Delta E/h\omega_0)$, the bucket area per bunch is given by

$$A = 8R\sqrt{\frac{2(e)V_1(1-\eta_{sc})E_0\gamma\alpha^2}{h^3c^2\pi\eta}} \tag{2}$$

where the space charge factor $\eta_{sc}$ is expressed by

#Corresponding author: tangjy@ihep.ac.cn



ISBN 978-3-95450-118-2

# HIGH INTENSITY LONGITUDINAL DYNAMICS STUDIES FOR AN ISIS INJECTION UPGRADE

R.E. Williamson, D.J. Adams, C.M. Warsop, ISIS, Rutherford Appleton Laboratory, STFC, UK

*Abstract*

ISIS is the world's most productive pulsed neutron and muon source, located at the Rutherford Appleton Laboratory in the UK. Operation is centred on a loss-limited 50 Hz proton synchrotron which accelerates $3\times10^{13}$ protons per pulse from 70 MeV to 800 MeV, delivering a mean beam power of 0.2 MW.

Recent upgrade studies at ISIS have centred on a new 180 MeV linac for injection into the existing ring offering the possibility of beam powers in the 0.5 MW regime through reduction in space charge and optimised injection. A central and critical aspect of such an upgrade is the longitudinal dynamics including beam stability, associated RF parameters, space charge levels and stringent requirements on beam loss.

This paper outlines possible longitudinal injection schemes for the injection upgrade meeting key design requirements such as minimising halo, maximising the bunching factor and satisfying the Keil-Schnell-Boussard (KSB) stability criterion throughout acceleration. Details of simulation models including calculation of KSB are given together with associated assumptions. Latest results from studies to understand and confirm stability limits on ISIS via simulation and experiment are presented.

## INTRODUCTION

Present ISIS operations centre on an 800 MeV rapid cycling synchrotron (RCS) accelerating $3\times10^{13}$ protons per pulse (ppp) on the 10 ms rising edge of a sinusoidal main magnet field. At the repetition rate of 50 Hz this corresponds to 0.2 MW. A high intensity proton beam is accumulated via charge-exchange injection of a 70 MeV un-chopped $H^-$ beam. Injection begins 0.4 ms prior to main magnet field minimum, lasting ~200 µs (~135 turns). The proton beam is 'adiabatically' trapped in two bunches by the ring dual harmonic RF system. The RF system consists of 10 ferrite tuned cavities with peak design voltages of 160 and 80 kV/turn for the $h$=2 and $h$=4 harmonics respectively.

A range of ISIS upgrade routes, increasing beam power into the megawatt (MW) regime, is under study [1]. The favoured path increases beam power by a factor of ~4 by adding a ~3.2 GeV RCS onto the output of the present 800 MeV synchrotron, providing 1 MW or more. Subsequently the ~3.2 GeV ring can then be adapted for multi-turn charge-exchange injection from a new 800 MeV linac, increasing beam current and delivering 2 – 5 MW beam powers.

However, with a focus on reliability and affordability priority has been given to the replacement of all, or part of, the 70 MeV $H^-$ injector. This could address obsolescence issues with the current linac and ensure more reliable future operation.

Current studies are centred on the option of installing a new, higher energy (~180 MeV) linac with an optimised injection system into the existing 800 MeV synchrotron [2, 3]. Injecting at higher energy reduces space charge and allows for an increase in beam current and hence power. It also enhances the other upgrade routes mentioned.

A critical aspect of the injection upgrade is the longitudinal beam dynamics in the ISIS RCS. Accelerating a substantially higher intensity beam from 180 to 800 MeV whilst satisfying the necessary constraints is non-trivial. The main constraints include painting a suitable beam (1D and 3D); maintaining slow adiabatic changes and avoiding halo generation; maximising the bunching factor; controlling the momentum spread; achieving near zero loss and staying below known instability thresholds whilst keeping the RF system parameters practical.

For the injection upgrade studies a nominal intensity of $8\times10^{13}$ ppp has been assumed, corresponding to ~0.5 MW operation. The effect this increase in beam current has on the longitudinal space charge and associated instabilities is considerably more challenging than on the present machine. Other key aspects of the injection upgrade such as transverse dynamics and injection studies are covered elsewhere [4, 5].

The basic viability of accelerating $8\times10^{13}$ ppp with realistic RF parameters has been reported [6] simulating a dual harmonic idealised, invariant Hofmann-Pedersen [7, 8] distribution created at main magnet field minimum. Two plausible injection schemes have also been presented [6].

In this paper, following further optimisations, three possible longitudinal injection schemes are presented together with simulation results. The implementation of the KSB stability criterion in the longitudinal dynamics code is elaborated and its output compared to results from the present ISIS.

## INJECTION SCHEMES

Several parameters are available to optimise longitudinal painting over injection. These include the flexibility inherent in dual harmonic RF defined by Equation 1, allowing manipulation in phase space with first and second harmonic voltages ($V_{h=2}$, $V_{h=4}$) and the phase between them ($\theta$).

$$V = V_{h=2}\sin\varphi - V_{h=4}\sin(2\varphi+\theta)\,, \qquad (1)$$

where $\varphi$ is the RF phase.



ISBN 978-3-95450-118-2

# HIGH INTENSITY ASPECTS OF J-PARC LINAC INCLUDING RE-COMMISSIONING AFTER EARTHQUAKE

M. Ikegami, K. Futatsukawa, T. Miyao, Y. Liu, KEK/J-PARC, Tokai, Japan
T. Maruta, A. Miura, J. Tamura, JAEA/J-PARC, Tokai, Japan

*Abstract*

In the course of the beam commissioning of J-PARC linac after nine-month shutdown due to an earthquake, we have experienced beam losses which were not seen before the earthquake. One of the main cause for the beam loss was the irregular RF setting for accelerating cavities to avoid multipactor at a cavity, which started to pose difficulty in the nominal operation after the earthquake. In an effort to mitigate the beam loss, we tried a few RF settings, some of which resulted in noticeable beam loss. In this paper, we discuss the particle simulation attempted to reproduce the beam loss with the irregular RF setting, and its comparison with the experimental result.

## INTRODUCTION

We had a magnitude-9.0 earthquake in Tohoku region in Eastern Japan in March 2011. It caused severe damage to J-PARC facilities which forced us to shutdown for nearly nine months [1]. After significant restoration efforts, we started beam operation of J-PARC linac in December 2011 and user operation in January 2012. The linac beam power when we resumed the user operation was 7.2 kW. Then, it is increased to 13.3 kW in March 2012, which is the same as just before the earthquake. While the linac beam operation was restored in terms of the beam power, we have experienced higher beam losses than before the earthquake. Thus, we have been trying to mitigate the beam loss while supporting the user operation.

One of the main causes of the beam loss was multipactor at an accelerating cavity, which started to pose difficulty in the nominal operation after the earthquake. The multipactor forced us to adopt irregular RF setting, which resulted in excess beam losses. After trying a few RF settings, we finally succeeded in suppressing the beam loss to a comparable level to before the earthquake.

The history of the beam start-up after the earthquake was reported in other literatures [2, 3, 4]. Then, we don't reiterate it in this paper. Instead, we discuss in this paper a particle simulation study intended to reproduce the beam loss we experienced in the beam commissioning.

This paper is organized as follows. We start with briefly reviewing the multipactor at an accelerating cavity in the next section. Then, we describe three RF settings we tried to avoid the multipactor in the beam commissioning. After presenting the experimentally observed beam losses, we move to particle simulation. We then try to deduce a picture on the mechanism for the experimentally observed beam loss comparing the experimental and simulation results.

## MULTIPACTOR AT AN RF CAVITY

J-PARC linac consists of a 50-keV negative hydrogen ion source, 3-MeV RFQ (Radio Frequency Quadrupole linac), 50-MeV DTL (Drift Tube Linac), and 181-MeV SDTL (Separate-type DTL) [5]. The multipactor mentioned above is observed in one of SDTL tanks. The SDTL section consists of 30 SDTL tanks with $2\beta\lambda$ inter-tank spacing. Here, $\beta$ and $\lambda$ denote the particle velocity scaled by the speed of light and the RF wavelength, respectively. Each SDTL tank consists of five $\beta$-graded cells, and two neighboring SDTL tanks are driven by a klystron. The relative RF amplitude and phase of the tank pair are supposed to be kept balanced with the low-level RF control system. However, we noticed just before the resumption of beam operation in December 2011 that the fifth tank pair, or SDTL5, shows some unstable behavior. For this tank pair, one of the tanks tends to have arcing, or presumably multipactor, which makes the balance of RF amplitude and phase easily lost. This unstable behavior arises in a certain range of RF amplitude which contains its design amplitude. Although similar behavior has been noticed for SDTL1 to SDTL6 since before the earthquake, it caused no difficulty in operating with the design tank level [6]. Therefore, we suspect that the multipactor in SDTL5 become severer at the earthquake for some reason to cause practical difficulty in the nominal operation.

As we can avoid the multipactor by adopting higher or lower RF amplitude for SDTL5, we adopt 109 % of the design amplitude in starting the user operation in January 2012. However, the unstable band was widened during the beam operation and forced us to increase the operating amplitude to 116 % later. In this paper, we focus on the operation with 116 % amplitude for SDTL5. We don't delve into the details on the multipactor itself. Further detail of the multipactor will be found in the reference [7].

## THREE RF SETTINGS

We here describe three RF settings we tried to avoid multipactor at SDTL5. We assume the RF amplitude of 116 % for SDTL5 in these cases.

### *Case-I: Phase-amplitude Scan Tuning Result*

In setting the RF amplitude and phase for SDTL tanks after the earthquake, it was required for us to perform the phase and amplitude scan tuning [8]. In the tuning, we needed an unusual treatment for SDTL5. Namely, we fixed the amplitude for SDTL5 to be 116 % of the design and performed the phase scan only to find the phase setting to realize the design energy gain. After conducting the tuning

ISBN 978-3-95450-118-2

# BEAM DYNAMICS OF CHINA-ADS LINAC*

Z.H. Li, F. Yan, J.Y. Tang, H.P. Geng, C. Meng, P. Cheng, B. Sun, Z. Guo, IHEP, Beijing, China

*Abstract*

An ADS study program was approved by Chinese Academy of Sciences at 2011, which aims to design and build an ADS demonstration facility with the capability of more than 1000 MW thermal power in about twenty years. The driver linac is defined to be 1.5 GeV in energy, 10 mA in current and in CW operation mode. To meet the extremely high reliability and availability, the linac is designed with much installed margin and fault tolerance. It is composed of two parallel 10-MeV injectors and a main linac. The superconducting acceleration structures are employed except the RFQs. The general considerations and the beam dynamics design of the driver accelerator will be presented.

## INTRODUCTION

China has increased its investment on the nuclear power in the past two decades and this trend is foreseen to be continued in the following decades in order to satisfy the increased energy demands for the economic development. Thus it is more and more urgent to find a solution to transmute the long-lived radioactive wastes produced by the nuclear reactors. A sub-critical system using externally provided additional neutrons is very attractive, it allows maximum transmutation rate while operating in a safe manner. In the beginning 2011, China-ADS project (or C-ADS) was launched in China which will be carried out in three or four phases, with the final goal to develop an ADS demonstration facility with 1000 MW thermal power at 2032. The project is supported financially by the central government and administrated by the Chinese Academy of Sciences. The driver accelerator of 15 MW beam power in the final stage is to be designed and constructed jointly by Institute of High Energy Physics (IHEP) and Institute of Modern Physics (IMP), both under CAS.

Table 1: Specifications for C-ADS Accelerator

| | |
|---|---|
| Energy | 1.5 GeV |
| Current | 10 mA |
| Beam Power | 15 MW |
| Frequency | (162.5)325/650MHz |
| Duty factor | 100% |
| Beam loss | <1 W/m |
| Beam Trips/Year[1] | <25000 1s<t<10s<br><2500 10s<t<5min<br><25 t>5min |

As the key part of the C-ADS facility, the driver accelerator is a CW proton linac of very high beam power. It uses superconducting acceleration structures except the RFQs. The design specifications for the proton beam are shown in Table 1. For the first phase, the project goal is to build a CW proton linac of 50 MeV and 10 mA by about 2015. The first phase itself will be executed progressively in several steps, with the first step to build two 5-MeV test stands of different designs by IHEP and IMP in parallel.

The C-ADS linac of 15 MW in beam power is far beyond the capability of the existing proton linacs. The 10-mA beam current looks not so ambitious compared with the existing pulsed machines, but the required beam loss level of $10^{-8}$ /m at high energy asks for a very delicate dynamics design. Furthermore, the CW operation will give even more difficulties. In order to avoid the risk of thermal problems, superconducting structures are applied from very low energy (3-5 MeV), which will introduce further difficulties in dynamics design. Besides these, the very stringent requirements on beam trips are believed to be potential "show stopper" for the ADS project and need to be considered at the very beginning of the design, and special measures have to be taken to satisfy these requirements.

## DESIGN PHILOSOPHY AND GENERAL LAYOUT

For the C-ADS, the linac has very high beam power and very high reliability that is not possessed by any of the existing linacs. This requires special design strategies to be integrated at the beginning of the design.

### *Fault Tolerant Design [2]*

For an ADS application, any beam trip lasting more than a few seconds will be considered as a major accelerator failure, possibly leading to the reactor core cool-down. Thus, the philosophy prevailing on current pulsed machines to cope with component failures should be reconsidered. In particular, for each failure analysis, the design should look at the ability to either maintain the beam under safe conditions, or to recover the beam through, in less than several seconds. This requirement appears to be highly challenging, given the state-of-the-art in the accelerator reliability. It is clear that suitable design strategies have to be followed early in the conceptual design stage. The main guidelines are: a strong design (which makes extensive use of component derating and proper redundancy) and a high degree of fault tolerance (i.e. the capability to maintain beam operation within nominal conditions under a wide variety of accelerator component faults) by means of local compensation or hot spare.

It is the common knowledge that any main component failure at low energy is difficult to be compensated by adjusting neighbouring elements so that large beam loss will happen in the downstream linac. At the C-ADS, we

* Work supported by NSFC (10875099, 91126003), the China ADS Project (XDA03020000), IHEP special funding (Y0515550U1)
#lizhihui@ihep.ac.cn



ISBN 978-3-95450-118-2

# SIMULATION AND MEASUREMENTS IN HIGH INTENSITY LEBT WITH SPACE CHARGE COMPENSATION

N. Chauvin*, G. Adroit, O. Delferrière, R. Duperrier, Y. Gauthier, R. Gobin, F. Harrault, P.A.P. Nghiem, J.B. Pontier, F. Sénée, O. Tuske, M. Valette, D. Uriot
CEA, IRFU, F-91191 Gif-sur-Yvette, France

*Abstract*

Over the last years, the interest of the international scientific community for high power accelerators in the megawatt range has been increasing. One of the major challenges is to extract and transport the beam while minimizing the emittance growth in the Low Energy Beam Transport (LEBT) line. Consequently, it is crucial to perform precise simulations and cautious design of LEBT. In particular, the beam dynamics calculations have to take into account not only the space charge effects but also the space charge compensation of the beam induced by ionization of the residual gas.

The code SolMaxP has been developed in CEA-Saclay to perform self-consistent calculations taking into account space charge compensation. Extensive beam dynamics simulations have been done with this code to design the IFMIF LEBT (Deuteron beam of 125 mA at 100 keV, cw). The commissioning of the IFMIF injector started a few months ago and emittance measurements of $H^+$ and $D^+$ beams have been done. The first experimental results will be presented and compared to simulation.

## INTRODUCTION

The International Fusion Materials Irradiation Facility will produce a high flux ($10^{18}$n.m$^{-2}$.s$^{-1}$) of 14 MeV neutron dedicated to characterization and study of candidate materials for future fusion reactors. To reach such a challenging goal, a solution based on two high power cw accelerator drivers, each delivering a 125 mA deuteron beam at 40 MeV to a liquid lithium target, is foreseen [1].

In a first phase, called EVEDA (Engineering Validation and Engineering Design Activities), the 125 mA cw/9 MeV deuteron Linear IFMIF Prototype Accelerator (LIPAc) will be constructed, tested and operated at Rokkasho-Mura, in Japan [2]. This accelerator is composed by an ECR ion source, a low energy beam transport (LEBT) line, a RFQ [3], a matching section, a superconducting radio-frequency accelerator (based on Half Wave Resonator cavities), and finally a high energy beam line equipped with a diagnostic plate and a beam dump.

The purpose of the LEBT is to transport the 140 mA/100 keV deuteron beam extracted from the ECR source and to match it for its injection into the RFQ. A previous work [4] showed the beam dynamics simulations that have been achieved to perform the design and the validation of this LEBT. This paper will recall briefly the simulations that have been done and then presents the preliminary experimental results obtained during the IFMIF LEBT commissioning.

* Nicolas.Chauvin@cea.fr

## LOW ENERGY BEAM LINE LAYOUT

### *ECR Ion Source and Extraction System*

The IFMIF ECR source, based on the SILHI design, will operate at 2.45 GHz [5]. The extraction system has been optimized to increase the total beam intensity from 150 mA to 175 mA (in order to meet the required 140 mA $D^+$ , as $D_2^+$ and $D_3^+$ are also produced in the ECR source, see Table 1) and the energy from 95 keV to 100 keV. A four electrode system has been calculated to minimize the beam divergence.

Table 1: Beam Parameters After the Extraction System

| Extracted Species | Intensity (mA) | Emittance ($\pi$ mm.mrad) |
|---|---|---|
| $D^+$ | 141 | 0.064 |
| $D_2^+$ | 26.5 | 0.043 |
| $D_3^+$ | 8.8 | 0.042 |

### *Low Energy Beam Transport Line*

The LEBT is based on a dual solenoid focusing system to transport the beam and to match it into the RFQ. The total length of the beam line, from the plasma electrode to the internal face of the RFQ entrance flange is 2.05 m (see Fig.1). A pumping system and beam diagnostics (Faraday cup, Emittance Measurement Unit (EMU) and four-grid analyser) are inserted between the two solenoids. A regulating valve is also foreseen in order to inject a controlled flux of a specific gas in the beam line.

At the end of the LEBT, a cone with an half-angle of 8° is located just before the RFQ injection. The role of this cone is to allow the injection of the beam of interest ($D^+$) while stopping the other beam species (i.e. $D_2^+$ and $D_3^+$) to prevent their injection into the RFQ, that would cause subsequent beam losses. The cone injection hole is 12 mm diameter. A circular electrode negatively polarized, called

ISBN 978-3-95450-118-2

# BEAM HALO DEFINITIONS AND ITS CONSEQUENCES

P. A. P. Nghiem*, N. Chauvin, W. Simeoni Jr. , D. Uriot
CEA/DSM/IRFU, 91191 Gif-sur-Yvette Cedex, France

*Abstract*

In high-intensity accelerators, much attention is paid to the beam halo: formation, growth, interaction with the beam core, etc. Indeed, beam losses, a critical issue for those high-power accelerators, directly depend on the beam halo behaviour. But in the presence of very strong space-charge forces, the beam distribution takes very different shapes along the accelerator, often very far from any regular distributions, with very varied halo extensions. The difficulty is then to find a general definition of the halo capable of describing any distribution type. This paper proposes a definition of the beam halo, studies its consequences and compares it to the most usual ones. It is an introduction to a discussion session on Beam Halo Definition during the HB2012 workshop.

## INTRODUCTION

In high-intensity accelerators, great importance is given to emittance growth and halo growth. It can even be said that, in case there is no injection into a circular accelerator, the importance of emittance is only due to its suspected connection with halo formation. The latter should therefore be at the centre of every attention. The reason is that halo directly leads to beam losses, which even tiny, cannot be neglected when considering the high bam power (MW class) induced by the high intensity.

Halo is definitely the figure of merit in nowadays high-intensity accelerators. Paradoxically, a concrete, precise and general definition of halo is still missing. Typically, the four following questions have no clear answers:

- During beam design stage or machine operating, it is well known that halo should be minimised. But how much at which part of the beam exactly should be minimised?
- Scrapers are often employed to cut the halo and it is known that halo can grow up downstream more or less quickly. But where is the halo and where is the core? Is this cut not enough or too much? How to quantify the speed of halo re-formation?
- There is a need to develop dedicated beam diagnostics to measure beam halo. But how much and which part of the beam exactly should be measured?
- When failing to know exactly what halo growth is, it is common to consider instead 1 RMS emittance growth. But is there a clear connection, qualitatively or quantitatively, between emittance growth and halo growth?

The answers to these questions may depend on the definition given to halo. This paper considers the existing approaches aiming at defining beam halo, then suggests a concrete approach to qualify beam halo. Finally, the consequences on the above questions are examined.

*phu-anh-phi.nghiem@cea.fr

## THE EXISTING DEFINITIONS

Many attempts have been made to attribute a quantitative definition to beam halo. A special international workshop, HALO'03 [1] has been organised to assess the ways to define and to measure halo, but no consensus has emerged on how to define what halo is. From this workshop however, it is more and more common to characterise halo by comparing the "far" beam centre to "close" beam centre areas of the particle distribution. How "far" or how "close" may be somewhat arbitrary.

It is for example the ratio of beam sizes including in

$$\frac{m\,RMS}{n\,RMS} \quad (1)$$

with n being generally 1 and m between 3 or 5. Another way is to consider the ratio

$$\frac{Emittance\,(x)}{Emittance\,(1RMS)} \quad (2)$$

where x can be between 90% and 100% of the distribution. In the same spirit, a "halo parameter" has been defined as the ratio of nth moments of the distribution

$$\frac{4th\ moment}{2nd\ moment} \quad (3)$$

The latter was first suggested by [2] for a 1-D geometrical space and then extended to a 2-D phase space [3]. The idea was to characterise the kurtosis, a measurement of the difference in the peakedness with a Gaussian distribution. Contrarily to the definitions (1) and (2) which are model independent, (3) involves a dynamical point of view, as such a halo parameter is an invariant of motion in the presence of only linear forces.

The definitions of these types are useful in the sense that they give an idea of the relative importance of the halo. That is why the term of "halo parameter" is more suitable as they are rather abstract quantities that do not aim to give a concrete measurement of the halo itself. They suffer nevertheless from three defaults:

- They presuppose where the core part is and where the halo part is. The first one is presupposed to be 1 RMS or 2nd moment while the second is presupposed to be 3 or 5 rms, or 95% of the beam, or 4th moment.
- The reference distribution is the Gaussian one, which is not free of halo. In high-intensity machines, beam distributions significantly differ from Gaussian one, with a halo tail more or less important, independently to the

ISBN 978-3-95450-118-2

# TEST OF OPTICAL STOCHASTIC COOLING IN FERMILAB*

V. A. Lebedev#, FNAL, Batavia, IL 60510, USA
M. S. Zolotorev, LBNL, Berkeley, CA 94720, USA

*Abstract*

A new 150 MeV electron storage ring is planned to be build at Fermilab. The construction of a new machine pursues two goals a test of highly non-linear integrable optics and a test of optical stochastic cooling (OSC). This paper discusses details of OSC arrangements and choice of major parameters of the cooling scheme. At the first step the cooling will be achieved without optical amplifier (OA). It should introduce the damping rates higher than the cooling rates due to synchrotron radiation. At the second step we plan to use an OA. The passive cooling scheme looks as a promising technique for the LHC luminosity upgrade. Its details are also discussed.

## INTRODUCTION

The stochastic cooling suggested by Simon Van der Meer [1,2] has been successfully used in a number of machines for particle cooling and accumulation. However it is not helpful for cooling of dense bunched beams in proton-(anti)proton colliders. In the case of optimal cooling the maximum damping rate can be estimated as:

$$1/\tau \approx 2W\sigma_s/(NC) \ ,$$

where $W$ is the bandwidth of the system, $N$ is the number of particles in the bunch, $\sigma_s$ is the rms bunch length, and $C$ is the machine circumference. For the LHC proton beam ($\sigma_s = 9$ cm, $C = 26.66$ km) and one octave system band with upper boundary of 8 GHz one obtains $\tau = 12000$ hour. Effective cooling requires damping rates that are higher by at least 3 orders of magnitude. The OSC suggested in Ref. [3] can have a bandwidth of $\sim 10^{14}$ Hz and, thus, suggests a way to achieve required damping rates. The basic principles of the OSC are similar to the normal (microwave) stochastic cooling. The key difference is the use of optical frequencies, which allow an increase of system bandwidth by 4 orders of magnitude.

In the OSC a particle emits e.-m. radiation in the first (pickup) wiggler. Then, the radiation amplified in an OA makes a longitudinal kick to the particle in the second (kicker) wiggler as shown in Figure 1. Further we will call these wigglers as the pickup and the kicker. A magnetic chicane is used to make space for an OA and to bring the particle and the radiation together in the kicker wiggler. In further consideration we assume that the path lengths of particle and radiation are adjusted so that the relative particle momentum change is equal to:

$$\delta p/p = -\kappa \sin(k\,\Delta s) \ . \qquad (1)$$

Here $k = 2\pi/\lambda$ is the radiation wave number, and $\Delta s$ is the particle displacement on the way from pickup to kicker relative to the reference particle which obtains zero kick:

$$\Delta s = M_{51}x + M_{52}\theta_x + M_{56}(\Delta p/p) \ . \qquad (2)$$

Here $M_{5n}$ are the elements of 6x6 transfer matrix from pickup to kicker, $x$, $\theta_x$ and $\Delta p/p$ are the particle coordinate, angle and relative momentum deviation in the pickup center.

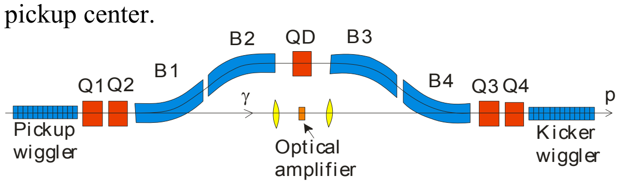


Figure 1: OSC schematic.

For small amplitude oscillations the horizontal and vertical cooling rates are [4]:

$$\begin{bmatrix}\lambda_x \\ \lambda_s\end{bmatrix} = \frac{k\kappa}{2}\begin{bmatrix} M_{56} - C\eta_{pk} \\ C\eta_{pk}\end{bmatrix} , \qquad (3)$$

where $\eta_{pk} = (M_{51}D_p + M_{52}D'_p + M_{56})/C$ is the partial momentum compaction determined so that for a particle without betatron oscillations and with momentum deviation $\Delta p/p$ the longitudinal displacement relative to the reference particle on the way from pickup to kicker is equal to $C\eta_{pk}\,\Delta p/p$, and $D$ and $D'$ are the dispersion and its derivative. Here we also assume that there is no $x$-$y$ coupling. Introduction of $x$-$y$ coupling outside the cooling area allows redistribution of the horizontal damping rate into both transverse planes. The sum of damping rates, $\Sigma\lambda_n = k\kappa M_{56}/2$, does not depend on the beam optics outside of the cooling chicane.

An increase of betatron and synchrotron amplitudes results in a decrease of damping rates [4]:

$$\begin{aligned} \lambda_x(a_x,a_s) &= F_x(a_x,a_s)\lambda_x \ , \\ \lambda_s(a_x,a_s) &= F_s(a_x,a_s)\lambda_s \ , \end{aligned} \qquad (4)$$

where the fudge factors are:

$$\begin{aligned} F_x(a_x,a_s) &= 2J_0(a_s)J_1(a_x)/a_x \ , \\ F_s(a_x,a_s) &= 2J_0(a_x)J_1(a_s)/a_s \ , \end{aligned} \qquad (5)$$

and $a_x$ and $a_s$ are the amplitudes of longitudinal particle motion due to betatron and synchrotron oscillations expressed in the units of e.-m. wave phase:

$$\begin{aligned} a_x &= k\sqrt{\varepsilon_1\left(\beta_p M_{51}{}^2 - 2\alpha_p M_{51}M_{52} + \left(1+\alpha_p{}^2\right)M_{52}{}^2\right)} , \\ a_p &= kC\left|\eta_{pk}\right|(\Delta p/p)_{\max} \ . \end{aligned} \qquad (6)$$

Here $\varepsilon_1$ is the Courant-Snyder invariant of a particle, and $(\Delta p/p)_{\max}$ is the particle maximum momentum deviation. As one can see from Eqs. (4) and (5) a damping rate changes its sign if any of amplitudes exceeds the first root of the Bessel function $J_0(x)$, $a_{x,}a_s > \mu_0 \approx 2.405$.

The following conclusions can be drawn from Eqs. (3) and (6). $M_{56}$ depends only on focusing inside the chicane, while $\eta_{pk}$ additionally depends on the dispersion at the

*Work supported by Fermi Research Alliance, LLC, under Contract No. DE-AC02-07CH11359 with the United States Dep. of Energy
#val@fnal.gov



ISBN 978-3-95450-118-2

# MEASUEMENT OF OPTICS ERRORS AND SPACE CHARGE EFFECTS

K. Ohmi, Y. Sato, J. Takano, KEK, Tsukuba, Ibaraki, Japan
S. Hatakeyama, JAEA, Tokai, Ibaraki, Japan

*Abstract*

Emittance growth and beam loss due to the space charge force are enhanced by errors of the lattice. Nonlinearities of the space charge force and lattice components are integrated with Twiss and x-y coupling parameters into one turn map. Twiss and x-y coupling parameters are measureable quantities. We study space charge effects based on the measured Twiss-coupling parameters.

## INTRODUCTION

Emittance growth and beam loss are caused by chaotic behavior near nonlinear resonances induced by space charge force and nonlinear accelerator components. One turn map including the space charge and the nonlinear components characterizes the nonlinear property for long term behavior. The space charge force is incorporated into one turn map by integrating with a finite propagation step. The one turn map is constructed by connecting the nonlinear transfer maps, the nonlinear accelerator components and space charge force, with linear transformation (represented by transfer matrix) between them.

The beam shape, which characterizes the space charge force, is determined by one turn map. The one turn map is determined self-consistently by the space charge map with the beam shape.

The linear optics parameters are measurable, where they are for zero intensity. Transfer matrix and revolution matrix is reconstructed by the measured optics parameters. One turn map is constructed with the measured optics parameters. The one turn map based on measured optics is deviated from the design one. Simulation using the map gives worse emittance growth and beam loss than design one. The degradation should appear in actual accelerators. The beam loss caused by the optics errors can be recovered by an optics correction.

In this paper, we discuss measurement of linear optics parameters. One turn map is constructed by the measured linear optics parameters, where the strength of nonlinear components is assumed to be correct. Simulations using the one turn map have been performed for J-PARC MR. Some results, which is preliminary at present, are shown.

## LATTICE TRANSFORMATION AND SPACE CHARGE FORCE

One turn map ($\mathcal{M}$) is defined how dynamical variables, $\boldsymbol{x}(s) = (x, p_x, y, p_y, z, \delta)^t$, are tarnsferred in a revolution,

$$\boldsymbol{x}(s + C) = \mathcal{M}(s)\boldsymbol{x}(s), \tag{1}$$

where $C$ is the circumference. The transverse momentum is normalized by design momentum $p_0$, and the longitudinal variables are defined by arrival time and momentum deviation as $z = v(t_0 - t)$ $\delta = \Delta p/p_0$, respectively. One turn map including the space charge force is expressed as follows,

$$\mathcal{M}(s) = \prod_{i=0}^{N-1} \mathcal{M}_0(s_{i+1}, s_i)e^{-:\Phi(s_i):}, \tag{2}$$

where $\mathcal{M}(s_{i+1}, s_i)$ is nonlinear transformation from $s_i$ to $s_{i+1}$. $\Phi(s_i)$, which is the space charge potential, is given by solving Poisson equation with the beam distribution at $s_i$.

The expression using the symbol $:\Phi:$ is

$$e^{-:\Phi(s_i):}p_\ell = p_\ell - \frac{\partial \Phi(s_i)}{\partial x_\ell}. \tag{3}$$

where $p_\ell = p_x, p_y$ or $\delta$, and $x_\ell = x, y$ or $z$. The integration step ($\Delta s = s_{i+1} - s_i$) should be chosen $\Delta s \ll \beta$, since betatron phase advance for $\Delta s$ should be small ($\ll 1$).

One turn map including only lattice nonlinear components is decomposed by nonlinear map of the components and transfer matrix between the components as follows,

$$\mathcal{M}_0(s) = \prod_{i=0}^{N_{nl}-1} M_0^{-1}(s_{i+1}, s_i)e^{-:H_{nl}(s_i):}. \tag{4}$$

where $M(s_{i+1}, s_i)$ is transfer matrix from $s_i$ to $s_{i+1}$, and

$$e^{-:H_{nl}(s_i):}p_\ell = p_\ell - \frac{\partial H_{nl}(s_i)}{\partial x_\ell}. \tag{5}$$

For example, $H_{nl}$ for sextupole magnet is expressed by

$$H_{nl}(s_i) = \frac{K_2(s_i)}{6}(x^3 - 3xy^2) \qquad K_2 = \frac{eB"}{p_0} \tag{6}$$

One turn map including space charge force (Eq. 2) is expressed by the nonlinear transformation and linear transfer matrix as follows,

$$\mathcal{M}(s) = \prod_{i=0}^{N-1} M_0(s_{i+1}, s_i)e^{-:H_I(s_i):}, \tag{7}$$

where $N = N_{nl} + N_{sc}$, and $H_I = \Phi$ or $H_{nl}$. Simulation codes for space charge effects have been developed based on the description in Eq. 7 [1].

ISBN 978-3-95450-118-2

# SPACE CHARGE EFFECTS IN THE NICA COLLIDER RINGS

O. Kozlov, A.Eliseev, S.Kostromin, I.Meshkov, A.Sidorin, A.Smirnov, G.Trubnikov,
JINR, Dubna, Russia
T.Katayama, GSI, Darmstadt, Germany

*Abstract*

The **N**uclotron-based **I**on **C**ollider f**A**cility (NICA) is a new accelerator complex being constructed at JINR aimed to provide experiments with colliding heavy ions up to Au for experimental study of hot and dense strongly interacting baryonic matter and search for possible signs of the mixed phase and critical endpoint in the centre-of- mass energy range $\sqrt{s_{NN}}$ = 4-11 GeV. Two beam cooling systems – stochastic and electron will be used in the collider rings. Parameters of cooling systems, proposed scenario of operation and particular features of their design intended to achieve required average luminosity of the order of $10^{27}$cm$^{-2}$s$^{-1}$at high energies are presented in this report.

## INTRODUCTION

The goal of the NICA project is construction at JINR of the new accelerator facility that consist of [1]: cryogenic heavy ion source of Electron String type (ESIS) with 6T solenoid; source of polarized protons and deuterons, the existing linac LU-20 of Alvaretz type (energy up to 5 MeV/u); a new heavy ion linear accelerators RFQ-DTL (3 MeV/u); a new 600 MeV/u superconducting Booster-synchrotron placed inside the decommissioned Synchrophasotron yoke; the existing and modernized proton and heavy ion synchrotron Nuclotron (4.5 GeV/u maximum kinetic energy for ions with Z/A=1/3); the new system of beam transfer channels, and two new superconducting storage rings of the collider.

The facility will provide ion-ion (1-4.5 GeV/u), ion-proton collisions and collisions of polarized pp (5-12.6 GeV) and polarized dd (2-5.8 GeV) beams. The collider will have two interaction points. The Multi Purpose Detector (MPD) will be used for the first IP, the Spin Physics Detector will be used for the second one.

Collider operation at fixed energy without acceleration of the injected from the Nuclotron beam is considered. Beam storage at some optimum energy and slow acceleration in the collider (at field ramp rate < 1 T/s) is presumed as a reserve option. The maximum energy of the experiment is determined by the Nuclotron maximum magnetic rigidity of 45 T·m. The main purpose of the NICA facility is to provide the collider experiments with heavy ions (e.g. Au) at average luminosity of to $1{\cdot}10^{27}$ cm$^{-2}$ s$^{-1}$ in the maximally wide energy range up to 4.5 GeV/u.

Therefore we discuss only heavy ion mode of the facility operation and $^{197}$Au$^{+79}$ ions as the reference particles. The space charge effects in the high intensity ion beams are considered. The corresponding beam cooling technique is proposed for collider rings to achieve the required beam parameters.

## COLLIDER LUMINOSITY

Two collider rings have the maximum magnetic rigidity of 45 Tm corresponding to the maximum rigidity of Nuclotron. The rings are vertically separated (32 cm between axes) and use "twin aperture" superconducting magnets (dipole and quadrupoles) [2] except the common Interaction Region part. The maximum field in dipoles of 1.8 T and maximum gradient in quadrupoles of 23 T/m are chosen to avoid the saturation effects in iron yokes. Each ring consists of two bending arcs and two long straight sections representing the racetrack shape with the circumference of 503 m that is exactly two Nuclotron sizes. Collider ring optics is based on FODO periodic cell in arc, 12 cells per each arc. FODO optics shows its more preference in comparison with other optics from the view point of IBS rates, stochastic cooling time reserve for Intra Beam Scattering (IBS) suppression, more convenient scheme for beam injection [3]. In Fig. 1 the assembly of one ring is shown for ion mode of operation, where the layout of stochastic cooling system for that ring and electron cooling, RF systems for both rings are pictured.

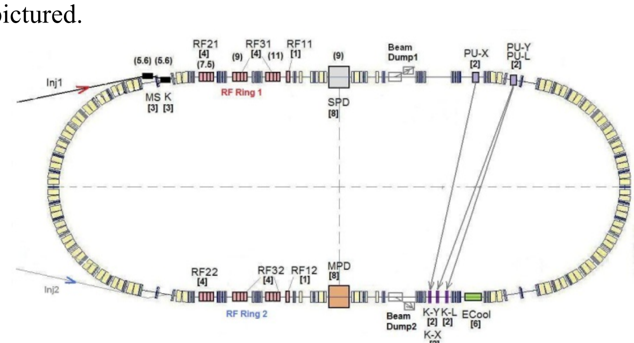


Figure 1: Collider ring composition.

The collider operation in luminosity range of $10^{26}\div10^{27}$ cm$^{-2}$ s$^{-1}$ allows to perform experiments to measure all hadrons comprising multi-strange hyperons, their phase-space distributions and collective flows.

For identical colliding bunches of round shape cross-section the peak luminosity can be written as

$$L = \frac{N_i}{4\pi\varepsilon\beta^*} F_{coll} f_{HG}(\sigma_s, \beta^*), \tag{1}$$



ISBN 978-3-95450-118-2

# BROAD-BAND TRANSVERSE FEEDBACK AGAINST E-CLOUD OR TMCI: PLAN AND STATUS*

C. Rivetta†, J. Cesaratto, J. Fox, M. Pivi, K. Pollak, O. Turgut, S. Uemura, SLAC, CA 94025, USA
W. Hofle, K. Li, CERN, Geneva, Switzerland

*Abstract*

The feedback control of intra-bunch instabilities driven by electron-clouds or strong head-tail coupling (Transverse mode coupled instabilities, TMCI) requires bandwidth sufficient to sense the vertical position and apply multiple corrections within a nanosecond-scale bunch. These requirements impose challenges and limits in the design and implementation of the feedback system. To develop the feedback control prototype, different research areas have been pursued to model and identify the bunch dynamics, design the feedback control and implement the GigaHertz bandwidth hardware. This paper presents those Research & Development lines and reports on the progress as it stands today. It presents preliminary results of feedback systems stabilizing the transverse intra-bunch motion, based on macroparticle simulation codes (CMAD / HeadTail) and measurement results of the beam motion when it is driven by particular excitation signals.

## INTRODUCTION

Intrabunch instabilities induced by electron clouds and strong head-tail interactions are one of the limiting factors to reach the maximum beam currents in the SPS and LHC rings[1, 2]. Different schemes to control both electron cloud instabilities (ECI) and transverse mode coupling instabilities (TMCI) are under investigation to achieve the required High Luminosity in LHC. The effect of coating the SPS vacuum pipes with low secondary electron yield materials has been studied to effectively suppress the electron cloud build-up, and mitigate intrabunch ECI. CERN is proposing a plan to coat large part of the SPS and LHC chambers in order to mitigate electron cloud instabilities. Continuous testing of the limitations of these techniques and the design of the necessary infrastructure to apply the coating are currently conducted at CERN [3]. These techniques cannot mitigate TMCI and research is conducted at CERN to lower the transition energy in the SPS and thus increasing the synchrotron tune which has shown to increase the instability threshold for TMCI[2, 4].

Feedback techniques can stabilize bunch instabilities induced not only by electron clouds but also induced by strong head-tail interactions (TMCI). Complementary to the plan previously described, the US LHC Accelerator Research Program (LARP) is supporting a collaboration between US Labs and CERN to study the viability of controlling intrabunch instabilities using feedback control techniques. A collaboration among SLAC / LBNL / CERN (under the DOE LARP program) started evaluating the limitations of this technique to mitigate both instabilities and other possible head-tail distortions in bunches [5, 6].

The application of feedback control to stabilize the bunch is challenging because it requires a bandwidth sufficient to sense the transverse position and apply correcting fields to multiple sections of a nanosecond-scale bunch. These requirements impose technology challenges and limits in the design [7]. Additionally, the intra-bunch dynamics is more challenging than the beam dynamics involving the interaction between bunches. The collaboration has defined different interdependent working lines to study the problem, to design a feedback control channel and to develop the hardware of a control system prototype to prove principles and evaluate the limitations of this technique by stabilizing a few bunches in the CERN SPS machine. This paper gives an overview of the research areas and plans, measurements and results of present studies, and goals and future directions.

## RESEARCH & DEVELOPMENT - GOALS

A CERN - US collaboration has been working to mitigate via GigaHertz bandwidth feedback systems electron clouds, TMCI, and other intra-bunch distortions and instabilities at SPS and LHC. The near term goal for this ECI/TMCI feedback is to analyze and define design techniques for the system, study the limitations of the feedback technique to mitigate those instabilities, and build the hardware of a minimum prototype to control a few bunches and measure the limiting performance. the design of a practical prototype system capable of controlling a full SPS fill is a future project based on the results of this first stage.

The collaboration has defined different working lines that involve:

1. Development of reduced mathematical models of the bunch dynamics interacting with electron clouds and machine impedances. Identification of those reduced models based on machine measurements. Design of control feedback algorithms based on the reduced models.

2. Inclusion of realistic feedback models in advanced multi-particle simulation codes to test the models, possible feedback designs and diagnostic tools.

* Work supported by the U.S. Department of Energy under contract DE-AC02-76SF00515 and the US LHC Accelerator Research Program (LARP).

† rivetta@slac.stanford.edu

ISBN 978-3-95450-118-2

# PROTON BEAM INTER-BUNCH EXTINCTION AND EXTINCTION MONITORING FOR THE MU2E EXPERIMENT*

E.J. Prebys, Fermilab, Batavia, IL 60510, USA

*Abstract*

The goal of the Mu2e experiment at Fermilab is the search for the conversion of a muon into an electron in the field of a nucleus, with a precision roughly four orders of magnitude better than the current limit. The experiment requires a beam consisting of short (≈200 ns FW) bunches of protons separated by roughly 1.7 $\mu$sec. Because the most significant backgrounds are prompt with respect to the arrival of the protons, out of time beam must be suppressed at a level of at least $10^{-10}$ relative to in time beam. The removal of out of time beam is known as "extinction". We will discuss the likely sources of out of time beam and the steps we plan to take to remove it. In addition, two possible techniques for monitoring extinction will be presented.

## MOTIVATION

The goal of the Mu2e experiment [1] is to search for the conversion into an electron of a muon which has been captured by a nucleus ($\mu N \rightarrow eN$). This is related to the search for $\mu \rightarrow e\gamma$, but is sensitive to a broader range of physics.

A key component of the experimental technique is the proton beam structure. The beam consists of short (≈200 ns FW) proton bunches with 8 GeV kinetic energy. These strike a production target, producing muons which are in turn transported and captured on a secondary target. The pulses are separated by approximately 1.7 $\mu$s, during which time the captured muons either decay normally or *potentially* convert into electrons. The most important background comes from the radiative capture of pions, which are prompt with respect to the primary proton. To suppress this background, it's vital that the interval between the bunches be free of protons at a level of at least $10^{-10}$ relative to the beam in the bunches [2]. Some of this suppression will come from the method used for generating the bunches, but active suppression in the transport line should be designed for an additional suppression factor of at least $10^{-7}$.

## BEAM DELIVERY SCHEME

The details of the beam delivery scheme are described elsewhere [3], and Fig. 1 shows the relavent components of the Fermilab accelerator complex. A "batch" of approximately $4 \times 10^{12}$ protons is accelerated to 8 GeV kinetic energy in the Fermilab Booster and injected into the Recycler permanent magnet storage ring. There, a 2.5 MHz RF system splits the batch into four bunches of $10^{12}$ protons each. These are transferred one at a time to the Delivery Ring (formerly the Antiproton Accumulator Ring). Each bunch is resonantly extracted, forming a chain of $3 \times 10^7$ proton bunches, separated by the 1.7 $\mu$sec period of the Delivery Ring.

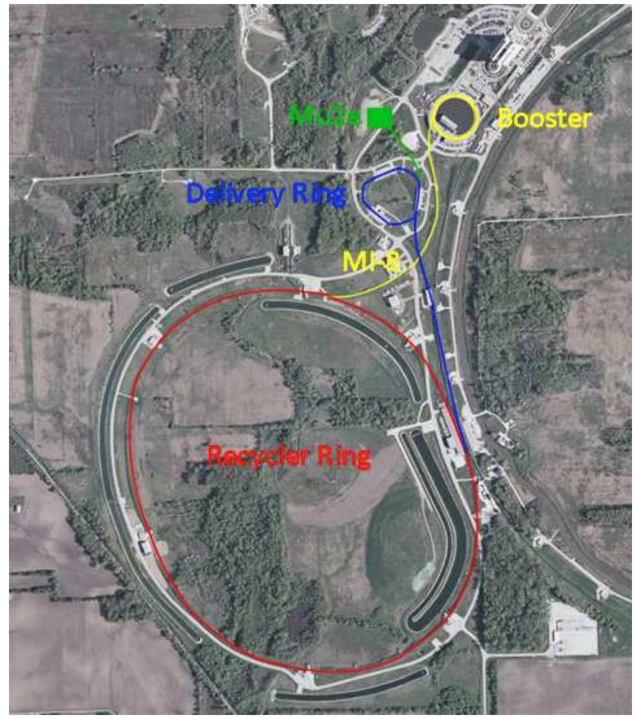


Figure 1: The elements of the Fermilab complex used for the Mu2e experiment. Beam is transported from the Booster to the Recycler to the Delivery Ring (formerly the Antiproton Accumulator). The experiment itself will be built in a new detector hall.

The average beam intensity will be 8 kW or $2 \times 10^{16}$ protons/hour. At that rate, it will take approximately three years to collect $3.6 \times 10^{20}$ protons on target, the nominal data set for the experiment.

## IN RING EXTINCTION

Our goal is to maintain an extinction level of $10^{-5}$ or better for the beam which is extracted from the Delivery Ring. The transfer scheme described above insures that bunches going into the Delivery Ring will have at least this level of extinction, and the concern is that beam will leak out of time during the slow extraction process. The mechanism for protons to drift out of time involves changes in energy that cause particles to migrate to the boundaries of the bucket, or to leak out of the bucket entirely.

* Work supported by the United States Department of Energy under Contract No. DE-AC02-07CH11359



ISBN 978-3-95450-118-2

# SRF TECHNOLOGY CHALLENGE AND DEVELOPMENT

A. Facco#, INFN-Laboratori Nazionali di Legnaro, I-35020 Legnaro, Padova, Italy
Facility for Rare Isotope Beams (FRIB), Michigan State University, East Lansing, MI 48824 USA

*Abstract*

SRF technology for particle accelerators is in continuous evolution, providing a large variety of high gradient- low loss resonators with large apertures, suitable for many different beam current and energy regimes. Recent development was aiming not only at highest gradient and Q but also at improving field quality, reliability and cost reduction for large production. The SRF R&D effort, once concentrated mostly in the high energy electron machines, is increasingly focused to heavy ion linacs, energy recovery linacs and also to cavities for special applications. A concise overview of the present state of the art will be given, with emphasis to very recent publications.

## INTRODUCTION

Superconducting (SC) technology is nowadays the first choice for large accelerators, after a development lasting several decades and still ongoing [1][2][3]. Well known advantages over normal-conducting (NC) one are: low rf losses, leading to energy savings, reduced rf system cost, possibility of cw or long pulse operation at high gradient; large beam aperture, leading to low beam losses, low wakefields, low beam impedance for Higher Order Modes (HOM). Moreover, some new applications like Energy Recovery Linacs (ERL [4]) would not be possible without SC technology. Of course there is a price to pay: high quality factor Q reduces the cavity rf bandwidth, making it difficult to provide reliable phase- and amplitude-lock; HOMs have a long lifetime and must be damped with additional couplers; SC operation makes cavities more prone to quench due to NC transition of even a small area, and make multipacting (MP) problems more severe; SC technology implies the use of more expensive materials, more strict cleanliness and vacuum requirements; cryogenic cooling technology is technically more difficult and more expensive than water cooling. However, due to high gradient and unique capabilities, the overall construction and operation cost of SC technology can be lower than NC one in many applications, becoming the main one in present large accelerator projects.

The goal of SC cavity development is to produce close-to-ideal resonators characteristics:

- High gradient, up to the fundamental limits of their SC materials;
- High Q in the desired resonant mode (only);
- High shunt impedance for the desired resonant mode (only);
- No multipacting;
- Stable resonant frequency determined only by the tuner position;
- Ideal axially symmetric field distribution (or planar for deflecting cavities);
- Possibility of coupling a large amount of rf power without affecting the resonator properties.

R&D on SC resonators is pushing not only for high gradient and Q, but also for overall efficiency, beam quality, reliability and low cost. Activities are involving numerous laboratories and institutions, and the impressive progress reached so far is moving the new accelerator specifications to higher and higher levels. However, there is still way to go to reach ultimate performance and there are still physical aspects which have not yet been fully understood and which are subject of an active and productive research.

## MAIN RESONATOR TYPES IN USE

The evolution of SC resonators has selected a few main resonators types, finally excluding some of the early successful types, like spiral and split ring ones. Development of new geometries, or the use of old geometries for new applications, is still ongoing. R&D, initially focused mostly on cavities for high energy electron machines, is now devoted in a large part also to low beta cavities for ion linacs, which performance (normalized to the different cavity parameters) is steadily approaching the ones of elliptical cavities.

The main resonator geometries in use for particle acceleration can be classified as follows (a good introductory description can be found in [5][6]):

- Elliptical cavities ($\sim 0.6 \leq \beta \leq 1$) widely used in high beta machines, both linear or circular, for electron and ions;
- Quarter-wave resonators (QWR, $\sim 0.02 \leq \beta \leq 0.16$), with 2 or 4 gap, used in several low beta ion linacs in operation and in new projects;
- Half-Wave resonators (HWR, $\sim 0.09 \leq \beta \leq 0.5$), of Coaxial or Spoke type. Until now, only a few coaxial HWRs (and no Spoke) are in operation, but hundreds of such cavities are going to be installed in several new ion linac projects;
- CH resonators ($\sim 0.02 \leq \beta \leq 1$), multigap Spoke cavities widely studied and prototyped, not yet in operation but proposed in several projects too. $\beta=1$ multi-spoke have been recently proposed also for electron acceleration [25].

It should be noted that other, less common types of resonators are presently in use:

*facco@lnl.infn.it



ISBN 978-3-95450-118-2

# SRF CAVITY RESEARCH FOR PROJECT X

Robert Kephart Fermilab, Batavia, IL 60510, USA
for the Project X Collaboration

*Abstract*

Project X is a new SRF linac based multi-MW class proton source proposed for construction at Fermilab. It consists of a 3 MW, 1 mA, CW H$^-$ SRF linac that feeds an Intensity Frontier Physics program and a 3-8 GeV pulsed linac that accelerates ~4% of the output of the CW linac for injection into the Fermilab Main Injector synchrotron. The Main Injector then provides an additional 2 MW of beam power at 60-120 GeV in support of a world-class long baseline neutrino program. The project has chosen operating frequencies that are sub-harmonics of 1.3 GHz and is developing 6 separate Superconducting Radio Frequency (SRF) cavity designs for acceleration of H$^-$ particles with various velocities. An R&D program is in progress to develop these cavities, the associated cryomodules, and the required fabrication and test infrastructure. A status and progress report on this R&D program is presented.

## PROJECT X GOALS

Project X is being developed to meet the requirements described in strategic plans developed by Fermilab and HEPAP [1, 2]. Design goals are based on three principal physics goals defined within these strategic plans:

- A neutrino beam for long baseline neutrino oscillation experiments. The desired beam power is in excess of 2 MW, available at any energy over the range 60-120 GeV.
- High intensity, low energy proton beams for kaon, muon, and nuclei based precision experiments. The desired beam power is in excess of several 100 kW per experiment, in the energy range 1-8 GeV. It is essential that the delivered beams be available with a variety of duty factors and bunch configurations and that the program can operate simultaneously with the neutrino program.
- A path toward a muon source for a possible future Neutrino Factory and/or a Muon Collider. This requires an upgrade potential to ~4 MW of beam power in the energy range 5-15 GeV, and the ability to deliver this beam in intense pulses.

## PROJECT X REFERENCE DESIGN

A schematic of the Project X Reference Design [3, 4] is shown in Fig 1. The design is based on a 3 GeV continuous wave (CW), superconducting H$^-$ ion linac followed by a 3-8 GeV superconducting (SC) linac that is used to accelerate a portion of the beam to the injection energy of the existing Fermilab Main Injector synchrotron. The 3 MW, CW linac operates with an average current of 1 mA, but with peak currents as high as 5 mA for times less than the ~ 1 μsec required to extract <<1% of the stored energy of the SC cavities. When combined with a broad band chopper and RF separation cavities, this permits beam intensities, pulse duration, and repetition rates to be tailored to a wide range of rare decay experiments. Provisions will be included in the design of the first 1 GeV of the CW linac to accelerate 2 mA which will permit generation of as much as 1 MW of beam power at 1 GeV to support a future low energy nuclear physics or materials irradiation program. Couplers for the CW SRF cavities are designed for average currents as high as 5 mA to support future machine upgrades. Approximately 4% of the 3 GeV CW linac beam power is diverted to the pulsed linac for acceleration to 8 GeV. This pulsed linac operates with 4.3% duty factor and sends beam into the existing 8 GeV fixed energy Recycler Ring via many turn injection. The 8-GeV linac also services a separate 8 GeV Physics program. When sufficient beam is accumulated in the Recycler, it is transferred by single turn injection into the existing Main Injector ring and accelerated to 60-120 GeV before extraction to serve the long baseline neutrino program.

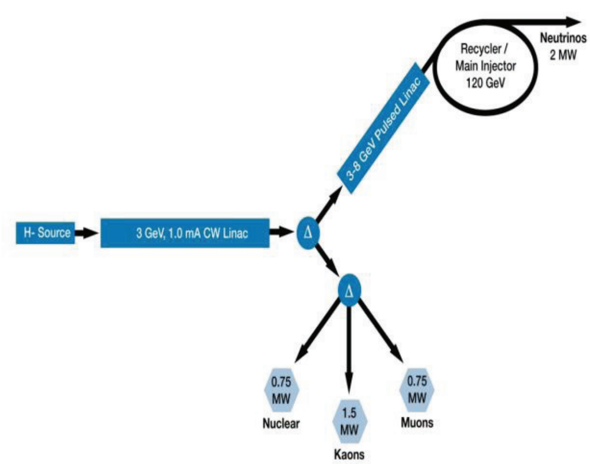


Figure 1: Project X schematic layout.

The machine parameters for the Project X reference design are shown in Table 1. Key to the broad physics reach of the planned experimental program is that large beam powers can be delivered simultaneously to the 1 GeV, 3 GeV, 8 GeV, and 60-120 GeV programs. Moreover, the planned broadband chopper at 2.1 MeV and RF selection will enable a variety of bunch patterns to be delivered simultaneously to a broad program of rare decay experiments.

ISBN 978-3-95450-118-2

# BEAM DYNAMICS STUDIES OF H- BEAM CHOPPING IN A LEBT FOR PROJECT X*

Qing Ji#, David Grote, John Staples, Thomas Schenkel, Andrew Lambert, and Derun Li
Lawrence Berkeley National Laboratory, Berkeley, CA 94720, USA

*Abstract*

Project X is proposed as a high intensity proton facility at Fermilab to support a world-leading program in neutrino and flavor physics over the next several decades. The front-end consists of an $H^-$ ion source, low-energy beam transport (LEBT), and 162.5 MHz CW Radio-Frequency-Quadrupole (RFQ) accelerator. The LEBT design, currently under study at LBNL, would comprise two solenoids, a dipole magnet and a chopper. The LEBT chopper is designed to achieve 1 MHz beam chopping of a partially neutralized 30 keV, 5 mA H- beam. Preliminary simulation studies show that chopping the beam before the second solenoid is more efficient in terms of chopper bias voltages. However, the space charge neutralization will be lost along the beam after the chopper and through the second solenoid. A beam dynamics study, using WARP 3D (a Particle-in-cell simulation code), has been carried out to investigate both the time dependence of the partial neutralization in the segment after the chopper, as well as the emittance growth. Beam emittances have been measured at various chopping repetition rates. The experimental results can be used to benchmark future transport simulations.

## INTRODUCTION

Project X is a multi-functional high intensity proton facility being proposed by Fermilab to support the intensity frontier of future high energy physics programs in the US [1]. As a critical centrepiece of the technology development R&D program toward the success of Project X, Project X Injector Experiment (PXIE) is aimed at studying, building and validating the concept for the Project X front-end, thereby minimizing a primary technical risk element within the reference design. The PXIE system will have a DC $H^-$ ion source (up to 10 mA cw $H^-$ production), a solenoid-based low energy beam transport (LEBT) system, a 162.5-MHz 2.1-MeV CW radio-frequency quadruple (RFQ), MEBT with wideband choppers and two SC cryomodules to accelerate beam to 30 MeV.

Solenoid-based LEBTs do not spark, can withstand uncontrolled beam losses, and transport high current, space-charge neutralized ion beams [2]. But solenoid-based LEBTs are typically longer then electrostatic LEBTs. When the beam is chopped, e.g. at MHz frequencies, the space charge neutralization will be partially lost along the chopper, which causes beam emittance growth and mismatch into the RFQ and these detrimental effects are aggravated for longer LEBTs.. Hence, it is crucial to understand the time- dependent beam dynamics, in particular beam matching into the RFQ after the LEBT chopper where the beam transitions from nearly neutralized to un-neutralized.

WARP 3D is a particle-in-cell code, developed to achieve end-to-end 3D self-consistent time-dependent simulations of beams [3-5]. The WARP code includes a variety of physical models that make it useful for a broad range of research in plasma physics and computational electrodynamics. It can model acceleration, focusing and compression along accelerators, particle loss at walls, particle interaction with desorbed gas and electrons, neutralization from plasma etc. We used WARP 3D to study beam dynamics in the PXIE LEBT and chopper.

## ION SOURCE AND LEBT

### *H- Ion Source*

A filament-discharge $H^-$ ion source was chosen as the PXIE baseline ion source. The ion source has been tested and confirmed to deliver 10 mA DC $H^-$ beam without using any Cs [6]. The normalized rms emittance for the 10 mA beam was measured to be less than 0.2 π mm mrad [7]. As the filament is a consumable component in the ion source, there is a limited time of operation before filament replacement is necessary. The filament lifetimes are approximately 350 and 500 hours for 5 mA and 10 mA operating levels, respectively. A LEBT design with two ion sources and a switching magnet has been proposed to significantly shorten the beam downtime due to ion source service cycles.

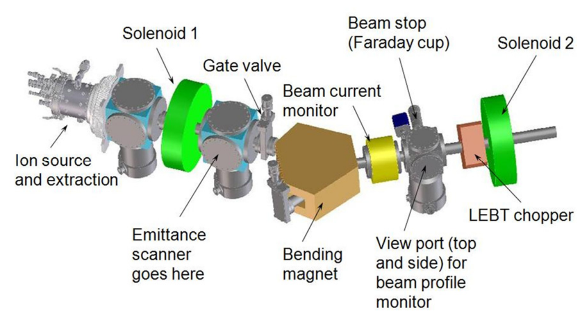


Figure 1: Schematic drawing of a two-solenoid LEBT proposed to PXIE.

### *LEBT*

In Figure 1 we show a LEBT beamline (approximately 1.3 meters long), consisting of a two-solenoid magnetic lens system and chopper, which is being evaluated for

*Work supported by the Office of Science, Department of Energy under the contract number DE-AC02-05CH11231.
#qji@lbl.gov



ISBN 978-3-95450-118-2

# INTENSE HIGH CHARGE STATE HEAVY ION BEAM PRODUCTION FOR THE ADVANCED ACCELERATORS[#]

L. Sun, Institute of Modern Physics, CAS, 509 Nanchang Rd., Lanzhou 730000, China

*Abstract*

Modern advanced heavy ion beam accelerators have strong needs for either dc or pulsed intense high charge state heavy ion beams, such as dc beams for FRIB project, SPIRAL2 project, HIRFL/IMP facility, RIBF/RIKEN facility etc., and pulsed beams for RHIC, LHC, FAIR project. After decades' development, only several typical ion sources have found their applications in these accelerators, i.e. Electron Beam Ion Source (EBIS), Laser Ion Source (LIS) and Electron Cyclotron Resonance Ion Source (ECRIS). This paper gives a general review of the advantages and limitations of these three types of ion source with their latest development and performance.

## INTRODUCTION

Modern particle physics, nuclear physics and high energy physics and medical and industrial applications as well are the driving force for the fast development of heavy ion accelerators, such as FRIB project, SPIRAL2 project, HIRFL facility, RIBF project, RHIC, LHC, FAIR and etc. The preinjectors for those accelerator facilities are essentially important. Higher Q/M or charge state Q from an ion source makes the downstream accelerators more compact and less costly. High Charge state Ion (HCI) beam at the preinjector is delivered from a HCI source. But because of the capacity and characteristics of an ion source is inherent, the choice of ion beam charge state is a trade-off between ion beam intensity and charge state. Therefore, the choice of the ion source is also strongly depending on the accelerator needs, for instance, EBIS is the ion source solution to RHIC preinjector [1], and ECRIS is the only choice for FRIB project [2]. Before any discussion on ion source technology, let us recall the physics behind the HCI production with an ion source. Ions production in an ion source is realized by energetic electron impact with neutrals. Atomics physics reveals that the probability of the producing multiply charged ions by a single electron impact falls off rapidly with increasing ion charge state Q. Therefore the only efficient way for the production of HCIs is by means of successive ionization or step by step striping. Then we have to increase τ the exposure time of the ions to a cloud of energetic electrons so as to ionize the ions to the desired charge sate before they are lost. For HCIs production the optimum electrons' energy ($T_e^{opt}$) must be in the range of keVs, which should be generally 3~5 times the threshold energy of the incident subshell electron that should be removed to obtain the desired charge state. Actually, there is a strong correlation between the product of ($n_e\tau$) and Teopt. For certain $T_e^{opt}$, a corresponding minimum value of ($n_e\tau$) for the transition of any ion Q-1 to the next charge state Q is mandatory. In Figure 1, Golovanivsky's diagram of the ($n_e\tau$) Teopt criteria gives the typical values of ($n_e\tau$) and $T_e^{opt}$ for the ionization of hydrogen-like ions to become fully stripped nuclei and also some other partially stripped ions that can be produced with the same ($n_e\tau$) $T_e^{opt}$ values [3]. For HCI production, the vacuum condition is also essential. The residual neutral density n0 must be low enough to minimize the charge exchange process. The critical neutral density to produce certain charge state Q is correlated with the electron density, the ion species and the $T_e^{opt}$ value as well [4].

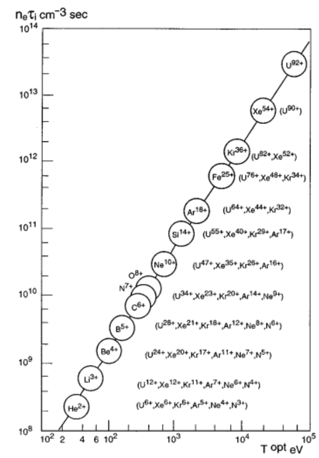


Figure 1: Golovanivsky's diagram of the *($n_e\tau$)$T_e$* criteria.

With the knowledge as discussed above, an ion source that can produce intense HCI beam must be able to provide necessary control of ($n_e\tau$) $T_e^{opt}$ values. Taking three types of HCI beam sources EBIS, LIS and ECRIS that are most popularly studied HCI machines today for example, in EBIS, one can have precise and independent control of the parameters, while in ECRIS these parameters are coupled , and in LIS, one can have the least independent control over all the parameters [5].

## EBIS

EBIS or Electron Beam Ion Source was first proposed in 1967 and lately demonstrated in 1968 by Dr. Donets in Dubna. In an EBIS, an electron gun produces high current electron beam on one end which is then compressed to high current density as it passes through a long solenoid field. The electron beam is decelerated and stopped in an electron collector on the other end of the device. During a definite period of time, gas or singly charged ions from external ion source of working substance is injected into trap. Electrostatic potentials are applied to cylindrical electrodes in the solenoid bore to trap ions axially, and the radial trapping of ions are established by space charge of the electron beam. Since the HCIs are produced through stepwise ionization by the energetic electrons, the longer

[#]sunlt@impcas.ac.cn

ISBN 978-3-95450-118-2

# HIGH INTENSITY OPERATION AND CONTROL OF BEAM LOSSES IN A CYCLOTRON BASED ACCELERATOR

M.Seidel, J.Grillenberger, A.C.Mezger, PSI, Villigen, Switzerland

*Abstract*

This paper discusses aspects of high intensity operation in PSI's cyclotron based proton accelerator (HIPA). Major beam loss mechanisms and tuning methods to minimize losses are presented. Concept and optimization of low loss beam extraction from a cyclotron are described. Collimators are used to localize beam losses and activation. Activation levels of accelerator components are shown. Other relevant aspects include the beam trip statistics and grid to beam power conversion efficiency.

## INTRODUCTION TO PSI'S HIPA FACILITY

The HIPA facility produces a continuous wave 590 MeV proton beam for the generation of muon beams and neutrons in a spallation target. Acceleration is done in a classical Cockroft-Walton pre-accelerator and, after bunching, in a chain of two isochronous cyclotrons. The cyclotrons are realized as separated sector cyclotrons, employing box resonators at 50.6 MHz for the acceleration of the beam. The facility contains also a source for ultracold neutrons (several 100 neV) which is operated in pulsed mode with a duty factor of 100.

Muons are produced as decay products of pions, which are generated when the high intensity proton beam passes through two rotating graphite targets with thicknesses of 5 mm and 40 mm. The targets are cooled simply by radiation cooling at temperatures up to 1700 K. Muon rates are of the order of $5{\cdot}10^{8}\,s^{-1}$ per beamline. The significant emittance blowup after the second target requires collimation of 30% of the proton beam intensity, in order to allow the further transport of the beam to the SINQ spallation target. The spallation target consist of lead filled Zircaloy tubes which are packed closely in a target enclosure. This target is cooled by a circuit of heavy water $D_2O$, which exhibits a neutron capture cross section three orders of magnitude smaller than normal water. The UCN source uses the same type of target, however equipped with a moderator employing frozen deuterium. Ultracold neutrons can be stored with small losses in a closed volume, and so the storage time is dominated by the natural lifetime of the neutrons. The storage volume is filled with freshly generated neutrons roughly every 10 minutes by a proton pulse of 8 seconds.

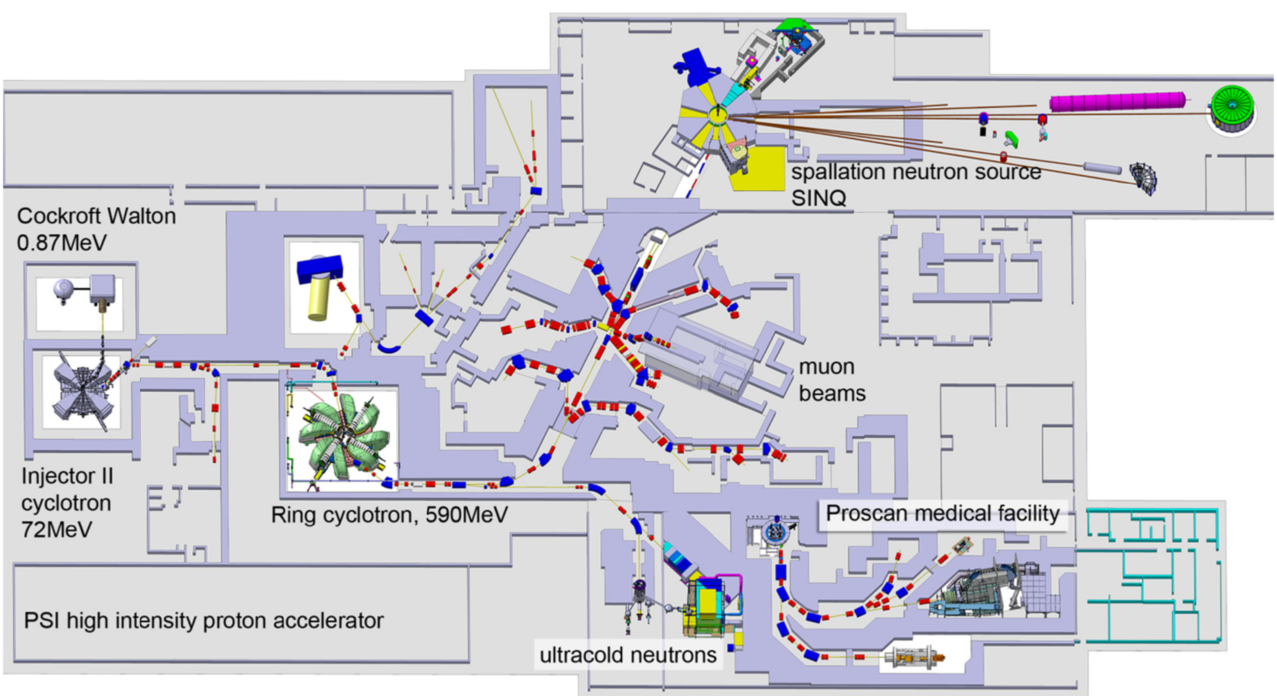


Figure 1: Layout of the PSI high intensity proton accelerator including the two meson production targets (center of image) and the spallation neutron source SINQ with related experimental facilities. The proton therapy facility for cancer treatment was originally connected to HIPA, but uses a separate superconducting cyclotron now.

ISBN 978-3-95450-118-2

# BEAM LOSS CONTROL IN THE ISIS ACCELERATOR FACILITY

D.J. Adams, B. Jones, A. H. Kershaw, S.J. Payne, B.G. Pine, H.V. Smith, C.M. Warsop, R.E. Williamson, D.M. Wright, STFC, RAL, UK

*Abstract*

The ISIS spallation neutron and muon source has been in operation since 1984. The accelerator complex consists of an $H^-$ ion source, 665 keV RFQ, 70 MeV linac, 800 MeV proton synchrotron and associated beam transfer lines. The facility currently delivers ~2.8x10$^{13}$ protons per pulse (ppp) at 50 Hz, which is shared between two target stations.

High intensity performance and operation are dominated by the need to minimise and control beam loss, which is key to sustainable machine operation allowing essential hands on maintenance. The dominant beam loss in the facility occurs in the synchrotron due to high intensity effects during the $H^-$ injection and longitudinal trapping processes. Losses are localised in a single region using a collector system. The measurement, simulation and correction systems for these processes are described. Emittance growth during acceleration can also drive extraction and beam transport loss at 800 MeV - measurement and control systems for these are also outlined.

## INTRODUCTION

The ISIS accelerator complex has been delivering beams for neutron and muon experiments since 1984. The facility consists of an $H^-$ ion source, 665 keV RFQ, 70 MeV $H^-$ linac, 70 MeV $H^-$ beamline (HEDS), 800 MeV proton synchrotron and two 800 MeV extract proton beam lines, EPB1 and EPB2, delivering beams to Target Stations 1 and 2 respectively. The facility operates at 50 Hz delivering 160-200 kW of beam power shared between two target stations. This equates to synchrotron intensities of 2.5-3.0x10$^{13}$ ppp. A schematic layout of the facility can be found in Fig. 1.

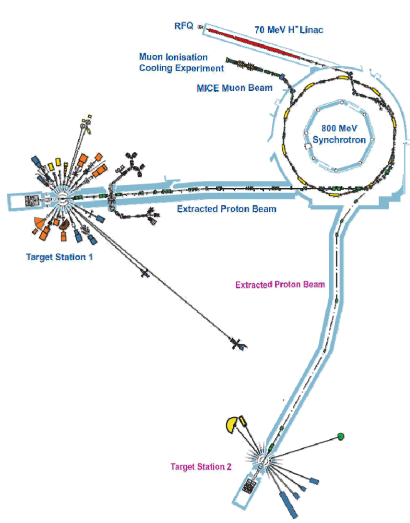


Figure 1: Schematic layout of the ISIS facility.

Operation of the facility depends upon the control of beam losses, particularly in the synchrotron where the high beam intensities have significant effects. This paper describes the beam loss diagnostics on ISIS and how they are presented in a Main Control Room (MCR) environment. Operating levels throughout the facility are presented and methods of optimisation are discussed. Beam loss mechanisms are described and hardware upgrades addressing some of these processes are discussed. Future areas of study are also presented.

## ISIS BEAM LOSS DIAGNOSTICS

Beam losses on the accelerators are mainly detected using two diagnostics: resonant current transformers (intensity monitors) and argon gas filled coaxial ionisation tubes (beam loss monitors). Intensity monitors have a sensitivity of ±3 μA in the injector and ±3x10$^{10}$ ppp in the ring and EPBs. Beam losses are calculated based on difference measurements between two points or times in the accelerator. Beam loss monitors (BLMs) are located ~2 m from the beam axis and detect epithermal neutrons produced when a $H^-$ or proton beam hits an accelerator component such as a magnet or vacuum vessel. They are 3 to 4 m long and are distributed to cover almost the whole accelerator to ensure any significant loss is detected. These monitors have a sensitivity of ~1.2x10$^9$ to 7x10$^6$ lost protons between 70 and 800 MeV respectively.

Interlock systems compare signals from both diagnostic types to trip levels on a pulse by pulse basis to turn the machine off in the event of a fault. Table 1 shows the distribution of these monitors across the facility.

Table 1: Beam Diagnostic Layout

| | Intensity Monitor | Beam Loss Monitors |
|---|---|---|
| Ion Source | 1 | 0 |
| RFQ | 2 | 0 |
| Linac | 4 | 9 |
| HEDS | 4 | 8 |
| Synchrotron | 1 | 39 |
| EPB1 | 6 | 10 |
| EPB2 | 5 | 15 |

Scintillators are also used to detect particle losses in regions where installation of normal beam loss monitors is not practical. At ISIS we use plastic scintillators (BD408) with dimensions 150x100x3 mm. They produce analogue signals in a similar manner to our beam loss



ISBN 978-3-95450-118-2

# PERFORMANCES AND FUTURE PLANS OF THE LHC RF

P. Baudrenghien, T. Mastoridis, CERN, Geneva, Switzerland

*Abstract*

The ramp-up of the LHC operation has been exceptionally fast: from the first acceleration of a single bunch at nominal intensity (1.1E11 p) to 3.5 TeV/c on May 2010, to the accumulation of 11 $fb^{-1}$ integrated luminosity two years later (June 2012). On the RF side this was made possible by a few key design choices and several developments, that allow reliable LHC operation with 0.35 A DC beam at 4 TeV/c (1380 bunches at 50 ns spacing, 1.5E11 p per bunch). This paper reviews the RF design and presents its performance. Plans are also outlined that would allow operation with 25 ns bunch spacing (doubling the beam current) and even increased bunch intensity with the target of above 1A DC current per beam, without big modification to the existing RF power system.

## THE LHC RF

The LHC RF system consists of 8 RF stations per beam. The RF system accelerates the beam during the ramp, compensates the small energy losses during coasting, and also provides longitudinal focusing. A simplified block diagram of the LHC RF system is shown in Figure 1.

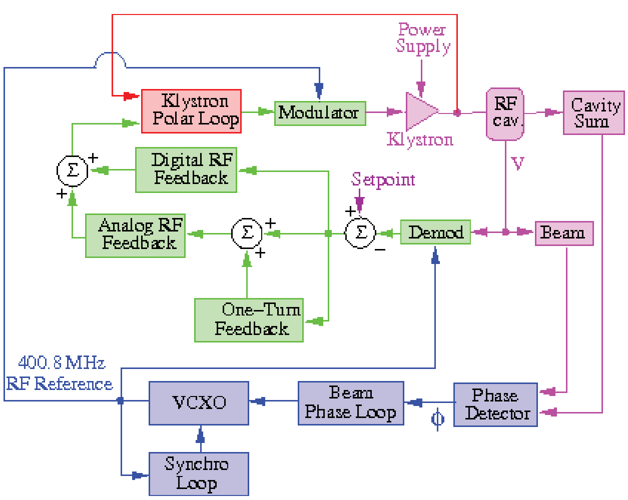


Figure 1: Simplified block diagram of the RF system. Cavity controller in green, beam phase loop in blue, klystron polar loop in red, and other RF components and beam in magenta.

Each RF station includes an accelerating superconducting cavity, a 330 kW klystron (currently operated with reduced DC settings limiting the power to 200 kW), and the Low Level RF (LLRF) system consisting of the klystron polar loop, the cavity controller, and the beam phase loop. The superconducting cavity has an $R/Q$ of 45 Ω, a resonance frequency $f_o$ of 400.8 MHz, and a mechanical tuner with a 100 kHz range. For nominal intensity beams, the cavity voltage $V$ and loaded quality factor $Q_L$ are set to 0.75 MV and 20,000 respectively during injection (flat bottom) and to 1.5 MV and 60,000 during collision (flat top). The cavity controller acts to compensate for the transient beam loading and to reduce the RF station fundamental impedance as sampled by the beam to increase longitudinal stability. It incorporates digital and analog paths, as well as the One-Turn feedback (OTFB), which acts to reduce the impedance at the revolution harmonics. The klystron polar loop (amplitude/phase) as implemented at the LHC acts to stabilize the klystron gain and phase response against variations due to high voltage power supply fluctuations and operation point (DC settings) changes. There is one klystron loop per cavity. The beam phase loop is a narrow bandwidth loop which acts on the Voltage-Controlled Crystal Oscillator (VCXO) to damp out barycentric longitudinal motion around the synchronous phase, motion driven by the noise in the RF system or by other mechanisms. There is one beam phase loop per ring. The beam phase loop averages the beam phase over all bunches in the ring.

## CHALLENGES ON LHC RF OPERATION

The design and operational choices for the LHC RF were largely defined by the anticipated challenges and limitations due to the beam parameters and system specifications. The main challenges, the solutions implemented and their performances are outlined below.

### *Transient Beam Loading and Coupled-bunch Instabilities*

The cavity characteristics greatly influence transient beam loading effects and coupled-bunch instabilities.

Filling in the LHC is done by the injection of up to twelve successive batches in each ring. During filling, the field in the empty buckets is perturbed by the beam in the filled buckets (transient beam loading). In the case of optimum detuning for the average beam current, and with a constant klystron drive, the peak phase modulation $\Delta\phi$ on the RF voltage caused be a beam gap is given by [1]

$$\Delta\phi \approx \pi f_0 \frac{R}{Q} \frac{I_{b,rf}}{V} t_{gap} \quad (1)$$

where $I_{b,rf}$ is the RF component of the beam current, and $t_{gap}$ the beam gap length. This phase modulation causes an injection phase error if the injection phase is kept constant, and results in capture losses. The effect is minimized by using superconducting cavities with a low $R/Q$ (45 Ω) and high RF voltage. Furthermore, strong RF and One-Turn feedback systems were developed to keep

ISBN 978-3-95450-118-2

# STATUS AND BEAM COMMISSIONING PLAN OF PEFP 100-MeV PROTON LINAC*

J. H. Jang#, H. J. Kwon, D. I. Kim, H. S. Kim, J. Y. Ryu, B. S. Park, K. T. Seol, Y. G. Song, S. P. Yun, S. S. Cha, Y. M. Li, Y. S. Cho, PEFP/KAERI, Daejeon, Korea

*Abstract*

The proton engineering frontier project (PEFP) is developing a 100-MeV proton linac which consists of a 50-keV injector, a 3-MeV RFQ (radio frequency quadrupole), and a 100-MeV DTL (drift tube linac). The installation of the linac was finished on March this year. The beam line magnets were also installed in the experimental halls. The utilities will be prepared at the end of October 2012 and accelerator commissioning will start in this winter. The beam commissioning is scheduled in February 2013 with the goal to deliver 100-MeV proton beam into a 100-MeV target room. This work summarized the status of the PEFP linac development and the beam commissioning plan.

## INTRODUCTION

Proton Engineering Frontier Project is the 100-MeV proton linac development project which was launched at 2002 as a 21st century frontier R&D program of Korean government [1,2]. The final goals of the project are constructing a proton linear accelerator with the final energy of 100 MeV and the peak beam current of 20 mA, developing technologies for the proton beam utilizations and the accelerator applications, and promoting industrial applications with the developed technologies.

The PEFP proton linear accelerator consists of two parts. The low energy part includes an 50-keV ion source, a low energy beam transport (LEBT), a 3-MeV radio frequency quadrupole (RFQ), and a 20-MeV drift tube linac (DTL) . The high energy part consists of seven DTL tanks which accelerator proton beams from 20 MeV to 100 MeV. A medium energy beam transport (MEBT) system will be installed after the 20-MeV DTL. It includes a 45-degree bending magnet for 20-MeV beam extraction and 2 DTL-type tanks with 3 cells for both transverse and longitudinal beam matching. The basic parameters of the linac are summarized in Table 1.

The PEFP experiment hall includes 10 beam lines, 5 for 20-MeV beams and 5 for 100-MeV beams. One of the main characteristics of PEFP beam lines is using AC magnet to distribute proton beams into 3 target rooms in both 20-MeV and 100-MeV beam lines. Each target room was assigned to special purposes as shown in Table 2 and Table 3. The main application fields are the bio-medical application, the material science, the energy and environmental application, the semiconductor production and research, the space science, and the isotope production.

The 20-MeV linac system has been successfully installed and tested at the Daejeon site of KAERI. In this operation of the linac from 2007 to 2011, we studied the characteristics of the low energy part of the linac and also supplied 20-MeV proton beams to users. The fabrication of the remaining DTL tanks was finished in 2010. The linac was installed into the accelerator tunnel in March 2012. In the process, we disintegrate and moved the 20-MeV linac into the project site at Gyeongju city. After completing utility test, the accelerator and beam commissioning will start. The proton beam will be provided to users from spring 2013.

Table 1: Basic Parameters of PEFP Linac

| Parameter | Value |
|---|---|
| Frequency | 350 MHz |
| Beam Energy | 100 MeV |
| Operation Mode | Pulsed |
| Max. Peak Current | 20 mA |
| Pulse Width | <1.33 ms (< 2.0 ms for 20 MeV) |
| Max. Beam Duty | 8% (24% for 20 MeV) |
| Max. Beam Power | 160 kW ( 96 kW for 20 MeV ) |

Table 2: Specification of 20-MeV Beam Lines

| Target Room | Application Field | Average Current | Irradiation Condition |
|---|---|---|---|
| TR21 | Semiconductor | 600 μA | Hor. Ext. 300 mmΦ |
| TR22 | Bio-Medical Appl. | 60 μA | Hor. Ext. 300 mmΦ |
| TR23 | Materials, Energy & Environment | 600 μA | Hor. Ext. 300 mmΦ |
| TR24 | Basic Science | 60 μA | Hor. Ext. 100 mmΦ |
| TR25 | Radio Isotopes | 1200 μA | Hor. Vac. 100 mmΦ |

Table 3: Specification of 100-MeV Beam Lines

| Target Room | Application Field | Average Current | Irradiation Condition |
|---|---|---|---|
| TR101 | Radio Isotopes | 600 μA | Hor. Ext. 100 mmΦ |
| TR102 | Medical Research (Proton therapy) | 10μA | Hor. Ext. 300 mmΦ |
| TR103 | Materials, Energy & Environment | 300 μA | Hor. Ext. 300 mmΦ |
| TR104 | Basic Science Aero-Space tech. | 10 μA | Hor. Ext. 100 mmΦ |
| TR105 | Neutron Source Irradiation Test | 1600 μA | Hor. Vac. 100 mmΦ |

*This work was supported by Ministry of Education, Science and Technology of the Korean government
#jangjh@kaeri.re.kr



ISBN 978-3-95450-118-2

# RECENT COMMISSIONING OF HIGH-INTENSITY PROTON BEAMS IN J-PARC MAIN RING*

Y. Sato#, S. Igarashi, M. Shirakata, N. Yamamoto, T. Toyama, M. Tejima, K. Satou, Y. Hashimoto, M. Okada, K. Hara, C. Ohmori, K. Ohmi, K. Ishii, T. Sugimoto, S. Yamada, S. Nakamura, J. Takano, K. Niki, N. Kamikubota, M. Uota, Y. Hori, M. Shimamoto, Y. Kurimoto, M. Yoshii, H. Hotchi, S. Hatakeyama, F. Tamura, T. Koseki,
J-PARC (KEK/JAEA), Tokai-Mura, Ibaraki, Japan

*Abstract*

J-PARC main ring (MR) provides high power proton beams of 200 kW to the neutrino experiment. Beam losses were well managed within capacity of collimation system. Since this beam power was achieved by shortening the repetition rate, the following tunings were applied in order to reduce the beam losses, such as improvement of tune flatness, chromaticity correction, upgrades of injection kickers, dynamic bunch-by-bunch feedback to suppress transverse oscillation, beam loading compensation using feedforward technique, and balancing the collimators of MR and the injection beam transport line. Especially, the dynamic bunch-by-bunch feedback was effective to reduce the beam losses to one-tenth during injection and beginning of acceleration. Moreover, with the beam loading compensation, impedance seen by the beam was significantly reduced, longitudinal oscillations were damped, and the beam power was increased over 5% without increasing the beam losses. Monitors were upgraded to find time structure and location of the beam losses, even in first several turns after each injection. In this presentation these commissioning procedures and beam dynamics simulations are shown, and our upgrade plan is discussed.

## OVERVIEW

The Japan Proton Accelerator Research Complex (JPARC) consists of a series of three proton accelerators, a $H^-$ linac, a 3 GeV Rapid-Cycling Synchrotron (RCS) and a Main Ring synchrotron (MR), and three experimental facilities [1]. Typically more than 93% of the 3 GeV protons from RCS are directed to muon and neutron production targets in the Materials and Life Science Experimental Facility (MLF). The rest protons are transported into MR through a beam transport (3-50BT) and accelerated to 30 GeV, and extracted with the fast extraction method (FX) or the slow extraction method (SX). The protons into the SX line are guided to the hadron experimental facilities, and the protons into the FX line are delivered to the neutrino target for the Tokai to Kamioka Japan (T2K) experiment. A different operational period is set for each extraction method. In the high power operation of MR in FX mode, 145 kW proton beams had been delivered to the neutrino target by March 2011, before the Tohoku earthquake, and 200 kW by June 2012. The repetition time had been shortened from 3.2 s to 2.56 s. The beam power was increased with controlling the beam losses to be localized at the MR collimator area and the averaged lost power under 450 W, the collimator capacity till this summer. In the next section, the tunings to reduce the beam losses, the monitoring properties during the tunings, and our near upgrade plan are discussed.

## HIGH-INTENSITY OPERATION

MR high-intensity operation in the FX mode restarted on December 24th, 2011 after the 9-month-shutdown from March 11th, 2011. User operation for the T2K experiment restarted on March 5th, 2012, and continued till June 9th, 2012. Figure 1 shows the history of the MR power, and Figure 2 shows the total beam losses during the period. The achieved beam power to the neutrino target was 190 kW in May, 2012, and 200 kW in June, 2012, the latter of which signified 1.08E14 protons per pulse (ppp) in 2.56 s cycle. The beam losses were measured with DC current transformer (DCCT). In Fig. 2, the red line is the loss power based on 1 ms averaged DCCT signal, and the green line based on 10 μs DCCT signal. Except for machine study periods, the total beam losses during the user operation were successfully controlled below the collimator capacity, which was 450 W. It will be 2 kW in this fall. The delivered protons on the neutrino target were ~3E20 POT (protons on target) from January, 2010, the beginning of the T2K user operation, to June 9th, 2012. The T2K experiment observed 11 candidate events, where a muon neutrino appeared to be transformed into an electron neutrino. The transformation from muon neutrino to electron neutrino occurs with 99.92% probability (3.2 sigma) [2].

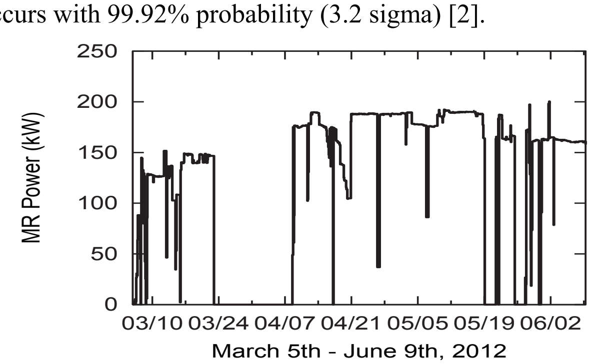


Figure 1: MR beam power in the FX mode from March 5th to June 9th 2012. 190 kW in mid-May, 200 kW in June.

*J-PARC is managed by KEK and JAEA.
#yoichi.sato@j-parc.jp



ISBN 978-3-95450-118-2

# OPTICAL TRANSITION RADIATION FOR NON-RELATIVISTIC ION BEAMS

B. Walasek-Höhne, C. Andre, F. Becker, P. Forck, A. Reiter, M. Schwickert,
GSI Helmholtz Centre for Heavy Ion Research GmbH, Darmstadt, Germany
A. Lumpkin, Fermi National Accelerator Laboratory, Batavia, USA

*Abstract*

The precise transverse ion beam profile measurement is an ongoing research field at GSI. Usually beam profiles are measured with Secondary Electron eMission Grids (SEM-Grid), scintillating screens or Beam Induced Fluorescence (BIF) monitors [1]. As an alternative, the feasibility of Optical Transition Radiation (OTR) has been investigated using an 11.4 MeV/u ($\beta = 0.16$) Uranium beam at the GSI UNIversal Linear ACcelerator (UNILAC). The experiment was prompted by successful measurements at the CLIC Test Facility 3 with 80 keV electrons and a feasibility study for UNILAC and SIS18 energies at GSI.

OTR is a classical electro-dynamic process where the emitted photon number depends on the square of the ion charge state. Usage of a stripping foil during the experiment increased the mean charge state of ions, compensated the low β and allowed imaging the ion beam with an Image Intensified CCD camera (ICCD). Various experiments, using a non-relativistic beam, have been performed to estimate signal strength and evaluate the working regime of the OTR technique. The precise ICCD gating feature, as well as the emitted light spectrum, was used to distinguish the prompt OTR signal from any background sources with longer emission time constant e.g. blackbody radiation. In this contribution, the results of applying the OTR beam profile monitor technique to a non-relativistic ion beam are presented.

## INTRODUCTION

Optical Transition radiation is produced by the ions of charge q and velocity β when they cross the interface of two media of different dielectric constants.

OTR has become a popular method of beam imaging since it was first introduced in beam diagnostics applications forty years ago by Wartski [2]. There are extensive experiences with OTR imaging of relativistic electron and proton beams [3]. In these cases $\gamma >> 1$ and $\beta \sim 1$ were hold.

Ginzburg et al. [4] considered a non-relativistic charge q moving from vacuum to an ideal conductor with $v << c$. For the number of emitted photons I, theory predicts the proportionality $I \propto q^2 \cdot \beta^2 \cdot N$ where N is the number of particles.

The OTR signal of a non-relativistic ion beam has been evaluated for the first time by Lumpkin [5]. A comparison with successful non-relativistic [6] and relativistic [4] electron and proton [3] measurements is shown in Table 1. Since the charge state $q >> 1$ for heavy ions like $U^{28+}$ seems to compensate the low value β, a pilot OTR experiment was carried out at the UNILAC.

Table 1: Comparison of Various Particle Beam Cases with Estimated Photon Number [5]

| Particle | E (MeV) | q | β | N | Photon Number |
|---|---|---|---|---|---|
| e | 0.08 | 1 | 0.63 | $4 \cdot 10^{11}$ | $7 \cdot 10^{5}$ |
| e | 150 | 1 | 0.99 | $6 \cdot 10^{9}$ | $1.2 \cdot 10^{7}$ |
| p | $1.2 \cdot 10^{5}$ | 1 | 0.99 | $1 \cdot 10^{11}$ | $1 \cdot 10^{8}$ |
| U | $2.6 \cdot 10^{3}$ | 28 | 0.16 | $1 \cdot 10^{11}$ | $4 \cdot 10^{6}$ |

## EXPERIMENTAL SETUP

The GSI linear accelerator UNILAC is designed to accelerate all ions from protons to Uranium with energies up to 11.4 MeV/u. For OTR tests the diagnostics test bench (beam line X2), equipped with different profile and current measurement methods, was used.

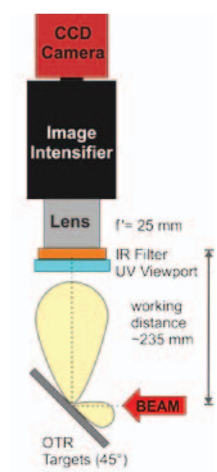


Figure 1: Scheme of the OTR experiment at the X2 area with the OTR screen tilted 45° to the beam direction and the ICCD.

Figure 1 shows a scheme of the experimental setup consisting of the OTR targets (500 µm stainless steel and 10 µm aluminized Kapton) and the imaging system.

In order to detect even single photons an image intensified camera system (ICCD from ProxiVision Company) was use where the photons are converted into electrons by a Bialkali photocathode and accelerated to a double Multi Channel Plate with $10^6$ fold amplification. The electrons then hit a phosphor screen to create photons



ISBN 978-3-95450-118-2

# MOMENTUM SPREAD DETERMINATION OF LINAC BEAMS USING INCOHERENT COMPONENTS OF THE BUNCH SIGNALS

P. Kowina, P. Forck, R. Singh, GSI Darmstadt, Germany
F. Caspers, CERN, Switzerland

*Abstract*

Measurements of the momentum spread of the particles in a beam are of great importance when optimizing Linac setup for high current operation concerning controlled longitudinal phase space occupation. A new method of the momentum spread determination was tested at GSI heavy ion linear accelerator. It is based on the analysis of incoherent components of the bunch signal. A significant enhancement of signal to noise ratio was achieved by means of resonant cavity pick-up of pile-box shape. Spectra were analyzed on $36^{th}$ harmonic of the rf-frequency i.e. at 1.3 GHz. This reduced contribution of the coherent components in the frequency spectrum of the bunched beam. Fast digital processing and gating synchronized to the bunch train allowed a drastic reduction of the measuring time and additionally suppressed a noise in the frequency spectrum, respectively. This contribution describes the measurement setup and discusses the first results obtained with heavy ion beams. Since measurements were taken just two days before conference started the results presented here are to be treated as a very preliminary.

## MEASUREMENT PRINCIPLES

In the case of the linear accelerator the longitudinal phase space is critically influenced by for any parameters variations. Therefore its knowledge is extremely important for any beam dynamics calculations and calls for precise measurements. There are several methods, e.g. based on the measurements of arrival time and time-of-flight between two particle detectors [1] or basing on the measurements using dipole magnet and kicker [2]. However, these methods are either destructive for beam [1] or require, besides diagnostics elements, an installation of an dedicated kicker [2]. A good alternative is measurements of the two projections of the longitudinal phase space using two independent but non-intercepting devices. In this case the projection of the phase deviation $\frac{\Delta\phi}{\phi}$ axis can be determined by means of e.g. Bunch Shape Monitor, as described e.g. in [3].

The other projection of the phase i.e. the momentum spread $\frac{\Delta p}{p}$ may be determined via analysis of incoherent component of the bunch signals. This would be an analogy to longitudinal Schottky noise measurements for bunched beams commonly used at nearly any circular accelerators [4]. Originally Schottky noise was analyzed for high vacuum diodes that can be considered as a kind of linear accelerator. Let us assume a large synchrotron with big number of circulating bunches like e.g. LHC [5]. At injection 2808 bunches are circulating with revolution frequency of $f_0 = 11.24$ kHz and period of $T_0 = 89\ \mu$s. An interesting question is whether one can observe any Schottky signal within measurement time reduced to let us say 80 $\mu$s, i.e. when bunches are passing Schottky pick-up only once. This situation corresponds to the measurements made at a Linear accelerator. The only difference is absence of dispersion in the Linac case. A relationship between the momentum spread and the frequency spread can be obtained from generalization of the momentum compaction function $\alpha$ for transfer line which should be applicable also in the particular case of Linac [6]. The relative change in orbit $\frac{\Delta L}{L_0}$ per relative momentum change $\frac{\Delta p}{p_0}$ is given by:

$$\alpha(s, s_0) = \frac{\Delta L/L_0}{\Delta p/p_0} = \frac{1}{L_0}\int_{s_0}^{s} \frac{D(t)}{\rho(t)}dt \text{ with } L_0 = \int_{s_0}^{s} dt,$$

and $D$ and $\rho$ being dispersion and mean bending radius, respectively. The relative change in time of flight per relative momentum spread $\eta(s, s_0)$ is:

$$\eta(s, s_0) = \frac{\Delta t/t_0}{\Delta p/p_0} = \frac{p_0}{t_0}\frac{\Delta(L/v)}{\Delta p} = \alpha(s, s_0) - 1 + \frac{v^2}{c^2},$$

where $v$ is the velocity of the reference particle. If there is no dispersion (no dipole in lattice) one reads:

$$\eta(s, s_0) = -1 + \frac{v^2}{c^2}.$$

For ultra-relativistic particles a Linac would be isochronous i.e. all particle would arrive simultaneously. However, for GSI Linac $v/c \sim 15\%$ [7] which results in $\eta \simeq -0.98$. Therefore, momentum spread and frequency spread are related to each other via:

$$\frac{\Delta p}{p} = \frac{1}{\eta}\frac{\Delta f}{f}.$$

## EXPERIMENTAL SETUP

The measurements described here were performed at GSI *Unilac* [7]. A pill-box cavity with the inner diameter of 236 mm was used as pick-up, see Fig. 1. The frequency of the $TM_{010}$ mode was tuned to 1.30089 MHz i.e. to $36^{th}$ harmonics of Unilac rf-frequency of 36.136 MHz. This high harmonics number allows rejection of coherent component of the bunch signal[1]. The coupling loop was

[1] Power density of the coherent signal depend on the bunch length and decreases with the harmonic number. On the contrary, the power spectrum density per Schottky band remain constant.

ISBN 978-3-95450-118-2

# BEAM INDUCED FLUORESCENCE - PROFILE MONITORING FOR TARGETS AND TRANSPORT

F. Becker*, C. Andre, C. Dorn, P. Forck, R. Haseitl, B. Walasek-Hoehne, GSI, D-64291 Darmstadt
T. Dandl, T. Heindl, A. Ulrich, Physik Department E12 TU-München, D-85748 Garching
J. Egberts, J. Marroncle, T. Papaevangelou, Centre CEA de Saclay, F- 91191, France

*Abstract*

Online profile diagnostic is preferred to monitor intense hadron beams at the Facility of Antiproton and Ion Research (FAIR). One instrument for beam profile measurement is the gas based Beam Induced Fluorescence (BIF)-monitor. It relies on the optical fluorescence of residual gas, excited by beam particles. In front of production targets for radioactive ion beams or in plasma physics applications, vacuum constraints are less restrictive and allow a sufficient number of fluorescence photons, even at minimum ionizing energies. Unwanted effects like radiation damage and radiation induced background need to be addressed as well. A profile comparison of BIF and Ionization Profile Monitor (IPM) in nitrogen and rare gases is presented. We studied the BIF method from $10^{-3}$ to 30 mbar with an imaging spectrograph. Preferable fluorescence transitions and fundamental limitations are discussed.

## MOTIVATION

Compared to synchrotrons with typical vacuum pressures $p_{SYN}$ of $1\cdot10^{-12}$ to $1\cdot10^{-9}$ mbar, beam transport sections are usually operated in the range $p_{TS}$ of $1\cdot10^{-9}$ to $1\cdot10^{-6}$ mbar. This fact increases the set of possible instrumentation in the FAIR HEBT sections, since the expected signal strength for gas based profile monitors scales $\propto p$, see [1, 2]. Beside Ionization Profile Monitors (IPMs) with MCP amplification for high sensitivity or applications with high read out rates [3], compact BIF installations or strip line IPMs are foreseen. Within a collaboration between CEA-Saclay and GSI-BD an IPM prototype, designed for the IFMIF/EVEDA facility [4] was characterized at the GSI LINAC experimental branch for various beam and gas conditions [5]. Together with the IPM a BIF monitor was installed in the same plane and profiles of a 1.1 mA $Xe^{21+}$ beam with 250 $\mu$s pulse length @ 4.8 MeV/u were recorded in nitrogen and rare gases.

At low duty cycles, temporarily triggered gas puffs beyond $1\cdot10^{-4}$ mbar could be provided with pulsed gas valves. In front of production targets for radioactive ion beams or in plasma physics applications, vacuum requirements are less restrictive or even protective gases are used with typical pressures $p_{TAR}$ from $1\cdot10^{-4}$ mbar to atmospheric pressure. In order to characterize the BIF monitor at gas pressures $\geq 1\cdot10^{-4}$ mbar, imaging spectroscopy was performed in a separated gas cell at the Munich Tandem van de Graaff accelerator. With a DC 200 nA $S^{8+}$ beam at 3.75 MeV/u former results [6] for gas pressures $\leq 1\cdot10^{-3}$ mbar could be confirmed. This data-basis was now extended to gas pressures up to 30 mbar.

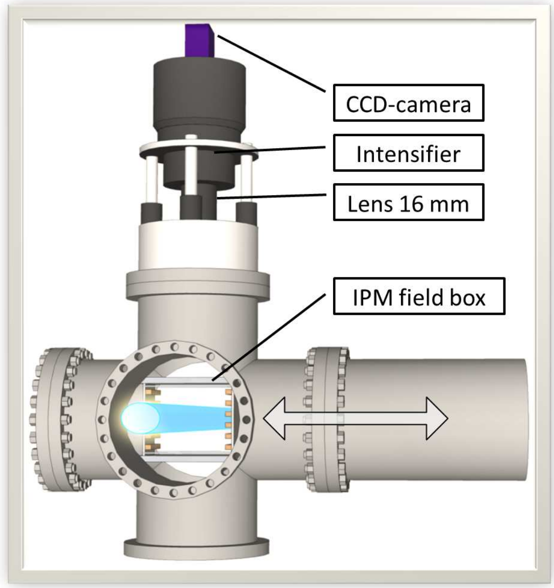


Figure 1: Schematic drawing of the experimental setup with the IPM and BIF monitor mounted in the same plane on a blackened vacuum chamber (DN100CF). The IPM field box could be moved out the chamber with a stepper motor controlled linear drive (to the left).

## BIF IPM - EXPERIMENTAL SETUP

In order to compare horizontal profiles of the different monitors, we decided to place both systems in the same transversal plane, see Fig. 1. During IPM operation the electric field box was centered in the chamber and moved out of the optical path for BIF operation. The vacuum chamber was sandblasted and blackened by electrochemical surface treatment to suppress stray-light from the chamber walls during BIF operation. The experimental branch is equipped with a 700 l/s turbomolecular pump and reaches a typical base pressure of $2\cdot10^{-7}$ mbar. Furthermore, it is equipped with a remote controlled gas dosing system. This way, purified gases (e.g. nitrogen and rare gases) could be applied in a dynamic equilibrium within an accessible pressure range from $10^{-6}$ to $10^{-3}$ mbar. For cleaning purpose during gas exchange, the vacuum system was evacuated to base pressure.

The IPM illustrated in Fig. 1, consists of a 55x61 $mm^2$ field box with 833 V/cm electric field for ion detection and

* Frank.Becker@gsi.de



ISBN 978-3-95450-118-2

# LONGITUDINAL BEAM DIAGNOSIS WITH RF CHOPPER SYSTEM

T. Maruta*, J-PARC center, Japan Atomic Energy Agency, Tokai, Ibaraki, Japan
M. Ikegami, High Energy Accelerator Research Organization, Tsukuba, Ibaraki, Japan

*Abstract*

The RF chopper system is one of the key items for the upcoming 400 MeV and 50 mA upgrade of the injection linac of Japan Proton Accelerator Research Complex (J-PARC). The system scrapes unnecessary beams for the following 3 GeV Rapid Cycling Synchrotron (RCS). Since the remnant beam causes a beam loss in RCS, it is required to maintain the sufficient elimination power for the stable operation after the upgrade. The elimination power heavily depends on the beam width in the phase direction at the RF chopper cavity. The confirmation of the present status is important for the consideration of the upgrade properly. Therefore, we obtained the beam width from the measurements of the RCS beam loss with varying the RF settings of the chopper. In this paper, we discuss the measurement method and results.

## INTRODUCTION

Japan Proton Accelerator Research Complex (J-PARC) is a high intensity proton accelerator facility designed for a MW-class beam. The accelerator complex is currently comprising a 181 MeV linac, a 3 GeV Rapid Cycling Synchrotron (RCS) and a 30 GeV Main Ring (MR). A 3 GeV beam is also transported to Materials and Life Science Experimental Facility (MLF). In the injector linac, The design peak current is 30 mA, the macro pulse is 0.5 msec with the repetition rate of 25 Hz. 50 keV negative hydrogen ions ($H^-$) are extracted from an ion source (IS), then they are accelerated by a 3 MeV Radio Frequency Quadrupole (RFQ), a 50 MeV Drift Tube Linac (DTL), and a 181 MeV Separate-type DTL (SDTL) [1]. All cavities are operated at the frequency of 324 MHz.

A 3 MeV beam transport line so-called MEBT1 is a 3 m long transport line connecting the RFQ and DTL as shown in Fig. 1. There are two major issues. One is a matching of the beam to the DTL acceptance in both longitudinal and transverse phase space by eight quadrupole magnets and two buncher cavities while transferring the beam to DTL. To measure the beam qualitatively, we place beam current monitors (CTs), beam position monitors (BPMs) and wire scanner monitors (WSMs) [2] throughout MEBT1. The other issue is a shaping of a macro pulse. The RF frequency of RCS is 0.938 MHz and it is different from the frequency of the linac. If a macro pulse is injected to RCS without any shaping, a part of the macro pulse stays out of the RF bucket and it is lost in the middle of acceleration. The beam loss causes a serious radioactivation of accelerator components. It is the key issue for the stable operation to mitigation of the beam loss, i.e. the rejection of the beam out the RF bucket for RCS. Therefore, we configure another pulse structure to a macro pulse so-called medium pulse. The RF chopper system in MEBT1 conducts the forming of the medium pulse. The system is comprised from a RF deflector cavity and a scraper. During RF on, beam is horizontally deflected by sinusoidal RF wave in the cavity, and then the beam is absorbed in the scraper as shown in Fig. 2. The detail of the RF chopper system is introduced in the next section.

The linac has a plan to extend the peak current to 50 mA from currently 30 mA by the replacement of the front-end part (IS and RFQ) in the next summer. The simulation of new RFQ by LINACSrfqSIM indicates that the longitudinal beam emittance in the 50 mA operation increases more than 20 percent from the present operation of 15 mA [3], i.e. beam width in phase direction at 50 mA operation is wider than present. Since the RF becomes smaller as the synchronous phase shifts from 0 deg (for cosine wave), the increase of beam width in phase direction causes an insufficient deflection for beam elimination at beam envelope. Therefore, we need to confirm whether the 20 % emittance enhancement is problem for the RF chopper system or not. And if the chopper system cannot sustain the 50 mA operation, we must upgrade the chopper system with the reasonable estimation. For the estimation, the understanding of present status is absolutely imperative. However there is no monitor to measures a longitudinal beam profile in MEBT1. It motivates us to measure the beam width in phase direction by existing apparatus.

## RF CHOPPER SYSTEM

The RF chopper system is comprised from an RF chopper cavity and a scraper which is located at 0.72 m downstream from the cavity. The beam is horizontally deflected by the chopper cavity during the RF on, and then the deflected beam is absorbed in the scraper.

We employ an RF deflector (RFD) for the beam chopping [4]. The RFD is operated in a $TE_{11}$-like mode with the frequency of 324 MHz, which is same frequency as the other cavities. Since no higher order harmonic is supplied, the RF wave is sinusoidal. There are two RF gaps in the cavity at a interval of $3\beta\lambda$, where $\beta$ is the velocity of beam normalized by the speed of light and $\lambda$ is RF wave length. For the supplement of RF from the single amplifier, the two RF gaps are connected in series via a coaxial tube with length of $2\lambda$ in order to deflect a beam at the same RF phase by two gaps. The design deflection angle of each RF gap is 6 mrad at the electric field of 1.6 MV/m of which an RF power is 22 kW. The power source of the chopper cavity is

* tmaruta@post.j-parc.jp

ISBN 978-3-95450-118-2

# FIBER BASED BLM SYSTEM RESEARCH AND DEVELOPMENT AT CERN

S. Mallows, The University of Liverpool, UK
E.B. Holzer, J. van Hoorne, CERN, Geneva, Switzerland

*Abstract*

The application of a beam loss measurement (BLM) system based on Cherenkov light generated in optical fibers to a linear accelerator with long bunch trains is currently under investigation at CERN. In the context of the Compact Linear Collider (CLIC) study, the machine protection role of the BLM system consists of its input to the 'next cycle permit'. In between two cycles it is determined whether it is safe to commit the machine for the next cycle. A model for light production and propagation has been developed and validated with beam measurements. Monte Carlo simulations of loss scenarios established the suitability in terms of sensitivity and dynamic range. The achievable longitudinal position resolution of the system, considering that the bunch trains and the optical fiber length are comparable in size is discussed.

## INTRODUCTION

Beam loss monitors (BLMs) are common devices used in lepton and hadron accelerators. They can be used as a diagnostics tool and/or as a crucial part of the machine protection system. Typically, a BLM is placed outside the vacuum chamber and observes the secondary particle shower generated when the lost particles interact with the vacuum chamber walls or beamline components. At high energy accelerators, the BLM system should detect the magnitude and location of losses and, when necessary, trigger a beam interlock system.

The Compact Linear Collider (CLIC) study investigates the feasibility of a high-energy electron-positron linear collider optimized for a centre of mass energy of 3 TeV. To achieve the high accelerating gradients, the RF power is produced by a novel two-beam acceleration method in which a decelerating drive beam supplies energy to the main accelerating beam. The linacs are arranged in modular structures referred to as the two beam modules (TBMs) which cover $\sim$42 km of beamline. Losses from either beam can have severe consequences due to the high intensity drive beam and the high energy, small emittance main beam.

To monitor beam losses in the TBMs, it is estimated that a total of more than $\sim$45,500 localised monitors would be required [1]. It is therefore desirable to investigate cost effective technology choices that cover large distances along the beam line, particularly for the drive beam decelerators which would account for $\sim$41,500 of the required localized detectors. However, the BLM system based on Cherenkov fibers currently under development is in no way specific to CLIC and can be applied to any hadron machine.

## MULTIMODE CHERENKOV FIBERS AS A BLM

### *Detection Principle*

Cherenkov radiation is emitted when the velocity of a charged particle travelling through the fiber exceeds that of the phase velocity of light in the fiber. The photons are emitted along a cone with opening angle, $\theta_c$, given by:

$$cos\theta_c = \frac{1}{n\beta} \tag{1}$$

where $\beta = v/c$ and $n$ is the refractive index of the fiber core.

The number of photons produced per unit wavelength is given by:

$$\frac{d^2N_{ph}}{d\lambda dL} = \frac{2\pi\alpha z^2 \cdot sin^2\theta_c}{\lambda^2} \tag{2}$$

where $\alpha$ is the fine structure constant, $\lambda$ the wavelength of the light produced, and $L$ the path length of the charged particle traversing the fiber.

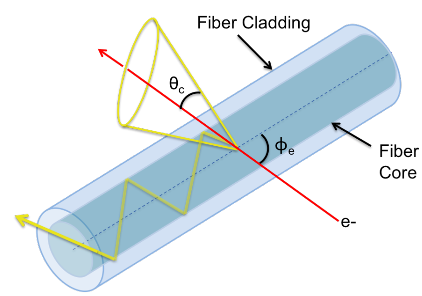


Figure 1: Schematic to illustrate the detection principle for Cherenkov beam loss monitors.

A multi-mode optical fiber will only propagate light entering the fiber within a certain 'acceptance cone'. The numerical aperture (NA) characterizes the range of angles over which the fiber can transmit light. Thus, when estimating the signal from Cherenkov fibers, one has to consider not only the probability of production of light, but the probability that it is trapped and propagates to the fiber end face. Without considering attentuation effects, the probability, $P_{e,a}$ that the photons are trapped and exit within the 'the nominal acceptance cone', is defined by [2]:

$$\mathrm{P_{e,a}} = \frac{1}{\pi}cos^{-1}\left[\frac{\beta\sqrt{n^2 - \mathrm{NA}^2} - \cos\phi_e}{\sin\phi_e\sqrt{\beta^2n^2 - 1}}\right] \tag{3}$$

where $\phi_e$ is the angle between the direction of propagation of the charged particle and the fiber axis.



ISBN 978-3-95450-118-2

# ON-LINE CALIBRATION SCHEMES FOR RF-BASED BEAM DIAGNOSTICS

P.-A. Duperrex*, U. Müller, PSI, Villigen, Switzerland


*Abstract*

RF-based beam diagnostics, such as beam current monitors and beam position monitors (BPMs), rely on precise RF signal measurements. Temperature drifts and differences in the overall measurement chain gain make such measurements very challenging and calibration can drift with time. On-line calibration schemes for BPMs and current monitors have been developed to address these issues. These innovative schemes are based on the use of a pilot signal at a frequency offset from the measurement frequency.

This paper presents the techniques that have been developed to overcome such problems in a proton cyclotron with 2mA current. Results, advantages and disadvantages of such schemes are discussed.


## INTRODUCTION

RF-based beam diagnostics rely on precise RF signal measurements. The measurement chain (Fig.1) may comprise one or several sensors, some amplification stages, long cables, some front-end electronics and a processing unit.

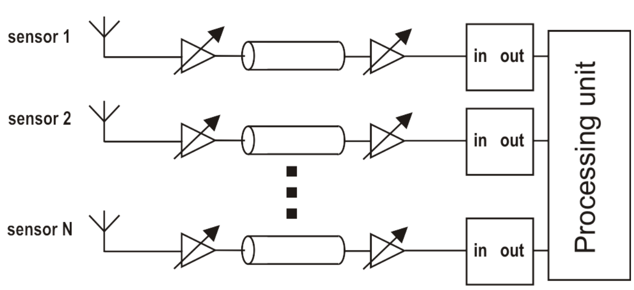


Figure 1: A typical measurement chain with sensors, amplification stages, cabling, signal shaping and processing unit.

To compensate possible different sensor sensitivities, differences between the overall gain of the different lines and electronics temperature drift, calibration procedures are unavoidable. These procedures may require effort and time and need usually to be repeated after repairs. For these reasons, on-line automatized calibration is attractive.

The concept developed for the on-line calibration scheme is to use a test signal (the pilot signal) to calibrate on-line the measurement chain. This has been first applied for a beam current monitor that suffers large gain drifts at high beam intensity. The second application was for calibration of beam position monitors.

## ON-LINE CALIBRATION FOR BEAM CURRENT MONITORS

### System Description

A beam current monitor, called MHC5, is used to measure the transmission at a 4 cm thick graphite target (the so-called target E) for muon and pion production. Transmission measurements at this point are very important. If a portion of the beam were to bypass the target E, the beam footprint on the next target (the SIN-Q spallation neutron source target) could be reduced. This would lead to an overheating of the SIN-Q target surface. Thus, to avoid such possible damage, the transmission at this point must be carefully monitored.

The MHC5 is placed in vacuum behind the graphite target and is subject to heavy heat load due to the energy deposition of the scattered particles. The resulting mechanical thermal expansion induces a drift of the resonance frequency. Because of the dynamic nature of the calibration drift effect, it was not possible to solve this problem by calibrating the monitor at different beam intensities.

The current monitor (Fig.2) consists of a re-entrant resonator, symmetric around proton beam pipe. The open-end gap in the beam pipe couples some of the wall current into the resonator. This gap acts also as a capacitor and determines the resonance frequency. The resonance frequency is set to 101.26 MHz, the 2nd harmonic of the proton beam bunch frequency. This harmonic is used because of the better signal-to-noise ratio, the RF noise components from the generator being mainly at the odd harmonics. No significant shape dependency of the 2nd harmonic amplitude for relatively short beam pulses is expected [1]. The oscillating magnetic field in the resonator is measured using a magnetic pick-up loop, the signal being proportional to the beam current. Advantages of such resonator are that its construction is simple and it is rugged with respect to radiation. Disadvantages are that it is sensitive to temperature and it is not an absolute measurement; the signal has to be calibrated.

The monitor is made of aluminium (Anticorodal 110), with a 10µm coating layer of silver to improve the electrical conductivity. The inner diameter is 225mm, the outer diameter 420mm, its height 224mm. The capacitor gap is 4mm and small movable plates are used for the fine tuning of the resonance. It has an active water cooling system (maximum water speed: 2m/s).

The monitor itself is in vacuum and the external surfaces were chemically blackened to increase the emissivity for additional cooling.

ISBN 978-3-95450-118-2

# SUMMARY OF WORKING GROUP A ON "BEAM DYNAMICS IN HIGH-INTENSITY CIRCULAR MACHINES"

G. Franchetti, GSI, Darmstadt, Germany
J. Holmes, ORNL, Oak Ridge, Tennessee, USA
E. Métral, CERN, Geneva, Switzerland

*Abstract*

In this proceeding we summarize the presentations of the HB2012 Workshop session on "Beam Dynamics in High-Intensity Circular Machines" as well as the outcome of the discussion session.

## INTRODUCTION

This working group hosted 29 presentations in dedicated sessions plus 5 presentations in a joint session with the working C. In this summary, only one talk from the joint session is included (the one from J. Holmes, see below), i.e. 30 talks are discussed. Many thanks to all the speakers who gave excellent and well-prepared talks! In addition to all the talks, a discussion session took place on Thursday afternoon, where the hot topics of the workshop were discussed.

Eight (i.e. ~ 27 %) speakers were from Asia-Russia (3 IHEP Beijing, 3 J-PARC, 1 KEK, 1 JNR), eleven (i.e. ~ 37 %) from Europe (7 CERN, 2 GSI, 2 RAL) and eleven (i.e. also ~ 37 %) from North America (1 BNL, 3 FNAL, 1 ORNL, 2 LBNL, 1 UMD, 1 JLAB, 1 SLAC, 1 TRIUMF). We summarize below the highlights of the working group. A brief summary (1 slide) per talk can be found in the Appendix of the slides of the summary given on Friday morning for those interested [1].

## NEW INTERESTS / IDEAS: BEAM-BEAM AND CIRCULAR MODES

At HB2010, the issue of the interplay between space charge and beam-beam in colliders was raised [2]. This year, two talks were devoted to beam-beam, one from RHIC [3] and one from LHC [4]. The next goal for RHIC is to double the current luminosity by increasing the proton bunch intensity from $1.7\times10^{11}$ p/b up to $3\times10^{11}$ p/b with an upgraded polarized proton source, and to (partially) compensate the beam-beam head-on tune spread by two electron lenses, whose installation started this year. The maximum beam-beam parameter reached so far during p-p (polarized) runs is 0.017 with $1.7\times10^{11}$ p/b and a transverse rms. norm. emittance of ~ 2.5 µm. Several observations still need to be fully understood: 1) fast beam losses during the first 1-2 hours of the fills; 2) no clear transverse emittance growth during the stores (due to dynamic aperture?); beam-beam coherent π-mode seen only in the vertical plane and not in the horizontal one (due to stabilization by coupling between the transverse planes?). In the LHC, the luminosity was considerably increased in 2011 and 2012, reaching a record peak luminosity of ~ 77% of the design luminosity of $10^{34}$ cm$^{-2}$s$^{-1}$. Many Machine Developments (MDs) took place and the one from Ref. [4] will be treated below. Furthermore, the interplay between beam-beam and impedance is under discussion at CERN to try and better understand observed instabilities (see below).

Circular modes (already proposed in the past) and their possible application (with flat beams) for the LHC [6] have been presented at HB2012. X / Y eigenmodes, in uncoupled case, may have clockwise / counter-clockwise optical modes, which is called a circular optics. To have a circular optics, the focusing has to be rotationally invariant in the transverse plane (which can be obtained with solenoids as focusing elements and bending magnets with special field index, or approximately with skew quads). A. Burov suggested using circular optics with flat beams to [6]:

1) Fight against space charge in the LHC complex at low energy. With circular modes, the space charge limit comes from the larger transverse emittance, whereas in the usual planar modes, it comes from the smaller one;

2) Increase the LHC luminosity using flat beams (instead of round ones as currently used) as in this case the luminosity is inversely proportional to the square root of the smaller emittance.

These concepts should be studied in detail to evaluate the real quantitative (maximum) gain for the LHC luminosity: this includes effects of dispersion and any other perturbation, as well as the Intra-Beam Scattering (IBS) with the small transverse emittance in one plane. Circular optics is also considered in the MEIC project to realize the matched electron cooling for diminishing the space charge impact [7].

## PHYSICS OF COLLIDERS, STORAGE RINGS AND SYNCHROTRONS

IOTA (Integrable Optics Test Accelerator) is a future test ring in FNAL for Non-Linear Optics and OSC (Optical Stochastic Cooling) studies [8]. V. Lebedev already gave a talk at HB2010 on OSC in the Tevatron, where the OSC's concept was reviewed. The principle is similar to the normal stochastic cooling except with much larger bandwidth (~ 200 GHz): undulators replace the PU and Kicker. In this study, a new/better understanding is proposed and a possible application for the LHC is discussed. OSC seems a promising technique for the LHC, which would allow a well-controlled luminosity leveling and which could potentially double the average luminosity. However, the next step for the moment is to validate the cooling principles in IOTA.



ISBN 978-3-95450-118-2

# WG-B: BEAM DYNAMICS IN HIGH INTENSITY LINACS

D. Raparia, BNL, Upton, USA
P. A.P. Nghiem, CEA, Saclay, France
Z. Li, IHEP, Beijing, China

*Abstract*

Emittance coupling, equipartioning and losses were a few topics, which were discussed thoroughly during parallel session for beam dynamics in high intensity linacs (group B). Linac designs for the future, under construction, upgrade and the existing linacs from around the world were presented in three working sessions.

A total of 18 talks were presented. Five presentations are general beam dynamics in nature and twelve talks were project specific. The detail of each contribution can be found in these proceedings. Here we report the summary of the discussions and some concluding remarks of the general interest to all the projects presented in the working group.

## INTRODUCTION

Beam Dynamics of High Intensity Linacs (working group B) had 18 invited talks and 15 poster presentations. These presentations included three on linac beam dynamics, nine on design of linac for specifics projects, two reports from operating linacs, one on RFQ design recopies, one on loss mechanism in H- linacs and one for multi MW proton linac design challenges. Out them two talks were designed to generate discussion and had one two hours long discussion session.

## GENERAL BEAM DYNAMICS FOR HIGH INTENSITY LINACS

Hofmann discussed in detailed emittance coupling in the intense beam and can be summarized as (1) equipartition beam is not necessary to avoid emittance exchanged, it is enough if one avoid resonance region in Hofmann charts, (2) emittance exchanged depends on the crossing speed (inversely proportional) of resonance stop-bands and (3) on equipartition, even main resonance will disappear but splitting of emittances and consistent emittance growth may happen.

Lagniel raised question about validity of equipartition in his talk entitled, "Equipartition Reality or Swindle", which was followed by long and lively discussion. Discussions hinted there is more work (simulations) needed to reach any conclusion.

Nghiem tried proposed a new definition of the halo particles arguing existing definitions are too abstract and definitions decide in advance where should be the halo. According to proposed definition the location of steepest density variation, i.e. where the second derivative is maximum in case of 1-D distribution, separate halo particles from the core particles.

## BEAM DYNAMICS DESIGN OF LINACS

Table 1 give a brief description of the linacs discussed in the WG-B at HB2012. These linacs accelerate variety of particles to different energies and beam powers using different frequencies. The block diagram of these linacs depends on the mode of operation; pulse or continuous wave (CW). The pulse linac usually used as injector to circular machine with higher pulse current and lower beam power compared to CW linacs. CW linacs are used for fix target except ESS, which is a pulse linac. The front-end of these linacs have the same structure namely, a source, a low energy transport (LEBT), and a RFQ. Following structure depends on the nature of operations, CW linac start superconducting structure right after RFQ to avoid large power consumption and associate problems of structure cooling. Pulse linacs have warm cavities after RFQ. The transition energy between warm and superconducting part of the linac is coming down as the superconducting technologies getting mature. For example, in case of SNS the transition energy is about 187 MeV whereas ESS proposing about 80 MeV. Superconducting structures at lower energies have much lower (< factor of 5) phase advance per meter in compare to warm structures (DTL, CCDTL). The lower longitudinal focusing forces per meter make beam susceptible to longitudinal beam halo, which tends to loss at higher energies. Although spoke cavities have not yet seen any beam through it, every future linac design have these cavities.

An essential element for pulse linac is a chopper and is generally located after RFQ, to provide gap in the pulse train for rise time of a kicker magnet (to kick the beam out of beam line or out of circular machine). The most demanding requirement for the chopper is in the case of Project-X, where beam need to chop bunch-by-bunch basis. It is interesting to see CSNS move chopper from MEBT to LEBT to reduce losses in linac, whereas ESS added the chopper after the RFQ.

A different design recipe for RFQ was presented. In this method the focusing parameter B is varied as the beam bunches to compensate RF defocusing, instead keeping it constant as in the present RFQs.

In spite of all these differences and peculiarities, the design guide line is the same for all these linacs: (1) a zero-current phase advance per period less than 90 degrees to avoid structure resonances, (2) a smooth phase advance per meter to avoid mismatches, (3) tunes chosen to avoid the radial – longitudinal coupling resonances in the Hoffmann chart (4) and tried to follow equipartition rule.



ISBN 978-3-95450-118-2

# ACCELERATOR SYSTEM DESIGN, INJECTION, EXTRACTION AND BEAM-MATERIAL INTERACTION: WORKING GROUP C SUMMARY REPORT

D. Li, LBNL, Berkeley, CA 94720, USA,
N.V. Mokhov, FNAL, Batavia, IL 60510, USA

## INTRODUCTION

The performance of high beam power accelerators is strongly dependent on appropriate injection, acceleration and extraction system designs as well as on the way interactions of the beam with machine components are handled. The experience of the previous ICFA High-Brightness Beam workshops has proven that it is quite beneficial to combine analyses and discussion of these issues in one group, WG-C at this Workshop. A broad range of topics was presented and discussed in twenty talks at four WG-C sessions as well as at two joint WG-A/C and WG-B/C sessions. The presentations are listed at the end of this report. Highlights from these talks, outstanding issues along with plans and proposals for future work are briefly described in the sections below.

## INJECTION

Stripping foils – carbon or aluminum oxide - is the standard techniques for the $H^-$ injection in the existing machines and projects under consideration. As an example, Fig. 1 shows a typical layout of the system. At ISIS, the serially powered dipoles are used to generate a 45mrad – 65mm vertical bump. Horizontal painting on a 50-µg/cm$^2$ thick $Al_2O_3$ foil is done via the closed orbit movement.

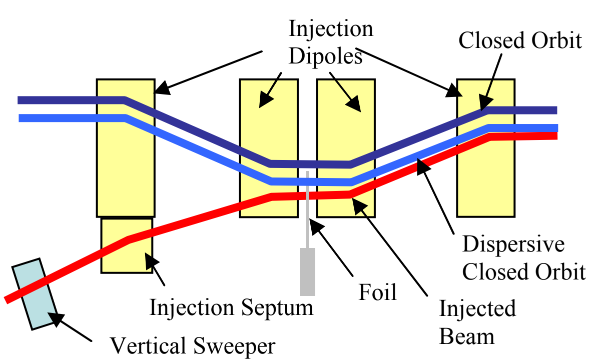


Figure 1: Schematic layout of ISIS stripping foil injection.

Impressive analysis is performed at SNS to reveal the role of multiple and single Coulomb scattering, energy loss, elastic and inelastic nuclear interactions in stripping foils as a source of beam loss in the machine. The space charge effect is one of the phenomena specific to the high-power accelerators. Detailed 2D and 3D ORBIT simulations done for ISIS and Project X allowed quantification of this effect for the technique performance, prediction of beam loss distributions and foil heating. A trick proposed by the ISIS–JPARC collaboration - use of a double-layer foil set – results in a 20% reduction of the peak temperature compared to a standard single-foil setup.

Attention to details and several modifications of the injection system within the Proton Improvement Plan (PIP) would double the 8-GeV proton production in the Fermilab Booster. PIP includes: aperture improvement, better orbit control, magnet re-alignment, a notcher relocation from the L5 straight section to the L12 one along with changing its action from vertical to horizontal, implementation of new stronger correctors for magnetic cogging, switch to 2-stage collimation as was designed originally, and an improved radiation protection scheme.

## BEAM LOSS, COLLIMATION AND EXTRACTION

Comprehensive studies of beam loss and collimation in the ESS Linac have demonstrated difficulties in this area for linear accelerators. The TraceWin tracking simulations were performed to propagate quadrupole and cavity errors allowing optimization of the scheme and loss limit on a graphite collimator. The findings in the MEBT studies are: halo growth occurs in the last half of the MEBT (sometimes in the final 10-20 cm); the standard scheme of two collimators separated by 90 deg is not the optimum for the ESS MEBT; the phase advance of an individual particle (angle in the normalized phase space) depends on its initial position due to a strong space charge; the angular distribution of halo particles is not uniform.

A drastic underestimation of equipment activation due to beam loss in the ESS RFQ (<3 MeV) and DTL (<79 MeV) was found compared to that predicted by the "1 W/m" rule. NVM, as a co-author of that rule, pointed out that "The **1 W/m rule** for beam loss doesn't apply here as we derived it for continuous loss of $E_p$ > 100-200 MeV beam resulting in contact dose (30 day/1 day) of 0.5-1 mSv/hr on an outer surface of a typical (massive) accelerator magnet" (Beam Halo and Scraping, Ed. N.V. Mokhov, W. Chou, 7th ICFA Workshop on High Intensity High Brightness Hadron Beams, Lake Como, Wisconsin, 13-15 Sep. 1999).

The amazing performance of the most powerful PSI accelerator complex is based – among other things – on excellence and innovations in the collimation, extraction



ISBN 978-3-95450-118-2

# SUMMARY OF THE WORKING GROUP ON COMMISSIONING AND OPERATION

Michael Plum, ORNL, Oak Ridge, Tennessee, USA, Yoichi Sato, J-PARC, Tokai, Japan, Rudiger Schmidt, CERN, Geneva, Switzerland

## INTRODUCTION

The conveners of Working Group D (Michael Plum, Yoichi Sato, and Rüdiger Schmidt) have built a program focussed on answering the following issues:

- observation of beam losses (e.g. time structure, other parameters,...)
- reducing beam losses with operational parameters away from the design set points
- reducing beam losses (or concentrating beam losses at a few locations) using collimators
- minimizing beam losses due to beam transfer from one accelerator to the following accelerator - what parameters are important?

The issue of reducing beam losses with operational parameters away from the design set points is especially valuable as it is rarely discussed.

## TALKS IN THE SESSION

1. Beam losses at LHC and its injector, Laurette Ponce (CERN, Geneva)
2. Collimation experience at the LHC, Stefano Redaelli (CERN, Geneva)
3. Performance and Future Plans of the LHC RF, Philippe Baudrenghien (CERN, Geneva)
4. High Intensity Operation and Controlling Beam Losses in a Cyclotron Based Accelerator, Mike Seidel (PSI, Villigen)
5. The result of beam commissioning in J-PARC 3-GeV RCS, Hiroyuki Harada (J-PARC, Tokai)
6. Recent Commissioning of High-Intensity Proton Beams in J-PARC Main Ring, Yoichi Sato, JPARC (J-PARC, Tokai)
7. Beam Loss Control for FNAL/Booster: Present and Plans for the Future, Fernanda Gallinucci Garcia (Fermilab, Batavia)
8. Characterizing and Controlling Beam Losses at the LANSCE Facility, Lawrence Rybarcyk (LANL, Los Alamos, New Mexico)
9. Beam Loss Mitigation in the Oak Ridge Spallation Neutron Source SNS, Michael Plum (ORNL, Oak Ridge, Tennessee)
10. Beam Commissioning Plan for CSNS Accelerators, Sheng Wang (IHEP, Beijing)
11. Beam Loss Control in the ISIS Accelerator Facility, Christopher Warsop (STFC/RAL/ISIS, Chilton, Didcot, Oxon)
12. Status and Beam Commissioning Plan of PEFP 100-MeV Proton Linac, Ji-Ho Jang (KAERI, Daejeon)

### *High Intensity Operation and Controlling Beam Losses in a Cyclotron Based Accelerator, Mike Seidel*

PSI has two cyclotrons accelerating protons up to an energy of 590 MeV. The beam power is with 1.3 MW still the worldwide record. During tests even a beam power of 1.4 MW was achieved. The beam is sent to several targets.

Acceleration is in CW mode with an extraction efficiency of 99.98 %. Clean extraction requires large turn separation between turns, this can be achieved by "closed orbit distortions". A gain by a factor of 3 can be achieved using this technique. A fine control of the tune is required to minimise losses. Longitudinal space charge requires high gap voltage.

The tomographic phase reconstruction using wire scanner data allows measurement of beam tails.

The last 20-50% of the full current are achieved by minimising beam loss with fine tuning, this process depends to some extent on the operator skills.

Beam losses today are down to $5*10^{-5.}$ An increase of the beam power is only accepted if the losses do not increase.

Activation in general is in the order of 1 mSv/h, some areas 10 mSV/h, the accumulated dose for personnel is constant over the years.

Very high power operation requires loss monitoring, interlocks, addressing thermo-mechanical cooling problems and remote handling of components.

### *Beam Loss Control in the ISIS Accelerator Facility, Christopher Warsop*

The ISIS synchrotron accelerates protons from 70 MeV to 800 MeV at 50 Hz. The total beam power is 200 kW, the power is limited by beam losses leading to activation.

Monitoring is with BLMs (ionization chambers and few scintillators) and BCTs. The protection systems issue beam dumps or warnings in case of too high losses.

For the injector, beam losses are minimised by careful tuning. Injection into the synchrotron is with H- beams, the foil stripping efficiency ~98 %, leading to some losses downstream of the foil. Trapping loss are 5-10 %, and losses during acceleration <1 %.

It is favoured to generate losses at low energy and localise losses in one area on collectors, even if the betatron phase for the collector is not optimised.

A new septum with larger acceptance decreased the losses at extraction. However, to reduce beam losses during the entire cycle (in particular at extraction) the

# QINCLOSING PLENARY SUMMARY OF WORKING GROUP E DIAGNOSTICS AND INSTRUMENTATION FOR HIGH-INTENSITY BEAMS

R. Dölling, Paul Scherrer Institute, Villigen, Switzerland
N. Hayashi, J-PARC, J-PARC, JAEA, Tokai, Ibaraki, 319-1195, Japan
V. Scarpine, FNAL, Fermilab, Batavia, IL 60510, USA

## OVERVIEW

Working group E was charged with presentations and discussions on diagnostics and instrumentation of high intensity beams. We had 2 sessions, consisting of a total of 12 talks, each of 20 minutes for presentation followed by some discussion. One session was followed by a discussion session of two hours. All sessions took place in parallel with the sessions of WG-D (Commissioning, operations and performance), inevitably preventing some possibly useful overlap. In addition, seven posters, regarding beam diagnostics, were presented in the single poster session.

## PRESENTATIONS

The following **talks** were presented:
*T. Xu: "The Beam Diagnostics of CSNS"*, presented an overview on the progress on diagnostics for the Chinese spallation neutron source. This talk includes an overview of the CSNS accelerator, progress on the development of diagnostics and prototype testing and plans for commissioning the CSNS front-end starting next year. *V. Scarpine: "Instrumentation Development and Beam Studies for the Fermilab Proton Improvement Plan Linac Upgrade and New RFQ Front-End"*, presented beam measurements from Fermilabs new front-end injector system, including proton beam energy from time-of-flight, delivered by the new 201 MHz RFQ.
*L. Nebot Del Busto: "Detection of Unidentified Falling Objects at LHC"*, described the detection of sudden beam loss around the LHC ring at millisecond time scales. These losses were detected exclusively by the LHC BLM system. The talk described the techniques employed to identify such beam loss events.
Specific beam instrumentation and methods:
*E. Holzer: "Fiber Based BLM System R&D at CERN"*, presented The application of a beam loss measurement (BLM) system based on Cherenkov light generated in optical fibers, where a longitudinal resolution of beam loss detection of ~1m over 100 m may be possible.
*P. Duperrex: "On-line Calibration Schemes for RF-based Beam Diagnostics"*, described improvements of BPMs and current monitors used in a high radiation environment.
*P. Saha: "Online Monitoring for the Waste Beam in the 3 GeV RCS of J-PARC"*, discussed the detection of a small fraction (about 0.4%) of un-stripped $H^0$ and $H^-$ waste beam in comparison to the full beam.
*R. Singh/O. Chorniy: "Measurement and Interpretation of the Betatron Tune Spectra of High Intensity Bunched Beam in the SIS18"*, described their two measurement system and compared their head-tail mode measurements with a simple model. The predicted modifications of tune spectra, due to space charge effects based on analytical models, were studied.
*W. Blokland: "Recent Developments on High Intensity Beam Diagnostics at SNS"*, reported on improvements of electron beam scanner that performs non-interceptive measurements of the transverse and longitudinal profiles of the proton beam in the SNS ring. Also presented are temperature measurements of the stripper foil and the target imaging system.
*F. Becker: "Beam Induced Fluorescence – Profile Monitoring for Targets and Transport"*, reported on the use of these monitors at higher gas pressures. Beam profiles from ionic transition N2+ appear unchanged from $10^{-3}$ to 30 mbar.
*B. Walasek-Hohne: "Optical Transition Radiation for Non-relativistic Ion Beams"*, reported on the first use of this technique at lower energy heavy ion beams, which was proposed by A. Lumpkin from FNAL. First results on OTR $q^2$ dependency were also presented.
*T. Maruta: "Longitudinal Beam Diagnostics with RF Chopper System"*, presented a measurement of the longitudinal bunch distribution with a large dynamic range (order of $10^{-6}$), obtaining the beam profile on the phase axis by measuring the beam loss in RCS with various RF settings of the chopper cavity.
*P. Kowina: "Momentum Spread Determination of Linac Beams Using Incoherent Components of the Bunch Signal"*, reported on the first, still preliminary, indications, that it may be possible to obtain a Schottky signal in a linac. Very preliminary spectrum were presented from different bunching conditions.
The following **posters** were presented:
*O. Chorniy: "A Method to Measure the Incoherent Synchrotron Frequencies in Bunches"*,
*M. Hempel: "Bunch-by-Bunch Beam Loss Diagnostics with Diamond Detectors at the LHC"*,
*Y. An: "The Study on Measuring Beta Functions and Phase Advances in the CSNS/RCS"*,
*S. Redaelli et al.: "A Tool Based on the BPM-interpolated Orbit for Speeding up LHC Collimator Alignment"*,
*H. Hassanzadegan et al.: "Beam Position Monitor System of the ESS Linac"*,
*R. Dölling: "Progress with Bunch-shape Measurements*

ISBN 978-3-95450-118-2